Microtribological Performance of Metal-doped MoS_2 Coatings

Pantcho Stoyanov

Department of Mining and Materials Engineering
McGill University
Montreal, Quebec
Canada

February, 2011

A thesis submitted to McGill University
in partial fulfillment of the requirements of the degree of
Doctor of Philosophy

Abstract

The mechanical and tribological properties of pure MoS_2, pure Au, Au-MoS_2 and Ti-MoS_2 coatings were evaluated and examined at a microscopic scale. The metal doped MoS_2 coatings had varying metal content, 5-10at% for Ti and 10-90% for Au. Reciprocating sliding wear tests were performed with a range of initial Hertzian contact pressures from 0.41 to 3.5 GPa and in air at two humidity levels (i.e. "low" being 3-5%RH and "high" being 30-40%RH). Titanium and gold were chosen for this study as metal additives due to their positive influence on the mechanical properties of the coating. The friction and wear behavior at the micro-scale were directly compared to tribological properties at the macro-scale, which were performed using an *in situ* tribometer. Reciprocating micro- and macro- wear tests were performed with spherical diamond tip (with 10 and 50 µm radii) and a sapphire tip (with a radius of 3.175 mm), respectively. The range of initial Hertzian contact pressures for macro-scale (i.e. between 0.41GPa and 1.2GPa) overlapped with that for micro-scale. However, the initial Hertzian contact diameters (2*a) were very different (i.e. 0.8-2.3 µm for micro-scale and 60-180 µm for macro-scale).

It was observed that the small addition of Ti or Au to MoS_2 improved the microtribological properties (i.e. lower friction and less wear) compared to pure MoS_2 coatings. The improved microtribological properties with metal additions were attributed to an increase in the mechanical properties, decrease in adhesion, and a decrease in the interfacial shear strength.

In terms of the different length scales, lower steady state friction was observed for macrotribology compared to microtribology. The higher friction at the micro- scale was explained by the greater adhesion effects and additional velocity accommodation modes (e.g. microplowing or plowing). The microplowing or plowing at the microscopic scale was attributed to the tip roughness and the inability to sustain a stable transferfilm throughout the tests at high humidity. In addition, using *in situ* and *ex situ* techniques, three different stages for solid lubrication were identified based on differences in contact area, tip shapes, and environmental conditions. The first stage has been previously observed with macrotribology on MoS_2 coatings at low humidity levels. The second stage, on the other hand, was observed for micro-tribology where the contact size is significantly smaller compared to stage one. The main wear mechanism is still adhesion, but there is also some micro-plowing. The final stage was observed for humid sliding in microtribology, where no transfer films were observed and therefore the main wear mechanism was plowing.

Résumé

Les propriétés mécaniques et tribologiques de revêtements de MoS_2 pur, d'Au pur, de Au-MoS_2 et de Ti-MoS_2 ont été évaluées et examinées à l'échelle microscopique. Les revêtements nanocomposites étudiés contenaient 5-10 % at. de Ti et 10-90 % at. d'Au. Des tests d'usure par glissement alternatif ont été mis en œuvre, l'échelle de pression Hertzienne de contact initiale variant de 0.41 à 3.5 GPa, dans une atmosphère d'air avec deux niveaux d'humidité contrôlée (le niveau le moins élevé se situant entre 3 et 5 % HR et le plus élevé entre 30 et 40 % HR). Pour cette étude, le titane et l'or ont été choisis comme additifs métalliques pour leur influence positive sur les propriétés mécaniques des revêtements. Les comportements de friction et d'usure des revêtements à l'échelle microscopique ont été directement comparés à leurs propriétés tribologiques à l'échelle macroscopique, dont les tests étaient effectués à l'aide d'un tribomètre *in situ*. Des tests sclérométriques alternatifs ont été réalisés aux échelles microscopiques et macroscopiques avec des pointes de diamant sphérique (10 et 50 μm de rayon) et une pointe de saphir (ayant un rayon de 3.175 mm). La gamme de pression Hertzienne de contact utilisée à l'échelle microscopique (entre 0.41 GPa et 1.2 GPa) était très proche de celle utilisée à l'échelle macroscopique. Cependant, le diamètre de contact Hertzien initial (2*a) était très différent, soit 0.8 – 2.3 μm à l'échelle microscopique et 60 – 180 μm à l'échelle macroscopique.

Les résultats montrent que l'ajout de faibles quantités de Ti ou d'Au au MoS_2 améliore les propriétés micro-tribologiques (comportements à la friction et à l'usure atténués) en comparaison avec des revêtements de MoS_2 pur. L'amélioration des propriétés micro-tribologiques due à

l'addition de métaux a été attribuée au renforcement des propriétés mécaniques, une adhésion plus faible et une baisse des contraintes de cisaillement interfaciales.

Si l'on compare des tests micro- et macro-tribologiques effectués sur des étendues de longueur variées, ces derniers étaient caractérisés par une friction en régime permanent moins élevée. Le comportement de friction plus accentué dans le cas des tests réalisés à l'échelle microscopique s'explique sur la base d'effets d'adhésion plus importants et des modes additionnels de compensation de vitesse (labourage ou micro-labourage). Les tendances au labourage ou micro-labourage observées à l'échelle microscopique ont été attribuées à la rugosité de la pointe de diamant et à la difficulté de maintenir une couche de film de transfert en place lors de tests effectués dans des conditions d'humidité élevée. L'utilisation de techniques *in situ* et *ex situ* a également permis de déterminer trois stades de lubrification solide, en se basant sur des différences observées à la zone de contact, dues aux formes des différentes pointes et aux conditions environnementales appliquées. Le premier stade, avait été identifié auparavant, lors de tests de macro-tribologie sur des revêtements de MoS_2, à un niveau d'humidité faible. Par contre, le deuxième stade n'a été observé que lors de tests de micro-tribologie où la taille de la zone de contact était bien plus petite que dans le cas du premier stade. A ce stade, le mécanisme d'usure est principalement relié au comportement d'adhésion du revêtement, avec une influence possible de l'effet de micro-labourage. Le stade final de lubrification a été observé lors de tests de micro-tribologie réalisés dans des conditions d'humidité élevée et caractérisés par l'absence du film de transfert. De cette observation, il a été déduit que le principal mécanisme d'usure du film à ce stade de lubrification correspondait au labourage.

Contributions of Authors

All papers have been published or submitted for publication with the supervisor, Prof. Richard Chromik, as a co-author. The supervisor assisted the author of this thesis in the writing the manuscripts and provided normal supervision and advice for the experiments and the analysis of the results.

Other authors of the manuscripts in this thesis include three undergraduate summer students; David Goldbaum, Zachary Fishman, and Shivani Gupta. Under my co-supervision, the contributions to the manuscripts of the summer students are as follows:

- David Goldbaum wrote the Matlab code that determines the area function of the tip based on atomic force microscopy measurements.
- Zachary Fishman measured mechanical properties of the coatings and wrote the first version of the Matlab code for analysing the friction data from microtribology experiments.
- Shivani Gupta conducted microtribology experiments on pure Au coatings and analyzed the results.

Holger Strauss, a PhD student at McGill University, is also a co-author on one of the publications. He built and programmed the *in situ* tribometer, provided training and performed some of the experiments.

Additional authors include Jeffrey Lince and Xiaoling Zhang, who provided the coatings that were tested for this PhD dissertation. They also took part in discussion of the results.

The author of this PhD thesis was responsible for the writing of all manuscripts. In addition, the author performed the experimental procedure and analysis of the mechanical and tribological properties measurements at the macro- and micro- scale of all thin film coatings presented in this thesis. The author also co-supervised three summer students throughout this study.

The papers that form some chapters in this thesis are as follows:

- Chapter 3: P. Stoyanov, J.Z. Fishman, J.R. Lince, and R.R. Chromik, *Micro-tribological performance of MoS_2 lubricants with varying Au content*, Surface and Coatings Technology, v 203, n5-7, p761-765, 2008
- Chapter 4: P. Stoyanov, R.R. Chromik, D. Goldbaum, J.R. Lince and X. Zhang. *Microtribological Performance of Au-MoS_2 and Ti-MoS_2 Coatings with varying Contact Pressure*. Tribology Letters, v40, n1, p199-211, 2010
- Chapter 5: P. Stoyanov, R.R. Chromik, S. Gupta and J.R. Lince, *Micro-scale sliding contacts on Au and Au-MoS_2 coatings, Surface and Coatings Technology*, Surface and Coatings Technology, v205, n5, p. 1449-1454, 2010
- Chapter 6: P. Stoyanov, H. Strauss, and R.R. Chromik, *Scaling Effects between Micro- and Macrotribology of Ti-MoS_2 Coatings*, (submitted to Wear)

Acknowledgements

The author would like to thank Prof. Richard Chromik for providing this interesting and challenging topic and for all his helpful hints and suggestions, encouragements, and patience. The author also gratefully acknowledges financial support from Fonds québécois de la recherche sur la nature et les technologies (FQRNT), program Établisssement de nouveaux chercheurs, NSERC Discovery Grant, and Lorne Trottier for the graduate Fellowship (McGill Engineering Doctoral Award). Parts of this work was also supported under The Aerospace Corporation's Mission Oriented Investigation and Experimentation program, funded by the U.S. Air Force Space and Missile Systems Center under Contract No. FA8802-09-C-0001. The author also acknowledges Dina Goldbaum, Holger Strauss, Zachary Fishman, David Goldbaum, and Shivani Gupta for their collaboration with experiments and with the Matlab code. The assistance of Francois Barthelet in conducting atomic force microscopy measurements is also gratefully acknowledged.

The author would like to express sincere gratitude to his sister Milena Stoyanova for all her help and encouragements. Last, but certainly not least, the author would like to thank his parents, Lilly Rousseva-Stoyanova and Peio Stoyanov, for all their love, understanding, and continuous support.

Table of Contents

List of Figures

List of Tables

Chapter 1
Introduction

1.1 Background

The word tribology originated from the Greek word ‘tribos’, which means rubbing. Tribology defines the science of two interfaces in contact with each other in relative motion. The science of tribology generally refers to friction, wear, and lubrication. Friction and wear are present in most systems that involve some sort of a movement or motion between components. Depending on the system, friction and wear can be productive and unproductive[1]. For example, productive friction can be observed in automotive components such as breaks and clutches and productive wear can be observed in polishing, machining, and writing with a pencil. On the other hand, low friction and low wear is preferred in components such as gears and bearings. In general, friction and wear can be controlled by selecting the proper materials or performing different surface modifications techniques.

Due to the lack of knowledge of many tribological systems, the average loss per year for the US is estimated to be about $200 billion dollars. Simply by improving our understanding of tribological systems, the US alone can save up to $16 billion per year[1]. Therefore, there is a desire of tribological research in order to better understand the behavior of surfaces in contact and to optimize tribological systems, which would minimize the losses resulting from friction and wear[1]. A general approach for minimizing the friction and wear in tribological systems is

to utilize various lubrication techniques[2]. These lubrication techniques typically include liquid lubrication (e.g. mineral oils and more recently environmental friendly oils) or solid lubricants such as diamond-like carbon (DLC) or molybdenum disulphide (MoS_2).

Solid lubricants are used in certain devices or under certain severe conditions where liquids are not useful[3] (i.e. vacuum, extreme temperatures, high contact pressures, radiation, sealing and containment limitation, etc.). Molybdenum disulphide, as a solid lubricant, is known to have a low coefficient of friction and high endurance life under vacuum conditions and high contact pressures due to its structure. Therefore, it is mostly used in some aerospace applications, such as satellites and spacecrafts[4]. Typically applied as a coating, MoS_2 provides sufficient tribological properties at a wide range of operating temperature (up to 500°C in air and up to 1000°C in vacuum)[5]. Furthermore, MoS_2 coatings exhibit a low coefficient of friction at high pressures, more or less independent of velocity, providing for a high endurance life and thus making it very useful for long term space applications[4]. Other current applications of molybdenum disulphide include applications in machining processes and as anti-adhesion coatings[4].

Due to its excellent lubrication properties, MoS_2 has been more recently considered as a potential candidate for lubricating microelectromechanical systems (MEMS). Today, the most dominant material used in MEMS is silicon, because of the available fabrication technology. Although silicon is a hard material, it is also brittle and has thus poor tribological properties[6]. Therefore,

other materials or solid lubricants, such as MoS_2, have to be considered for lubricating such microdevices. However, as a result of the decreased contact size in such devices, roughness and adhesion play a larger role in the sliding behavior. For these reasons, it currently remains unclear how a reduction in contact size will affect the tribological behavior of microsystems using solid lubricants such as MoS_2.

1.2 Modification Techniques

Due to the wide availability of potential applications for MoS_2, there is an increasing demand for making this coating robust to different environmental conditions (i.e. varying temperature and humidity levels). One approach to improve the performance of MoS_2 under different environmental conditions and different contact pressures is to modify its microstructure. For instance, the most common modification processes is the addition of metals or other materials by co-sputtering. The addition of a dopant (e.g. Ti, Au, Ni, Al, Pb, and Sb_2O_3) to MoS_2 increases the density, the hardness, and the oxidation resistance of the coating making it more suitable for tribology applications at higher relative humidity[7-10].

1.3 Scope of this Work

With the recent advent of microelectromechanical systems (MEMS), molybdenum disulphide could be considered a good alternative that would improve the tribological properties of these devices.[11] Furthermore, the small addition of MoS_2 to gold could also potentially improve the service life of microswitches. “However, it remains unclear how a reduction in contact size will

affect the viability of these materials, including their ability to self lubricate by the formation of transfer films"[12]. The research presented in this PhD dissertation seeks to answer this question for the specific case of molybdenum disulphide cosputtered with Au and Ti. In more specific terms the objectives of this PhD dissertation are as follows:

1. To develop experimental techniques for tribological testing at the micro- scale using a 'true' area of contact for different contact pressures and humidity levels.

2. To understand how a reduction in contact size affects the tribological behavior of solid lubricants in terms of transferfilm formation and interfacial shear strength.

3. To compare the influence of low and high gold content of Au- MoS_2 nanocomposite coatings on the mechanical and micro-tribological properties (i.e. in terms of the elastic and plowing contribution).

4. To compare the effect of different metal additives (i.e. gold and titanium) to molybdenum disulphide on the mechanical and micro- tribological properties in terms of friction, wear behavior, interfacial shear strength, adhesion, and transferfilm formation.

5. To establish a direct comparison between macro- and micro- tribological performance of solid lubricants and provide a detailed understanding of the transferfilm formation and the velocity accommodation modes (VAM) using an *in situ* tribometer at the macro- scale

and using atomic force microscopy for *ex situ* analysis on nanoindation tips at the micro-scale.

6. To provide an understanding of whether gold and titanium doped MoS_2 coatings could be potential candidates for lubrication of micro-electromechanical systems (MEMS).

1.4 Final Remarks

All of the manuscripts in this PhD thesis have already been published or submitted to a journal. The chapters in this thesis are presented in the same way as they were published and include an experiment procedure section, which might be the same or contain overlaps within the different manuscripts.

REFERENCES

[1] B. Bhushan, Micro/Nano Tribology, 2 ed, CRC, Columbus, 1999, p.3-5

[2] K. Holmberg, Coatings tribology : properties, mechanisms, techniques and applications in surface engineering 2ed, Elsevier Science, Amsterdam; Boston; London, 2009

[3] A.Z. Szeri, TRIBOLOGY: Friction, Lubrication, and Wear, Hemisphere Publishing Corporation, New York, 1980, p.548

[4] A. Savan, E. Pflueger, P. Voumard, and A. Schroeder, Modern Solid Lubrication: Recent Developments and Applications of MoS_2, Lubrication Science 12 (2000) 185-203

[5] A.R. Lansdown, Molybdenum Disulphide Lubrication, Elsevier Science B.V., 1999, p.86

[6] S. Deladi, J. W. Berenschot, M. J. De Boer, G. J. M. Krijnen, and M. C. Elwenspoek, Proceedings of the IEEE International Conference on Micro Electro Mechanical Systems (MEMS),Maastricht, Netherlands, (2004), 181-184

[7] J. R. Lince, Tribology of co-sputtered nanocomposite Au/MoS_2 solid lubricant films over a wide contact stress range, Tribology Letters 17 (2004) 419-428

[8] X. Ding, X. T. Zeng, X. Y. He, and Z. Chen, Tribological properties of Cr- and Ti-doped MoS_2 composite coatings under different humidity atmosphere, Surface and Coatings Technology 205 (2010) 224-231

[9] S. D. Dvorak, K. J. Wahl, and I. L. Singer, *In situ* analysis of third body contributions to sliding friction of a Pb-Mo-S coating in dry and humid air, Tribology Letters 28 (2007) 263-274

[10] T. W. Scharf, P. G. Kotula, and S. V. Prasad, Friction and wear mechanisms in MoS_2/Sb_2O_3/Au nanocomposite coatings, Acta Materialia 58 (2010) 4100-4109

[11] T. W. Scharf, S. V. Prasad, M. T. Dugger, P. G. Kotula, R. S. Goeke, and R. K. Grubbs, Growth, structure, and tribological behavior of atomic layer-deposited tungsten disulphide solid lubricant coatings with applications to MEMS, Acta Materialia 54 (2006) 4731-4743

[12] P. Stoyanov, Z. Fishman, J. R. Lince, and R. R. Chromik, "Micro-Tribological Performance of MoS_2 Lubricants with varying Au content," Surface and Coatings Technology 203 (2008) 761-765

Chapter 2
Background and Literature Survey

2.1 Introduction

In this chapter, a literature survey is presented on tribology and molybdenum disulphide as a solid lubricant. The first part of this chapter consists of a general background on friction, wear, and lubrication. This includes information about basic friction laws, friction regimes applicable to various materials, wear laws, and the mechanism of solid lubrication. In the second part of this chapter, a literature survey is provided on molybdenum disulphide as a solid lubricant including information on its microstructure, lubrication mechanism (i.e. transfer-/ tribofilm formation), friction behavior under different sliding conditions, and its effect on the tribological properties when doped with other materials. The last part of this chapter consists of a literature survey of microtribology. This part of the chapter is introduced with an extensive discussion on the differences between macro-, micro-, and nano- tribology and the factors that can influence the small scale contacts (e.g. roughness and contact shape). This section is concluded with literature on nano-/ microtribology of solid lubricants that have a potential to be used for microelectromechanical systems (MEMS).

2.2 Background

2.2.1 Friction

Friction is typically defined as the force that resists motion between two interfaces (also known as lateral force) and is parallel to the sliding direction. The friction force can be divided into two components[1]:

$$\mathbf{F = F_a + F_p} \qquad \textbf{(2.1)}$$

Where F_a is the friction force due to adhesion and F_p is the friction force due to plastic deformation of the surface (i.e. plowing friction). In the case of a pure elastic contact, which is typically the case for most tribological systems during steady state sliding, the friction force due to plastic deformation can be neglected.

The coefficient of friction[2] μ, is the lateral force (F) divided by the normal force (L) as it is expressed in the following equation:

$$\mathbf{\mu = F/L} \qquad \textbf{(2.2)}$$

It has also previously been shown that the shear stress has a linear relationship with the contact pressure:

$$\mathbf{S = S_o + \alpha P} \qquad \textbf{(2.3)}$$

where S is the shear stress, P is the contact pressure, and α is a constant (i.e. the limiting coefficient of friction). Dividing through the contact pressure in equation (2.3), and using equation (2.2), the coefficient of friction can also be expressed by the following equation:[2]

$$\mu = S/P + \alpha, \quad (2.4)$$

Furthermore, using the contact radius calculated from the Hertz model[3] for ball on flat surfaces,[2] equation (2.4) can be rewritten as

$$\mu = S\pi(3R/4E)^{(2/3)} * L^{(-1/3)} + \alpha, \quad (2.5)$$

where R is the radius of the spherical counterface, and E is the reduced modulus of the contact.[2] Equation (2.5) has been generally used for macrotribological tests on solid lubricants such as molybdenum disulphide (MoS_2) and diamond-like carbon (DLC).

For most tribological setups, friction values depend on many parameter, such as environmental conditions (i.e. humidity, temperature, etc.), contact pressures, velocity, materials pair, etc. Some of the typical friction values are summarized in table 2.1 for dry sliding[1]. Table 2.1 shows that the highest friction values is observed with metal to metal sliding contacts, whereas the lowest friction is seen with at least one surface being a solid lubricant (i.e. MoS_2, DLC, Graphite, etc.). Therefore, such lubricants are typically used in tribological systems where there is a metal on metal contact for the purpose to reduce the coefficient of friction and increase the endurance life.

Table 2.1. Friction values for different tribological system sliding in dry environment.

Sliding materials coefficient of friction	
Gold on gold	1-2
Aluminum on aluminum	0.8-1.2
Silver on silver	0.8-1
Titanium on titanium	0.5-0.6
Aluminum on mild steel	0.5-0.6
Titanium on mild steel	0.4-0.6
Gold on mild steel	0.4-0.5
Aluminum oxide on aluminum oxide	0.3-0.6
Diamond on diamond	0.1-0.2
Dry sliding in general	0.1 to 1.0
Graphite solid lubricant on hard surface	0.05-0.15
MoS_2 solid lubricant on hard surface	0.05-0.1
Rolling friction (balls or rollers)	0.001-0.01
DLC on DLC in dry nitrogen or argon	0.001-0.01
MoS_2 coating surface on steel in high vacuum	0.001 and below

2.2.2 Wear

Wear is usually defined as the material loss and the plastic deformation as a result of a contact and a sliding motion of two interfaces. The most common wear mechanisms are adhesive, abrasive, fatigue, and chemical wear[1], Figure 2.1[1]. Adhesive wear occurs when there is transfer from one material to the other during the sliding process, Figure 2.1(a). The material properties play a significant role for this type of wear mechanism. Abrasive wear occurs typically when one surface is harder than the other, Figure 2.1 (b). The harder asperities are pressed against the softer surface, which results in plowing and removal of the softer material. Fatigue wear occurs due to changing continuously the stress level by loading and unloading of the surface, Figure 2.1(c). Chemical wear is the result of a chemical reaction between the surfaces during the sliding. Oxidation wear is probably the most common type of chemical wear[1], Figure 2.1(d).

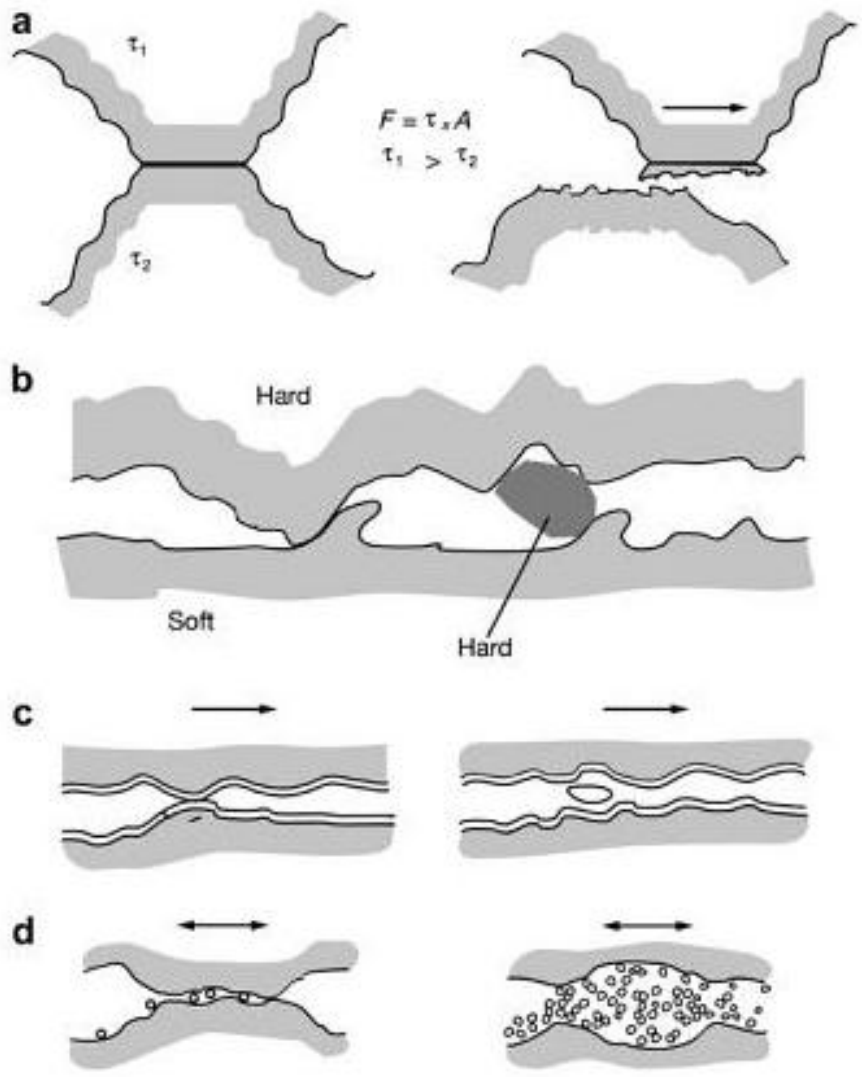

Figure 2.1. basic mechanisms of wear; (a) adhesive, (b) abrasive, (c) fatigue, and (d) chemical wear[1].

The wear depth and the wear volume are typically determined after a tribological tests using a technique that measures surface topography (i.e. profilometer, atomic force microscope, etc.). Using these values, the wear rate can be determined from Archard's wear equation:[4]

$$V/d = K*L/H \quad (2.6)$$

where V is the wear volume, L is the normal load, K is a material constant, H is the hardness and d is the sliding distance. In order to have a better understanding of the wear evolution with respect to sliding distance, one can use the wear rate equation developed by Siniawski et al. [5]:

$$K(n) = V(n)/d = K_1 * n^{\beta} \quad (2.7)$$

Where K(n) is the wear rate averaged over the first n cycles, V(n) is the wear volume during n cycles, d is the distance travelled by the ball, K_1 is the wear rate during the first cycle and the value β controls the time-dependence of the wear rate. For most tribological systems, the value of β falls in the range of $-1 \leq \beta < 0$, where for $\beta = -1$ all of the wear occurs in the first cycle, while $\beta=0$ corresponds to the case where the wear rate remains constant throughout the test. For some systems it is possible to obtain $\beta > 0$, which would represent a case where the wear rate increases with time.

2.2.3 Solid Lubrication

Solid lubricants are typically used for the purpose to reduce the coefficient of friction between two materials and to increase the wear resistance.[6] Currently, the most common solid lubricants consist of layer-lattice structures, such as graphite and molybdenum disulfide.[2] Other well known solid lubricants include soft metals (i.e. gold, copper, etc.), polytetrafluoroethylene (PTFE), diamond, dimond-like carbon, and some oxides.

The mechanism of using a solid lubricant in between two sliding surfaces is typically considered a two body problem and the coefficient of friction is related to the shear strength of the coating.[2] However, several recent investigations [2,7] have shown that the coefficient of friction has actually a strong dependence on the properties of the third body parts (transfer films), which are created during the sliding process and typically have the chemistry and the structure of the softer material or the solid lubricant.[2]

In general, however, for solid lubricants the tribological behavior (i.e friction and wear mechanism) is controlled by four main parameters, as defined by Holmberg and Matthews[1]:

a) The hardness relationship between the coating and the substrate
b) Thickness of the coating
c) Surface roughness
d) Shape and properties of lose debris

a) Hardness Effect

The hardness of the coating with respect to the slider, plays one of the most important roles in the tribological behavior of the coating. The frictional force is defined as the product of the shear stress and the contact area. When applying a hard slider to a soft coating, the contact area increases and therefore the friction is higher. When applying a hard slider on a hard coating, on the other hand, the contact area decreases but the shear strength increases and thus the friction

increases. Ideally, soft coatings, when deposited on hard substrates, are very effective in terms of reducing the friction. The friction force and the contact area in this case is reduced, which reduces the friction. This behavior can be seen clearly in Figure 2.2 (c)[1], which is based on Bowden and Tabor's theory[8]. In terms of reducing the wear, however, harder coating on a soft substrate can be very successful by preventing plowing of asperities.

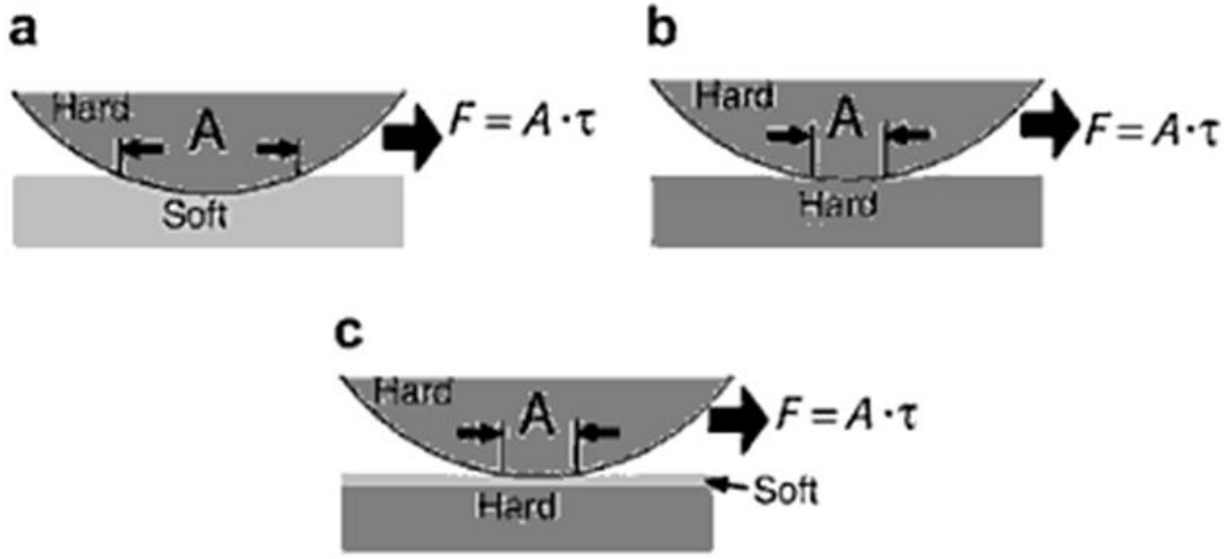

Figure 2.2. Depositing a thin soft film on a hard coating can reduce the coefficient of friction[1]

b) Thickness Effect

Thickness of the coating, in most systems, is also a very important parameter in terms of the friction and wear behavior[1]. When a hard slider is moving on a thin soft coating deposited on a hard substrate the friction depends on the shear strength of the coating following equation (2.4), which shows that the coefficient of friction is linearly proportional to the shear strength. For soft coatings, such as graphite and molybdenum disulphide, this would result in a low coefficient of

friction due to their low shear strength. There is however, a minimum thickness value for most coatings; if the thickness of the coating is below this minimum value, the coating will fail early and the substrate will be in contact with the slider. On the other side, if the soft film is very thick coating, the friction is significantly higher due to plowing and also an increase in contact area. When the coating is very thin it cannot support the load and plowing might occur in the substrate which would lead to an increase in friction. When the hard coating is thicker, on the other hand, it will be able to support the load and protect the softer substrate leading to virtually no plowing and therefore lower friction[1].

c) Roughness effect

The effect of substrate roughness for soft coatings is not as significant on the tribological properties as observed with the effect of thickness and hardness. This is particularly true in the case where the substrate roughness is significantly smaller than the coating thickness. However, for the case where the roughness is similar to the coating thickness, some minor changes in the friction coefficient have been previously observed, as reviewed by Holmberg[1]. If the roughness value of the slider is high relative to the coating thickness, on the other hand, some plowing of asperities might occur, which would result in an increased friction.

d) Effect of Debris particles

Debris particles are present at almost every tribological system. Depending on their shape, size and mechanical properties, debris particles can have a significant influence on the tribological

behavior of the coating. Godet[9] and Singer[2], have analyzed debris particles as a third body concept. Debris particles can be formed from the transferfilm through a chemical reaction with the environment, which then fall onto the wear track[2]. Throughout the sliding process, the debris particles can also reattach back from the wear track onto the slider and depending on the properties of the debris, this behavior can lead to debris shearing of the transferfilm, which would result in an increase in friction and wear. If the debris particles are significantly harder than the coating, then this could also lead to plowing of the coating and increase the friction.

In most tribological systems, the debris particles can also be collected on the slider from the end and the sides of the wear track. Dvorak et al.[10] observed this behavior with Pb-Mo-S coatings via *in situ* tribometry, where debris particles collected at the left and right edges of the contact. The authors were able to observe a difference in the debris behavior between sliding in dry and humid environments. In dry sliding the debris particles were attached to the counterface throughout most of the sliding test, whereas in humid environment the debris particles were not as stationary which resulted in higher friction.

2.3 Literature Survey on Macrotribology

2.3.1 MoS_2 Crystal Structure

The crystal structure of molybdenum disulphide is crucial for the tribological properties of the coating due to the physical and chemical changes that occur during a contact or a sliding process.[11] The crystal structure consists of molybdenum and sulfur atoms which are

composed of lattice layers and arranged in a hexagonal array as shown in Figure 2.3.[12] Each molybdenum atom is surrounded by six sulfur atoms and each sulfur atom is equidistant from three molybdenum atoms[13] with a typical distance of 2.41Å. The sulfur and the molybdenum atoms are covalently bonded and the bond between the lamellae consists of weak van der Waals forces, which results in a low shear strength during sliding and therefore a low coefficient of friction.[12] Furthermore, the size of the MoS_2 crystallites could also have a major influence on the tribological properties of the coating.

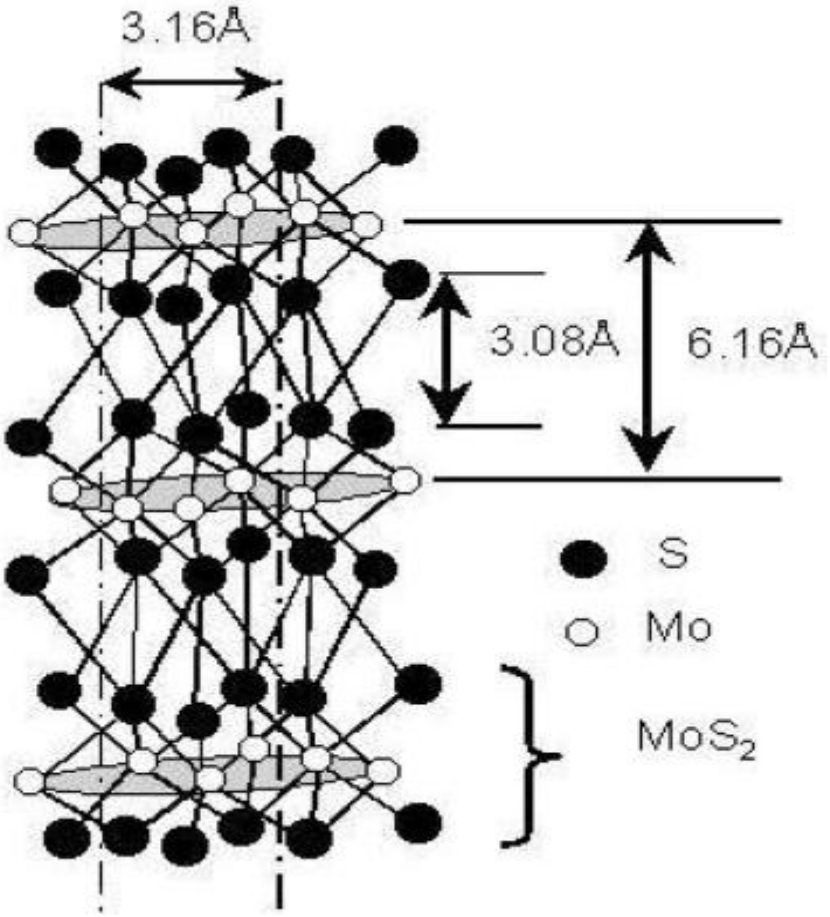

Figure 2.3 Crystal Structure of Molybdenum Disulphide[1]

2.3.2 Transfer of Molybdenum Disulphide

During a sliding contact between two surfaces, it is very ordinary for at least one of the materials to transfer to the other[13]. This transfer process is usually the result of plastic deformation, surface cracking, debris generation, and transfer or reaction layer formation[1], as shown in Figure 2.4. The transfer layer ranges between 0.01 and 50μm[1,14,15], but of course the amount and properties of the transferred material depend on the material and sliding conditions (i.e. contact pressure, contact area, environmental conditions, etc.). Godet et al.[9] described the third body concept in terms different velocity accommodation modes (VAM). Singer et al.[2] summarizes three more simplified ways that sliding is accommodated between a slider and a thin film, as shown in Figure 2.5 (i.e. Intrafilm flow, interface sliding, and interfilm sliding). Intrafilm flow occurs when the film is strongly adhered to both surfaces. In this case, the shearing occurs within the film and therefore, the friction behavior depends on the shear strength properties of the coating. The second velocity accommodation mode, interface sliding, occurs typically in a case with low normal loads and/ or single asperity contacts. For this VAM there is no material transfer onto the counterface, and the sliding occurs between the counterface and the coating. Interfilm sliding, on the other hand, occurs when the coating adheres to the counterface and the sliding takes place between the transferfilm and the coating. Throughout this sliding procedure, the shear strength is that of both films sliding against each other[2].

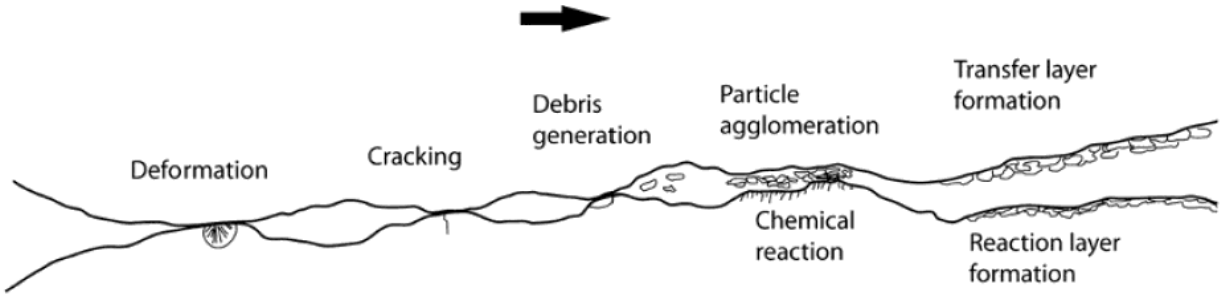

Figure 2.4. Process of transferfilm formation, as suggested by Holmberg et al.[1]

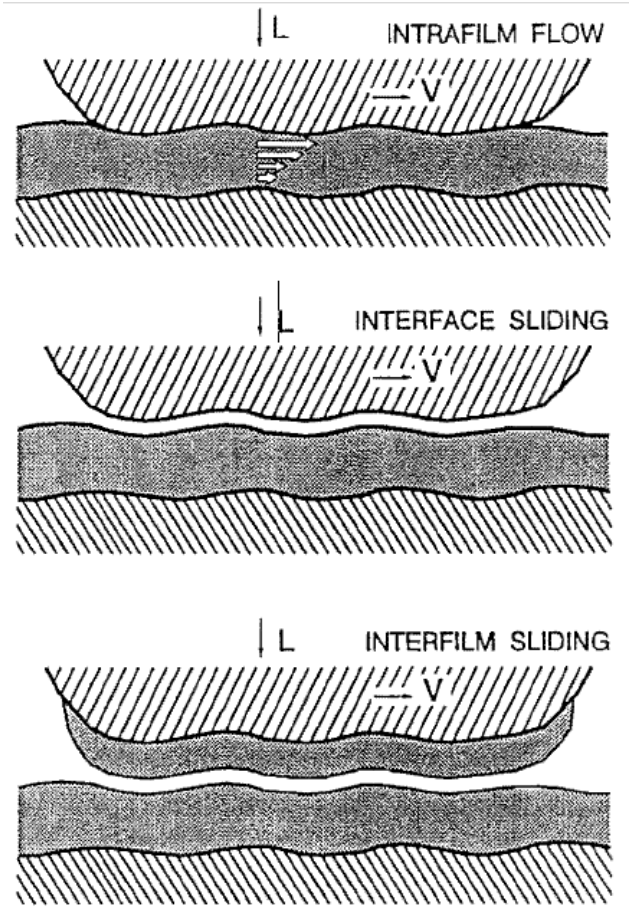

Figure 2.5. Three ways that sliding can be accommodated between a counterface and a thin film coating[2]

Molybdenum disulphide tends to transfer very readily to counterfaces, however, under ideal environmental conditions, the transfer occurs mostly during the initial stage (i.e. first few passes)[16] and stops after a stable and smooth transferfilm is formed [13]. Lansdown suggested that this process of the transferfilm formation occurs mainly by the transfer of crytellites instead of molecular transfer. Essentially, with molybdenum disulphide the stable transferfilm contributes to decrease in wear and a decrease in the coefficient of friction.

The group lead by Singer at the Naval Research Laboratory (NRL) has performed extensive research and describes in detail the process of the transferfilm formation of MoS_2 based coatings[10,14,17-20]. The group published a number of articles using an *in situ* Microraman tribometer, which allowed for monitoring the evolution of the transferfilm formation throughout the sliding process. By using this technique, the group found correlations between transferfilm characterization and tribological properties (i.e. friction and wear) at different sliding conditions. Dvorak et al.[10] investigated the third body process and velocity accommodation modes of Pb-Mo-S coatings using *in situ* tribometry. The authors found that when sliding on Pb-Mo-S coating, a MoS_2 transferfilm is formed during the first few cycles of the test which contributes to low friction coefficients in dry and humid environment. Furthermore, *in situ* monitoring revealed that the dominant velocity accommodation mode was interfacial sliding for both conditions. In humid air, however, a second velocity accommodation mode was observed (i.e. debris shearing).

More recently, Sharf et al.[21] investigated the tribo- and transferfilm behaviour of $MoS_2/Sb_2O_3/Au$ nanocomposite coatings in dry environment and in air (i.e. 50% relative humidity) using high resolution scanning electron microscopy (HRSEM) and cross-sectional transmission electron microscopy (TEM). Figure 2.6 and Figure 2.7 show high resolution scanning electron microscope (HRTEM) cross-sectional images of the worn surface and transfer film for the tests run in dry nitrogen and 50% relative humidity respectively. The presence of crystalline 2H-MoS_2 basal planes parallel to the sliding direction was observed on the worn surface for the case of dry nitrogen and 50% relative humidity, which indicated a transformation of the MoS_2 from amorphous to crystalline as a result of the frictional contact. However, the overall structure and chemistry of the worn surface was different for the two environmental conditions, as shown with the Automated eXpert Spectral Image Analysis (AXSIA) maps in Figure 2.6 (b) and Figure 2.7 (b). For the tests run under dry nitrogen Au nanoparticles were observed to be spread around close to the MoS_2 basal planes, whereas at 50% RH a continuous ~8nm thick crystalline Au layer was observed underneath the MoS_2 tribofilm. The transferfilms for both environmental conditions was approximately 1µm in thickness. Furthermore, TEM cross-sectional images of the transferfilms for both conditions revealed matching MoS_2 basal planes oriented parallel to the sliding direction, as shown in Figure 2.6(d) and Figure 2.7(c), which indicated the ‘basal on basal’ sliding contributed to a low friction and wear.

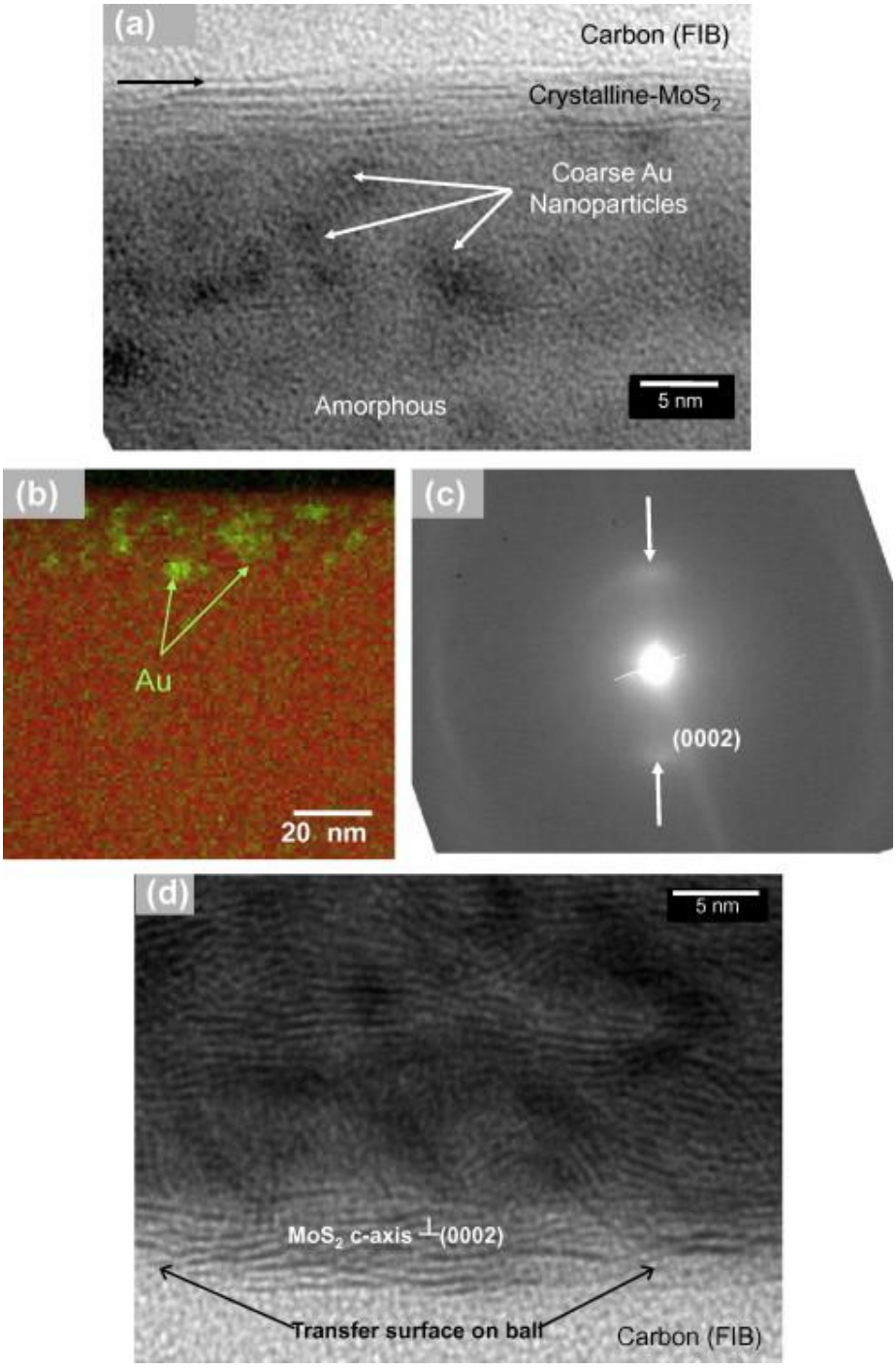

Figure 2.6. Cross sectional TEM image of the worn surface and transferfilm for tests run in dry nitrogen[21].

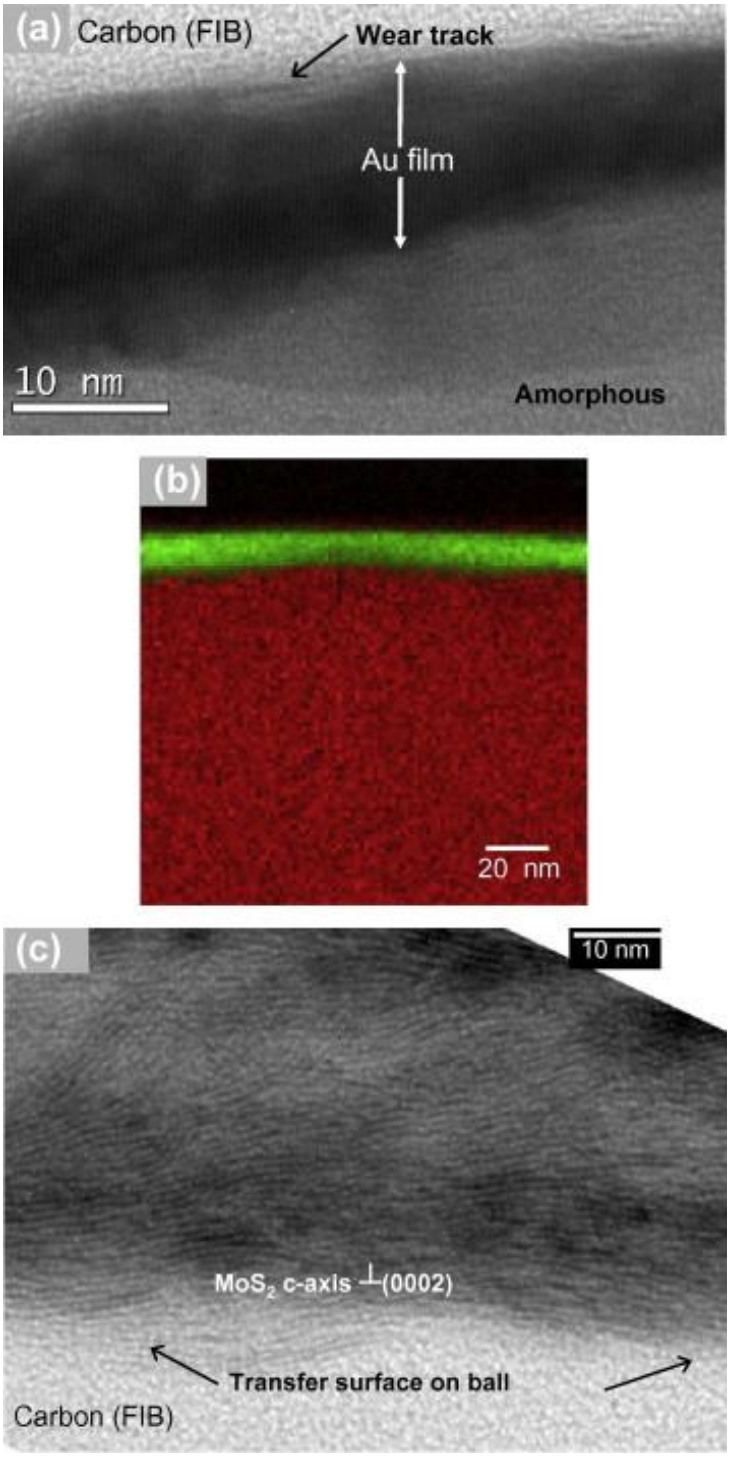

Figure 2.7. Cross sectional TEM image of the worn surface and transferfilm for tests run in air (i.e. 50% relative humidity).

2.3.3 Friction Behavior of MoS_2

In general, the friction behavior of molybdenum disulphide consists of four main stages, as seen in Figure 2.8: (1) Running in, (2) stable running, (3) coating break-down and (4) failure[11]. The run-in phase of the coefficient of friction can be explained by the reorientation of the crystallites and the formation of the transfer film. The lowest coefficient of friction, which is during the stable running stage, is obtained when the basal planes have a parallel orientation to the sliding direction and a stable transferfilm is developed on the counterface.[11] Eventually, the coating begins to break through, possibly due to oxidation of the coating and blister formation in between the coating and the substrate, followed by the final phase in the coefficient of friction, which consists of coating failure. During this stage, there is not enough lubricant left and the counterface is in contact with the substrate, resulting in a steep rise in the coefficient of friction.

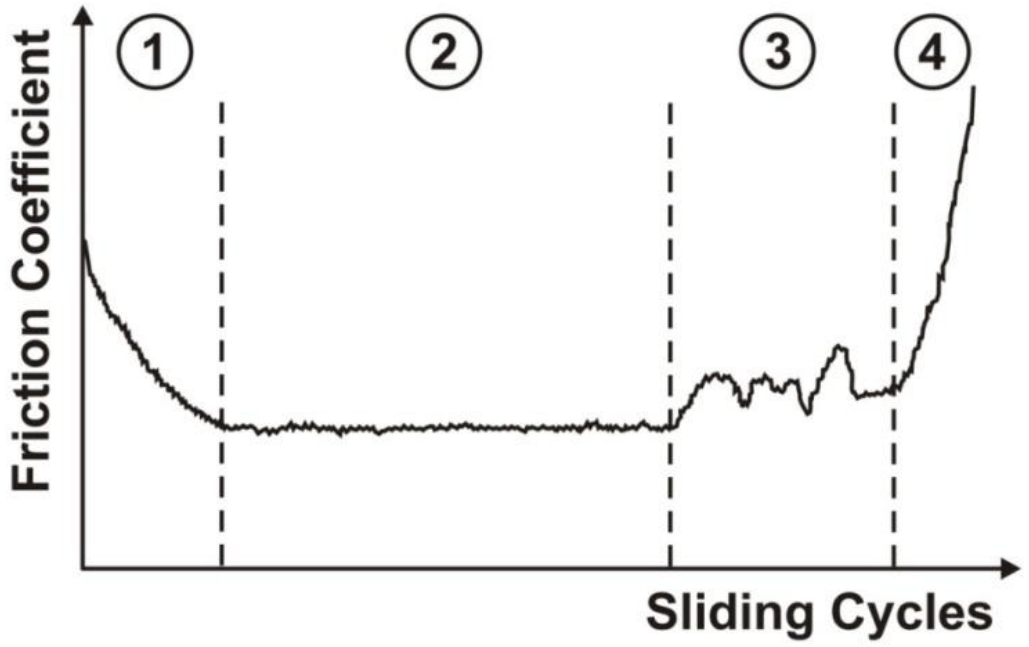

Figure 2.8. Typical stages in the friction performance of $MoS_{2[11]}$

Raman microscopy is a useful analysis technique to investigate the different sliding stages of molybdenum disulphide. Windom et al.[22] showed how Raman microscopy can be used to identify crystallinity and orientation of MoS_2 films. The authors performed Raman studies on microcrystalline MoS_2 powder and on natural MoS_2 crystal and discovered clear differences between the two samples; the bands in the natural crystalline MoS_2 spectra were much sharper and ratio between the 466 and 408cm^{-1} bands were significantly different between the two samples. In addition, a band at 422cm^{-1} for the natural MoS_2 crystal is not observed on the MoS_2 powder. A similar study[17], on Pb-Mo-S coatings, has also been performed using Raman spectroscopy side-by-side with high resolution transmission electron microscopy (HRTEM). The authors showed that when the film was observed to be crystalline with HRTEM, narrow bands consistent with MoS_2 were also observed in Raman spectroscopy. On the other hand, when the film was amorphous (e.g. unworn surface), no MoS_2 bands were observed with Raman spectroscopy. It is well accepted in the tribology community that Raman spectroscopy is a useful tool for studying the crystallinity and orientation of MoS_2-based surfaces and wear tracks[10,17,20,23-25]. Therefore, if the MoS_2 film is initially amorphous or nano-/ micro-crystalline, the transition between the run-in stage and the steady state stage will be observed with micro-Raman due to the increased degree of crystallinity in the steady state stage. Additionally, Windom et al.[22] described how Raman microscopy can also be used to observe the transformation from MoS_2 to MoO_3, and therefore identifying the transition between stage 3 and stage 4 of the sliding behavior (i.e. coating break-down and failure).

2.3.4 Wear life of MoS_2 under different sliding conditions

The wear life of molybdenum disulphide can typically be related to the coefficient of friction. The lowest wear rate is usually seen during the stable running stage of the coefficient of friction. Variables, such as humidity and coating thickness, can also influence the wear life. It has been shown that with low contact stresses, the wear life of molybdenum disulfide increases linearly with the coating thickness.[13] Furthermore, the presence of oxygen and water vapor decreases the wear life of the coating. This can be explained by the fact that with higher relative humidity levels, the coating oxidizes more rapidly and forms blisters which can lead to flaking of the coating. It has been proposed that the wear life of MoS_2 can be improved by simply improving the transfer film formation.[13]

2.3.5 Co-deposited molybdenum disulphide

The introduction of other elements within molybdenum disulphide coatings has been intensively investigated in order to improve the mechanical and tribological properties in different environmental conditions. Although different deposition techniques, such as burnishing and spray bonding, are well known and have been shown to be successful, this literature review concentrates on the co-sputtering process. There are many co-sputtering techniques that are currently being used, however, a good example is shown in Figure 2.9, which is the co-sputtering process used for MoS_2/Ti coatings and was developed and patented by Teer Coatings (www.teercoatings.co.uk). The chamber is kept at low pressures and typically Argon is used for the sputtering gas. The co-sputtering process is performed from two different targets sputtering at

the same time. In some special cases, the co-sputtered coating is produced by one composite target.[26]

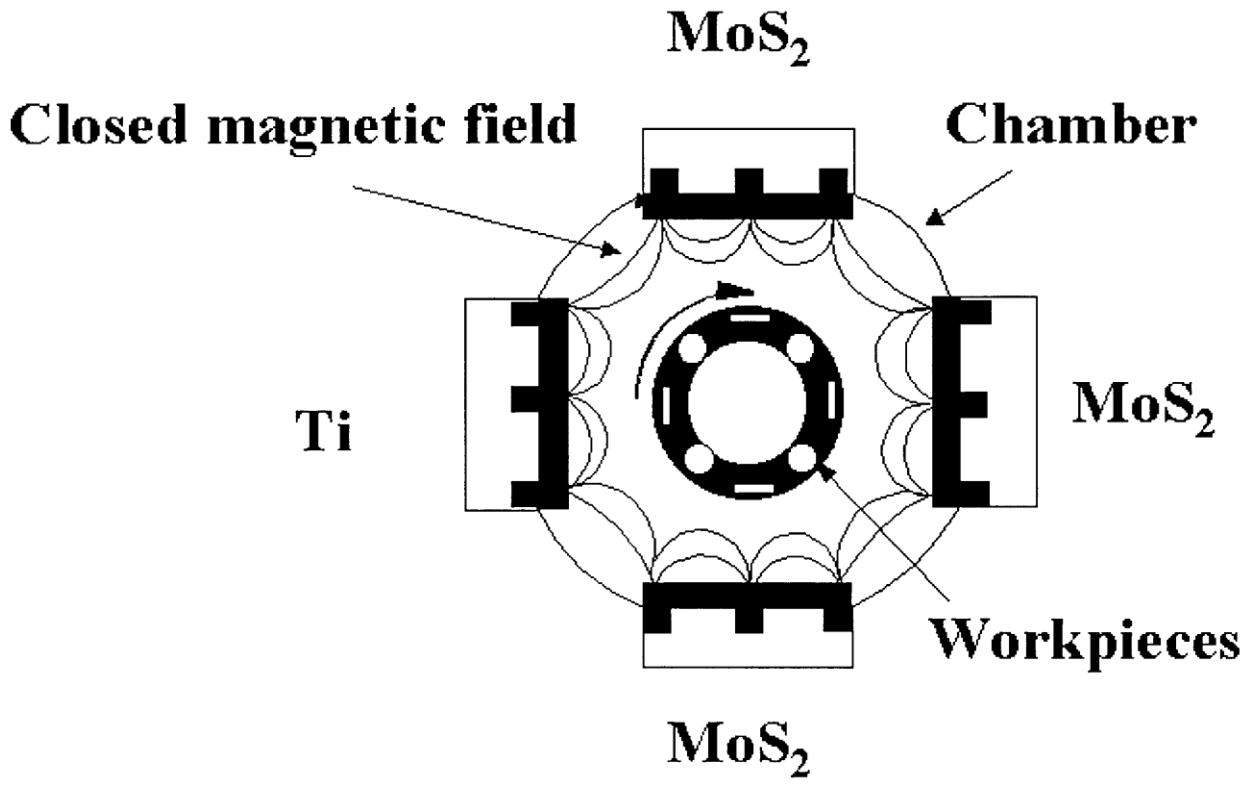

Figure 2.9. Schematic representation of the co-sputtering procedure developed and patented by Teer Coatings used for Ti and MoS_2[27]

2.3.6 Co-sputtered Au with MoS_2

The co-sputtering of gold with molybdenum disulfide has been studied most intensively in the last few years.[11,28] It is generally agreed that the addition of Au increases the density and the hardness of the coating.[28] Zabinski found that even a small amount of Au (2.5 at.%) causes coating densification and also an increase in the crystallite size, which seems to be in contradictory with Lince,[28] who stated that the larger amount of Au causes a reduction in the

MoS_2 crystallite size. Savan[11] suggested that the addition of gold promotes the preferential growth of the MoS_2 crystallites in the direction parallel to the surface, which results in a lower coefficient of friction.

Lince[28] studied the influence of contact stresses on co-sputtered MoS_2 coatings, with varying Au content. His coatings were deposited at the Space Materials Laboratory of The Aerospace Corporation (El Segundo, CA, USA) using a custom sputter deposition system.[28] These coatings were deposited on Si (100) wafers using a load locked deposition chamber and a base pressure of 1.33×10^{-7} Pa (1×10^{-9} Torr). The authors used Argon (99.999% nominal purity) as the sputtering gas, and kept the Ar pressure in the chamber during deposition at 4 Pa (3×10^{-3} Torr). The Au and MoS_2 sputtering power densities were 0.25 and 3.0 W/cm^2, respectively.

The tribological tests were performed using a pin-on-disk tribometer at a relative humidity below 1% with contact stresses ranging from 0.1MPa to 730MPa while varying the gold content between 42 and 100 at.%, Figure 2.10. At the low contact stresses, all of the coatings with the different Au content showed a lower coefficient of friction and higher endurance when compared to pure MoS_2, however, the best performance was seen with 75 at.% and 89 at.% Au. At the high contact stress, on the other hand, the coatings with the high gold content samples failed before the pure MoS_2 samples and the best performance (lowest coefficient of friction and highest endurance) was seen with 42 at.% and 59 at.%Au.[28]

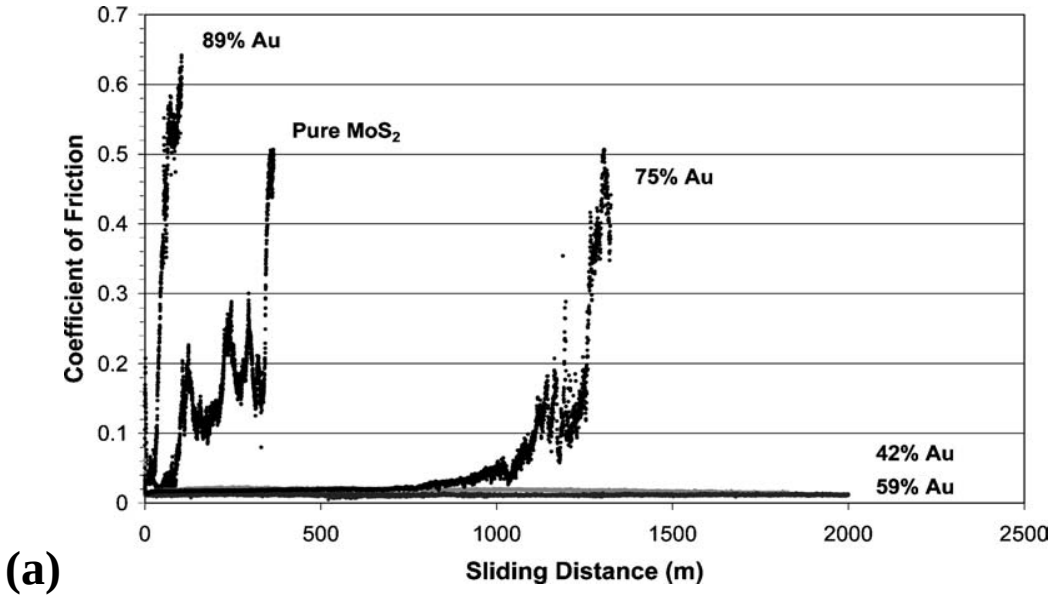

(a)

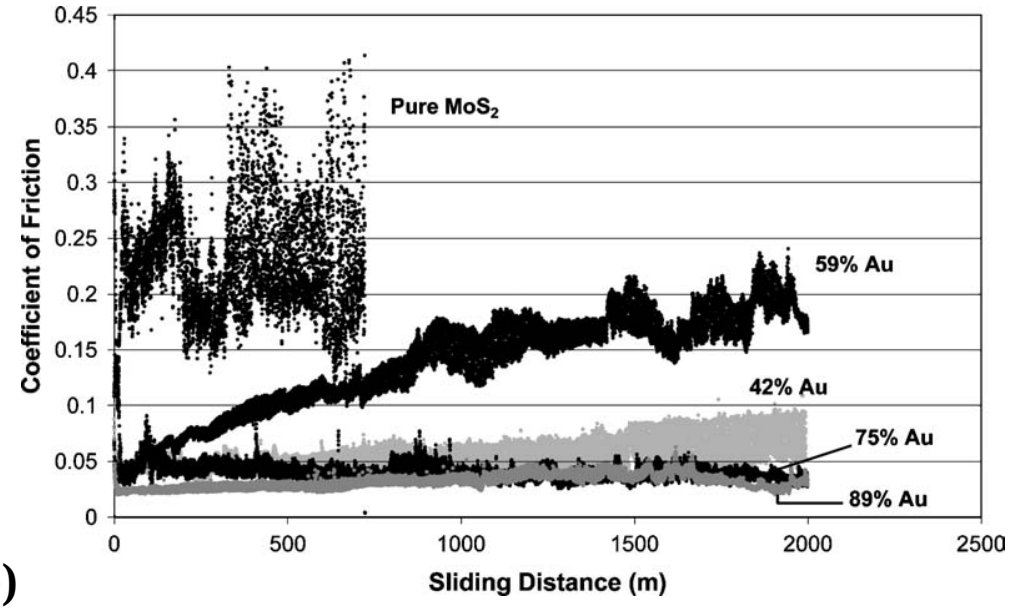

(b)

Figure 2.10. Coefficient of friction obtained at a contact stress of (a)730MPa and (b)0.1MPa for cosputtered MoS_2 coatings with 42, 59, 75, and 89 at.% Au[28]

Zabinski[29] investigated the effect of co-sputtering 2.5 at.% Au with molybdenum disulphide on the tribological properties. The tests were performed using a ball-on-flat tribometer under low and high relative humidity levels. The author found that the Au addition lowered the coefficient of friction for both environmental conditions when compared to pure MoS_2. Similar results were also seen by Spalvins[30] with a gold content of 5 at.%. The MoS_2/5%Au coating revealed a lower coefficient of friction and "a higher degree of frictional stability", Figure 2.11.[30]

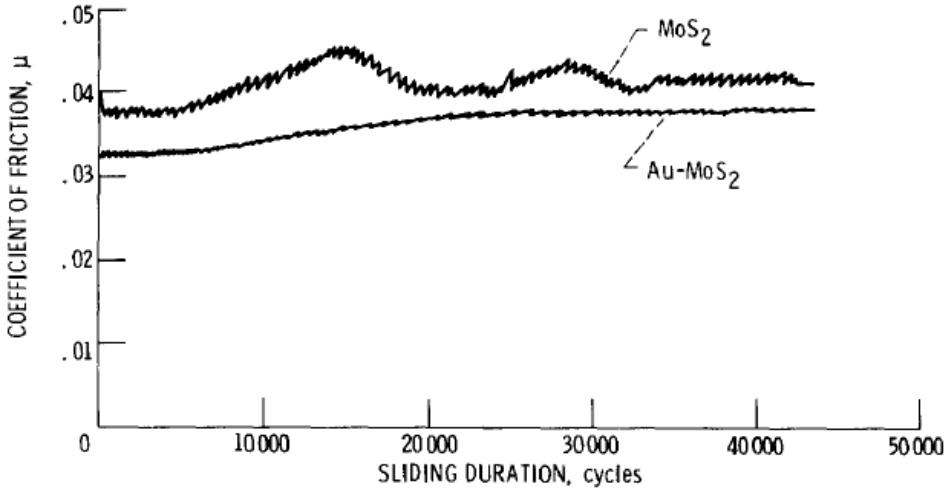

Figure 2.11. Coefficient of friction for MoS_2/Au compared to MoS_2 [30]

Further investigations of co-sputtering Au with MoS_2 was also performed by Roberts and Price.[31] Using a pin-on-disk tribometer under ambient environmental conditions, the authors showed that the optimum amount of Au is between 12 at.% and 15 at.%. The endurance life of the coating containing the optimum amount of Au was up to 4 times better than that from pure MoS_2. A similar result was also shown by Simmonds,[32] who found that the highest endurance

was for the co-sputtered coatings containing 15 at.% Au, which also correspond to the lowest coefficient of friction.[32]

2.3.7 Co-sputtered Ti with MoS_2

The co-sputtering of Titanium with molybdenum disulphide results in similar effects on the tribological properties as the Au dopant. The addition of titanium increases the hardness and the wear resistance of the coating and makes it less sensitive to humid environments during tribological testing, as shown by Renevier.[27] While varying the Ti content between 3 at.% and 11 at%, Simmonds[32] illustrated that there was a significant increase in the endurance life with the lower Ti content, Figure 2.12. The highest endurance life was seen between 5 and 6 at.% of Ti, however the higher coating lifetime did not correlate with a low coefficient of friction.[32] The author did not have an explanation for this phenomenon. However, it was suggested that it might be due to the different formation of the transfer film. The lower coefficient of friction resulted from a higher rate of the film formation and thus an easier breakthrough of the coating.[32]

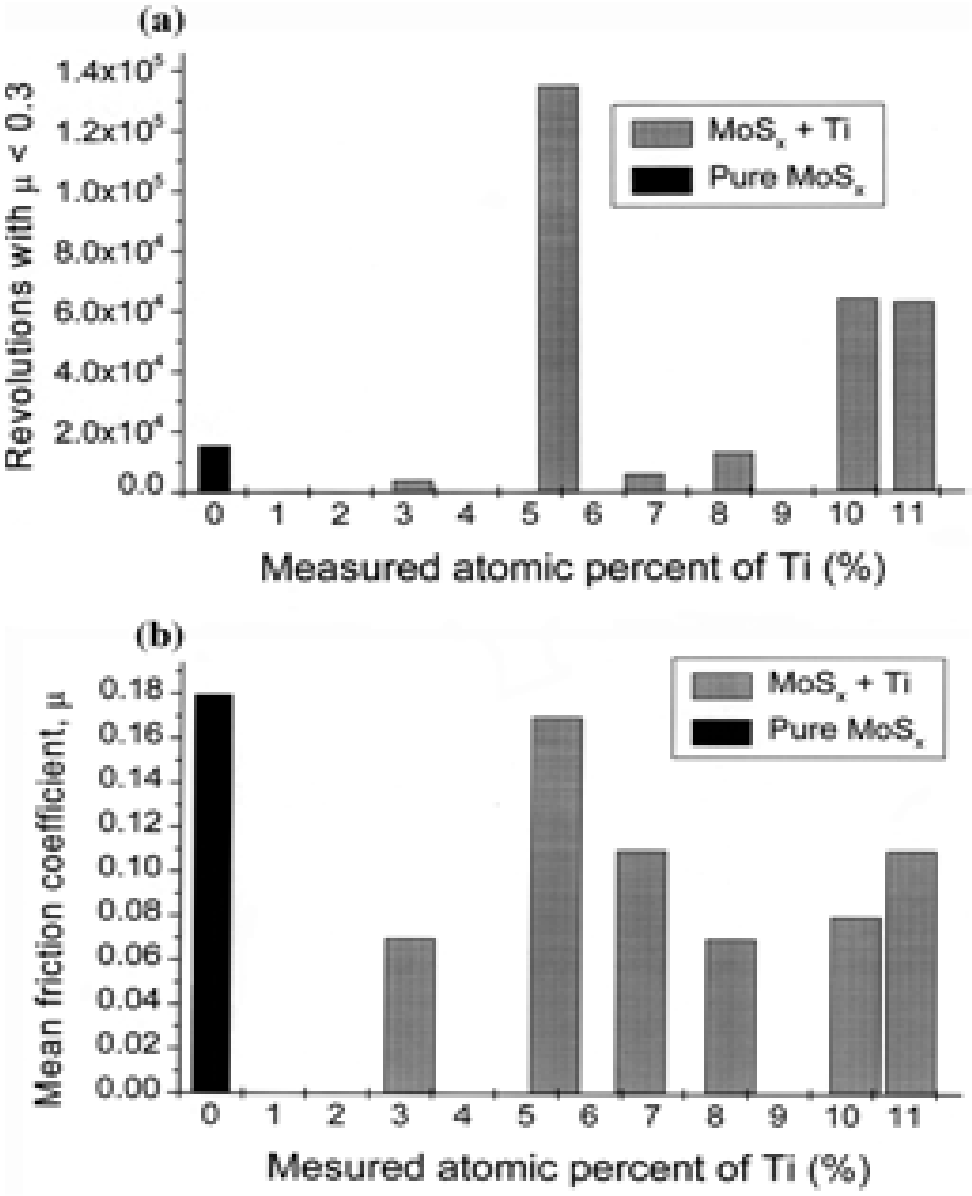

Figure 2.12. Tribological results for (a) endurance life, (b) mean coefficient of friction[32]

A more detail study on co-sputtered Ti with MoS_2 has been performed with MoST^{TM} coatings [Teer Coatings Ltd. (Worcestershire, UK)][27,33-38]. X. Ding et al.[39] investigated the

mechanical and tribological properties of Ti-MoS_2 coatings while varying the Ti content between 0 and 30 at%. The authors found that the hardness increased with increasing the metal content and the maximum hardness was observed with 20.2at% Ti (i.e. 8.4GPa), as shown in Figure 2.13. The increase in hardness of MoS_2 with the addition of Ti was explained by solution hardening effect and/ or densification of the coating. Renevier et al.[35] suggested that the titanium replaces the molybdenum in the MoS_2 matrix, and/or forms an interstitial solid solution in the 'a' and 'c' direction of MoS_2, as shown in Figure 2.14. However, with titanium content of more than 20.2 at%, X. Ding et al.[39] observed that the hardness values show a slight decrease. The authors suggested that this is possibly due to the formation of discrete metallic particles.

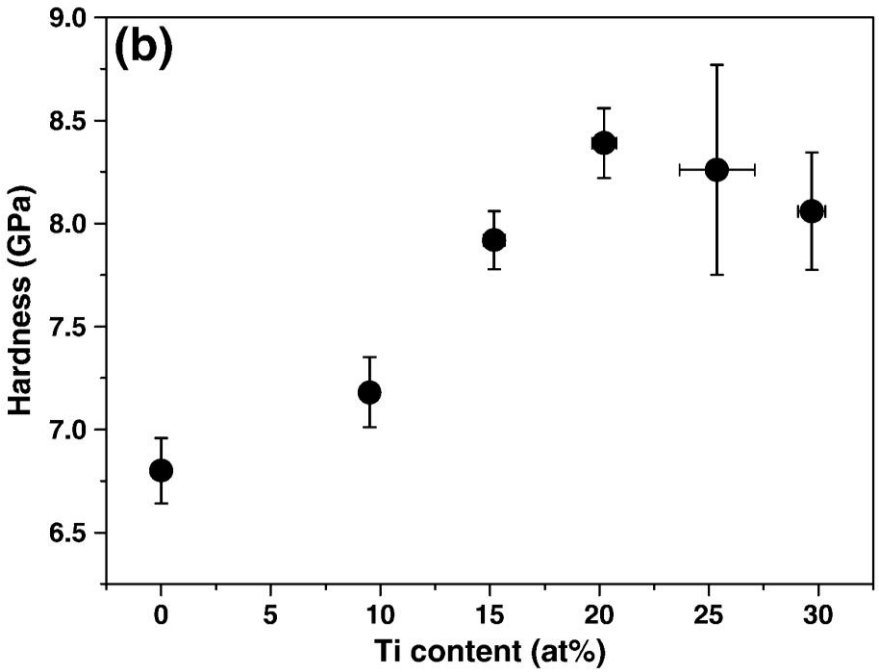

Figure 2.13. Hardness vs. Ti content for Ti-MoS_2 coatings[39].

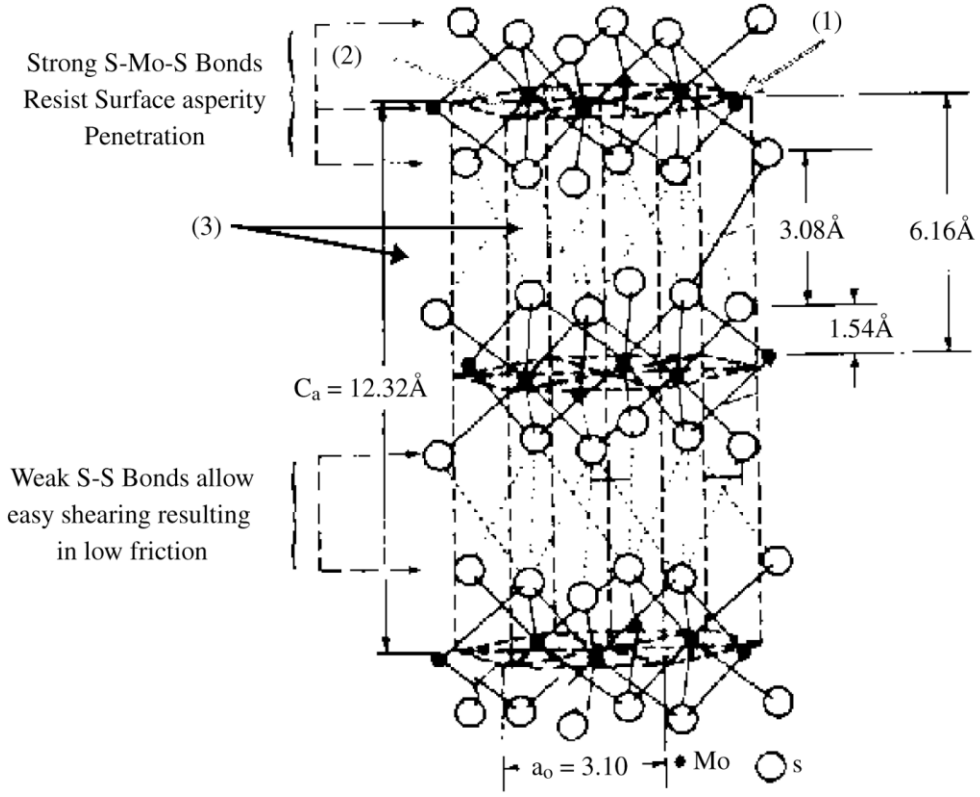

Figure 2.14. Hypothetical titanium addition to MoS_2 matrix[35]: (1) Replacing the molybdenum in the MoS_2 matrix, (2) interstitial solid solution of titanium in the a direction, and (3) interstitial solid solution of titanium in the c direction.

X. Ding et al.[39] also investigated the effect of different titanium content on the tribological properties, while varying the humidity levels between 0 and 100%. Figure 2.15 shows the friction coefficient results vs. relative humidity for Ti-MoS_2 with Ti content varying from 0 to 30 at%. The pure MoS_2 coating shows a very low coefficient of friction under dry atmosphere, as expected. However, the friction coefficient increases with increasing the relative humidity. The coating with Ti content of 9.5 at% was least affected by relative humidity; the friction coefficient remained low and nearly constant with all humidity levels. Ti-MoS_2 coatings with higher Ti

content (i.e. ≥20.2at%) revealed significantly higher friction values for all humidity levels, which also correlated with high wear rate values. The authors suggested that this is possibly due to tribo-oxidation of the Ti component, but also mentioned that these coatings would be investigated in more detail in future work. The wear rate vs. relative humidity for the low Ti content samples (i.e. ≤15.2 at%) is shown in Figure 2.16. The wear rate for the tests performed under dry air was similar for all three coatings. However, the pure MoS_2 coating was very sensitive to humidity and the wear rate increased significantly with increasing relative humidity. The Ti-MoS_2 coatings, on the other hand, showed low wear rates up to 75% relative humidity, as seen with the friction behavior. The lowest wear rate at 100% relative humidity was observed with the 9.5at% Ti content sample. The increased wear resistance with the Ti content samples for humid environments was explained by their ability to form a stable transferfilm.

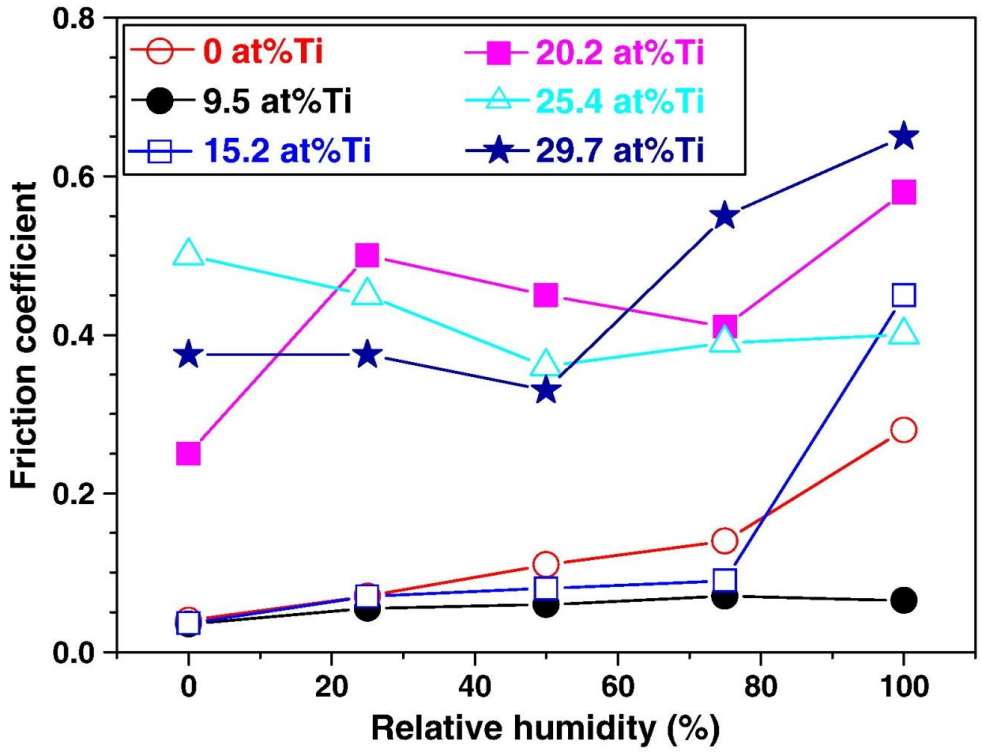

Figure 2.15. Friction coefficient vs. relative humidity for Ti-MoS_2 coatings with varying Ti content between 0 and 30 at%.

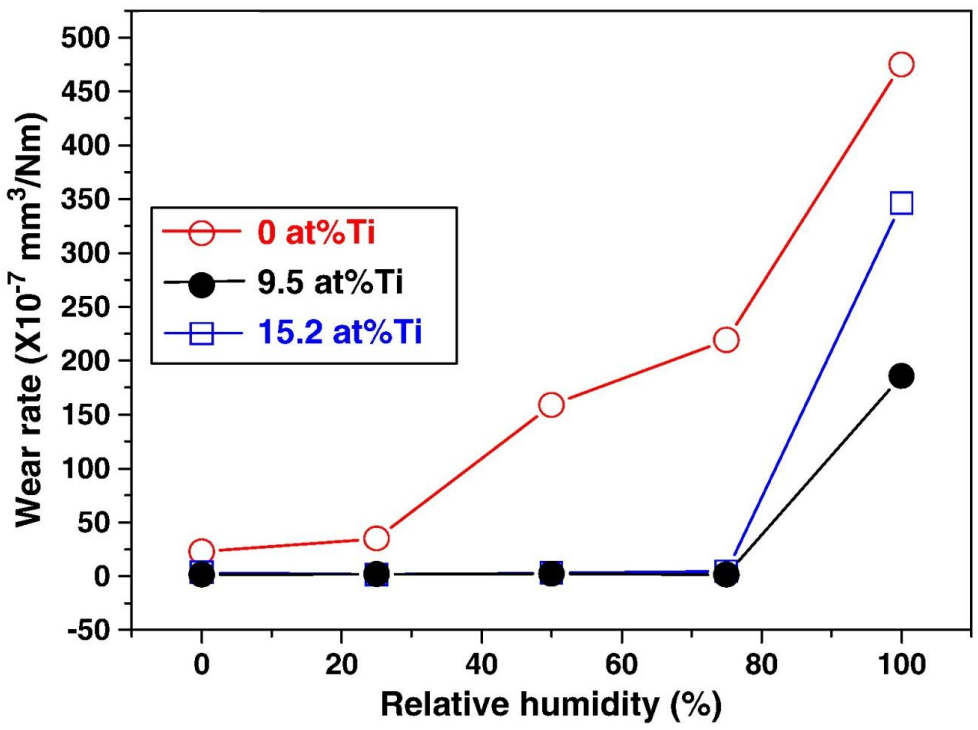

Figure 2.16. Wear rate vs. relative humidity for Ti-MoS_2 coatings with varying Ti content between 0 and 30 at%.

2.3.8 Effect of other Dopants

Zabinski[29] investigated the addition of 1.7%Fe to MoS_2. Planar and cross-sectional micrographs showed that Fe increased the crystallite size very little, but overall did not have a significant effect on the morphology, which is most likely due to the small amount of the dopant. Other metal additives on the other hand, such as chromium and cobalt, increase the size of the crystallites to about 35% and hardened the coating.[40] Other elements such as Pb and Sb, on the other hand are mostly used for sacrificial gettering of oxygen, protecting the MoS_2 from oxidizing.[11]

The mixture of co-sputtering two different materials with MoS_2, seems to be very successful. Zabinski found that co-sputtering Sb_2O_3/Au with MoS_2 results in a lower coefficient of friction in humid environments when compared to the addition of only Sb_2O_3 or Au with MoS_2. Similar MoS_2/Sb_2O_3/Au coatings were also investigated by Scharf et al.[21] in dry environment and humid environment (50% RH). The authors observed a significant increase in endurance life in humid environment for the MoS_2/Sb_2O_3/Au coatings when compared to pure MoS_2 (i.e. the Sb_2O_3/Au doped coatings did not fail up to 10,000 cycles whereas the pure MoS_2 failed at 4500 cycles). In terms of the coefficient of friction, Scharf et al. did not observe a significant difference between the MoS_2/Sb_2O_3/Au and pure MoS_2 coatings for tests run under high humidity and in dry air, Figure 2.17. However, the friction coefficient was significantly higher for both coatings at 50% relative humidity when compared to the friction in dry air (i.e. ~0.16 and ~0.006 respectively).

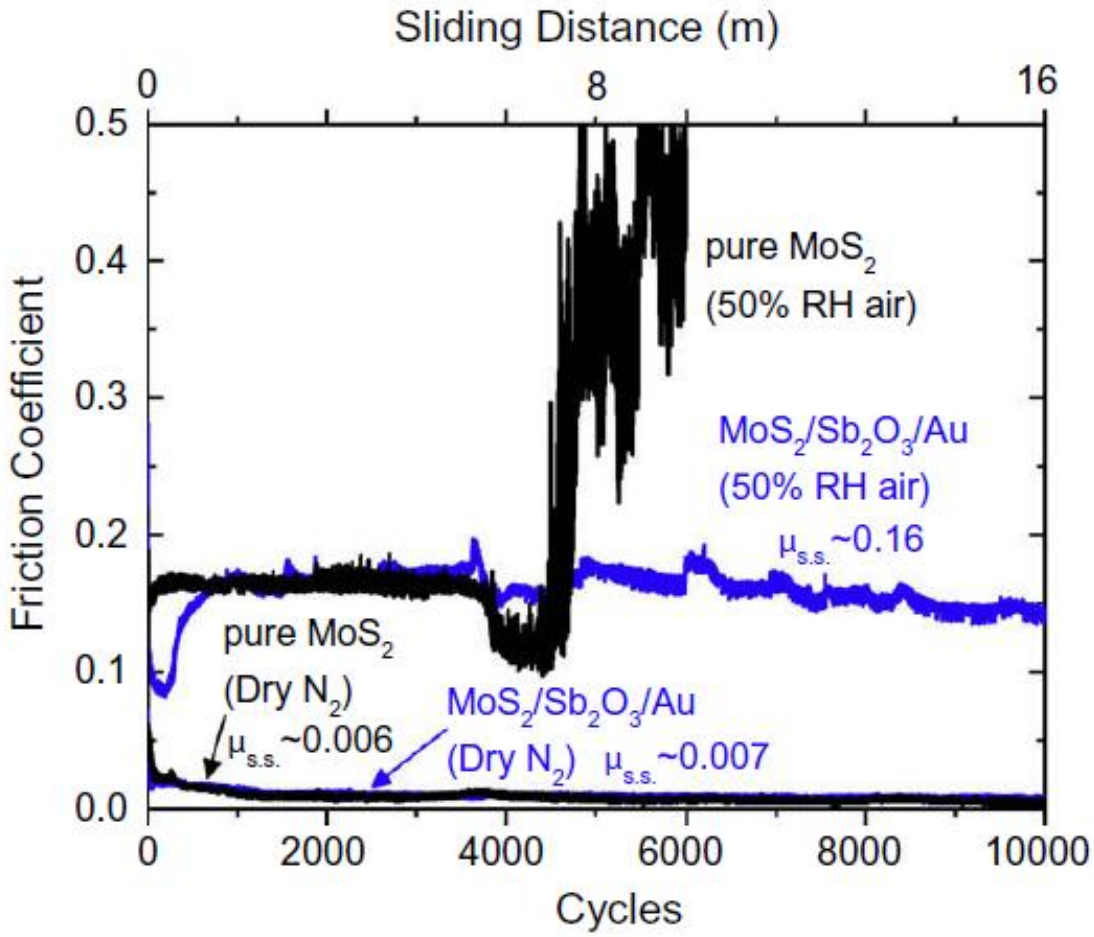

Figure 2.17. Coefficient of friction vs. cycles for $MoS_2/Sb_2O_3/Au$ and pure MoS_2 coatings[21].

2.3.8 Summary of Literature Survey on Macrotribology

In general, the tribological properties of a thin coating have a strong dependence on several parameters such as contact pressure, contact area, relative humidity, coating preparation and coating thickness. However, from this literature review, it can be agreed that the lowest coefficient of friction and the highest endurance life in humid environments for MoS_2 based coatings is seen with metal additives such as Au and Ti. This can be explained by the fact that

these coatings revealed the highest density with fine crystallite sizes.[29] The high density reduces the oxidation rate and the penetration of water vapor into the coating, whereas the finer grain structure of the MoS_2 reduces coating abrasion.[29] In addition, the finer crystallite size of the MoS_2 has a significant effect on the structure of the transfer film, as suggested by Lince.[28] The fine grain structure leads to a thin and more stable transfer film which reduces the coefficient of friction and increases the wear resistance.[28] The increase in the density of the coating with the metal dopant increases also the mechanical properties (e.g. hardness and reduced modulus), which leads to higher wear resistance following Archard's wear equation.

Most of the articles that were reviewed in this section investigate the effect of co-sputtering small amounts of dopants with molybdenum disulphide. Therefore, it still remains unclear how the higher dopant concentration will affect the tribological properties of the coating. As shown by Lince[28] with higher Au content, the higher amount of the dopant can certainly influence the mechanical properties of the coating and most importantly the formation of the transfer film.

Additionally, all of the research mentioned above has been performed at the macroscopic length scale. However, the tribological behavior (i.e. friction and wear resistance) of these coatings might be completely different when decreasing the contact size to the micro- and nanometer length scales. Therefore, there is an increasing desire to study the tribological properties of such solid lubricants at the micro- and nanometer length scale.

2.4 Literature Survey on Microtribology

2.4.1 Significance of Microtribology

Over the last few decades, the advance in new technology to measure friction, wear, adhesion, and surface topography at the micro- and nano- scale, has led to the establishment of fields such as microtribology and nanotribology[41-44]. These fields concentrate on the study of two interfaces in a sliding motion at the micro, molecular, and atomic level. Studies at these length scales are crucial in order to have a better understanding of a material's behavior during single and multi-asperity contacts and to possibly improve the tribological properties of micro- and nanostructures used in micro-electromechanical systems (i.e. MEMS and NEMS). However, there are several issues that may arise when decreasing the length scale down to the micro- and nano- level.

Figure 2.18 illustrates the difference between macrotribology (conventional), microtribology, and nanotribology in terms of the contact size (i.e. pin diameter) and the normal load. Even though similar pressures to the ones in macro-components may also be observed with micro devices, the contact area and normal load decreases up to six orders of magnitude. Such a decrease in normal load and contact size will decrease the real contact from millions of asperities to only a few asperities. Consequently, roughness and actual contact shape will play a larger role[45,46] in their behavior, which can have a significant effect on forces such as friction, adhesion, and surface tension. Due to these differences in the sliding mechanisms at the smaller length scales, the general macroscopic laws of friction are not always applicable for micro-/

nanoscale contacts, as summarized by Mo et al.[47] in table 2.2. Therefore, obtaining a fundamental understanding of the scaling effect is crucial for future innovations of micro- and nano- components.

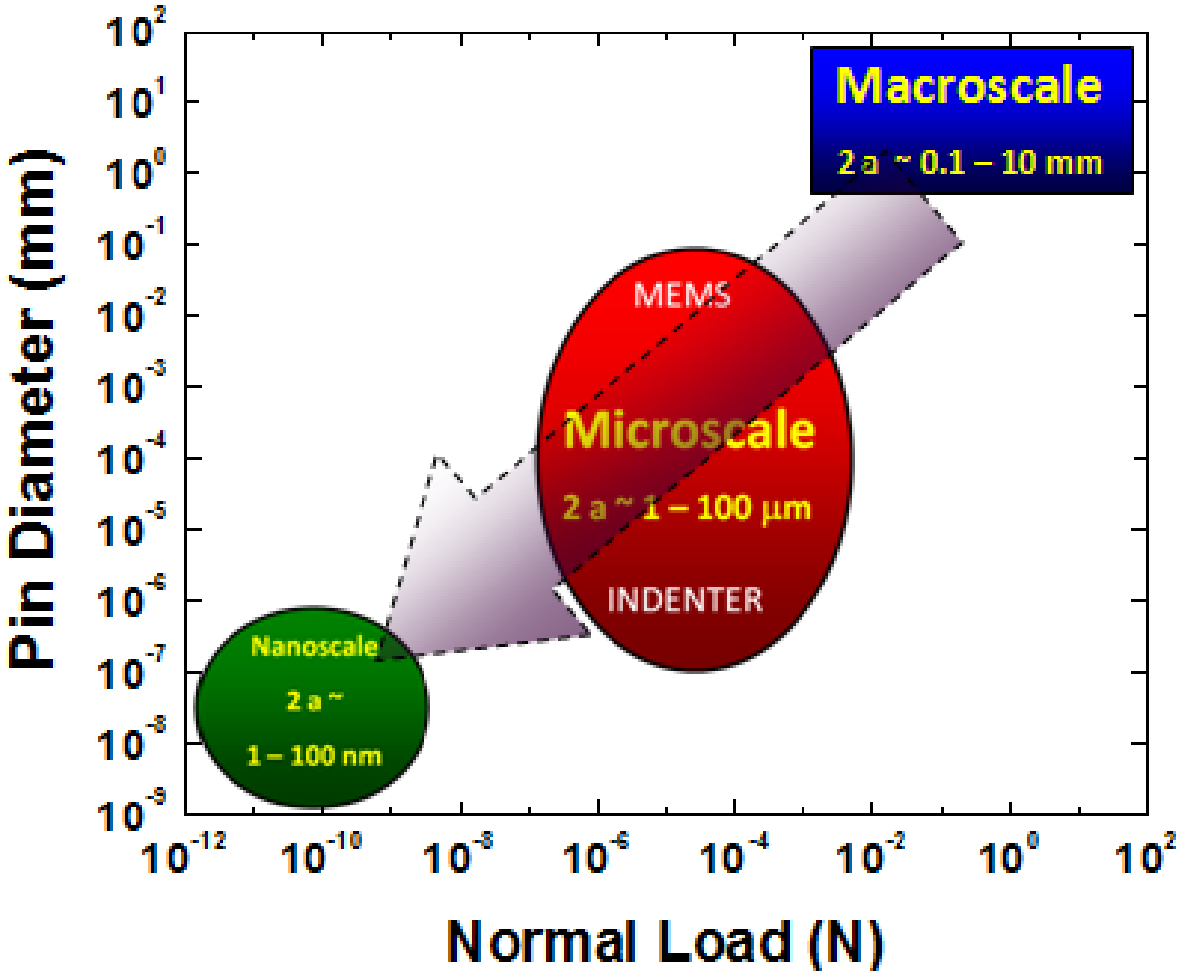

Figure 2.18. Difference between macrotribology (conventional), microtribology, and nanotribology in terms of the contact size (i.e. pin diameter) and the normal load. In this figure, 2*a represents the Hertzian contact diameter[48].

Table 2.2. Summary of friction laws[47]

Friction laws	F_f vs. area	F_f vs. L	Notes
Macroscale theories			
Amontons' law	Independent of A_{macro}	$F_f = \bar{\mu} \cdot L$	Law first discovered by Leonardo da Vinci
Bowden and Tabor	$F_f = \bar{\tau} \cdot \sum A_{asp}$	$F_f = \bar{\mu} \cdot L$	Law results from contact roughness
Single-asperity theories			
Non-adhesive (based on Hertz model)	$F_f = \tau \cdot A_{asp}$	$F_f \propto L^{2/3}$	Linear dependence of F_f on A_{asp} is generally believed to be true for microscale contacts, but has been questioned for nanoscale contacts
Adhesive (for example, Maugis–Dugdale)	$F_f = \tau \cdot A_{asp}$	Sublinear	

A_{macro} is the macroscopic contact area. A_{asp} is the contact area of a single asperity; A_{real} is the real contact area defined as the number of atoms N_{at} in contact multiplied by the average contact area A_{at} of an interfacial atom.

2.4.2 Applications of Microtribology

The interest in studying micro- and nano- tribology became significantly higher over the last few decades due to the advances in the production of microelectromechanical systems (MEMS). Such micro-devices are possible to be produced using silicon photolithographic process and a number of other micromachining methods that have recently been developed such as microcutting, microdrilling, micromilling, laser machining, etc.[1] An example of a MEMS fabrication process is shown in Figure 2.19 for a AlCuMgMn micro-tensile specimen[49]. The fabrication process of this specimen is described in more details elsewhere[49]. Briefly, the AlCuMgMn film is sputtered on top of the silicon wafer and then the Al alloy film and the silicon are etched away following the pattern of the tensile specimen cell. The only position where the metal is not etched away is in the center of the cell, which is the free test beam of the

Al alloy. Figure 2.20 shows a schematic representation of a micro-tensile cell and a processed waver.

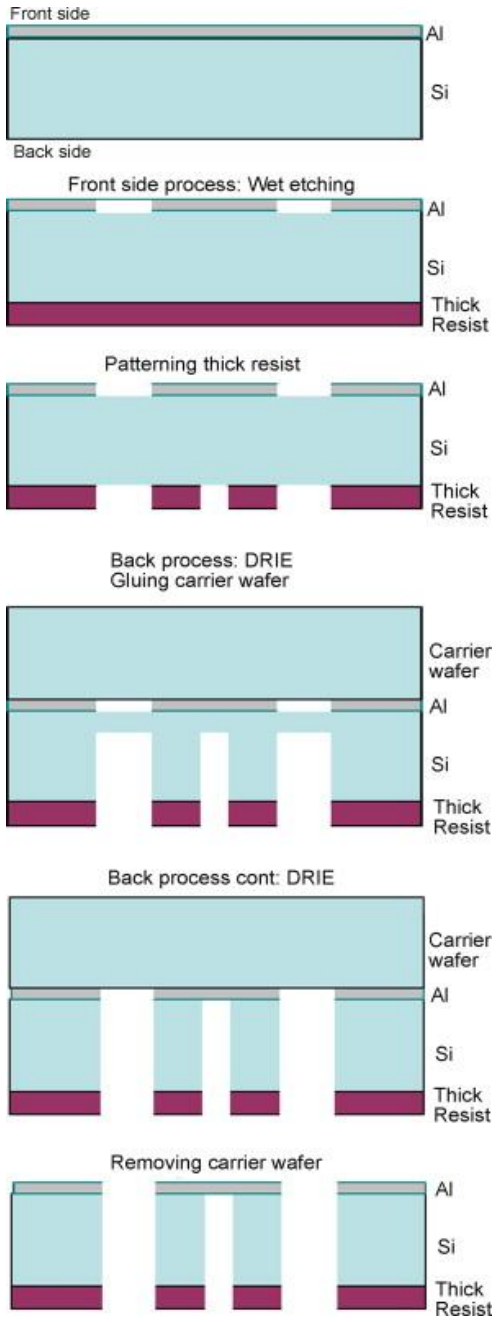

Figure 2.19. Typical fabrication process of a micro-tensile specimen[49]

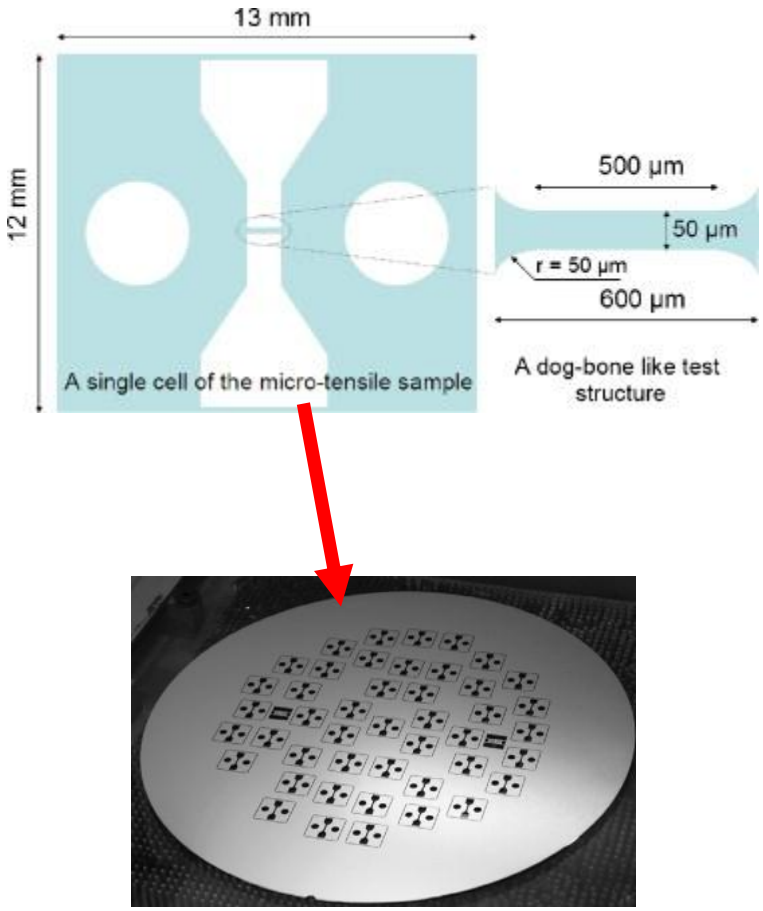

Figure 2.20. Micro-tensile cell and a processed wafer containing AlCuMgMn micro-tensile cells[49]

Using similar fabrication methods to the ones mentioned previously, there have been several successful MEMS designs, which are currently being used commercially; pressure sensor and air bag sensor for automotive industry, TI digital mirror display[50], RF MEMS capacitive switch[51] (Figure 2.21), Inkjet nozzles (HP), micro-gears (Figure 2.22), etc. There are also many potential applications for micro devices for applications in automotive, aerospace, and for medical instrumentation[41].

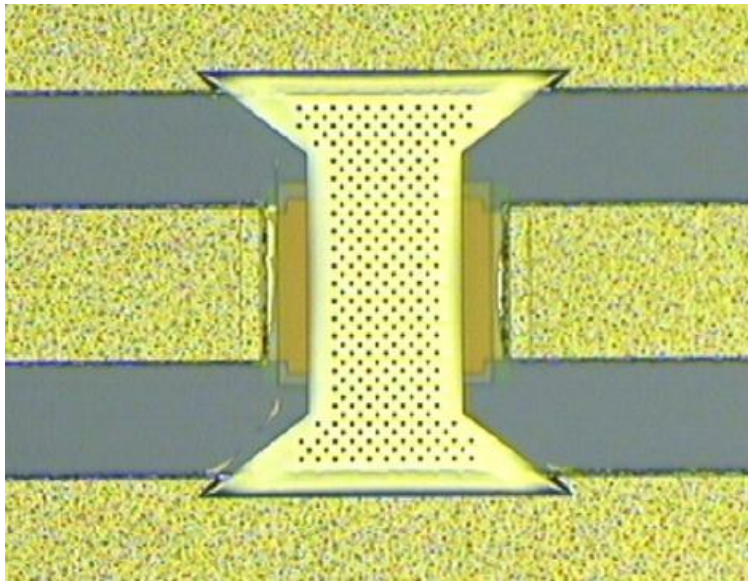

Figure 2.21. Top view of a shunt MEMS capacitive switch[51]

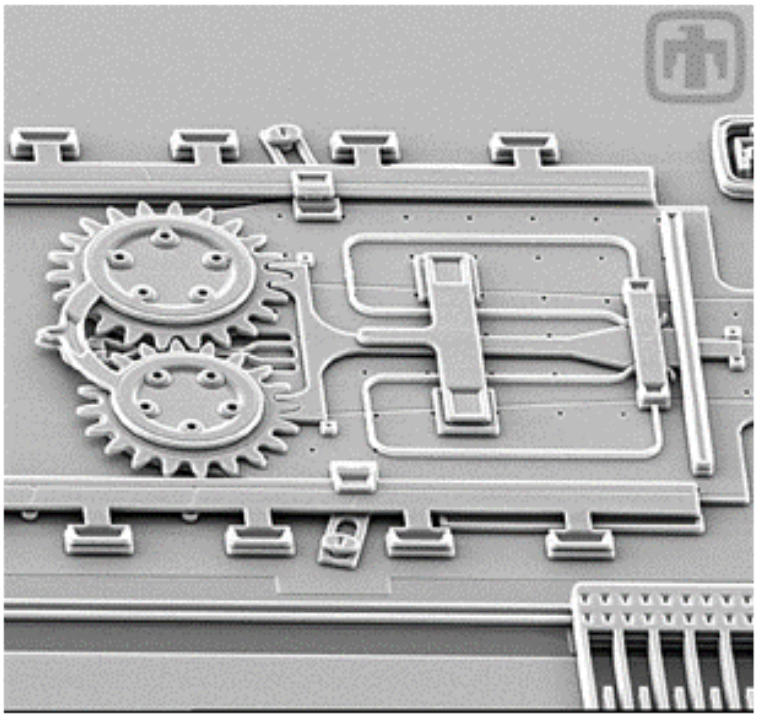

Figure 2.22. Micro gear designed in Sandia National Labs

In micro-devices similar to the ones shown in Figure 2.22, there is some type of a contact or a motion for which the friction and wear properties need to be controlled and minimized[52]. Currently the most common failure mechanisms in MEMS/NEMS are friction, wear, adhesion, fracture, and fatigue[53]. An additional major problem in microsystems is stiction (i.e. large static friction), which occurs due to the large surface area to volume ratio[53]. Therefore, the studying of properties such as adhesion, friction, and wear at the nano-/microscale has become crucial in order to improve the tribological performances of MEMS.

Today the most dominant material used in microdevices is silicon, because of the available machining technology[1]. However, bare silicon exhibits poor tribological properties (i.e. low wear resistance and high friction coefficient) and therefore needs to be coated or surface treated when used in microdevices. Figure 2.23 shows an example of a polysilicon microgear speed reduction unit and its components that after laboratory tribological testing [Sandia National Labs]. The images of the different component (i.e. hub, clip, and pinhole) clearly show that the main failure mechanism was wear. In addition, results from these tests showed that humidity had a significant influence on the wear of these components[53]. One solution to the tribological issue of the microgear speed reduction unit was to use a tungsten (W) coating with a thickness of 20nm. It was possible to deposit this coating on such a device using a chemical vapor deposition (CVD) technique[54]. Furthermore, Scharf et al.[55] showed that solid lubricants such as tungsten disulphide (WS_2) can also be deposited on microsystems using the atomic layer deposition (ALD) technique.

Other researchers[56] have also successfully deposited MoS_2 coatings on MEMS using the successive ionic layer absorption and reaction (SILAR) technique. In their study, the authors compared ALD deposited TiO_2 and ZrO_2 to SILAR deposited MoS_2 and ZrO_2 films on MEMS silicon test device. For low and high humidity levels, the ALD deposited samples showed to be more efficient in terms of reducing the friction coefficient of MEMS compared to the SILAR deposited films. Initially, when the sliding was mainly elastic (i.e. no wear), the MoS_2 film showed a decrease in friction, however, upon wear of the coating, a significant increase in friction was observed. Similarly to macroscopic sliding, the addition of Ti or Au to MoS_2 film has the potential to improve the microtribological properties of MoS_2 coatings making them more efficient in lubricating MEMS. However, the tribological properties (i.e. friction and wear) at the microscopic length scale of these types of coatings (i.e. Ti or Au doped MoS_2) are currently not fully understood.

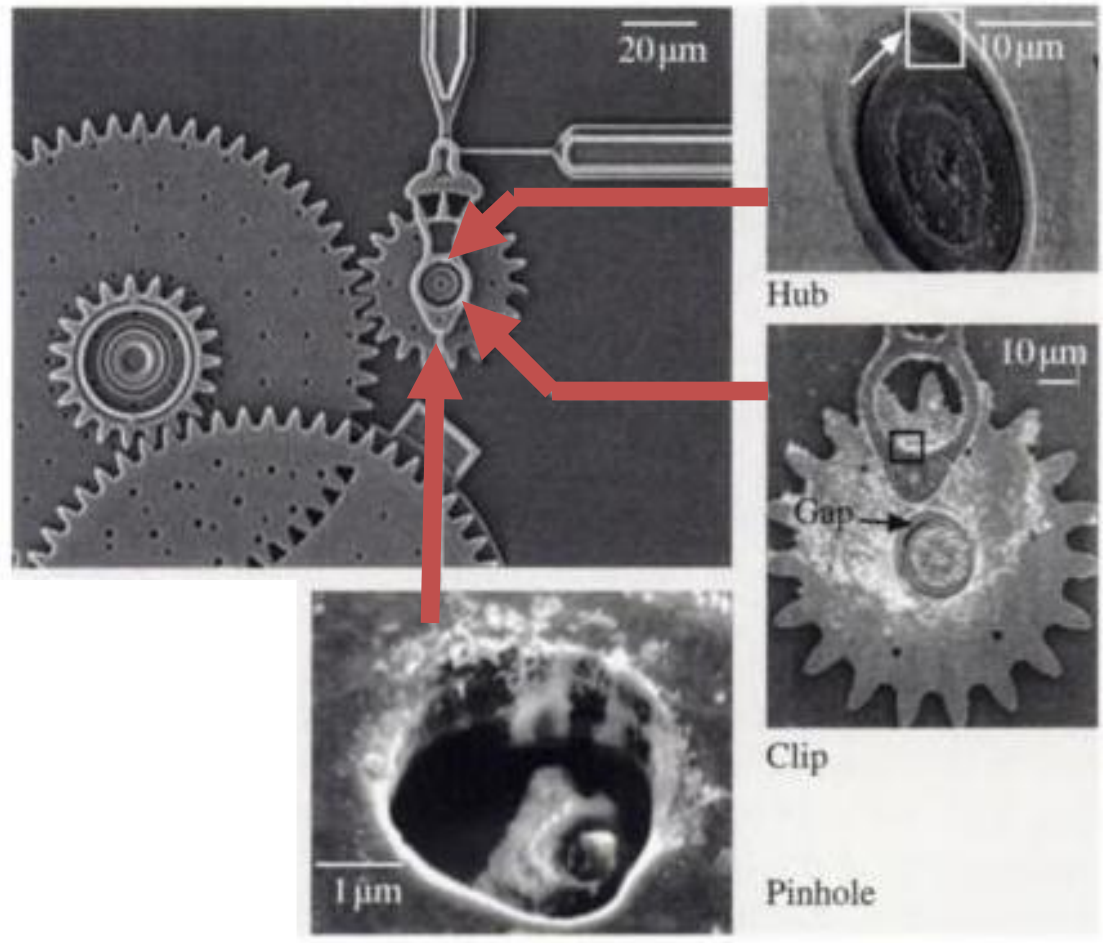

Figure 2.23. Examples of MEMS that fail due to tribological issues[57]

2.4.3 Techniques in Micro-/ Nano- tribology

The sliding mechanisms at the nano-/ micro- scale need to be fully understood in order to improve the tribological performances in micro-devices (i.e. increase endurance life and decrease friction). Therefore, there has been a significant demand for micro- /nanotribological studies to develop a good understanding of the interfacial phenomena in micro- /nanostructures[53].

Currently, the most widely used techniques for studying the mechanical and tribolocial properties at these small length scales are the surface force apparatus (SFA), the scanning tunneling microscopes (STM), the atomic force microscope (AFM), and the friction force microscope (FFM)[53]. This family of microscopes (i.e. that measure forces) are usually referred to as scanning force microscopy (SFM)[41].

Using a conductive atomic force microscopy (c-AFM), Kim et al.[58] studied the lubrication mechanism of cosputtered Au-MoS_2 coatings at the nano-scale. The authors were able to provide a visualization of the tribofilm on the worn surface of the Au-MoS_2 nanocomposite film, as shown in Figure 2.24. The tribofilm consisted of crystalline MoS_2 with the basal planes parallel to the sliding direction, which is consistent with literature on tribological properties of Pb-MoS_2 and PbO-MoS_2 coatings at the macroscopic scale. It was concluded that the tribofilm formation at the nanoscale is responsible for the low friction and high wear resistance of MoS_2 based coatings.

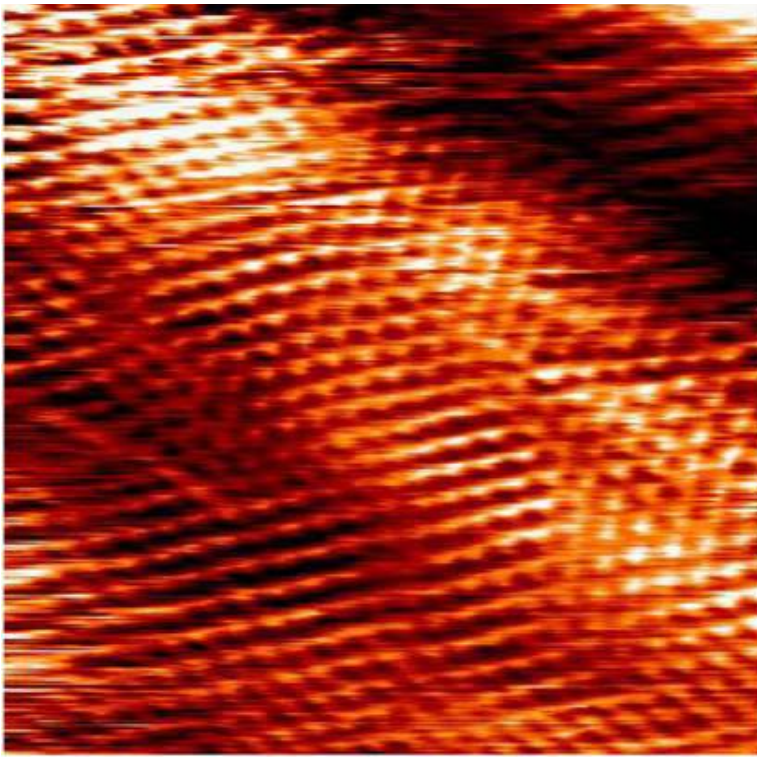

Figure 2.24. Topographic image of the worn surface of Au-MoS_2 coatings showing the hexagonal structure of the tribofilm (7nm x 7nm).

Another widely used technique for measuring tribological properties at the microscopic scale is the CSM microtribometer. Using this instrument, in reciprocating mode, Barriga et al.[59] studied the microtribological properties of sputter deposited gold and copper for potential applications in RF MEMS. The microtribological tests were performed with varying the normal load between 1 and 20mN at 33% and 84% relative humidity. The authors concluded that for Cu-Cu contacts the coefficient of friction at the microscale was affected by relative humidity (i.e. friction increased with increasing the in the relative humidity of 50%), whereas the friction coefficient for Au-Au contacts remained nearly unchanged with varying the humidity level

between 33% and 84%. The increase in the friction coefficient for the Cu-Cu contact was explained due to capillary forces at the higher relative humidity level.

Hysitron nanoindentation instrument is another widely used technique that has the capability of measuring the mechanical and tribological properties of materials at the microscopic length scale. This instrument operates with normal and lateral force loading configurations using a patented three-plate force displacement transducer[60], as shown in Figure 2.25. The force in this system is applied electrostatically, which results in pulling down the center plate towards the bottom plate. The normal force is calculated from the magnitude of the applied voltage. This design of the transducer allows for measurements to be performed using light loads ($\leq 25\mu N$). Depending on the design/ model of the instrument, the maximum normal load that is applied is 30mN. Usually, for mechanical properties measurements a diamond Berkovich tip is used and for microtribological a diamond spherical tip can be used.

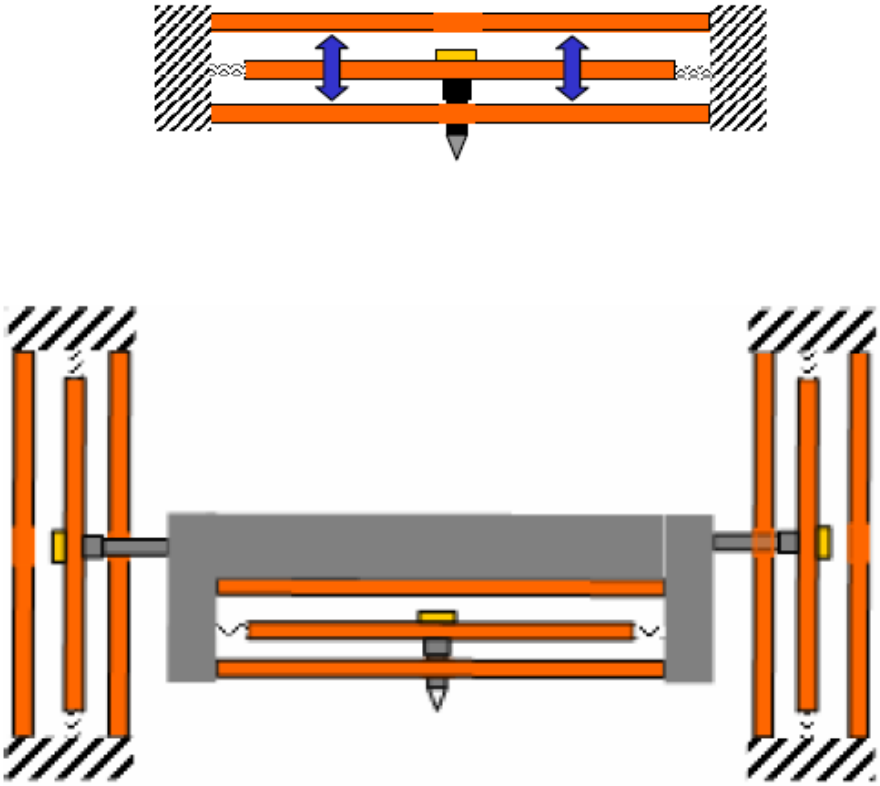

Figure 2.25. Cross-sectional representation of 1D (top) and 2D (bottom) transdusers used for Hysitron nanoindentation instruments[60]. The 1D transducer consists of two 'drive plates' which are parallel to each other and closely spaced with respect to the lateral dimensions. These plates are driven with an AC signal 180 degrees out of phase with one another. A force is then applied to the center plate and the tip simply by applying a large DC offset to the bottom or top plate[60].

Schiffmann and Hieke[61] investigated the micro-tribological properties of diamond-like carbon (DLC) coatings using a Hysitron Triboscope. The authors derived an equation which contains the elastic (Hertzian) component and an additional plowing term:

$$\mu = \mu_e + \mu_p = c_1 L^{(-1/3)} + c_2 L^m \qquad (2.8)$$

where c_1 and c_2 are constants and *m* is the plowing exponent.[61] Schiffmann[61] showed that with the lower load regimes the coefficient of friction was dominated by the elastic component and after a critical load the plowing component increases. This was explained by the fact that with the lower normal loads the tip is mostly sliding on the surface and with the higher normal loads the tip is plowing through the coating. Using the same equation, the authors were also able to show that the coefficient of friction is mainly dominated by the plowing component in the first few cycles of the test, whereas with the higher cycle number, the elastic component increases and eventually dominates, as shown in Figure 2.26.

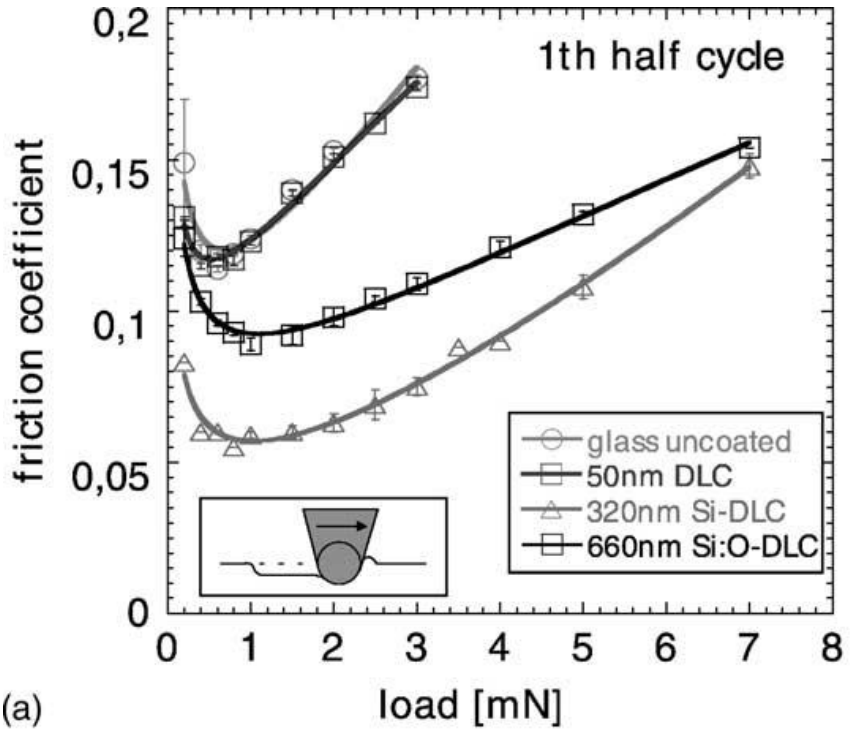

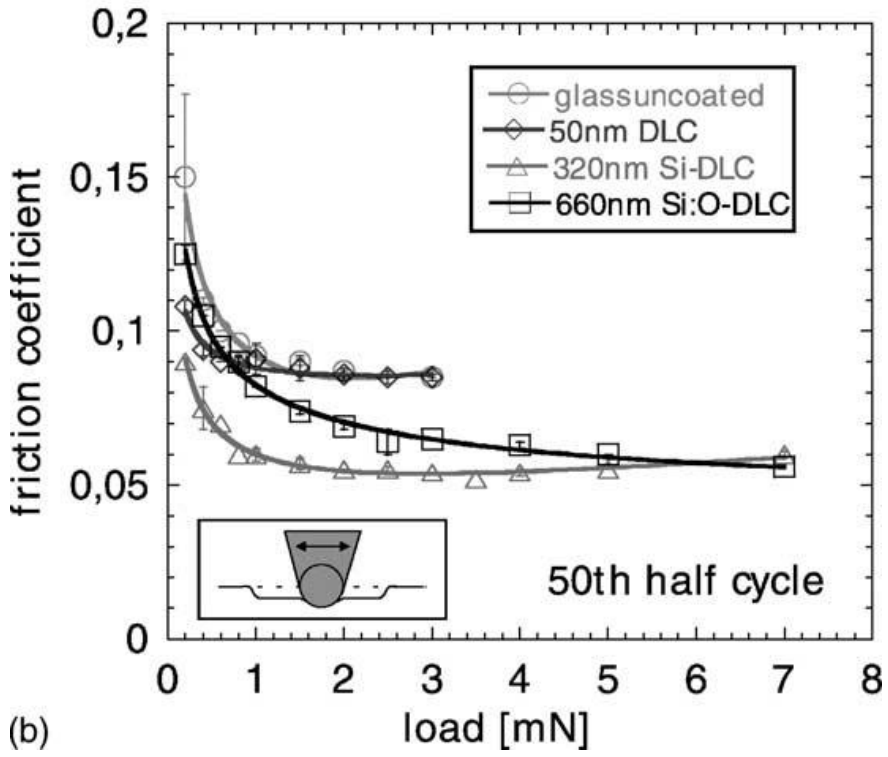

Figure 2.26. Coefficient of friction vs. load for DLC coatings[61] (a) 1st half cycle and (b) 50th half cycle. The data is fitted according to equation (2.8). It is observed that for the higher cycle numbers the friction remains relatively constant for the higher load regimes, Figure 2.26 (b). For the first few cycles on the other hand, the friction increases with the higher load regime, which resulted in higher plowing exponent *m*, Figure 2.26 (a).

2.4.4 Summary of Literature Survey on Microtribology

The most common tribological test used on MoS_2 coatings is a pin-on disk tribometer. Generally, this test provides sufficient results on the tribological properties of the coating at a macro scale, but it is not applicable for very small dimensions. The smaller length scale could certainly influence the friction behavior of these coatings in terms of the transfer film formation, the orientation of the basal planes and the oxidation rate or the wear track. It is possible that due to

the concise contact size for microtribology, the transfer film could be much smaller and thinner compared to the transfer film at macro scale and would most likely form easier, reducing the first stage of the coefficient of friction, [Figure 2.8]. Furthermore, considering the smaller transfer film and wear track, the presence of oxygen and water vapor could have a greater influence on the micro-tribological properties when compared to the macro-tribological properties.

It can be concluded that due to the good tribological properties (i.e. low friction and high endurance life), MoS_2 based coatings can be potential candidates for coatings in Micro-Electromechanical Systems (MEMS) and microswitches (e.g. RF-MEMS). Therefore, there is a need for testing these types of coatings at a micro- or nanoscale, using instruments that can simulate contact pressures to the ones observed in MEMS an experimental procedure similar to the one described by Schiffmann.[61]

REFERENCES

1 K. Holmberg, Coatings tribology : properties, mechanisms, techniques and applications in surface engineering 2ed, Elsevier Science, Amsterdam; Boston; London, 2009.

2 I.L. Singer, Solid Lubrication Processes, in: I.L. Singer and H.M. Pollock, Fundamentals of Friction: Macroscopic and Microscopic Processes, Netherlands, pp. 237-261, 1992.

3 H. Hertz, Über die Berührung fester elastischer Körper Journal für die reine und angewandte Mathematik 92 (1881) 156-171

4 J. Vizintin, M. Kalin, K. Dohda, and S. Jahanmir, Tribology of Mechanical Systems: A guide to present and future technologies, ASME Press, New York, 2004, p.336.

5 M. T. Siniawski, S. J. Harris, and Q. Wang, A universal wear law for abrasion, Wear 262 (2007) 883-888

6 A.Z. Szeri, TRIBOLOGY: Friction, Lubrication, and Wear, Hemisphere Publishing Corporation, New York, 1980, p.548.

7 S. D. Dvorak, K. J. Wahl, and I. L. Singer, In situ analysis of third body contributions to sliding friction of a Pb-Mo-S coating in dry and humid air, Tribology Letters 28 (2007) 263-274

8 F. P. Bowden and D. Tabor, The friciton and lubrication of solids, Clarendon Press, Oxford, 1950.

9 M. Godet, The third-body approach: a mechanical view of wear, Wear 100 (1984) 437-452

[10] S. D. Dvorak, K. J. Wahl, and I. L. Singer, In situ analysis of third body contributions to sliding friction of a Pb-Mo-S coating in dry and humid air, Tribology Letters 28 (2007) 263-274

[11] A. Savan, E. Pflueger, P. Voumard, and A. Schroeder, Modern Solid Lubrication: Recent Developments and Applications of MoS2, Lubrication Science 12 (2000) 185-203

[12] T. Spalvins, Lubrication with Sputtered MoS2 Films: Principles, Operation, and Limitations, Journal of Materials Engineering and Performance 1 (1992) 347-352

[13] A.R. Lansdown, Molybdenum Disulphide Lubrication, Elsevier Science B.V., 1999.

[14] I. L. Singer, S. D. Dvorak, K. J. Wahl, and T. W. Scharf, Role of third bodies in friction and wear of protective coatings, Journal of Vacuum Science & Technology A (Vacuum, Surfaces, and Films) 21 (2003) S232-S240

[15] T. W. Scharf and I. L. Singer, Monitoring transfer films and friction instabilities with in situ Raman tribometry, Tribology Letters 14 (2003) 3-8

[16] G. C. Barton and S.V. pepper, Transfer of molybdenum disulfide to various metals NASA Center: Glenn Research Center (1977) 17

[17] K. J. Wahl, D. N. Dunn, and I. L. Singer, Wear behavior of Pb-Mo-S solid lubricating coatings, Wear 230 (1999) 175-183

[18] K. J. Wahl, D. N. Dunn, and I. L. Singer, Effects of ion implantation on microstructure, endurance and wear behavior of IBAD MoS2, Wear 237 (2000) 1-11

[19] I. L. Singer, R. N. Bolster, J. Wegand, S. Fayeulle, and B. C. Stupp, Hertzian stress contribution to low friction behavior of thin MoS 2 coatings, Applied Physics Letters 57 (1990) 995-997

[20] C. C. Baker, R. R. Chromik, K. J. Wahl, J. J. Hu, and A. A. Voevodin, Preparation of chameleon coatings for space and ambient environments, Thin Solid Films 515 (2007) 6737-6743

[21] T. W. Scharf, P. G. Kotula, and S. V. Prasad, Friction and wear mechanisms in MoS2/Sb2O3/Au nanocomposite coatings, Acta Materialia 58 (2010) 4100-4109

[22] B. C. Windom, W. G. Sawyer, and D. W. Hahn, A Raman Spectroscopic Study of MoS_2 and MoO_3: Applications to Tribological Systems, Tribology Letters 42 (2011) 301-310

[23] D. Y. Wang, C. L. Chang, Z. Y. Chen, and W.Y. Ho, Microstructural and tribological characterization of MoS2-Ti composite solid lubricating films, Surface and Coatings Technology 120-121 (1999) 629-635

[24] C. Muratore, J. E. Bultman, S. M. Aouadi, and A. A. Voevodin, In situ Raman spectroscopy for examination of high temperature tribological processes, Wear 270 (2011) 140-145

[25] R.R. Chromik, C.C. Baker, A.A. Voevodin, and K. J. Wahl, In situ tribometry of solid lubricant nanocomposite coatings, Wear 262 (2007) 1239-1252

[26] B. C. Stupp, Performance of conventionally sputtered MoS2 versus co-sputtered MoS2 and Nickel (1984) 217-222

[27] N. M. Renevier, V. C. Fox, D. G. Teer, and J. Hampshire, Performance of low friction MoS2/titanium composite coatings used in forming applications, Materials & Design 21 (2000) 337-343

[28] J. R. Lince, Tribology of co-sputtered nanocomposite Au/MoS_2 solid lubricant films over a wide contact stress range, Tribology Letters 17 (2004) 419-428

[29] J. S. Zabinski, M. S. Donley, S. D. Walck, T. R. Schneider, and N. T. McDevitt, Effects of Dopants on the Chemistry and Tribology of sputter-deposited MoS2 films, Tribology Transactions 38 (1995) 894-904

[30] T. Spalvins, Frictional and morphological properties of Au---MoS2 films sputtered from a compact target, Thin Solid Films 118 (1984) 375-384

[31] E W Roberts and W B Price, Advances in Molybdenum Disulphide Film Technology for Space Applications, European Space Mechanisms & Tribology Symposium 6 (1995) 273-278

[32] M. C. Simmonds, A. Savan, E. Pfluger, and H. Van Swygenhoven, Mechanical and tribological performance of MoS2 co-sputtered composites, Surface and Coatings Technology 126 (2000) 15-24

[33] X. Wang, Y. Xing, S. Ma, X. Zhang, K. Xu, and D. G. Teer, Microstructure and mechanical properties of MoS2/titanium composite coatings with different titanium content, Surface and Coatings Technology 201 (2007) 5290-5293

[34] N. M. Renevier, J. Hamphire, V. C. Fox, J. Witts, T. Allen, and D. G. Teer, Advantages of using self-lubricating, hard, wear-resistant MoS2-based coatings, Surface and Coatings Technology 142-144 (2001) 67-77

[35] N. M. Renevier, V. C. Fox, D. G. Teer, and J. Hampshire, Coating characteristics and tribological properties of sputter-deposited MoS2/metal composite coatings deposited by closed field unbalanced magnetron sputter ion plating, Surface and Coatings Technology 127 (2000) 24-37

[36] N. M. Renevier, H. Oosterling, U. König, H. Dautzenberg, B. J. Kim, L. Geppert, F. G. M. Koopmans, and J. Leopold, Performance and limitation of hybrid PECVD (hard coating)--PVD magnetron sputtering (MoS2/Ti composite) coated inserts tested for dry high speed milling of steel and grey cast iron, Surface and Coatings Technology 163-164 (2003) 659-667

[37] N. M. Renevier, H. Oosterling, U. König, H. Dautzenberg, B. J. Kim, L. Geppert, F. G. M. Koopmans, and J. Leopold, Performance and limitations of MoS2/Ti composite coated inserts, Surface and Coatings Technology 172 (2003) 13-23

[38] V. Rigato, G. Maggioni, D. Boscarino, L. Sangaletti, L. Depero, V. C. Fox, D. Teer, and C. Santini, A study of the structural and mechanical properties of Ti---MoS2 coatings deposited by closed field unbalanced magnetron sputter ion plating, Surface and Coatings Technology 116-119 (1999) 176-183

[39] X. Ding, X. T. Zeng, X. Y. He, and Z. Chen, Tribological properties of Cr- and Ti-doped MoS2 composite coatings under different humidity atmosphere, Surface and Coatings Technology 205 (2010) 224-231

[40] B. C. Stupp, Synergistic effects of metals co-sputtered with MoS2, Thin Solid Films 84 (1981) 257-266

[41] B. Bhushan, Micro/Nano Tribology, 2 ed, CRC, Columbus, 1999.

[42] B.Bhushan, Micro/nanotribology and its applications to magnetic storage devices and MEMS, Tribology International 28 (1995) 85-96

[43] S. Majumder, N.E. McGruer, P.M. Zavracky, G.G. Adams, R.H. Morrison, and J. Krim, Tribology Issues and Opportunities in MEMS, Kluwer Academic Publishers, Dordrecht, 1998.

[44] M. Nosonovsky and B. Bhushan, Scale effect in dry friction during multiple-asperity contact, Transactions of the ASME. Journal of Tribology 127 (2005) 37-46

[45] C. K. Bora, E. E. Flater, M. D. Street, J. M. Redmond, M. J. Starr, R. W. Carpick, and M. E. Plesha, Multiscale roughness and modeling of MEMS interfaces, Tribology Letters 19 (2005) 37-48

[46] A. J. Bushby and N. M. Jennett, Determining the area function of spherical indenters for nanoindentation, presented at Fundamentals of Nanoindentation and Nanotribology II, 2001.

[47] Yifei Mo, Kevin T. Turner, and Izabela Szlufarska, Friction laws at the nanoscale, Nature 457 (2009) 1116-1119

[48] R. Chromik and K. Wahl, private communication

[49] R. Modlinski, R. Puers, and Ingrid De Wolf, AlCuMgMn micro-tensile samples: Mechanical characterization of MEMS materials at micro-scale, Sensors and Actuators A: Physical 143 (2008) 120-128

[50] P. F. van Kessel, L. J. Hornbeck, R. E. Meier, and M.R. Douglass, A MEMS-Based Projection Display, Proceedings of the IEEE 86 (1998) 1687-1704

[51] C. L. Goldsmith, Y. Zhimin, S. Eshelman, and D. Denniston, Performance of low-loss RF MEMS capacitive switches, Microwave and Guided Wave Letters, IEEE 8 (1998) 269-271

[52] J A Williams and H R Le, Tribology and MEMS, Journal of Physics D: Applied Physics 39 (2006) R201

[53] B. Bhushan, Springer Handbook of Nanotechnology, Springer - Verlag, 2004

[54] S. S. Mani, J. G. Fleming, J. A. Walraven, J. J. Sniegowski, M. P. se Beer, L. W. Irwin, D. M. Tanner, D. A. LaVan, M. T. Dugger, J. Jakubczak, and W. M. Miller, presented at the Reliability Physics Symposium, 2000. Proceedings. 38th Annual 2000 IEEE International, 2000

[55] T. W. Scharf, S. V. Prasad, M. T. Dugger, P. G. Kotula, R. S. Goeke, and R. K. Grubbs, Growth, structure, and tribological behavior of atomic layer-deposited tungsten disulphide solid lubricant coatings with applications to MEMS, Acta Materialia 54 (2006) 4731-4743

[56] C. Nistorica, J.F. Liu, I. Gory, G. D. Skidmore, F. M. Mantiziba, B. E. Gnade, and J. Kim, Tribological and wear studies of coatings fabricated by atomic layer deposition and by successive ionic layer adsorption and reaction for microelectromechanical devices, AVS 2005, v23, p836-840

[57] N.F. Smith, L. W. Irwin, P. Eaton, D. M. Tanner, K. S. Helgesen, J. J. Clement, W. M. Miller, J. A. Walraven, K. A. Peterson, P. Tangyunyong, M. T. Dugger, and S. L. Miller, MEMS Reliability: Infrastructure, Test Structures, Experiments, and Failure Modes, Sandia National Laboratories (2000) 2000-2091

[58] H. Kim and J. Lince, Direct visualization of sliding-induced tribofilm on Au/MoS2 nanocomposite coatings by c-AFM, Tribology Letters 26 (2007) 61-65

[59] J. Barriga, B. Fernández-Diaz, A. Juarros, S. I. U. Ahmed, and J. L. Arana, Microtribological analysis of gold and copper contacts, Tribology International 40 (2007) 1526-1530

[60] R. Cooper, Ubi 1 User Manual, Hysitron Incorporated, Minneapolis, 2007.

[61] K. I. Schiffmann and A. Hieke, Analysis of microwear experiments on thin DLC coatings: friction, wear and plastic deformation, Wear 254 (2003) 565-572

Chapter 3
Organization of Thesis

The organization of this PhD thesis is summarized in Figure 3.1. Chapter 4 provides a detailed description of the experimental setup and procedure for the mechanical and microtribological experiments. The objective of the study in chapter 4 is to understand the effects of low and high Au content (i.e. 32% and 84% Au respectively) with MoS_2 on the micro-tribological properties, Figure 3.1. For this study, the friction behavior was identified with a Hertzian elastic and a plowing component.

Chapter 5 provides an understanding of the influence of different metal additives (i.e. titanium and gold) to MoS_2 on the mechanical and micro-tribological properties. The results in this study were analyzed as a function of contact pressure and were correlated to the interfacial shear strength and different wear mechanisms.

Chapter 6 discusses lubrication strategies that improve the wear resistance of gold. In this study, the influence of 20 mol % MoS_2 co-sputtered with pure Au was compared to the microtribological behavior of pure Au. The microtribological results, with respect to the two coatings, were compared via different friction laws and velocity accommodation modes (VAM).

Chapter 7 concludes this thesis with a study showing a direct comparison between macro- and micro- scale tribology. A ‘real time’ study of the transfer film behavior and VAMs was

conducted with an *in situ* tribometer at the macro-scale and on the micro-scale transfer films were analyzed *ex situ* on the counterface (i.e. nanoindentation tips) by means of atomic force microscopy.

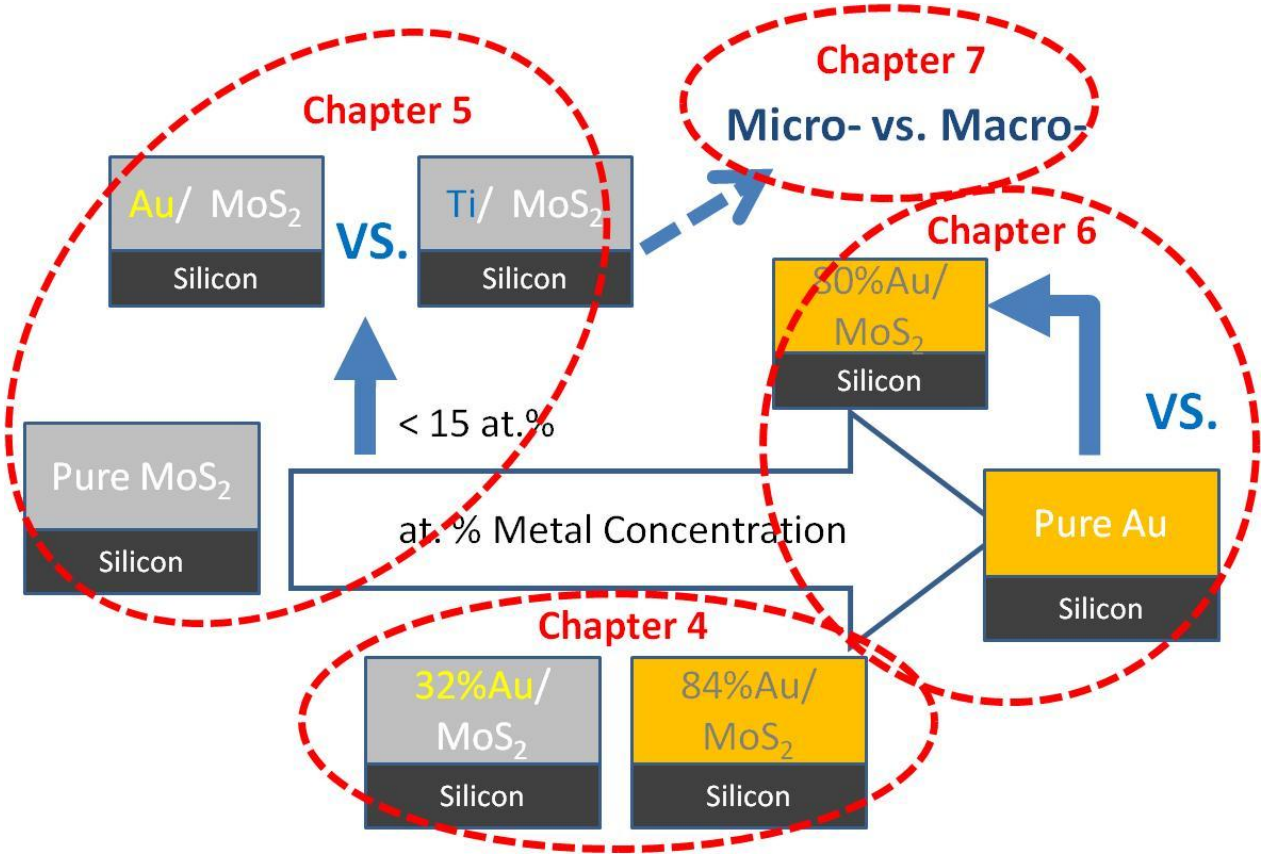

Figure 3.1. Organization of PhD thesis

Chapter 4

Micro-Tribological Performance of MoS_2 Lubricants with varying Au content

4.1 Abstract

Micro-tribological testing with a spherical diamond tip (radius = 100 μm) was conducted on two Au-MoS_2 coatings with 32at% and 84at% Au. For lower loads (0.2 to 2.0 mN), the performance of both coatings were similar, with minimal wear (<50 nm depth) and relatively stable friction coefficients. At higher loads (3.0 – 5.0 mN), similar trends were found for the 84at% Au specimen, but the 32at% Au sample wore severely and the friction became unstable. Non-linear curve fitting of friction coefficient versus normal load was conducted using a model containing an elastic (Hertzian) term and a plastic (plowing) term. Changes in the two contributions to the friction with time were used to explain the differences in performance observed between the two coatings.

4.2. Introduction

Solid lubricant coatings typically have a specific range of environmental and engineering conditions over which they are most effective. Many of these variables are well known (humidity, temperature, roughness, counterface material, etc.) and tribological performance has been characterized with them in mind for many years. More recently, with the advent of micro-electromechanical systems (MEMS) and a desire to use solid lubricants for these applications, [1] the variables of contact size and stress have become more important. More specifically, it

remains unclear how a reduction in contact size will affect the viability of these materials, including their ability to self lubricate by the formation of transfer films. [2]

Experimental efforts in this area may be sub-divided into two regimes: testing conducted on real MEMS devices that are constructed as miniature tribometers, [3,4] and those that simulate the conditions for a real device through micro- and nanotribological testing. [5-8] Both paths have pros and cons. The first, while able to provide conditions virtually identical to a real device, requires extensive investment in making the devices, which always have some finite yield from their microfabrication. Furthermore, any desired changes in contact size or material require additional devices to be made. For the second path, there are always questions on how accurately the experimental technique, such as atomic force microscopy (AFM), nanoindentation or microtribometry, simulates the contact conditions in MEMS. However, because tribology and lubrication is not well understood at these length scales, the ability of these techniques to more easily change contact conditions (size, chemistry, etc.) makes them a useful alternative that provides insight on the metrics that control friction at the reduced length scales of MEMS.

The microtribology of two Au-MoS_2 coatings with 32 and 84at% Au was studied with a nanoindentation instrument equipped with scratch capability. These coatings, depending on the Au content, were recently found to have good performance in macrotribology testing across a wide range of contact stresses. [9] In this study, the contact size is reduced while maintaining a similar contact stress, allowing an exploration of the potential of these coatings for MEMS and

other microtribological systems (e.g. electrical microswitches). Sliding wear experiments were conducted in a dry environment, and the contact size and stress were varied by changing the normal load. The friction results were analyzed using a combination of Hertzian elastic model and an additional plowing term. This analysis combined with wear measurements provided insight on the necessary contact conditions and preferred coating composition to provide lubrication for micro-scale sliding contacts.

4.3. Experimental Procedure

Nanocomposite coatings of Au and MoS_2 were co-deposited in a high vacuum chamber onto polished Si wafers. More details for the specimen preparation are found in the literature. [9] The composition of the coatings was measured by Auger spectroscopy (PHI 680 Auger Nanoprobe). Atomic force microscopy (Nanoman or Dimension 3100, Veeco) was used to determine the coating thickness from step-height measurements and the roughness from 20 x 20 μm^2 scans of the unworn coating.

Nanoindentation and sliding wear tests were performed using an instrumented indenter with a lateral force option (Hysitron TriboIndenter). A sphero-conical tip with a radius of 100 μm was used for the sliding tests and a Berkovich tip was used for the nanoindentation tests. Prior to the experiments, the area functions for both tips were determined from indentation on fused quartz. The hardness and elastic modulus of the coatings were determined from nanoindentation tests using a standard Oliver and Pharr analysis.[10] Between ten and twenty indentation tests were

conducted for each coating that resulted in contact depths between 10 and 50 nm (between 3 and 16% of the total coating thickness). The results from these tests were used to determine the average mechanical properties.

Sliding tests were performed under controlled temperature of 22°C and a relative humidity of 4.0 ± 0.2%. The relative humidity was controlled by flowing nitrogen gas, which passed through a desiccant (anhydrous $CaSO_4$) and into the instrument enclosure at a high flow rate for ten minutes and then a constant low flow rate throughout the sliding experiments. The results from the sliding experiments were analyzed using a custom-built analysis code with Matlab, Version 7.5.0. Wear depth measurements were determined from line profile measurements across wear track images acquired by AFM.

The sliding experiments were conducted with 8μm track lengths at a constant velocity of 4μm/sec. The normal load used for the experiments was 0.2, 0.5, 0.7, 1.0, 2.0, 3.0, and 5.0 mN. The total number of sliding cycles was 800, but due to limitation on the instrument software, the experiment consisted of "test cycles" of 40 sliding cycles each that were repeated twenty times consecutively at the same position. Each test cycle consisted of three phases, 1) a pre-scan, to image the topography at a 20 μN load, 2) an oscillating scratch, where the sample is worn under a high constant load for 40 sliding cycles, and 3) a post-scan with 20 μN load to image the topography of the resulting wear trace. [6,8] A plot of the normal force and lateral position

versus time are presented in Figure 4.1 for a test cycle with a normal load of 0.5 mN. In between test cycles, the tip briefly leaves the surface of the specimen and then re-engages with the surface at a small force (~ 2 μN). The tip then remains stationary at the center of the wear track for approximately 90 seconds while the next test cycle is loaded in the software. Based on the specifications of the instrument and images of wear tracks, any misalignment upon re-engaging the test is on the order a few nanometers.

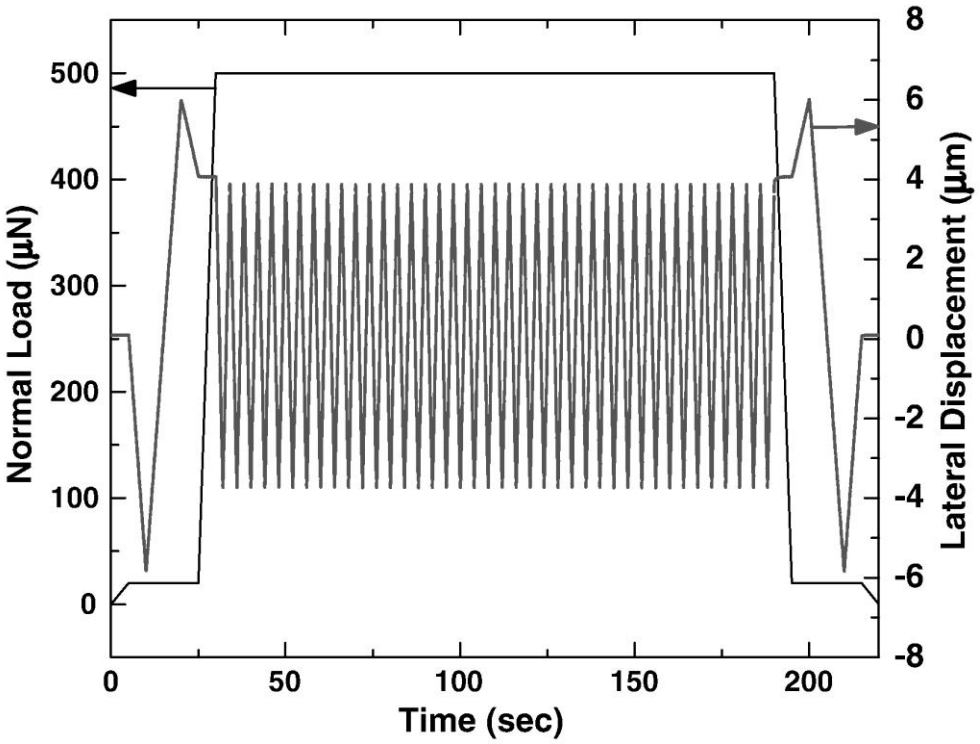

Figure 4.1. Normal load (black) and lateral displacement (gray) versus time for a test cycle with a normal load of 0.5 mN.

The coefficient of friction was calculated from the lateral force divided by the normal force. The average friction coefficient for each cycle was calculated from 39 data points corresponding to

the central 5μm of the track. Custom-built analysis code was used to conduct non-linear curve fitting of friction data versus normal load. This fitting was conducted for data near the end of each test cycle to investigate the evolution of both the Hertzian (elastic) and plowing (plastic) contributions to the total friction as a function of time. The equation used to model the two contributions was:

$$\mu = \mu_e + \mu_p = c_1 L^{(-1/3)} + c_2 L^m \quad (4.1)$$

where the first term is the Hertzian contribution and the second term is the plowing component. This equation has been used by Schiffman, et al. for similar sliding wear experiments on diamond-like carbon materials. [8] The fitting constant c_1 in Eq. 4.1 may be written as

$$c_1 = (S\pi(3R/4E))^{(2/3)} \quad (4.2)$$

where R is the radius of the spherical counterface, S is the shear stress and E is the reduced modulus of the contact.[11] The plowing portion of Eq. 4.1 is largely empirical, but can be considered to have c_2 inversely proportional to yield strength and the exponent, m, related to both yield strength and a strain hardening index.[8]

Figure 4.2 is an example of data for friction coefficient versus normal load where either the elastic or the plastic part of Eq. 4.1 is dominating. When the elastic part dominates, the curve has a smooth drop in friction with normal load, which matches closely to an $L^{-1/3}$ dependence (see inset in Figure 4.2 as well). When the plastic part of the sliding process has a significant effect, the data at higher loads typically has higher friction coefficients. In either case, and those in

between, Eq. 4.1 was found to confidently fit the friction measurements versus load as shown in Figure 4.2.

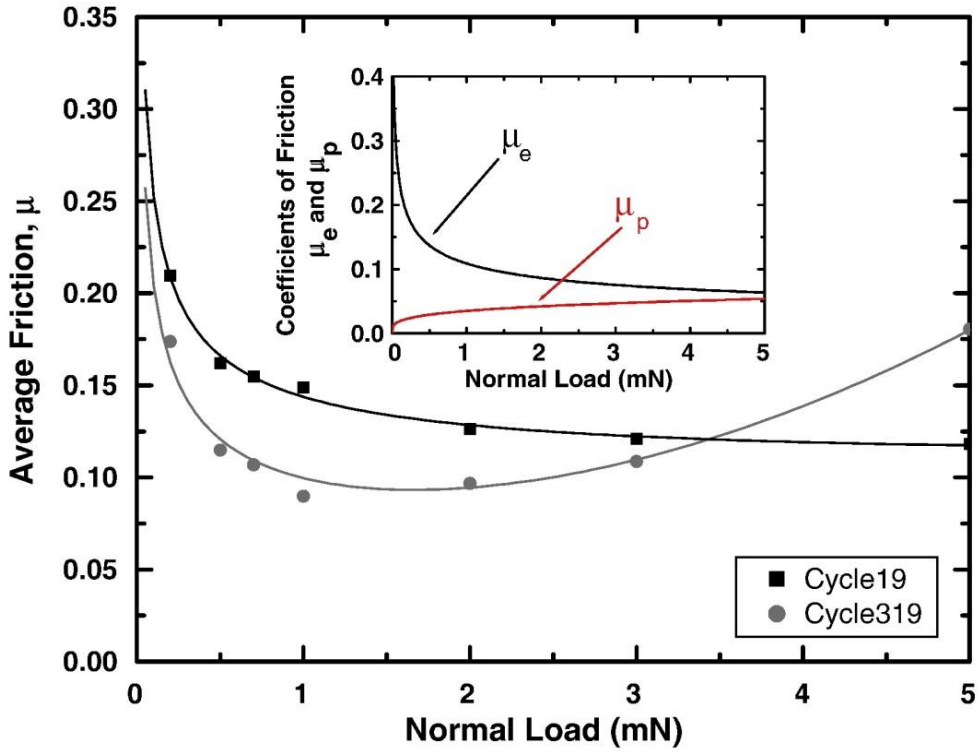

Figure 4.2. Average coefficient of friction versus normal load, fitted using a combination of Hertzian elastic model and an additional plowing term (see Eq. 1) for the 19th cycle on the MoS_2/84%Au and 319th cycle on the MoS_2/32%Au sample. The inset shows the typical shape of the elastic (μ_e) and plastic (μ_p) components.

4.4 Results

4.4.1 Coating Properties

The two coatings studied here had compositions of 32 and 84at% Au. The thickness and RMS roughness of the coatings were found to be nearly identical (see Table 4.1). The mechanical

properties of the coatings as determined by nanoindentation are contained in Table 4.1. The 32%Au coating was found to be softer and less stiff than the 84%Au coating. However, the H/E ratios for the two coatings were nearly identical.

Table 4.1. Properties of MoS_2/Au coatings.

Sample	Thickness (nm)	RMS roughness (nm)	Modulus, E (GPa)	Hardness, H (GPa)	H/E
MoS_2/32at%Au	310	6.3	43 ±11	1.1 ±0.3	0.025
MoS_2/84at%Au	320	4.7	88 ±18	2.0 ± 0.4	0.022

4.4.2 Friction Performance

For normal loads between 0.2 and 2.0 mN, both the 32%Au coating [Figure 4.3(a)] and 84%Au coating [Figure 4.3(b)] exhibited a rather smooth run-in to friction coefficients between 0.1 and 0.18. In general, larger loads resulted in a smaller friction coefficient. Also, for most tests, there was a rise in the friction coefficient every 40^{th} cycle, which coincided with the re-initiation of a subsequent test cycle. The friction rise could be due to numerous effects that might occur during a halt to sliding, such as: 1) adsorption of water vapor and mild oxidation of the wear track, 2) de-bonding of the transfer film or 3) a small misalignment of the tip upon re-initiation of the test cycle. To examine possible oxidation, experiments were conducted with increased time between test cycles. It was observed that the friction rises did not increase in magnitude with longer wait times. Based on this result and the observed low error in tip misalignment, our current understanding is that disturbance of the transfer film, probably during pre- and post-scanning (see Figure 4.1), is the mechanism having the greatest effect on the friction rises. While the

friction rises are unavoidable due to instrument limitations, their ultimate effect was found negligible on the eventual steady state friction behavior. This was confirmed by recent tests with an upgraded instrument allowing an increased number of sliding cycles. Similar run-in and steady state behavior without friction rises was observed for tests without pauses every 40 cycles.

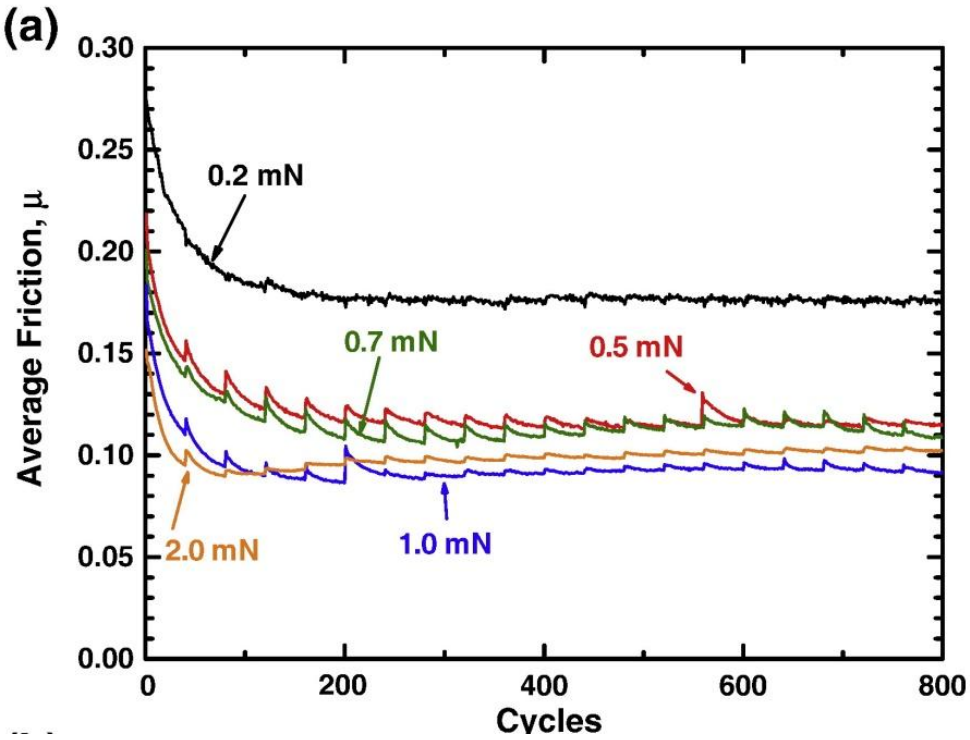

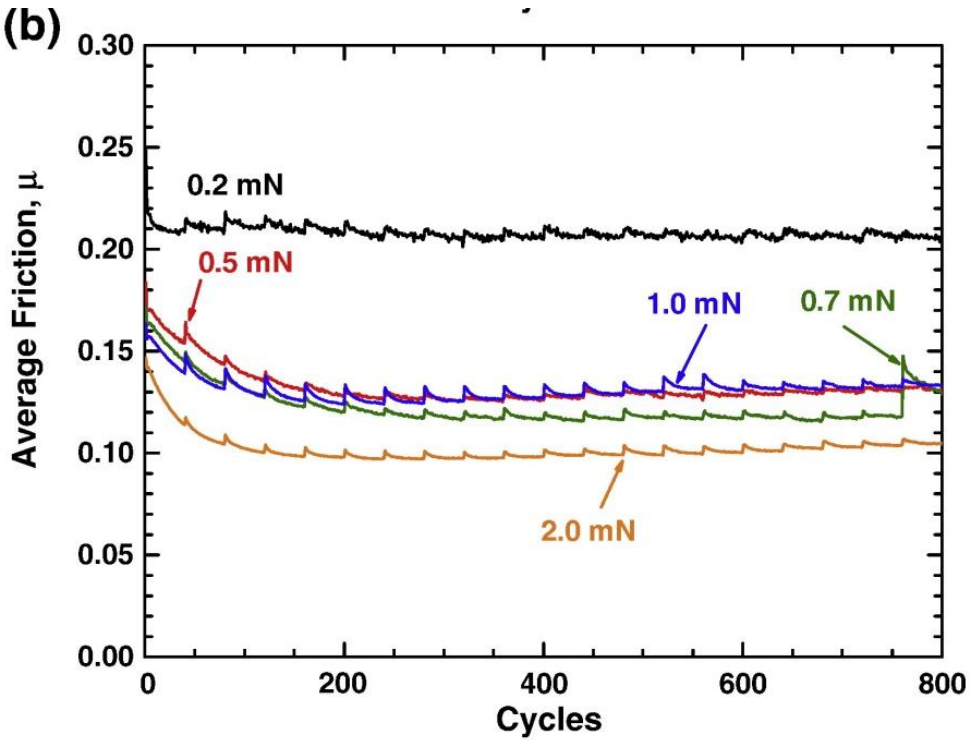

Figure 4.3. Average friction versus cycles for the MoS_2 coating with 32at% Au **(a)** and 84%Au **(b)** for normal loads from 0.2 mN to 2.0 mN.

For higher normal loads of 3.0 and 5.0 mN, the friction behavior of the 84% Au coating [Figure 4.4(b)] was similar to the behavior at smaller loads. However, higher load experiments on the 32% Au specimen resulted in markedly different behavior [Figure 4.4(a)]. For a load of 3.0 mN, a steady state friction of 0.1 is obtained after roughly 50 sliding cycles, but by cycle 300, the friction started to rise and was 0.17 by the end of the test. For a load of 5.0 mN, the friction coefficient started at approximately 0.14, rose steadily and then varied between 0.16 and 0.24 for the remainder of the test.

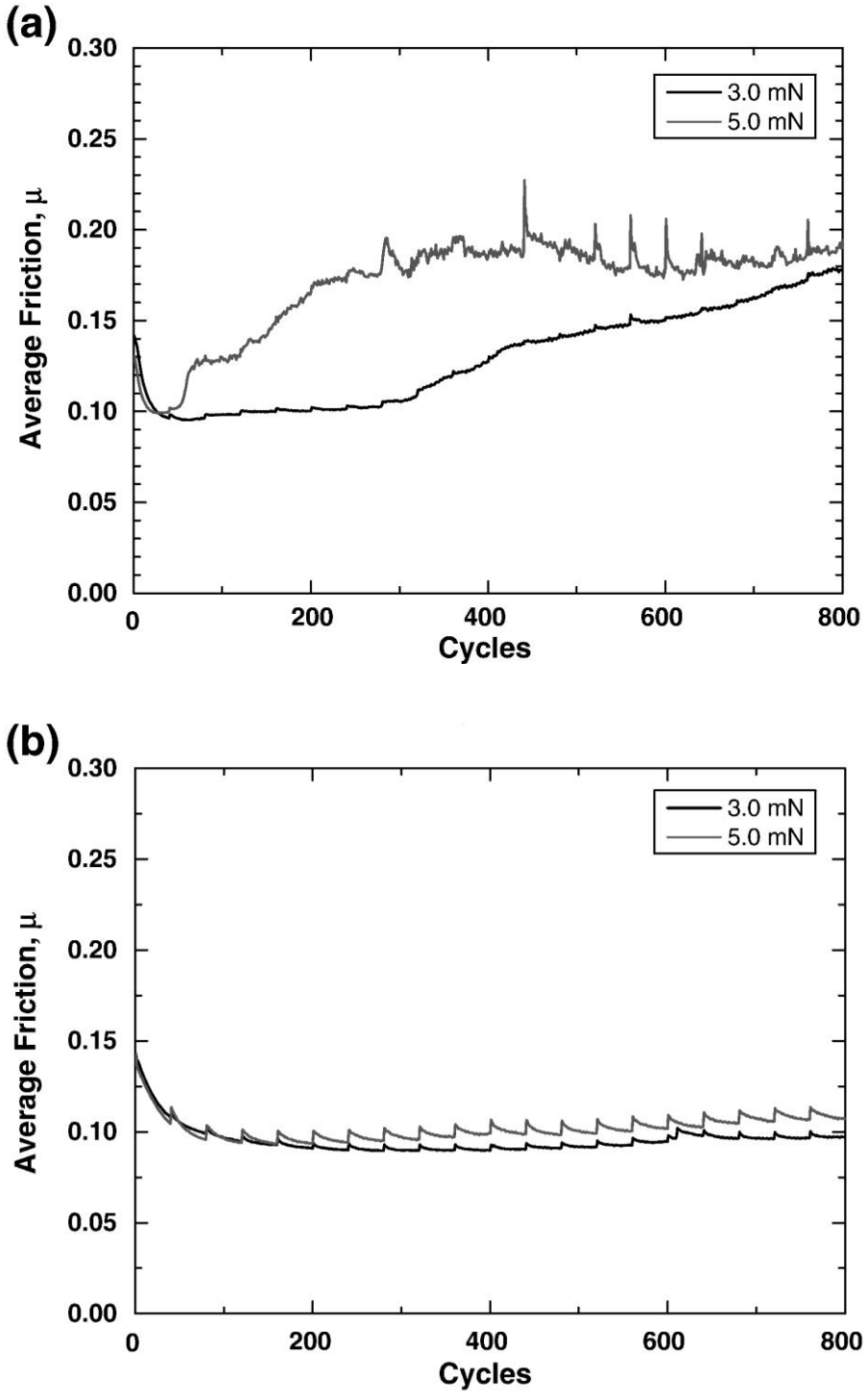

Figure 4.4. Average friction versus cycles for the MoS_2 coating with 32at% Au **(a)** and 84at% Au **(b)** for normal loads of 3.0 and 5.0 mN.

4.4.3 Wear

Wear depth measurements were obtained from AFM images of the wear tracks after 800 sliding cycles. Two line profiles were drawn across each wear track and an average was taken. Figure 4.5 is a plot of the wear depth versus the normal load for both coatings. For smaller normal loads between 0.2 and 1.0 mN, the wear depths for the two coatings are nearly identical. At higher normal loads between 2.0 and 5.0 mN, the wear for the 32% Au coating was greater than the 84% Au coatings. The difference in wear between the two coatings becomes greater with increasing normal load. All wear depths were less than the measured coating thickness except the 5.0 mN load test on the 32% Au coating, which has a wear depth of 350 nm, compared to the 310 nm coating thickness. This would indicate that wear of the Si substrate had commenced prior to the end of the test.

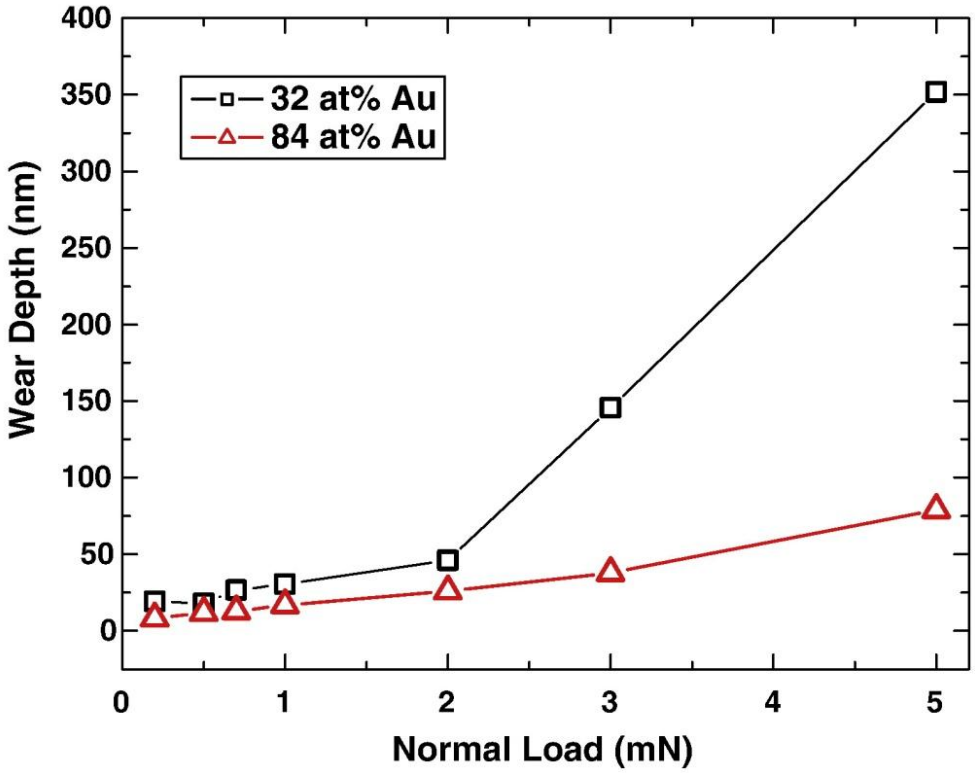

Figure 4.5. Wear depth, measured after 800 cycles, versus normal load.

4.5. Discussion

From the friction and wear results with normal loads below 2.0 mN, both coating have similar performance for the 800 cycles tested. While the 32% Au coating had slightly greater wear, this difference was minimal. When the normal load was increased, the performance changed significantly, with the 32% Au coating having much greater wear than the 84% Au coating. At the same time, the friction coefficient increased for the 32% Au specimen.

To consider the mechanisms for these differences in performance, an examination of the friction behavior with normal load was conducted that consisted of non-linear curve fitting with Eq. 1. For all of the data collected, the curve fitting results of friction coefficient data versus normal load yield curves qualitatively similar to those shown in Figure 4.2. While two extremes are shown in Figure 4.2 for primarily elastic and strongly affected by plowing, other data sets fell somewhere in between. These differences are most readily seen by plotting the two contributions to the total friction coefficient, μ_e and μ_p, separately. In this way, the evolution of the sliding process versus normal load or time may be explored. It should be noted that data used for this analysis was taken from the end of each test cycle, where the effect of the friction rises observed in Figures 4.3 and 4.4 were minimized.

To explore the evolution of the sliding process with time, μ_e and μ_p were plotted versus cycles. These results are plotted in Figure 4.6 for three normal loads (1.0, 3.0 and 5.0 mN). For all three loads, the elastic component for the 32% Au coating dropped during the run-in portion of the tests and then remained relatively constant [Figure 4.6(a)]. For the higher loads of 3.0 and 5.0 mN, the plastic component rose steadily throughout the test. For the 5.0 mN load, the plastic component becomes greater than the elastic early in the test (< 100 cycles). For the 3.0 mN load, this crossover occurs much later, at approximately cycle 600. While this crossover was not observed for a load of 1.0 mN, the curve for μ_p is steadily rising throughout the test, perhaps an indication that even at this load, the 32% Au coating will eventually fail. For the 84% Au coating [Figure 4.6(b)], the plowing component drops during run-in and then remains nearly constant. At

the same time the elastic component rises slightly at the start of the test and then also stays nearly constant. This evolution was observed for all normal loads and could be considered indicative of the steady state sliding taking place. There is a slight rise in μ_p with increasing cycle, possibly indicating that wear does progress for these coatings.

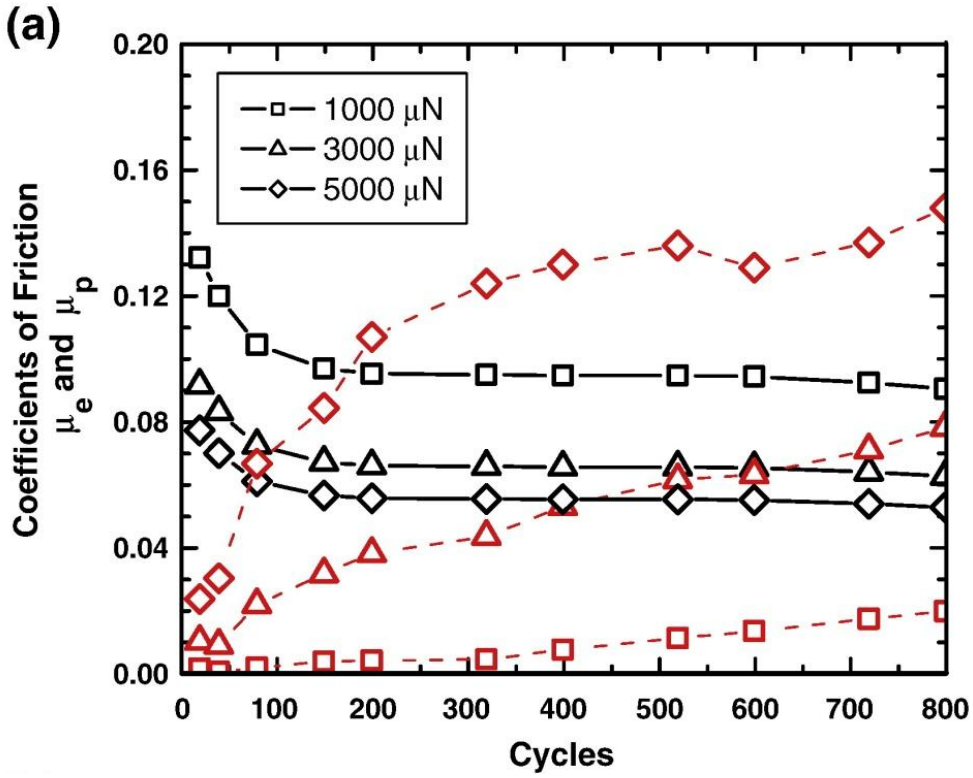

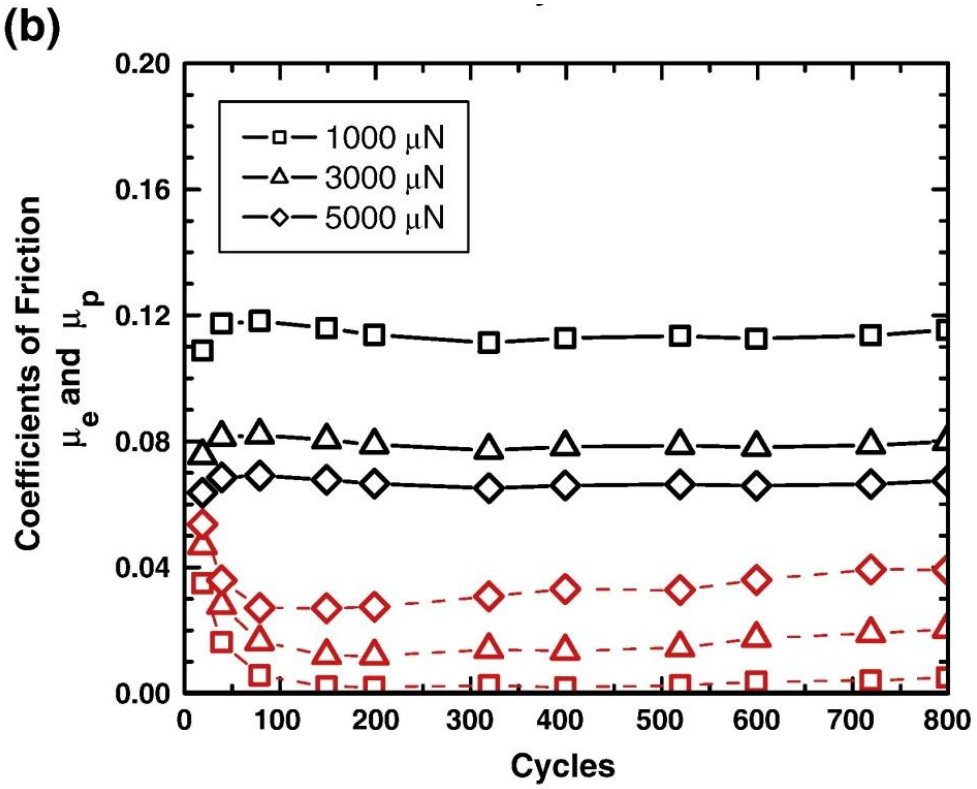

Figure 4.6. Calculated coefficients of friction, μe (solid lines) and μp (dashed lines), versus cycle number for the 32at% Au coating **(a)** and the 84at% Au coating **(b)**. These plots were constructed from the fitting results similar to those shown in Figure 4.2, where the best fit parameters were used to calculate the elastic and plastic contribution to the total friction coefficient.

Observations from Figure 4.6 are consistent with coating wear measurements (Figure 4.5). For the 84% Au coating, wear was minimal at all loads compared to the 32% Au coating. The 84% Au coating had nearly constant values of μ_e and μ_p with increasing cycles, and the plowing friction was always significantly smaller than the elastic component. When the 32% Au coating did not fail (at smaller normal loads), μ_e and μ_p were constant after run-in. When significant wear was observed, the plastic component steadily rose throughout the test. Combining the

observations from curve fitting of friction data and post-test wear analysis, it appears that sliding on the 84% Au coating results in a quick formation of a transfer film that remains stable throughout the test. At small loads, the same can be said for the 32% Au coating. However, at higher loads, the sliding on the 32% Au coating results in a plowing process. This plowing leads to coating wear and may also be associated with failure of the transfer films. Future work will explore these hypotheses. However, this discussion is consistent with differences in the coatings themselves. Higher metal content typically provides a harder, more fully dense coating that leads to thinner, more stable transfer films. Pure or lightly doped MoS_2 coatings are typically softer and will form patchy transfer films [9] that can lead to wear-related velocity accommodation modes, [2,12] such as plowing.

4.6. Conclusions

Microtribology experiments on Au-MoS_2 coatings in dry environments showed that a higher Au content coating (84at%) resulted in less wear and a more stable friction coefficient compared to a 32at% Au coating. Calculated values for the elastic (μ_e) and plastic (μ_p) components of the friction coefficient, obtained from non-linear curve fitting, were found to evolve with time. When coating wear was minimal, both μ_e and μ_p remained relatively constant after a reduction in the plastic component during run-in. When coating wear was significant, μ_e decreased and μ_p increased with increasing time.

Acknowledgements

The authors gratefully acknowledge financial support from Fonds québécois de la recherche sur la nature et les technologies (FQRNT), programme Établissement de nouveaux chercheurs. Support was also provided under The Aerospace Corporation's Mission Oriented Investigation and Experimentation program, funded by the U.S. Air Force Space and Missile Systems Center under Contract No. FA8802-04-C-0001.

REFERENCES

1 T. W. Scharf, S. V. Prasad, M. T. Dugger, P. G. Kotula, R. S. Goeke, and R. K. Grubbs, Growth, structure, and tribological behavior of atomic layer-deposited tungsten disulphide solid lubricant coatings with applications to MEMS, Acta Materialia 54 (2006) 4731-4743

2 I. L. Singer, S. D. Dvorak, K. J. Wahl, and T. W. Scharf, Role of third bodies in friction and wear of protective coatings, Journal of Vacuum Science & Technology A (Vacuum, Surfaces, and Films) 21 (2003) S232-S240

3 D. B. Asay, M. T. Dugger, and S. H. Kim, In-situ Vapor-Phase Lubrication of MEMS, Tribology Letters 29 (2008) 67-74

4 F.W. Delrio, M.P. De Boer, J.A. Knapp, E.D. Reedy Jr, P.J. Clews, and M.L. Dunn, The role of van der Waals forces in adhesion of micromachined surfaces, Nature Materials 4 (2005) 629-634

[5] R. Bandorf, H. Luthje, and T. Staedler, Influencing factors on microtribology of DLC films for MEMS and microactuators, Diamond and Related Materials 13 (2004) 1491-1493

[6] R.R. Chromik and K.J. Wahl, Friction of microscale contacts on diamond-like carbon nanocomposite coatings, presented at World Tribology Congress III, 2005.

[7] H. Liu and B. Bhushan, Nanotribological characterization of molecularly thick lubricant films for applications to MEMS/NEMS by AFM, Ultramicroscopy 97 (2003) 321-340

[8] K. I. Schiffmann and A. Hieke, Analysis of microwear experiments on thin DLC coatings: friction, wear and plastic deformation, Wear 254 (2003) 565-572

[9] J. R. Lince, Tribology of co-sputtered nanocomposite Au/MoS_2 solid lubricant films over a wide contact stress range, Tribology Letters 17 (2004) 419-428

[10] W. C. Oliver and G. M. Pharr, An improved technique for determining hardness and elastic modulus using load and displacement sensing indentation experiments, Journal of Materials Research 7 (1992) 1564-1583

[11] K.L. Johnson, Contact Mechanics, Cambridge University, Cambridge, UK, 1985, pp.84-106.

[12] M. Godet, The third-body approach: a mechanical view of wear, Wear 100 (1984) 437-452

Chapter 5

Microtribological performance of Au-MoS_2 and Ti-MoS_2 coatings with varying contact pressure

5.1 Abstract

Solid lubricant coatings with co-sputtered metal and MoS_2 have shown favorable macrotribological properties at a wide range of contact stresses and humidity levels. These materials are also candidates for use in microcontacts and micro-electromechanical systems (MEMS), but their performance at this scale is poorly understood. For this study, microtribological properties of Au-MoS_2 and Ti-MoS_2 coatings, with varying metal additives of less than 15 at.%, were examined using a nanoindentation instrument. Titanium and gold were chosen for this study as metal additives due to their different influence on the mechanical properties of the coating. The hardness and reduced modulus of the coatings increased with the addition of metal, when compared to pure MoS_2. Reciprocating microscratch tests were performed with two spherical diamond tips (50 µm and 10 µm radii) in dry air. A range of normal loads were used between 0.2 mN and 5.0 mN. Friction and wear measurements were analyzed with respect to the variation in the contact pressure and compared to literature studies performed at the macroscale. Correlations were found between the coating mechanical properties, tip-coating adhesion, interfacial shear strength, and the formation of transfer films and tribofilms.

5.2. Introduction

For a little more than a decade, the testing of nano- and micro-scale sliding contacts has been an important research area that seeks to improve the tribological performance of nano/micro-devices and to have a better understanding of a material's behavior during single and multi-asperity contacts [1-17]. Due to their applications in hard drives, diamond-like carbon (DLC) coatings have been well studied for their tribological behavior at these small length scales [12-18]. More recently, interest in other materials for microtribological applications has arisen. The demonstration of atomic-layer deposition of chalcogenides [19-20], such as WS_2, has provided the opportunity to include these materials, as solid lubricants, in micro-electromechanical system (MEMS). Additionally, there has been interest in using high metal additions to MoS_2 [8,10] for the possible use of these coatings in micromotors, switches or actuators.

Co-sputtered metal-MoS_2 solid lubricant coatings have shown favorable macrotribological properties at a wide range of contact stresses and humidity levels [21-31]. However, their microtribological performance is not nearly as well studied. Previous research has been performed using an atomic force microscope (AFM) [8] and a nanoindentation instrument [32-33] to investigate the influence of the gold content on the microtribological properties of MoS_2. It has been shown that higher gold content (i.e. 84 at% Au) shows the most promise for microtribological systems due to the better performance (i.e. lower coefficient of friction and lower wear rate) in humid environments and at higher contact pressure [32]. Other recent studies [34-35] have focused on lateral force microscopy of nanoparticles of MoS_2.

The co-sputtering of titanium with molybdenum disulphide results in similar effects on the macrotribological properties as the Au dopant. The addition of titanium increases the hardness and the wear resistance of the coating and makes it less sensitive to humid environments during tribological testing, as shown by Renevier [24]. While varying the Ti content between 3 at.% and 11 at%, Simmonds [25] illustrated that there was a significant increase in the endurance life with the lower Ti content. No reports in the literature were found on the microtribology of these coatings.

At present, it is well known that the low friction and high endurance life of metal-MoS_2 coatings is accomplished by the early formation of a stable and uniform transfer film (i.e. MoS_2 is transferred to the counterface) and tribofilm (i.e. a thin crystalline MoS_2 layer is formed on the worn surface), which can be directly correlated to a low interfacial shear strength. However, it still remains unclear if and how these tribological mechanisms change when decreasing the contact size to the microscale. The goal of this study was to investigate the influence of gold and titanium content on the microtribological properties of the co-sputtered molybdenum disulphide coatings developed by Lince [23] and Teer [28], and to compare the results to previous literature at the macro-scale. The friction measurements were analyzed as a function of the contact pressure and were correlated to the interfacial shear strength, the wear volume, and Raman spectroscopy of the wear track.

5.3. Experimental Procedure

Three coatings were studied in this work: sputtered MoS_2, co-sputtered Ti-MoS_2 (3.8 at.% Ti), and co-sputtered Au-MoS_2 (11.2 at.% Au). The gold and titanium concentration was measured using an energy dispersive spectrometer (EDS) on a field emission gun scanning electron microscope (Hitachi 4700-S FEG-SEM, Japan). The Au-containing and pure MoS_2 samples were produced at the Space Materials Laboratory of The Aerospace Corporation (El Segundo, CA, USA) using a custom sputter deposition system [23]. Briefly, coatings were deposited onto polished Si (100) wafers in a load locked deposition chamber with a base pressure of 1.33×10^{-7} Pa (1×10^{-9} Torr). Separate Au and MoS_2 radio frequency sputtering sources were used, which were operated in unbalanced mode to increase the ion flux on the substrate surface during deposition. Argon (99.999% nominal purity) was used as the sputtering gas, and the Ar pressure in the chamber during deposition was typically 4 Pa (3×10^{-3} Torr). The Au and MoS_2 sputtering power densities were 0.25 and 3.0 W/cm^2, respectively. The titanium content samples wear produced by Teer Coatings, Ltd. (Worcestershire, UK) using a close field unbalanced magnetron sputtering ion plating (CFUBMSIP) system operated in DC mode [28]. The preliminary chamber pressure before deposition was $5\sim6\times10^{-6}$ Torr. The argon sputtering pressure was approximately 3.0×10^{-3} Torr. The distance between the target and substrates was about 150 mm. Substrates were rotated in front of each of the targets in turn in a speed of 4.0 rpm. A pulsed DC power supply provided -350 V bias on the substrates during the 15 min pre-cleaning and -30 V during deposition. A thin adhesion layer of Ti was produced first and followed by the Ti-MoS_2 coatings. The substrate temperature during the deposition process was lower than 200 °C.

The films were characterized with various methods to determine their structure, coating thickness and roughness. Phase identification, bonding and degree of crystallinity was examined using a inVia-Raman microscope (Renishaw, Gloucestershire, UK) with a 514.5 nm Ar+ laser and x-ray diffraction (Bruker D8 Discover, Germany) in a standard Θ-2Θ geometry and with a Co-Kα x-ray source. The roughness of the coatings was measured using an atomic force microscope (AFM) (Veeco Dimension 3100, Santa Barbara, CA, USA) operated in contact mode using up to 50μm by 50μm scan size. The thickness of the coatings was measured from cross-sectional images obtained at high magnification using the FEG-SEM described above.

The mechanical properties of the coatings were measured with a Ubi 3 nanoindentation instrument (Hysitron, Inc. Minneapolis, MN, USA) with a 1D transducer and a diamond Berkovich tip. The hardness and reduced modulus values presented in this paper are averages taken from roughly ten indentations using indentation depths of up to 56nm, 43nm, and 180nm for the pure MoS_2, Au-MoS_2, Ti-MoS_2 coating, respectively. The same nanoindentation instrument and transducer were used for surface pull-off force measurements with a spherical diamond tip (50μm tip radius) and the instrument in displacement control feedback mode. The maximum displacement throughout the test was 60 nm with a hold time of one second. The pull-off force was measured from the retracting adhesion force on the unloading curve [36].

The shape of the two diamond tips (10μm and 50μm radii) that were used for microtribology were characterized with an AFM (Veeco Nanoman 3100, Santa Barbara, CA, USA) operated in closed loop scanning in tapping mode. Scans were used to characterize the radius, roughness,

and the area function of the spherical tips. This characterization was performed because, at smaller length scales, diamond indenters typically deviate from the ideal spherical shape due to the difficulty of machining them [37]. Therefore, it is crucial to obtain an accurate area function (which is the cross sectional area of the tip as a function of depth) in order to do any calculations that include the area of the tip as a variable. Over the depth range used for our tribological studies, the RMS roughness of the two tips were between 40 and 60 nm for the 10 μm tip and 5 and 15 nm for the 50 μm tip.

Tip area functions for both tips were produced using the AFM images and a custom-built pixel counting algorithm created in Matlab Version 7.5.0 (The Mathworks, Natick, MA, USA). This procedure was similar to the one described by Bushby [37]. The diamond tips were stationed vertically in a tip holder, without the ability of lateral and vertical movement. The indenter tips were scanned in the X and Y direction with scan sizes ranging from 5 μm to 30 μm. The scans were exported from the AFM software and converted into ASCII text files containing a 256x256 matrix. Each number in the matrix represents the height value, with the middle number in the matrix being the top of the tip. The column and row number represent the number of pixels as a function of the distance in the X and Y direction, respectively. In other words, each pixel represents a small square with the lengths being the scan size divided by 256 (i.e. the size of the matrix). Thus, using this matrix, the cross sectional area of the tip can be calculated at any given depth, where the depth is the value in the matrix. Figure 5.1 (a) and (b) shows the AFM images of the tips and plots of the area functions obtained from our pixel-counting algorithm compared to the ideal area functions for the 50 μm tip and the 10 μm tip, respectively.

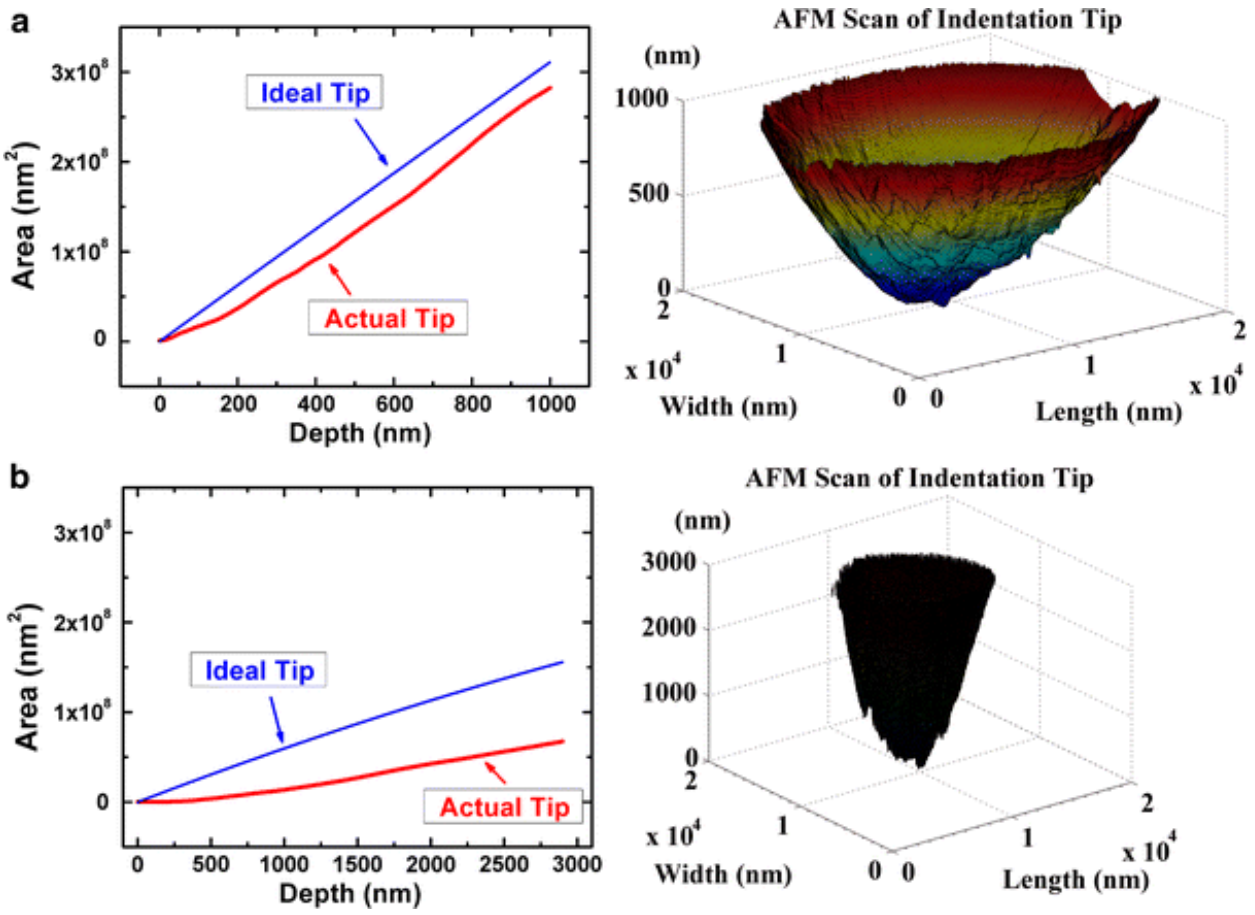

Figure 5.1. Tip area function vs. depth obtained using an AFM scan for (a) the 50μm tip and (b) the 10μm tip.

Microtribological testing with the spherical diamond tips was conducted using a Ubi 3 nanoindentation instrument with a 2D transducer. Sliding tests were performed under controlled ambient temperature and a relative humidity between 3.0 and 5.0%. The relative humidity was controlled by flowing compressed air, which passed through anhydrous $CaSO_4$ (desiccant) and into the instrument enclosure at a high flow rate for a few minutes and then a constant low flow rate throughout the sliding experiments.

The sliding experiments were conducted with an 8 μm track length at a constant velocity of 4μm/sec. All sliding experiments were repeated at least two times, and for some conditions, the sliding tests were repeated up to four times. The normal loads used for the experiments were varied between 0.2 and 5.0 mN, which resulted in a contact pressure between 0.4 and 3.5 GPa and a contact radius between 0.2 μm and 1.1 μm for the different tips. The total number of sliding cycles was 800, but due to limitation by the instrument software, only 400 cycles were performed at a time, and were repeated on the same position in order to achieve a total of 800 cycles. Each sliding test consisted of three phases, 1) a pre-scan, to image the topography at a 20 μN load, 2) an oscillating scratch, where the sample is worn under a constant load higher than 20 μN for 800 sliding cycles, and 3) a post-scan with 20 μN load to image the topography of the resulting wear trace. The experimental method is described in more detail elsewhere [32].

The results from the sliding experiments were analyzed using a custom-built analysis code written with Matlab software. The coefficient of friction was calculated from the lateral force divided by the normal force. The average friction coefficient for each cycle was calculated from 75(±2) data points corresponding to the central 5μm of the track. For *ex situ* examination of wear, the wear track was scanned using an AFM operated in contact mode, and the wear volume was calculated from the cross-sectional area in the middle of the track multiplied by the length of the wear track.

5.4. Results

5.4.1 Coating Characterization and Properties

Table 5.1 shows the properties of the coatings that were tested for this study. The hardness and the reduced modulus increased with the addition of metal to MoS_2. Also, the Ti-MoS_2 coating revealed higher reduced modulus and hardness values when compared to the Au containing coating.

Table 5.1. Coating properties of co-sputtered MoS_2, Au-MoS_2, and Ti-MoS_2

Sample	E_r (GPa)	H (GPa)	Thickness (nm)	RMS Roughness (nm)
MoS_2	29 (+/- 5)	1.2 (+/- 0.4)	770	4.9
MoS_2/ Au	68 (+/- 8)	3.3 (+/- 0.7)	330	5.2
MoS_2/ Ti	118 (+/- 9)	5.4 (+/- 0.3)	870	3.3

Figures 5.2 (a), (b), and (c) shows Raman spectra for the MoS_2, Au-MoS_2, and Ti-MoS_2 samples, respectively. For the MoS_2 coating, the scan revealed peaks which are consistent with the Raman active modes for MoS_2(2H) [38-40]. A small peak at 408 cm^{-1} was also observed with the Ti-MoS_2 sample, however no MoS_2 peaks were observed with the Au content samples for the as-prepared coating. The broad features between 250 and 500 cm^{-1} are commonly seen in MoS_2 coatings that have a low degree of crystallinity. Results from x-ray diffraction measurements (not shown) revealed no peaks for crystalline phases in any of the coatings. Based on these two techniques, the coatings appear to be primarily amorphous, consistent with previous publications on these materials [23,28].

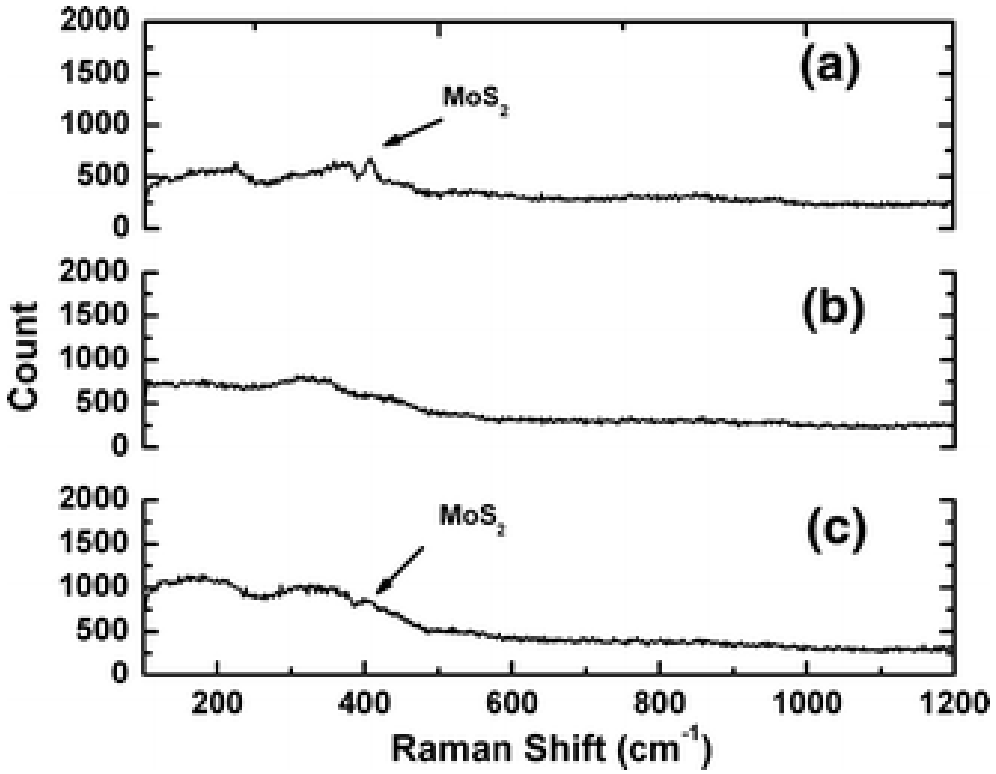

Figure 5.2. Film characterization on the unworn surface using a Raman microscope for the (a) MoS_2, (b) Au-MoS_2 , and (c) Ti-MoS_2 coating. Micro Raman scans show bands which are consistent with crystalline MoS_2 for the pure MoS_2 sample, however, no MoS_2 peaks are observed with the metal content samples.

5.4.2 Coefficient of Friction

Figures 5.3 (a), (b), and (c) show the average coefficient of friction vs. the cycle number using a 50μm tip for the MoS_2, Au-MoS_2, and Ti-MoS_2 samples, respectively. While three normal loads are plotted for each coating, sliding tests using normal loads in between and above the ones plotted were also performed and were used for the analysis in the discussion section. For all samples, both the run-in and steady state coefficients of friction decrease with increasing normal load, which is typically observed for MoS_2 coatings.

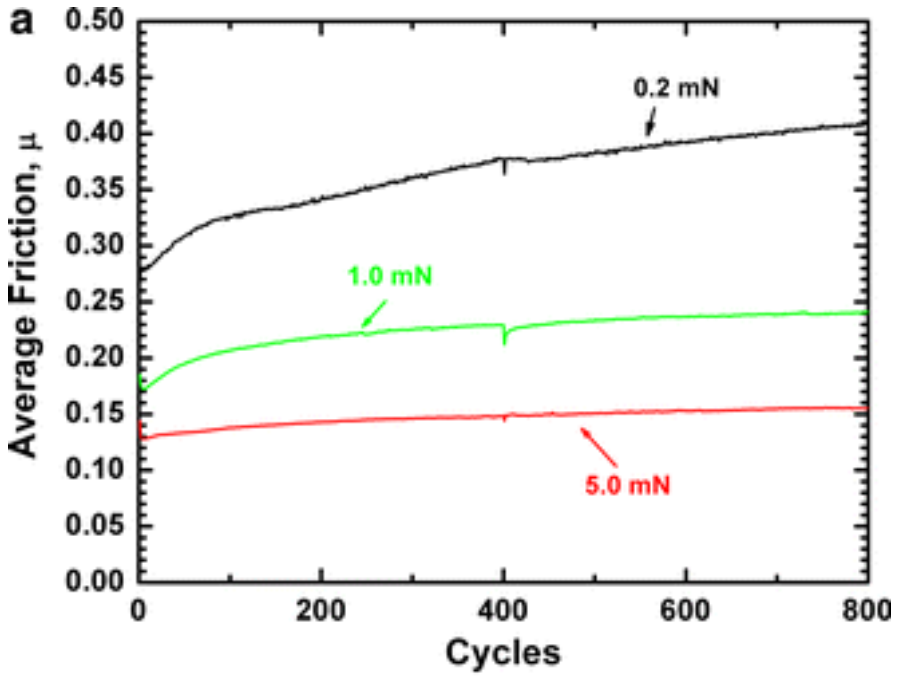
a
Average Friction, μ
0.50
0.45
0.40
0.35
0.30
0.25
0.20
0.15
0.10
0.05
0.00
0
200
400
600
800
Cycles
0.2 mN
1.0 mN
5.0 mN

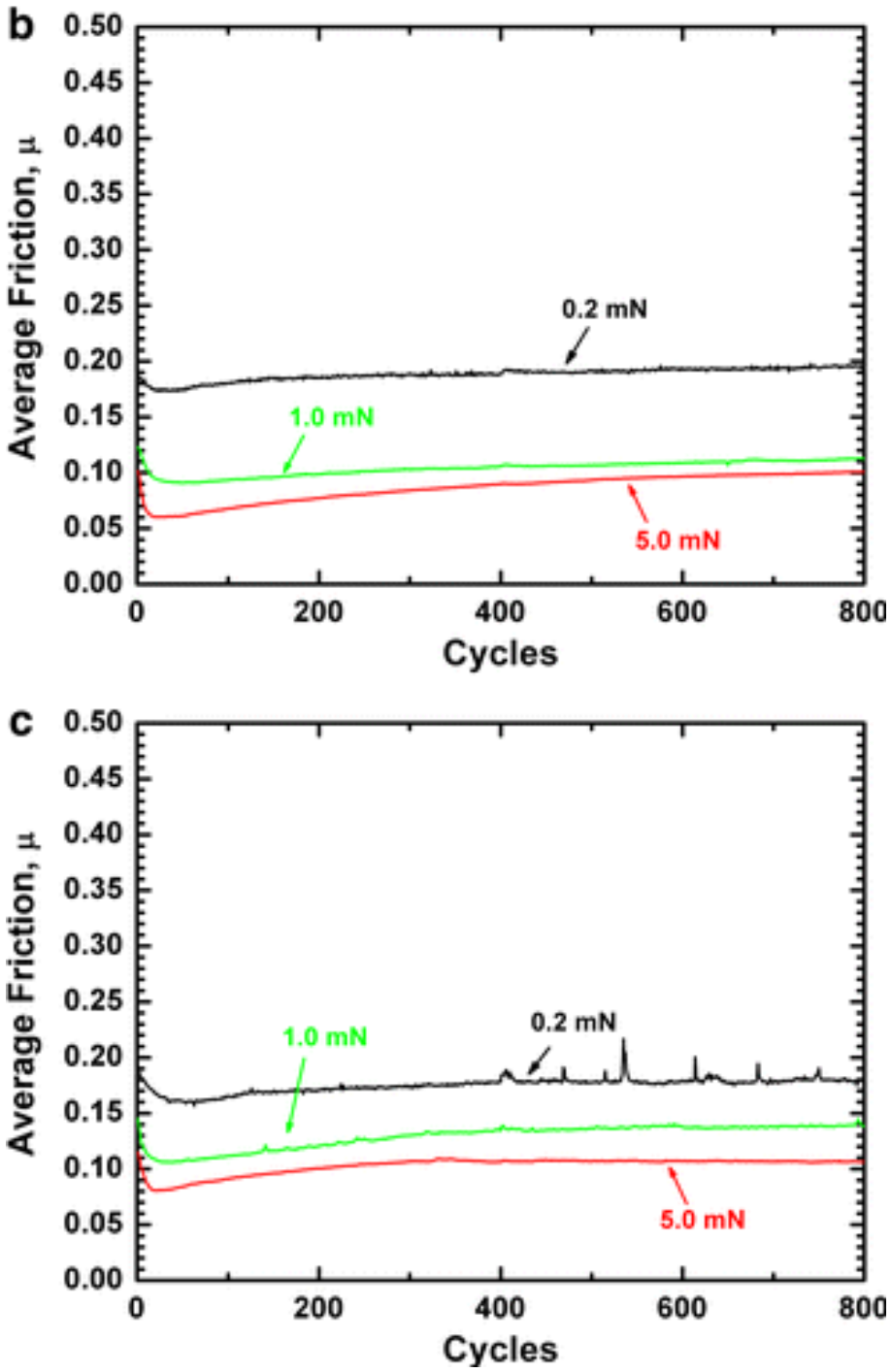

Figure. 5.3. Average coefficient of friction vs. cycle number for the 50μm using a normal load of 0.2mN, 1.0mN, and 5.0mN for (a) Pure MoS_2, (b) Au-MoS_2, and (c) Ti-MoS_2 [Contact Stress: 0.4 – 1.2GPa]

A different behavior in the coefficient of friction is observed with the 10 μm tip sliding against the MoS_2, Au-MoS_2, and Ti-MoS_2 samples (see Figures 5.4 (a), (b), and (c), respectively). The coefficient of friction does not decrease as significantly with increasing the normal load. In fact, the Au-MoS_2 sample reveals a higher friction coefficient with the highest normal load (see Figure 5.4 (b)). Furthermore, the MoS_2 sample shows an increase in the coefficient of friction with increasing the cycle number at the highest normal load (see Figure 5.4 (a)). Only the Ti-MoS_2 coating shows a similar, but not as significant, trend with the 10 μm tip (see Figure 5.4 (c)) when compared to the 50 μm tip (see Figure 5.3 (c)).

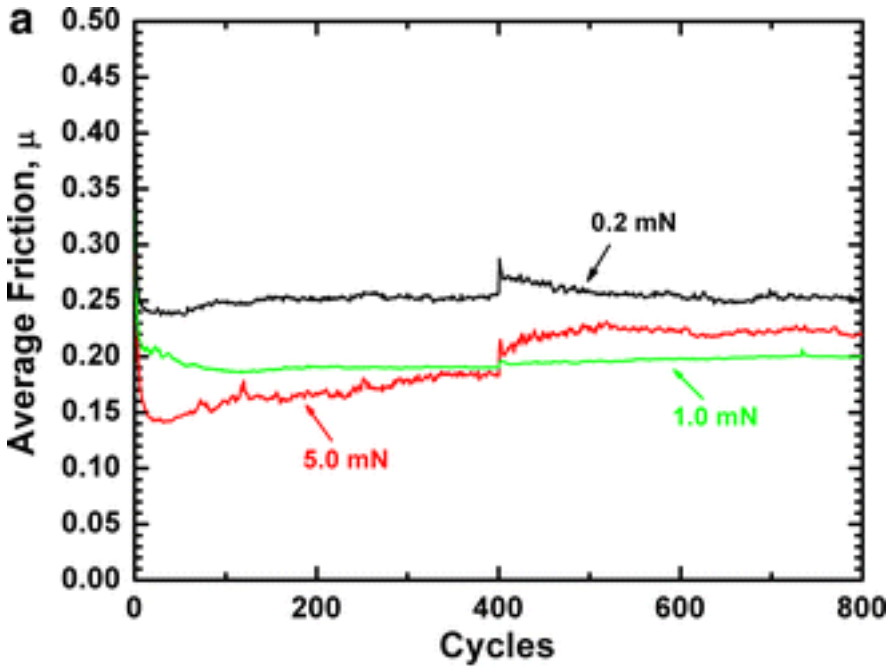

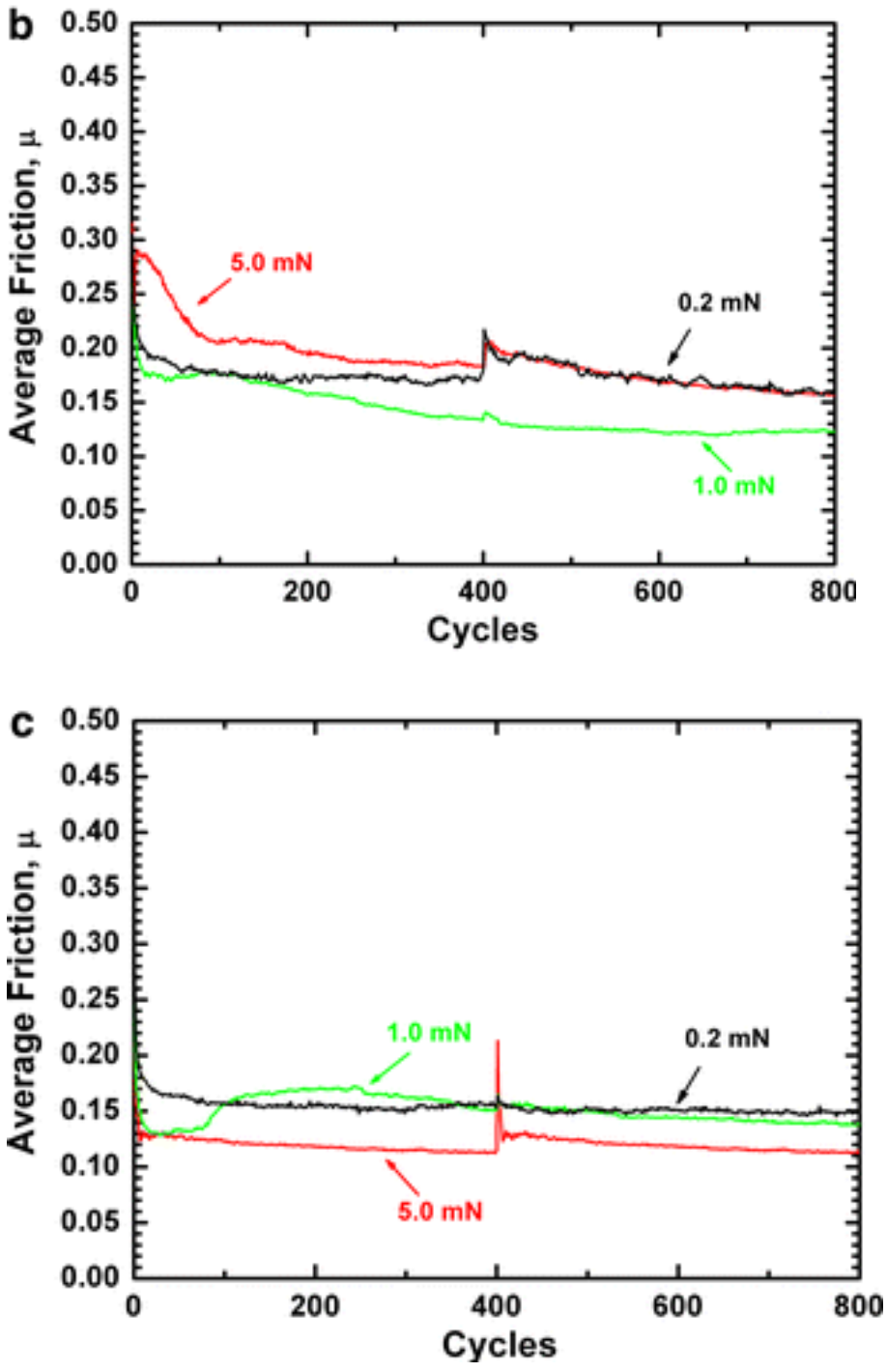

Figure 5.4. Average coefficient of friction vs. cycle number for the 10μm using a normal load of 0.2mN, 1.0mN, and 5.0mN for (a) Pure MoS_2, (b) Au-MoS_2, and (c) Ti-MoS_2 [Contact Stress: 1.2 – 3.5GPa]

Overall, higher coefficients of friction are observed with the MoS_2 coating compared to the coatings with Au or Ti. Figures 5.5 (a) and (b) show the difference in coefficient of friction between the metal containing coatings and the pure MoS_2 coating, calculated from averaging the last 100 cycles. The difference in coefficient of friction between the MoS_2 sample and the metal containing samples decreases with increasing the normal load for the 50 μm tip. However, with increasing normal load for the 10 μm tip, the differences in coefficients of friction remain relatively similar. In some instances, the comparisons made in Figure 5.5 are not representative of steady-state friction. That is, the friction coefficient for the MoS_2 sample never reaches steady state with the lowest normal load for the 50 μm tip, as it continuously increases throughout the whole test (see Figure 5.3 (a)).

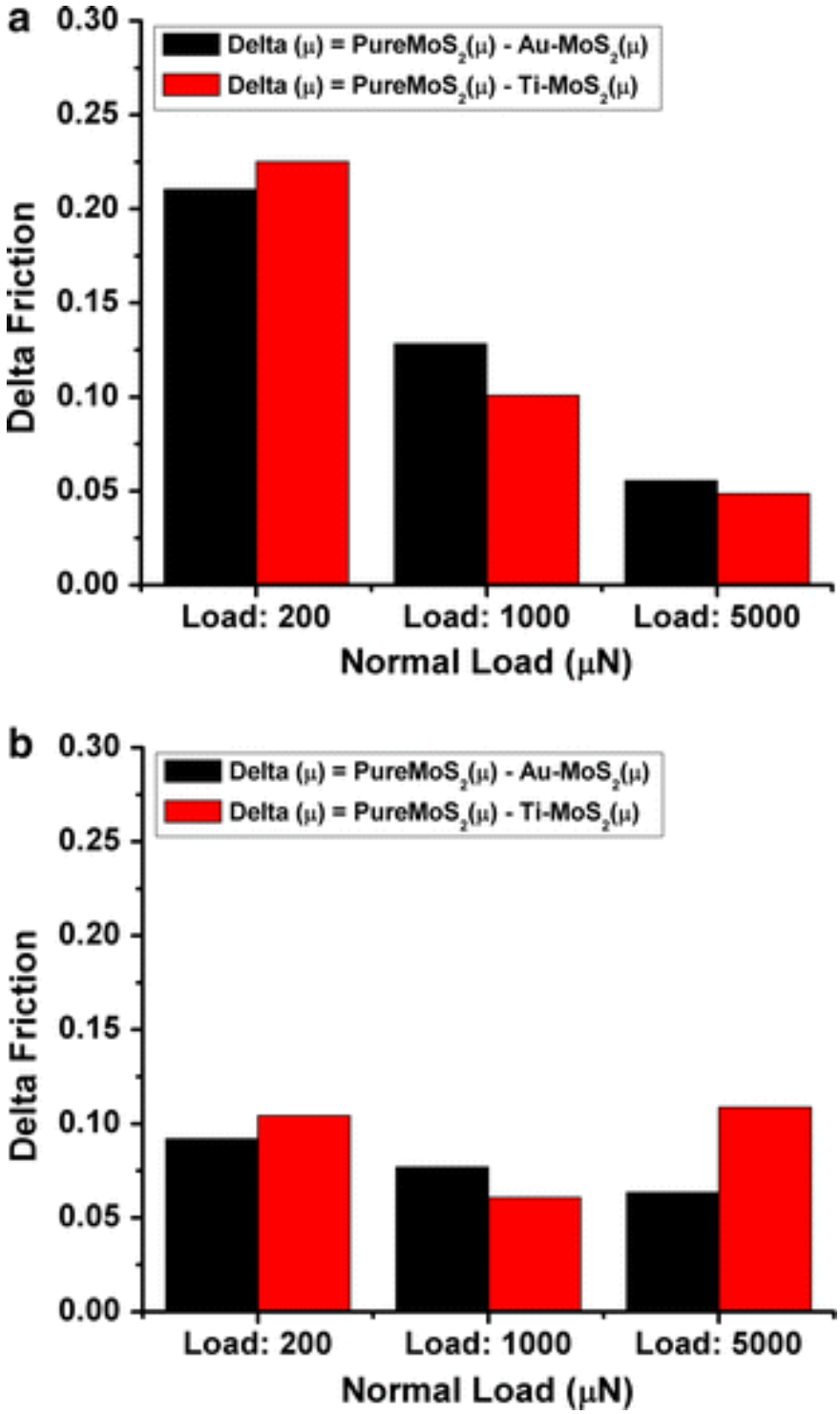

Figure 5.5. Delta Friction using (a) the 50μm Tip and (b) the 10μm Tip

5.4.3 Wear Results

Figure 5.6 (a) and (b) and (c) shows cross-sectional profiles of the wear tracks on the MoS_2, Au-MoS_2 and Ti-MoS_2 coatings, respectively. Results are provided for both tips, each at three different loads. In most cases, there is a clear trend of increasing wear depth and volume with increasing load. However, for the largest load with the 10 μm tip on the Au-MoS_2 coating, there are flat regions within the wear track that correspond to the Si substrate. Wear data for these instances of coating failure were not used for further analysis. Figures 5.7(a) and (b) show the wear volume for the 50 μm and 10 μm tip, respectively. The wear volume was plotted against the normal load, which varies between 0.2 and 5.0 mN. This corresponds to an initial Hertzian contact pressure between 0.4 and 1.2 GPa for the 50 μm tip and between 1.2 and 3.5 GPa for the 10 μm tip. For normal loads up to 1.0 mN with the 50 μm tip, very little wear is observed with the metal containing samples. In comparing to the MoS_2 coating, a magnitude in the wear volume similar to that for the coatings with Au and Ti was observed at the lowest loads (i.e. 0.2 and 0.5 mN). However, with the higher normal loads / contact pressures, the wear volume for the MoS_2 sample shows a linear increase when using the 50 μm tip, as seen in Figure 5.7 (a).

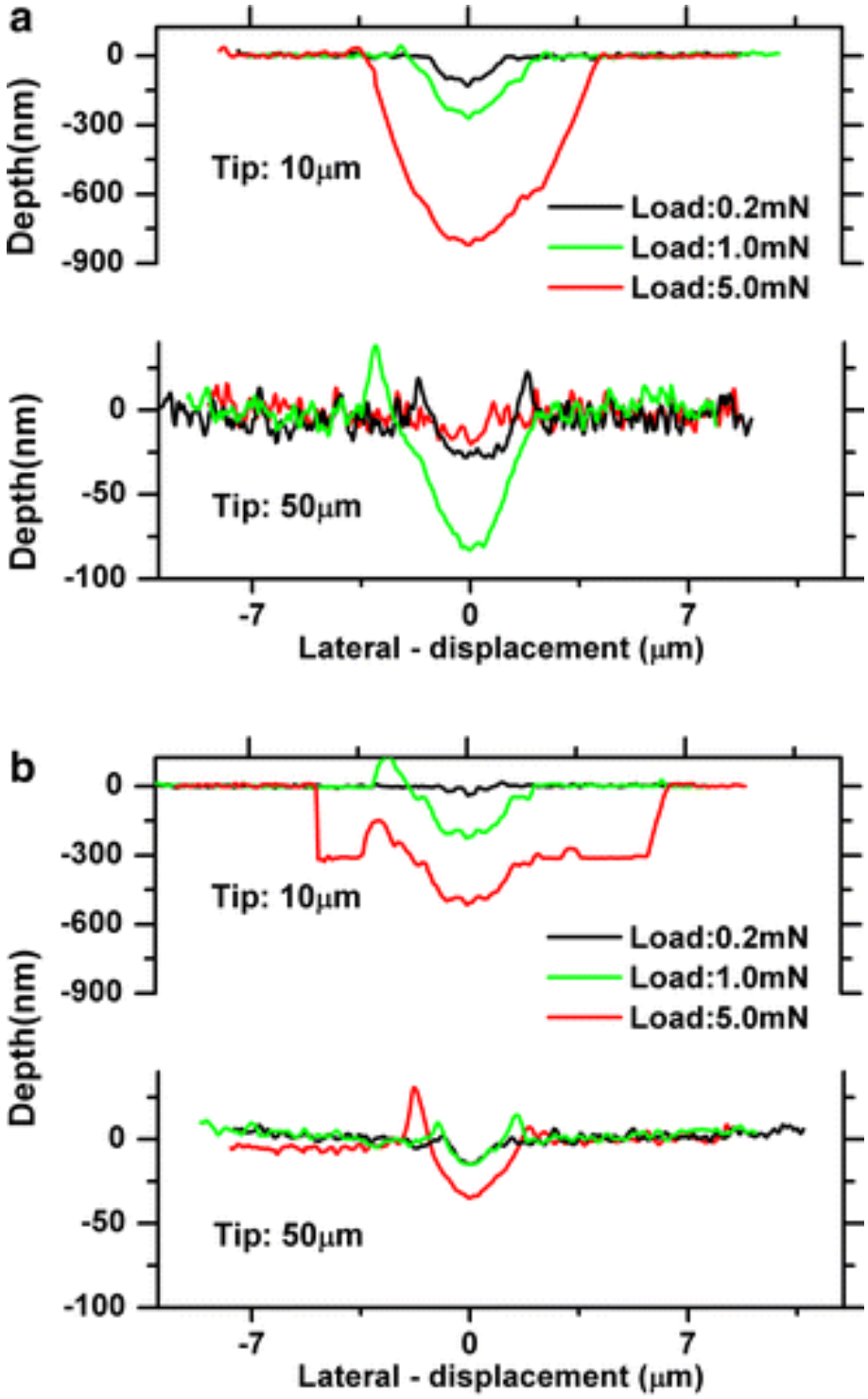
a
Depth(nm)
0
-300
-600
-900
Tip: 10μm
Load:0.2mN
Load:1.0mN
Load:5.0mN
Depth(nm)
0
-50
-100
Tip: 50μm
-7
0
7
Lateral - displacement (μm)
b
Depth(nm)
0
-300
-600
-900
Tip: 10μm
Load:0.2mN
Load:1.0mN
Load:5.0mN
Depth(nm)
0
-50
-100
Tip: 50μm
-7
0
7
Lateral - displacement (μm)

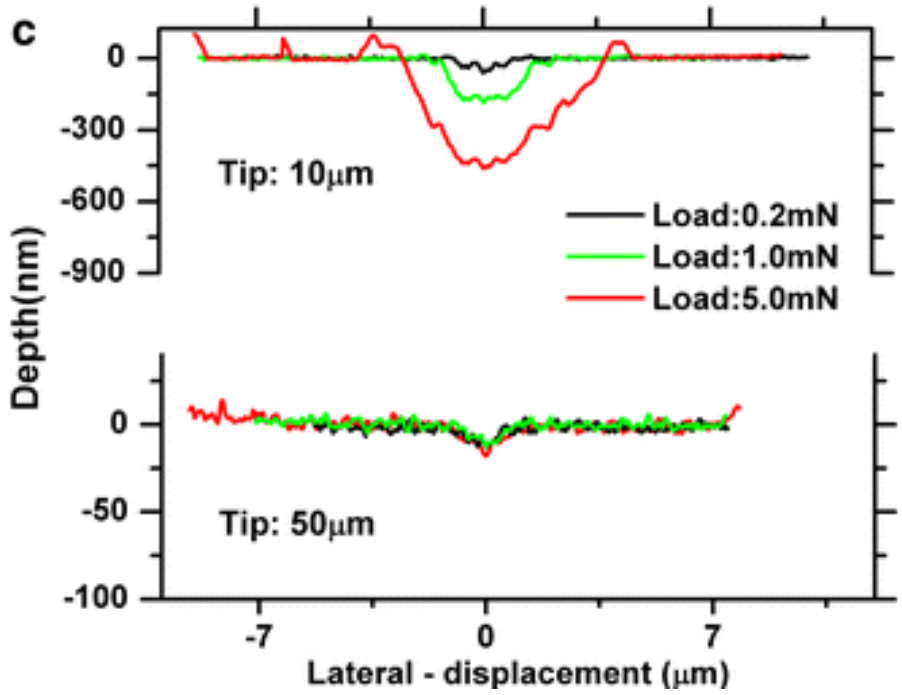

Figure 5.6. Cross-sectional plots of the wear tracks, which were created using normal loads of 0.2mN, 1.0mN, and 3.0mN and a tip radius of 10μm and 50μm on (a) Pure MoS_2, (b) Au-MoS_2, and (c) Ti-MoS_2 coatings.

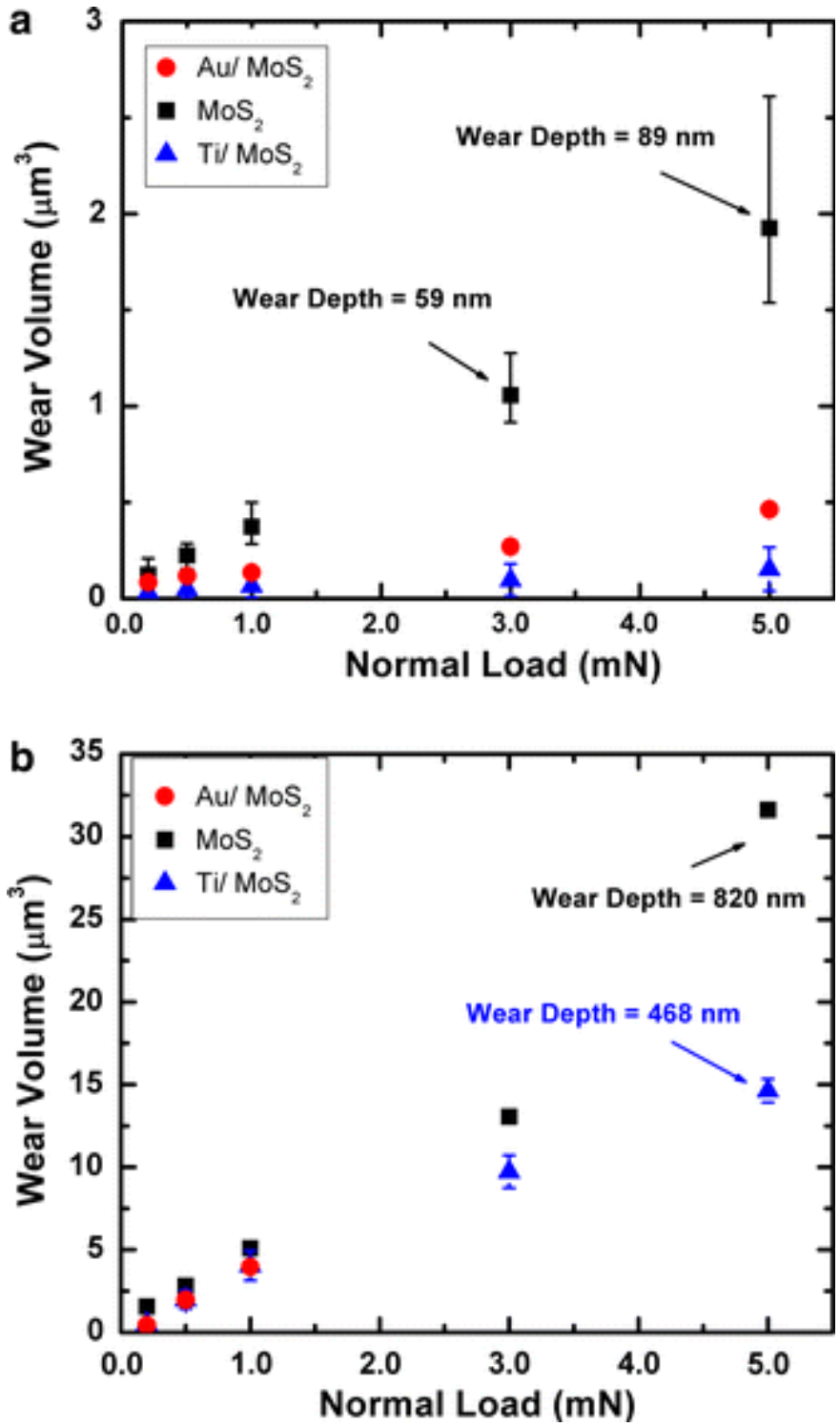

Figure 5.7. Wear volume vs. normal load for the (a) 50m tip and (b) 10m tip.

The 10 μm tip shows a different behavior in the wear volume, as shown in Figure 5.7 (b). For all samples, an increase in the wear volume is observed with increasing the normal load / contact pressure. Furthermore, with the highest contact pressure, the MoS_2 sample reveals the highest wear. It should be noted that for the highest contact pressure, the wear depth on the MoS_2 coating is higher than the actual coating thickness, indicating that the tip is sliding on the substrate. However, in Figure 5.6 (a), one can see that the substrate is not exposed in the same way as for the thinner Au-MoS_2 coating for the same sliding conditions.

5.4.4 Surface Characterization and Adhesion Measurements

Figure 5.8 shows the pull-off force measured for the three different coatings. The highest pull-off force was seen with the pure MoS_2 coating followed by the Au-MoS_2 sample. The smallest pull-off force was seen with the Ti-MoS_2 sample.

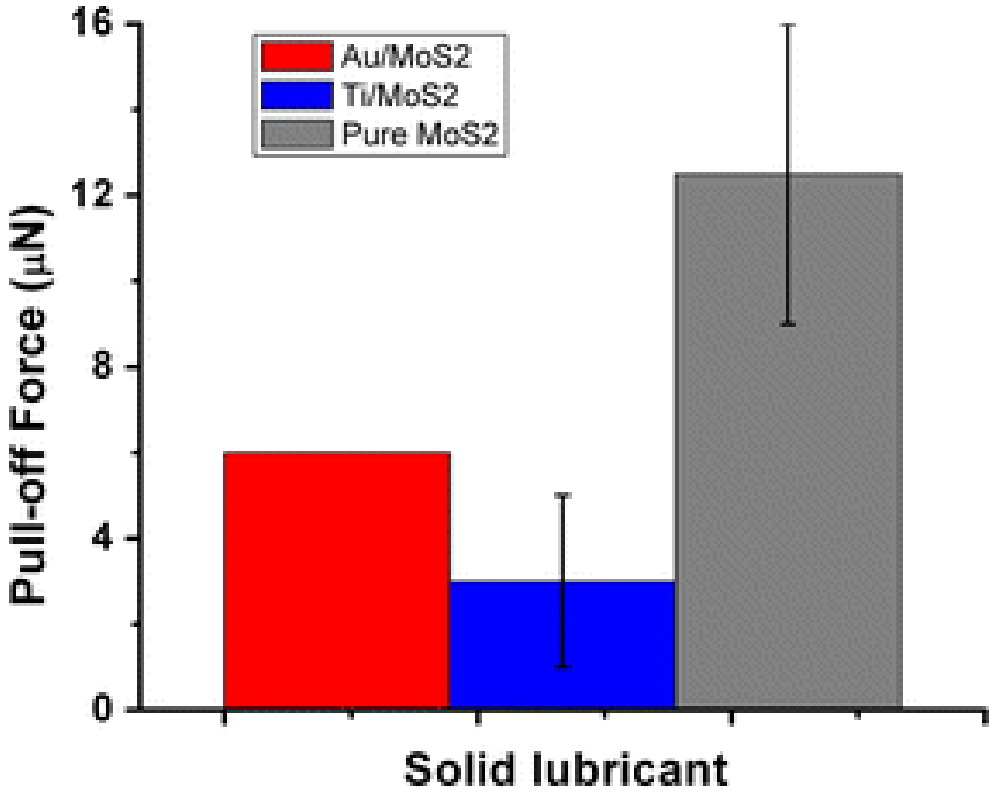

Figure 5.8. Pull-off force measurements on the three different coatings.

Figure 5.9 (a) shows the film characterization of the worn surface using a Raman microscope for 10μm tip using a normal load of 1.0mN. For all three coatings, the MoS_2 peaks observed for the worn surface are more distinct than prior to sliding (c.f. Figure 5.2). Similar results were obtained for the 10μm tip using a normal load of 0.2 mN (see Figure 5.9 (b)). However, the peaks for the Au-MoS_2 coating remained rather indistinct for this sliding condition. For sliding with the 50μm tip on the Au-MoS_2 sample and using a normal load of 5.0 mN, evidence of MoS_2 tribofilm formation was seen in as few as 20 cycles (see Figure 5.9 (c)).

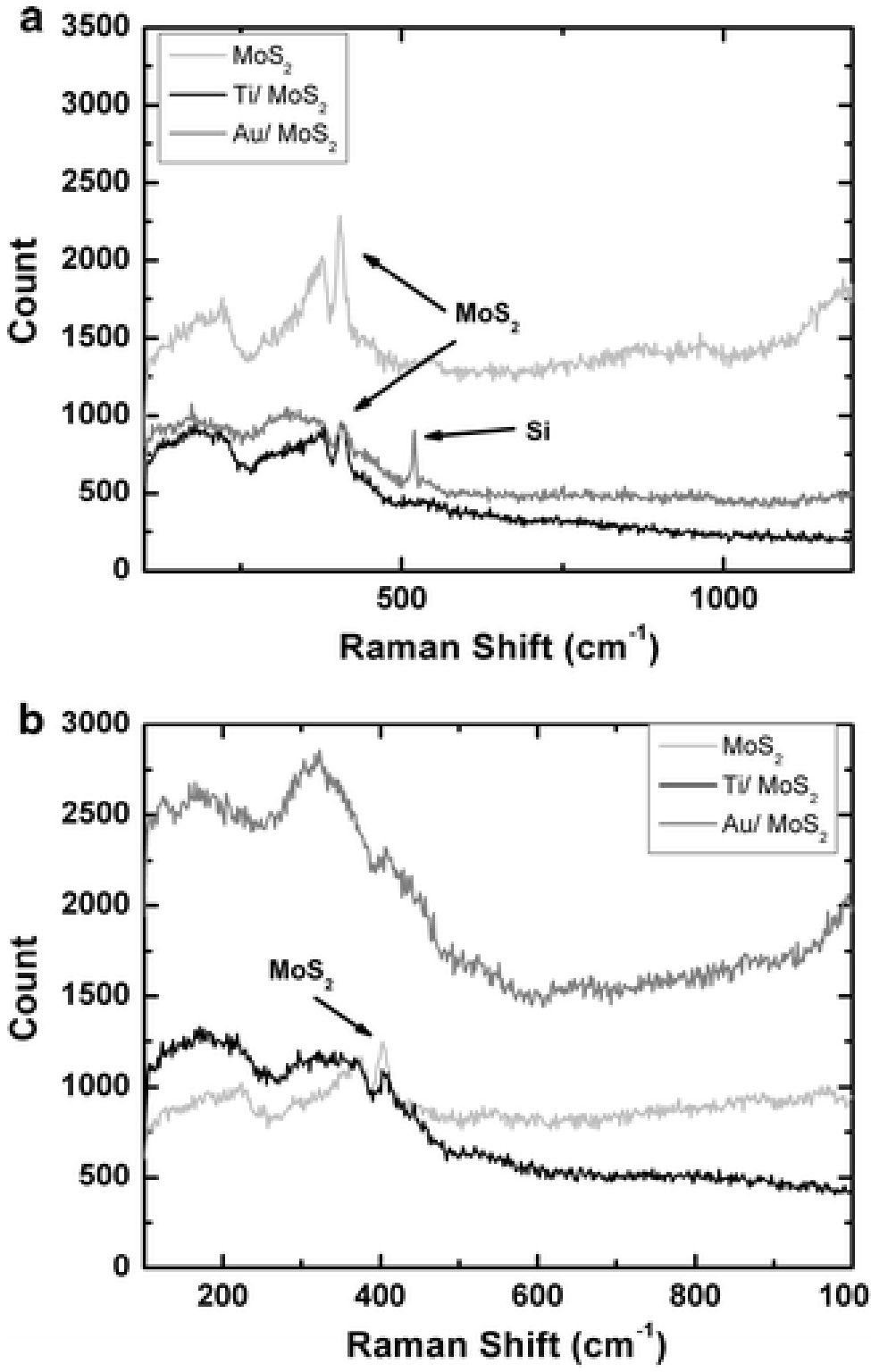
a
MoS2
Ti/ MoS2
Au/ MoS2
Count
MoS2
Si
Raman Shift (cm-1)
b
MoS2
Ti/ MoS2
Au/ MoS2
Count
MoS2
Raman Shift (cm-1)

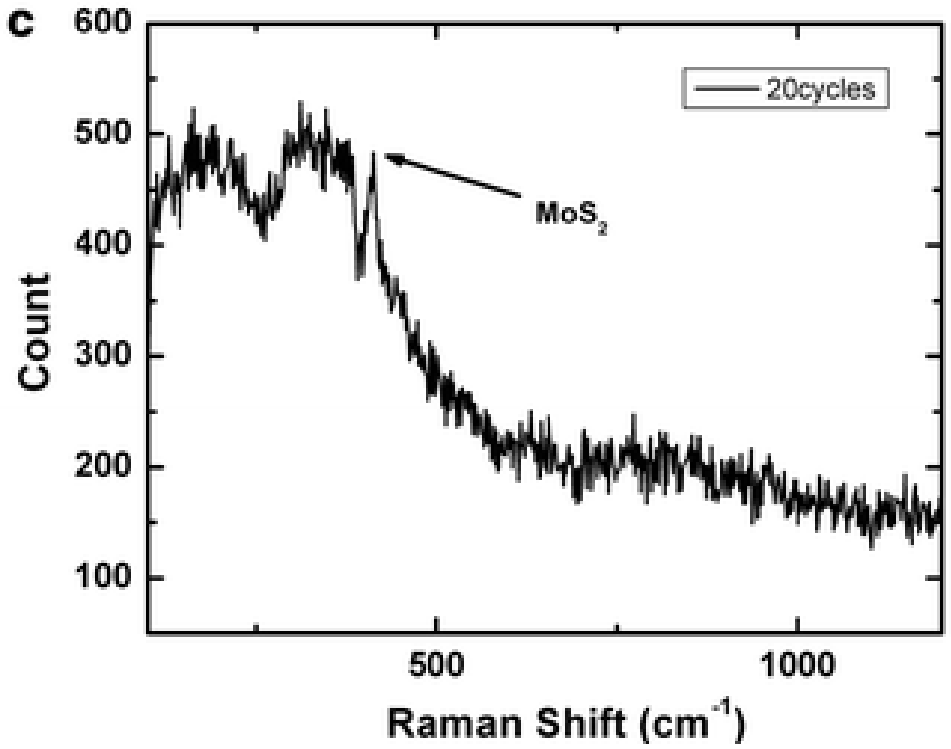

Figure 5.9. Film characterization of the worn surface using a Raman microscope for the (a) 10μm tip using a normal load of 1.0mN, (b) 10μm tip using a normal load of 0.2mN, and (c) 50μm tip on the Au-MoS_2 coating using a normal load of 5.0mN after 20 cycles. Micro Raman scans show bands which are consistent with crystalline MoS_2 for all samples. Crystalline MoS_2 is also seen by as few as 20 cycles.

5.5. Discussion

In comparing the performance of Ti-MoS_2 and Au-MoS_2 coatings to the pure MoS_2 coatings, it is first relevant to compare to macrotribology results in the literature [25-27,29]. Generally, metal is added to MoS_2 to enhance the mechanical and tribological properties, especially in the regime of higher relative humidity. Simmonds and co-workers studied the tribology of both Au-MoS_2 [29] and Ti-MoS_2 [25] coatings in 50% RH with an initial contact stress of 1 GPa. For Au-MoS_2 coatings with a similar Au content to those studied here, they observed a reduction of the friction

coefficient from 0.17 to 0.15 as compared to pure MoS_2 and an increase in the endurance. For Ti-MoS_2 coatings with a similar Ti content to those studied here, they observed a reduction of the friction coefficient from 0.18 to 0.07 as compared to pure MoS_2. Zabinski, et al. [26] studied Au-MoS_2 coatings with pin-on-disk tribometry with a initial contact stress of 0.98 GPa and found a reduction in the friction coefficient compared to pure MoS_2 in both dry (3-5% RH) and ambient conditions. For the coatings studied here, previous macrotribology research on Au-MoS_2 [23] and Ti-MoS_2 [24,28] demonstrated friction reduction and increase in endurance compared to pure MoS_2 The magnitude of the friction reduction in microtribology (c.f. Figure 5.5) was found to be similar to the macrotribology results. For a load of 5.0 mN on the 50 μm tip and 0.2 mN on the 10 μm tip, the initial contact stress is 1.2 GPa, similar to the stress in the macroscopic studies. The reduction in friction coefficient observed here is between 0.05 and 0.1. Despite the significant differences in %RH, this result compares favorably to those of Simmonds and co-workers [25,29], who saw a reduction in friction of 0.02 for Au-MoS_2 and 0.11 for Ti-MoS_2. Zabinski, et al. [26] observed a reduction in friction of 0.03 in dry conditions for Au-MoS_2 compared to pure MoS_2. Thus, a similar friction reducing capability of metal doping of MoS_2 is also observed for microtribology. Without running longer tests, it is not clear whether the same can be said for the effect on coating endurance. However, the wear for the Ti-MoS_2 and Au-MoS_2 coating were consistently less when compared to pure MoS_2 (c.f. Figure 5.7), especially at higher contact stresses.

Other observations of the microtribology experiments on MoS_2 and metal doped MoS_2 coatings showed both additional similarities and some subtle differences to macrotribology. The steady

state friction force (i.e. 800th cycle) was plotted against the normal force in log-log plots, Figures 5.10(a) and (b) for the 50μm and 10μm tip, respectively. A linear fit was conducted on the results according to $F \alpha L^m$, where m is the slope of the fit in the log-log scale. The linear fit showed that the m value was 0.94, 0.89 and 0.94 when using the 10μm tip and 0.78, 0.79, and 0.84 when using the 50μm tip for the MoS_2, Au-MoS_2, and Ti-MoS_2, coatings respectively. This indicates that with the 10μm tip, all three coatings show higher m values when compared to the 50 μm tip. Furthermore, when using the 50μm tip, the MoS_2 coating follows the relationship of $F \alpha L^{0.78}$, which is closer to $F \alpha L^{2/3}$ when compared to the other two coatings and the 10 μm tip. The Hertzian behavior of $F \alpha L^{2/3}$ has been previously observed in macrotribology studies of MoS_2 coatings by Singer et al. [41-42] and by several other authors [30,43]. The higher m values with the 10 μm tip can be explained by the difference in the tip shape, as seen in Figures 5.2 (a) and (b). The difference between the actual area function (i.e. measured using an AFM) and the ideal area function (i.e. ideal shape of a sphere) of the 10 μm tip is greater than the 50 μm tip. The 10 μm tip deviates from a spherical shape, which can cause a different F to L relationship. It has previously been shown that even small deviations from a spherical tip shape can result in increasing m values as high as one [44], as seen in our case with the 10 μm tip.

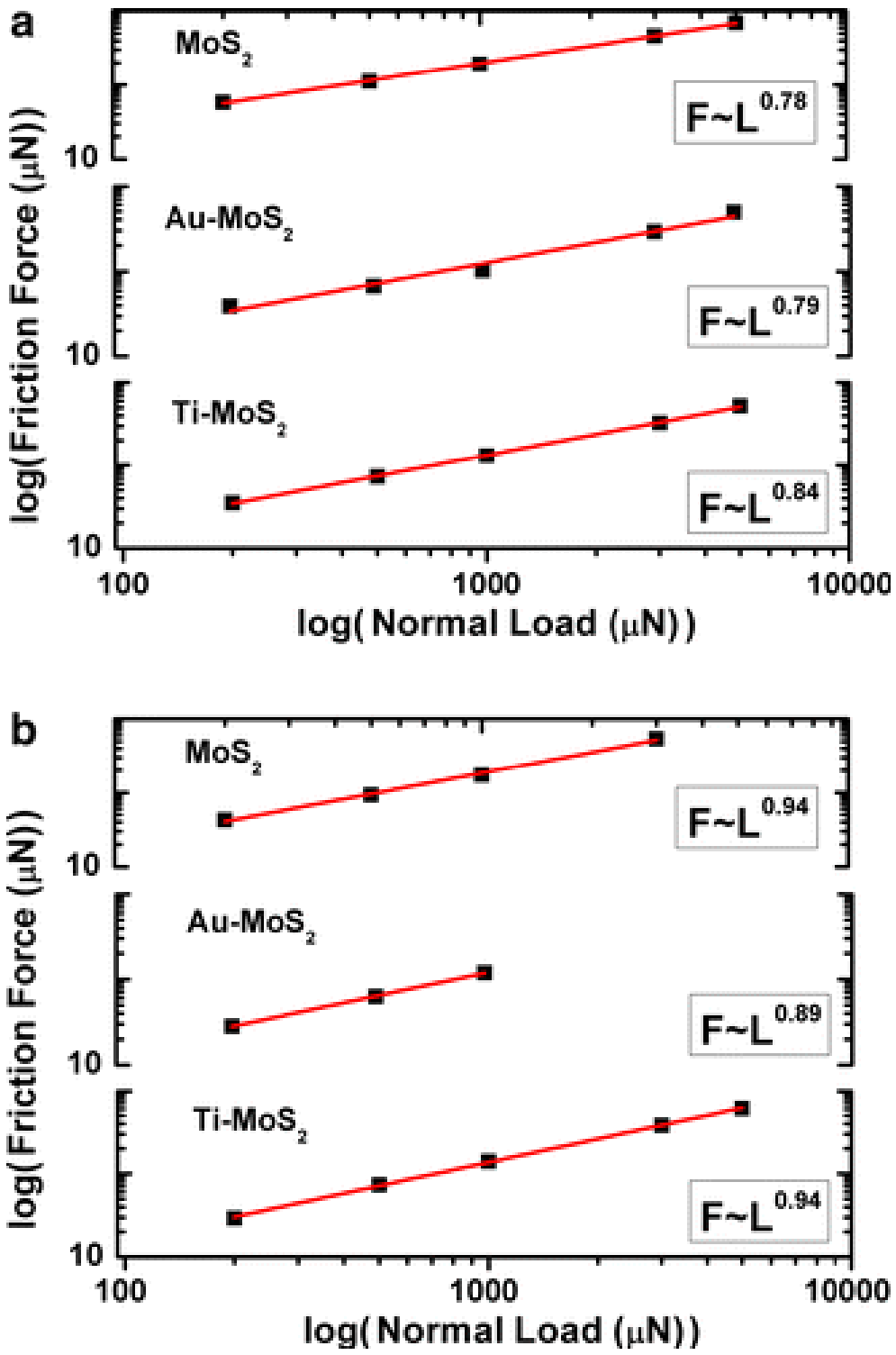

Figure 5.10. Friction Force vs. Normal Load for (a) the 50μm tip and (b) the 10μm tip for sputtered MoS_2 sample and co-sputtered Au-MoS_2 sample and co-sputtered Ti-MoS_2 sample

As described in the literature [41,43,45-46], the shear strength has a pressure dependence which can be approximated by

$$S = S_o + \alpha P \qquad \text{Eq. 5.1}$$

where S_o is the interfacial shear strength (Velocity Accommodation Parameter), P is the mean pressure of the contact, and α represents the limiting coefficient of friction [41]. This equation is often cast in terms of the coefficient of friction, μ, such that

$$\mu = S_o/P + \alpha \qquad \text{Eq. 5.2}$$

Thus, from Eq. 5.2, the coefficient of friction is inversely proportional to the pressure. This behavior was also confirmed when plotting the steady state friction coefficient (800^{th} cycle) vs. inverse pressure for the 50 μm tip on the MoS_2, Au-MoS_2, and Ti-MoS_2 coatings (see Figures 5.11 (a), (b), and (c), respectively). The pressure for this plot was calculated at the steady state condition (800^{th} cycle) using the normal force divided by the projected area of the tip. The area was determined from the results of the pixel counting algorithm of AFM images (see Figure 5.1). The value of the tip area at the 800^{th} cycle was calculated using the elastic depth, which was obtained from the difference in the normal displacement of the post scan (i.e. 3^{rd} phase of the sliding experiment) and the last sliding cycle.

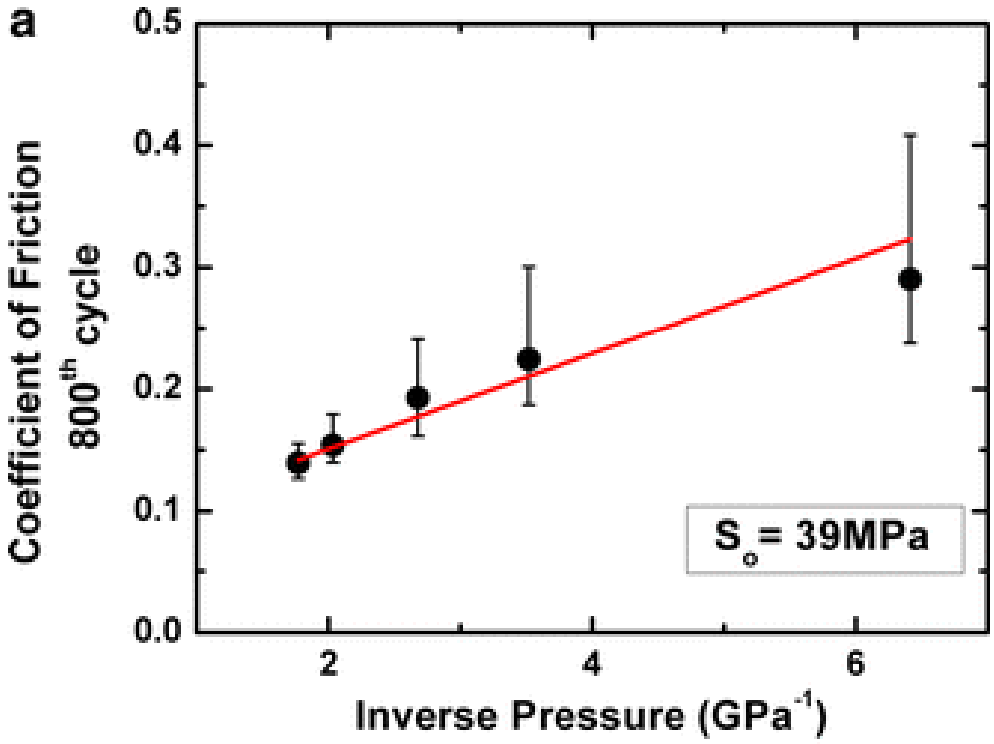
a
Coefficient of Friction
800th cycle
0.5
0.4
0.3
0.2
0.1
0.0
2
4
6
Inverse Pressure (GPa-1)
So = 39MPa

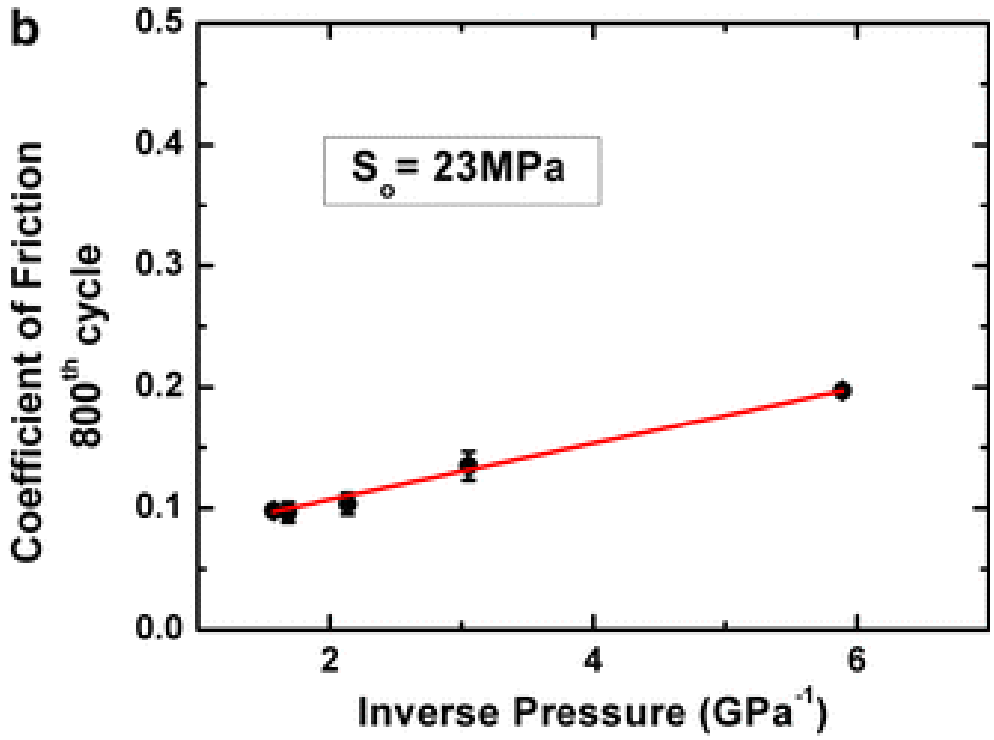
b
Coefficient of Friction
800th cycle
0.5
0.4
0.3
0.2
0.1
0.0
2
4
6
Inverse Pressure (GPa-1)
So = 23MPa

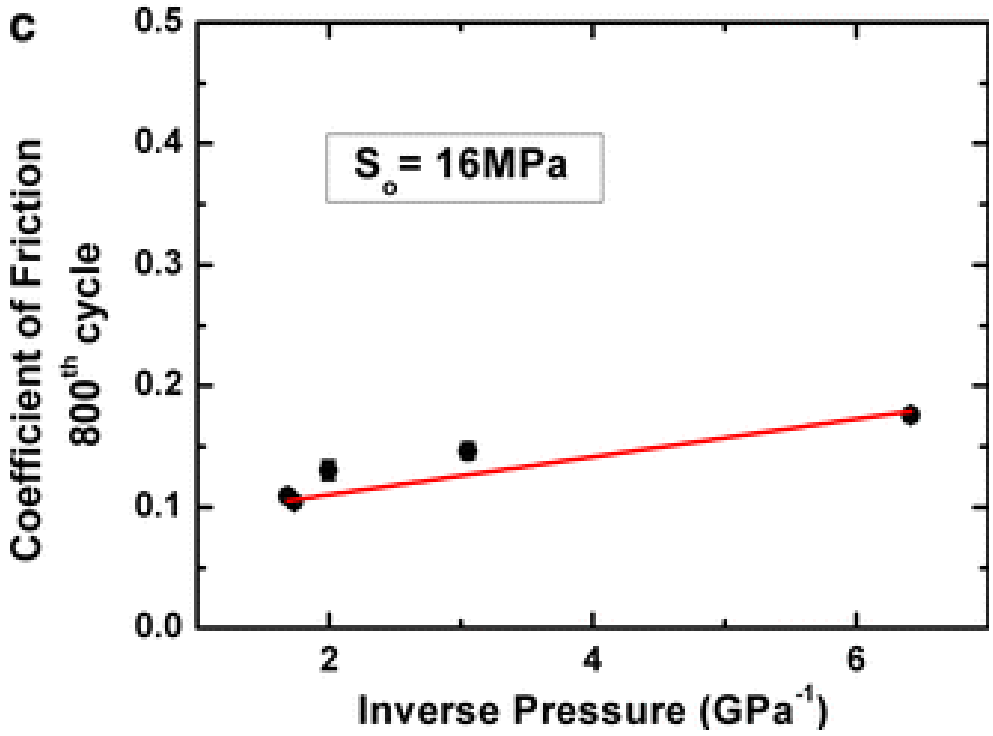

Figure 5.11. Coefficient of friction vs. inverse pressure using the 50μm for (a) sputtered MoS_2 sample and (b) co-sputtered Au-MoS_2 sample and (c) co-sputtered Ti-MoS_2 sample. Linear fit was performed on each coating and the slope ($\mathbf{S_o}$) and intercept (**a**) were obtained following the equation of $\boldsymbol{\mu = S_o/P + \alpha}$**.** The contact pressure is calculated at the 800th cycle using the actual area function of the tip.

Least square fit of a straight line was performed on each sample for the 50 μm tip, shown in Figure 5.11 (a), (b), and (c). Reasonable fits were not obtained for the 10 μm tip (not shown). This may be explained by the fact that not enough data points were used, because the tip was often in contact with the substrate at the higher normal loads. Furthermore, the higher contact pressures obtained with the 10 μm tip could also result in higher plowing, which leads to difficulty in measuring the actual contact area.

The fit with the 50 μm tip revealed a mean slope (S_o) and an intercept (α) for each sample, and the values are summarized in Table 5.2. The velocity accommodation parameter, S_o, decreases with the addition of metal to MoS_2. Also, the mean slope S_o shows the lowest value (15MPa) with the Ti content sample when compared to the other two samples (39MPa and 23MPa for the MoS_2 and the Au-MoS_2 samples, respectively). The y-intercept, α, showed similar values for all three coatings (see Table 5.2.). The lower S_o values for the Ti and Au coating compare favorably with S_o values obtained in macrotribology, for MoS_2 coatings, at low relative humidity levels [42] where low friction values were observed. The value for the pure MoS_2 coating is slightly higher than typically observed [41]. Considering that the higher wear at the larger normal loads for the MoS_2 coating may be affecting this analysis, a fit was conducted to the three data points for the lower normal loads. This results in a shear strength of 26 MPa, but with much higher uncertainty due to the large scatter in friction data for the lowest loads on the MoS_2 coating. Thus, we believe that the pure MoS_2 did give a similar response at the lower loads to the other coating and similar shear strength to the literature on macroscopic contacts on MoS_2.

Table 5.2. Microtribological properties summary for testing with the 50μm tip

	Wear Volume (μm^3) [L: 3.0/5.0mN]	**S_o (MPa)**	**α**	**Friction(μ) [L: 3.0/5.0mN]**	**Friction Force**
MoS_2	1.1/1.9	39 (±6)	0.07(±0.01)	0.15/0.14	$F \propto L^{0.78}$
Au-MoS_2	0.3/0.5	23.2 (±0.4)	0.061(±0.002)	0.10/0.10	$F \propto L^{0.79}$
Ti-MoS_2	0.1/0.2	15 (±3)	0.079(±0.006)	0.11/0.10	$F \propto L^{0.84}$

Further examination of data in Table 5.2. allows for comparisons of the hardness, velocity accommodation parameter (S_o), wear volume, coefficient of friction, and friction force relationship with normal load. In terms of the relationship between the friction force and the normal force (i.e. $F \alpha L^m$) the pure MoS_2 sample shows the closest value to 2/3, when compared to the two other coatings. However, the *m* value for the metal doped samples is very similar to the *m* value of the pure MoS_2 sample. Also, the limiting friction is similar for all coatings, and S_o is, in all cases, low and relatively comparable to measurements at macroscopic length scales [30,41-43]. However, the hardness was observed to increase with the addition of metal to MoS_2, and the highest hardness value was obtained with the Ti content sample followed by the Au-MoS_2 coating. This can be directly correlated with the wear volume of the three different coatings. The wear volume decreases with the addition of metal to MoS_2 and therefore decreases with increasing the hardness. As seen with the hardness values, the highest wear resistance is also observed with the Ti content sample.

While the wear resistance of a coating can sometimes simply be explained by the hardness, further analysis of the wear mechanisms was carried out using a modified version of the technique of Kuster and Schiffmann [16]. In their method, the wear contribution is separated into two components and directly correlated to the total depth during a sliding process, which consists of three contributions: elastic deformation, plastic deformation, and material loss. Kuster and Schiffmann [16] used three depth values in order to calculate each wear contribution; the depth after the initial loading (D_{IL}), the depth under normal load after the last cycle of the test (D_{LC}),

and the residual depth after unloading measured from the end scan (D_{RD}). Using these measurements the following equations can be derived:

$$\text{Elastic deformation} = D_{LC} - D_{RD}, \quad \text{Eq. 5.3}$$

$$\text{Material loss} = D_{LC} - D_{IL}, \quad \text{Eq. 5.4}$$

$$\text{Plastic deformation} = D_{RD} - [\text{Material loss}] = D_{RD} - (D_{LC} - D_{IL}), \quad \text{Eq. 5.5}$$

We used a slightly modified version of this method because it was difficult to measure the wear depth from the end scan of the sliding test (due to thermal drift and material pile up at the end of the wear track). Thus, the value of D_{IL} was calculated using the elastic-plastic wear depth from an indentation test and the value of D_{RD} was calculated using the wear depth obtained with an AFM.

The different depth contributions versus the normal loads for the 50 μm tip are plotted in Figure 5.12 (a), (b), and (c) for the pure MoS_2, Au-MoS_2, and Ti-MoS_2 coatings, respectively. The highest plastic deformation is observed with the pure MoS_2 coating, which can be explained by the lower hardness value. The Au and Ti content samples show similar contribution of plastic deformation to the wear, which is a smaller when compared to the one of the pure MoS_2 sample. However, the material loss is slightly higher with the Au content sample when compared to the Ti content sample and the highest contribution of material loss to the total wear is seen with the pure MoS_2 sample. For those loads that could be analyzed for the 10 μm tip, similar results were observed (see Figures 5.13 (a), (b) and (c) for the pure MoS_2, Au-MoS_2, and Ti-MoS_2 coatings, respectively).

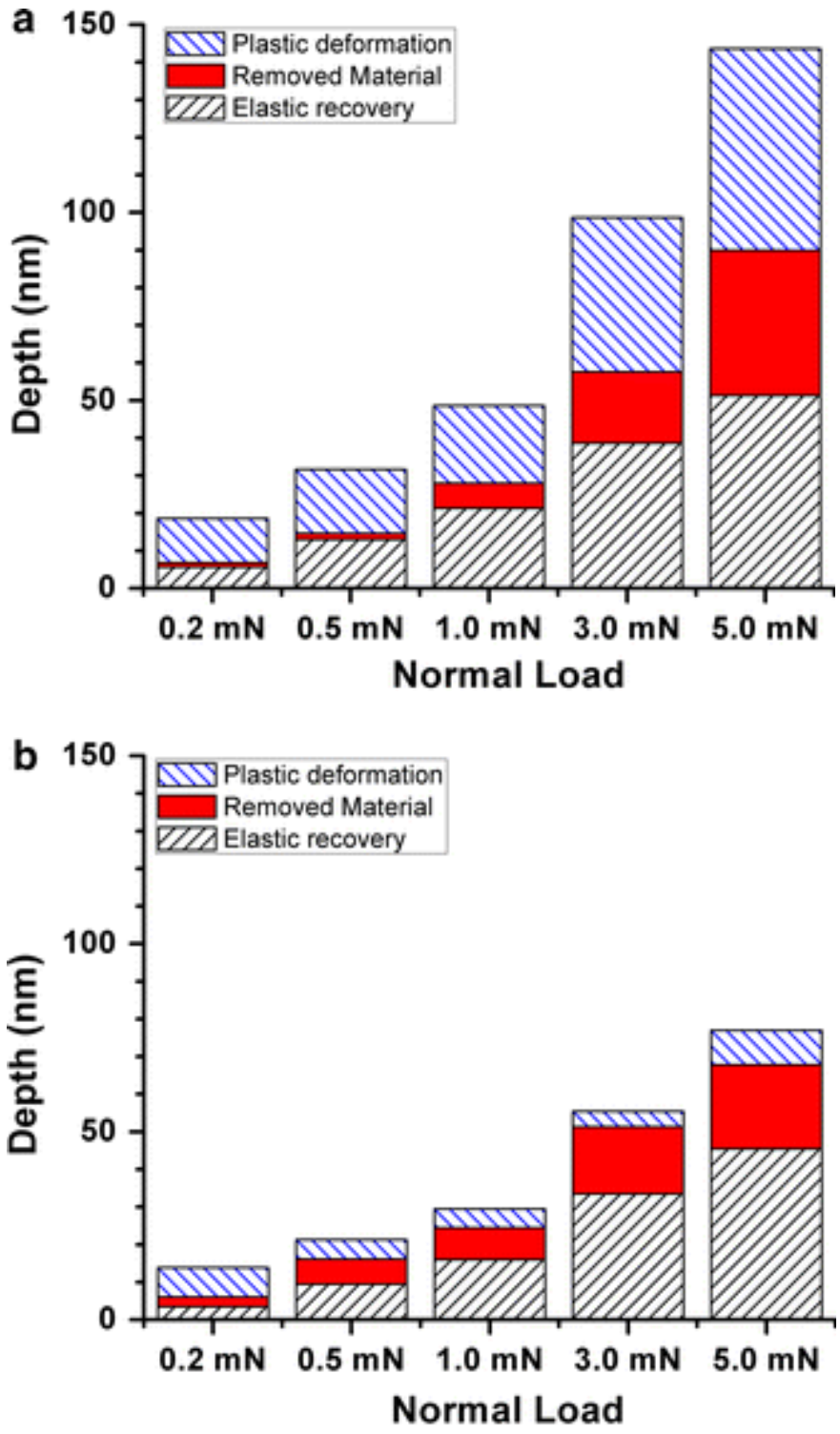
a
150
100
50
0
Depth (nm)
Plastic deformation
Removed Material
Elastic recovery
0.2 mN
0.5 mN
1.0 mN
3.0 mN
5.0 mN
Normal Load
b
150
100
50
0
Depth (nm)
Plastic deformation
Removed Material
Elastic recovery
0.2 mN
0.5 mN
1.0 mN
3.0 mN
5.0 mN
Normal Load

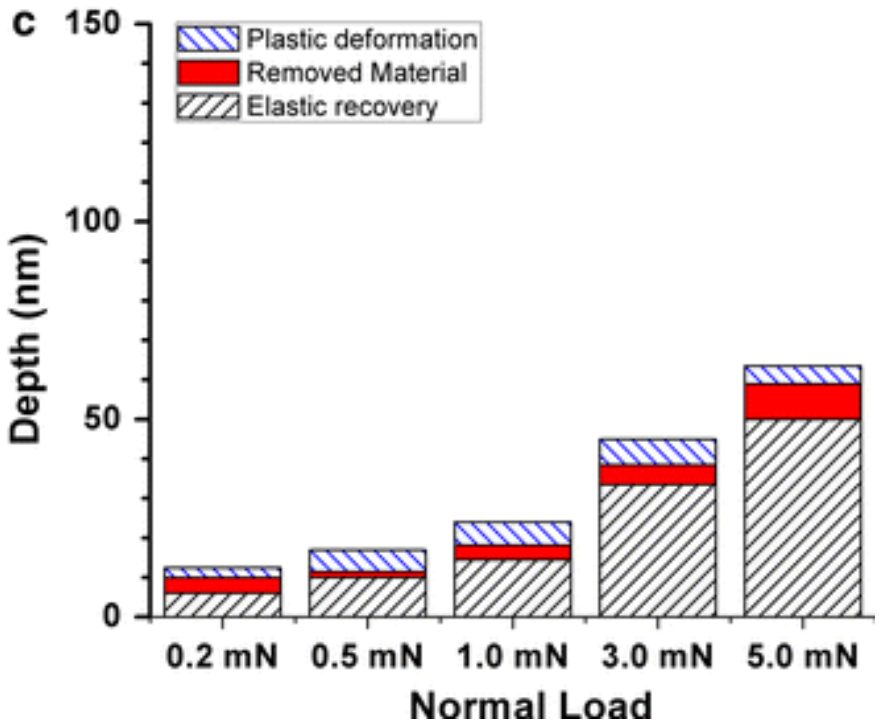

Figure 5.12 – Depth contribution during a sliding test using the 50 μm tip for (a) pure MoS_2, (b) Au-MoS_2, and (c) Ti-MoS_2

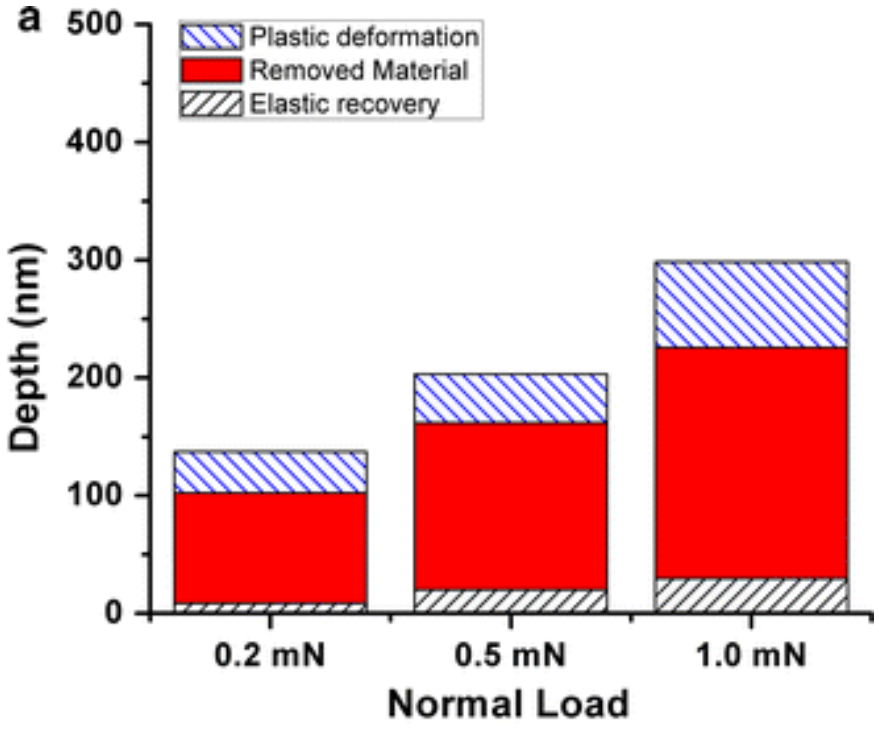

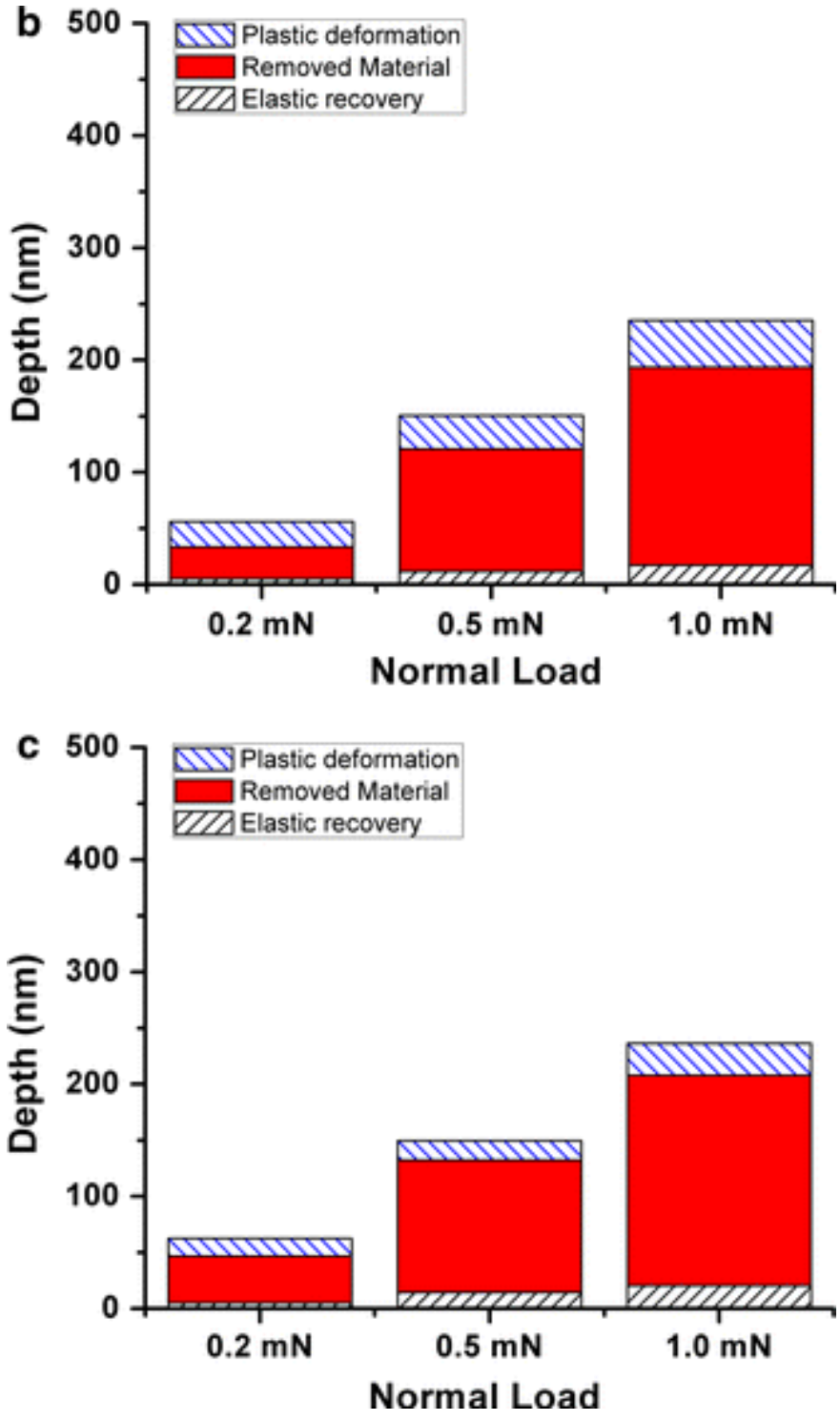

Figure 5.13 – Depth contribution during a sliding test using the 10 μm tip for (a) pure MoS_2, (b) Au-MoS_2, and (c) Ti-MoS_2

The removed material can be correlated to either plowed material or adhesive wear. While some plowing must occur during our tests, our steady-state analysis for the 50 μm tip revealed a nearly Hertzian relationship between the friction and the normal load. The small deviation from $L^{2/3}$, while possibly attributable to tip shape, may also be due to adhesion. Thus, differences in material loss might be also due to differences in the surface adhesion. As seen in Figure 5.8, the highest pull-off force was seen with the pure MoS_2 coating followed by the Au-MoS_2 sample and the smallest pull-off force was seen with the Ti-MoS_2 sample. Thus, if adhesive wear is part of the material loss, these measurements help to explain the trend in wear resistance of the coatings. The adhesion measurements are also consistent with the velocity accommodation parameter, S_o, which shows the same trend with decreasing interfacial shear strength from MoS_2 to Au-MoS_2 to Ti-MoS_2. It has been previously suggested that the S_o value represents a property of the interfacial shear strength between the transfer-film (i.e. MoS_2 transferred on the tip) and the tribofilm [41] (i.e. crystalline MoS_2 on the surface of the wear track), but could also include the shear strength of each film, depending on which velocity accommodation mode is active. The decrease in surface adhesion with the decrease in the S_o value may indicate that the metal doped samples form a uniform and stable transfer- and tribo- film, leading to lower interfilm shear strength.

It has been previously shown with macro- and nano- tribology [8,21], that a crystalline tribofilm is formed on the worn surface of the MoS_2 film, which contributes to a low shear stress and therefore a low coefficient of friction. This typically occurs in the run-in stage, where the basal planes become oriented in a parallel direction to the sliding path and transfer occurs to the

counterface. Similar behavior on the wear track may also be expected with microtribology. While the spectra presented in Figure 5.9 provide significant evidence of tribofilm formation on the wear track, additional experiments with Raman spectroscopy on the counterfaces revealed no peaks for MoS_2. Of course, a transfer film could be present that is either in such small quantity or such an amorphous state as to be undetectable by Raman spectroscopy. It should also be mentioned that while the evidence in Figure 5.9 was the predominant observation from the Raman studies, other tests revealed no peaks that would indicate tribofilm formation. Additional surface characterization experiments will be necessary to unambiguously determine the role of transfer films in microtribology on solid lubricant coatings such as those studied here.

5.6. Conclusion

The microtribological properties of co-sputtered Ti and Au with MoS_2 solid lubricants were investigated, with a wide range of contact pressures. It was observed that the small addition of Ti and Au to MoS_2 improved the tribological properties in dry air; the co-sputtered Ti and Au with MoS_2 solid lubricants showed lower friction and less wear compared to the pure MoS_2 coating. The improved tribological properties with metal additions were attributed to an increase in the mechanical properties, decrease in adhesion, and a decrease in the interfacial shear strength or "velocity accommodation parameter". The interfacial shear strength for the Ti and Au content samples was similar to literature values obtained at the macroscale, indicating a similar sliding behavior. This was also confirmed with the evidence of a tribofilm on the surface of the wear tracks, which was seen with Raman spectroscopy.

Acknowledgments

The authors gratefully acknowledge financial support from Fonds québécois de la recherche sur la nature et les technologies (FQRNT), program Établisssement de nouveaux chercheurs and Lorne Trottier for the graduate Fellowship (McGill Engineering Doctoral Award). This work was also supported under The Aerospace Corporation's Mission Oriented Investigation and Experimentation program, funded by the U.S. Air Force Space and Missile Systems Center under Contract No. FA8802-09-C-0001. The authors acknowledge Zachary Fishman for his collaboration with the Matlab code. The assistance of Francois Barthelet in conducting atomic force microscopy measurements is also gratefully acknowledged.

REFERENCES

1 B. Bhushan, Micro/NanoTribology and Micro/Nanomechanics of MEMS Devices, in: B. Bhushan (ed.), Handbook of Micro/Nano Tribology, CRC Press, Boca Raton, FL, pp. 797-834 (1999)

2 C. K. Bora, E. E. Flater, M. D. Street, J. M. Redmond, M. J. Starr, R. W. Carpick, and M. E. Plesha, Multiscale roughness and modeling of MEMS interfaces, Tribology Letters 19, 37-48 (2005)

3 F.W. Delrio, M.P. De Boer, J.A. Knapp, E.D. Reedy Jr, P.J. Clews, and M.L. Dunn, The role of van der Waals forces in adhesion of micromachined surfaces, Nature Materials 4, 629-634 (2005)

[4] M. T. Dugger, "Surface treatments for modifying the tribological behavior of microsystems," in World Tribology Congress III, American Society of Mechanical Engineers, New York, NY 10016, (2005), pp. 711-713

[5] M. G. Gee and A. D. Gee, A cost effective test system for micro-tribology experiments, Wear 263, 1484-1491 (2007)

[6] H. W. Liu and B. Bhushan, Adhesion and friction studies of microelectromechanical systems/nanoelectromechanical systems materials using a novel microtriboapparatus, Journal of Vacuum Science & Technology A 21, 1528-1538 (2003)

[7] M. Nosonovsky and B. Bhushan, Scale effect in dry friction during multiple-asperity contact, Transactions of the ASME. Journal of Tribology 127, 37-46 (2005)

[8] H. Kim and J. R. Lince, Direct visualization of sliding-induced tribofilm on Au/MoS_2 nanocomposite coatings by c-AFM, Tribology Letters 26, 61-65 (2007)

[9] K.I. Schiffmann, Microtribological/mechanical testing in 0, 1 and 2 dimensions: A comparative study on different materials, Wear 265, 1826-1836 (2008)

[10] J.R. Lince, H.I. Kim, P.M. Adams, D.J. Dickrell, and M.T. Dugger, Nanostructural, electrical, and tribological properties of composite Au-MoS_2 coatings, Thin Solid Films 517, 5516-5522 (2009)

[11] S. Deladi, J. W. Berenschot, M. J. De Boer, G. J. M. Krijnen, and M. C. Elwenspoek, "An afm-based device for in-situ characterization of nano-wear," in Proceedings of the

17th IEEE International Conference on Micro Electro Mechanical Systems (MEMS), Institute of Electrical and Electronics Engineers Inc. , Piscataway, United States (2004), pp. 181-184

[12] K. I. Schiffmann and A. Hieke, Analysis of microwear experiments on thin DLC coatings: friction, wear and plastic deformation, Wear 254, 565-572 (2003)

[13] S. I. U. Ahmed, G. Bregliozzi, and H. Haefke, Microfrictional properties of diamond-like carbon films sliding against silicon, sapphire and steel, Wear 254, 1076-1083 (2003)

[14] R. Bandorf, H. Luthje, and T. Staedler, Influencing factors on microtribology of DLC films for MEMS and microactuators, Diamond and Related Materials 13, 1491-1493 (2004)

[15] R.R. Chromik and K.J. Wahl, "Friction of microscale contacts on diamond-like carbon nanocomposite coatings," in World Tribology Congress III, American Society of Mechanical Engineers, New York, NY, (2005), pp. 829-830

[16] R. L. A. Kuster and K. I. Schiffmann, Nano-scratch testing on thin diamond-like carbon coatings for microactuators: friction, wear and elastic-plastic deformation, Zeitschrift fur Metallkunde 95, 306-310 (2004)

[17] B. Bhushan, Chemical, mechanical and tribological characterization of ultra-thin and hard amorphous carbon coatings as thin as 3.5 nm: Recent developments, Diamond and Related Materials 8, 1985-2015 (1999)

[18] B. Bhushan, H. W. Liu, and S. M. Hsu, Adhesion and friction studies of silicon and hydrophobic and low friction films and investigation of scale effects, Journal of Tribology-Transactions of the Asme 126, 583-590 (2004)

[19] T. W. Scharf, S. V. Prasad, M. T. Dugger, P. G. Kotula, R. S. Goeke, and R. K. Grubbs, Growth, structure, and tribological behavior of atomic layer-deposited tungsten disulphide solid lubricant coatings with applications to MEMS, Acta Materialia 54, 4731-4743 (2006)

[20] T. W. Scharf, S. V. Prasad, M. T. Dugger, and T. M. Mayer, "Atomic layer deposition of solid lubricant thin films," in Proceedings of the World Tribology Congress III - 2005, American Society of Mechanical Engineers, New York, NY, (2005), pp. 375-376

[21] S. D. Dvorak, K. J. Wahl, and I. L. Singer, *In situ* analysis of third body contributions to sliding friction of a Pb-Mo-S coating in dry and humid air, Tribology Letters 28, 263-274 (2007)

[22] K. J. Wahl, L. E. Seitzman, R. N. Bolster, and I. L. Singer, Low-friction, high-endurance, ion-beam-deposited Pb-Mo-S coatings, Surface and Coatings Technology 73, 152-159 (1995)

[23] J. R. Lince, Tribology of co-sputtered nanocomposite Au/MoS_2 solid lubricant films over a wide contact stress range, Tribology Letters 17, 419-428 (2004)

[24] N. M. Renevier, V. C. Fox, D. G. Teer, and J. Hampshire, Performance of low friction MoS_2/titanium composite coatings used in forming applications, Materials & Design 21, 337-343 (2000)

[25] M. C. Simmonds, A. Savan, E. Pfluger, and H. Van Swygenhoven, Mechanical and tribological performance of MoS_2 co-sputtered composites, Surface and Coatings Technology 126, 15-24 (2000)

[26] J. S. Zabinski, M. S. Donley, S. D. Walck, T. R. Schneider, and N. T. McDevitt, Effects of Dopants on the Chemistry and Tribology of sputter-deposited MoS_2 films, Tribology Transactions 38, 894-904 (1995)

[27] T. Spalvins, Frictional and morphological properties of Au-MoS_2 films sputtered from a compact target, Thin Solid Films 118, 375-384 (1984)

[28] X. Wang, Y. Xing, S. Ma, X. Zhang, K. Xu, and D. G. Teer, Microstructure and mechanical properties of MoS_2/titanium composite coatings with different titanium content, Surface and Coatings Technology 201, 5290-5293 (2007)

[29] M. C. Simmonds, A. Savan, E. Pflüger, and H. Van Swygenhoven, Microstructure and tribological performance of MoS_x/Au co-sputtered composites, Journal of Vacuum Science and Technology, Part A: Vacuum, Surfaces and Films 19, 609-613 (2001)

[30] J. L. Grosseau-Poussard, P. Moine, and M. Brendle, Shear strength measurements of parallel MoS_x thin films, Thin Solid Films 307, 163-168 (1997)

[31] A.R. Lansdown, Molybdenum Disulphide Lubrication, Elsevier Science B.V., Amsterdam (1999)

[32] P. Stoyanov, J.Z. Fishman, J.R. Lince, and R. R. Chromik, Micro-Tribological Performance of MoS_2 Lubricants with varying Au content, Surface and Coatings Technology 203, 761-765 (2008)

[33] P. Stoyanov, J.R. Lince, and R.R. Chromik, "Micro-scale sliding contacts on Au and Au-MoS_2 coatings," submitted to Surface & Coatings Technology (2010).

[34] R. R. Sahoo and S. K. Biswas, Microtribology and friction-induced material transfer in layered MoS_2 nanoparticles sprayed on a steel surface, Tribology Letters 37, 313-326 (2010)

[35] R. R. Sahoo, S. Math, and S. K. Biswas, Mechanics of deformation under traction and friction of a micrometric monolithic MoS_2 particle in comparison with those of an agglomerate of nanometric MoS_2 particles, Tribology Letters 37, 239-249 (2010)

[36] R. P. Nair and M. Zou, Surface-nano-texturing by aluminum-induced crystallization of amorphous silicon, Surface and Coatings Technology 203, 675-679 (2008)

[37] A. J. Bushby and N. M. Jennett, "Determining the area function of spherical indenters for nanoindentation," in Fundamentals of Nanoindentation and Nanotribology II, Materials Research Society, (2001), pp. Q7.17.11-Q17.17.16

[38] H. Shin, H. J. Doer, C. Deshpandey, P. Fuqua, B. Dunn, and R. F. Bunshah, Effect of niobium doping on the properties of molybdenum sulfides as cathode materials, Surface and Coatings Technology 36, 859-865 (1988)

[39] K. J. Wahl, D. N. Dunn, and I. L. Singer, Effects of ion implantation on microstructure, endurance and wear behavior of IBAD MoS_2, Wear 237, 1-11 (2000)

[40] T. J. Wieting and J. L. Verble, Infrared and Raman Studies of Long-Wavelength Optical Phonons in Hexagonal MoS_2, Physical Review B 3, 4286 (1971)

[41] I.L. Singer, Solid Lubrication Processes, in: I.L. Singer and H.M. Pollock (ed.), Fundamentals of Friction: Macroscopic and Microscopic Processes, Kluwer Academic, Dordrecht, pp. 237-261 (1992)

[42] I. L. Singer, R. N. Bolster, J. Wegand, S. Fayeulle, and B. C. Stupp, Hertzian stress contribution to low friction behavior of thin MoS_2 coatings, Applied Physics Letters 57, 995-997 (1990)

[43] B. J. Briscoe and A. C. Smith, The Interfacial Shear Strength of Molybdenum Disulfide and Graphite Films, Tribology Transactions 25, 349 - 354 (1982)

[44] U.D. Schwarz, O. Zwörner, P. Köster, and R. Wiesendanger, Quantitative analysis of the frictional properties of solid materials at low loads. I. Carbon compounds, Physical Review B 56, 6987 (1997)

[45] P. W. Bridgeman, Shearing Phenomena at High Pressure Particularly in Inorganic Compounds, Proc. Amer. Acad. of Arts and Sciences 71, (1936)

[46] A. Erdemir, R.A. Erck, and J. Robles, Relationship of hertzian contact pressure to friction behavior of self-lubricating boric acid films, Surface and Coatings Technology 49, 435-438 (1991)

Chapter 6

Micro-scale sliding contacts on Au and Au-MoS_2 coatings

6.1 Abstract

The microtribological properties of Au and Au-MoS_2 coatings were examined using a nanoindentation instrument. MoS_2 was chosen for this study as an additive to Au due to its positive influence on the mechanical and tribological properties. Reciprocating microscratch tests were performed using a diamond indenter with a tip radius of 50 μm and a range of normal loads between 0.2 mN and 5.0 mN. The friction and wear results, with respect to the two coatings, were correlated to different velocity accommodation modes and levels of adhesion. It was found that the addition of 20 mol% MoS_2 to Au reduced the adhesion and limiting friction and also improved the wear resistance significantly. This coating shows potential for applications in microcomponents and microswitches due to its wear resistance, relatively low friction and good electrical conductivity.

Keywords: Microtribology, MoS_2, Au, micro-electromechanical systems (MEMS), nanoindentation

6.2. Introduction

Gold is a noble material, which has been known for its excellent corrosion resistance, great electrical conductivity, and thermal properties [1]. Therefore, gold is widely used as an electrical conductor in microcomponents and microswitches [2]. These types of application include DC motor controls and RF micro-electromechanical systems (MEMS) [2-4]. The most common failure mechanisms are adhesion, melting, and increase in electrical resistivity due to failure of the coating [2]. Thus, numerous studies have been carried out on Au in order to improve its mechanical and tribological properties and increase the endurance life [5-9]. It has been proposed that the main wear mechanism of Au films in air is due to grains pull-off [10]. Therefore, the reduction in adhesion between the gold coating and the slider could have a significant effect on the tribological properties of the Au. While most of the applications described above involve only normal contact, some small sliding motion often occurs, and future microsystems may include sliding electrical contacts.

Recent macroscopic tribology experiments [6,11] showed that the addition of MoS_2 to Au increases the endurance life significantly. The authors observed that the optimum performance (i.e. lowest friction and highest endurance at macro-scale), in low contact stress regimes, was seen with Au coating containing between 10 to 25 mol% MoS_2. In addition, the largest reduction in pull-off force was seen with the addition of 25 mol% MoS_2. However, the smallest increase in electrical resistivity was observed by the addition of 20 mol% MoS_2.

In this article, we investigate the influence of 20 mol % MoS_2 co-sputtered with pure Au compared to the microtribological behavior of pure Au. A nanoindentation instrument was used to conduct sliding wear tests at similar contact stresses to those found in microsystems. The microtribological results, with respect to the two coatings, were compared via different friction laws and velocity accommodation modes (VAM) [1,12-13].

6.3. Experimental Procedure

Coatings were deposited onto polished Si (100) wafers in a load locked deposition chamber with a base pressure of 1.33×10^{-7} Pa (1×10^{-9} Torr). Separate Au and MoS_2 radio frequency sputtering sources were used, which were operated in unbalanced mode to increase the ion flux on the substrate surface during deposition. Argon (99.999% nominal purity) was used as the sputtering gas, and the Ar pressure in the chamber during deposition was generally 4 Pa (3×10^{-3} Torr). The Au and MoS_2 sputtering power densities were varied between 1 to 2.5 W/cm^2 to achieve films with varying Au:MoS_2 concentration ratios. More information on the deposition of these coatings may be found in Ref. 11. For this study, a pure Au coating and a MoS_2 – 80at. % Au coating were produced.

The films were characterized with various methods to determine: grain size, hardness, films thickness and roughness. Grain size and phase identification were determined using an x-ray diffractometer (Bruker D8 Discover, Madison, WI) using a standard Θ-2Θ geometry and Co-Kα radiation. Scherrer's equation and the method of integral breadths [14-17] were used to calculate the crystallite size. The roughness of the coatings was measured using an atomic force

microscope (AFM) (Veeco Dimension 3100, Santa Barbara, CA) operated in contact mode using up to 50μm by 50μm scan size. The thickness of the coatings was measured from cross-sectional images obtained at high magnification using a field emission gun scanning electron microscope (FEG-SEM) (Hitachi 4700-S, Japan).

The mechanical properties of the coatings were measured with a Nanoindentation instrument, Ubi 3 (Hysitron, Inc. Minneapolis, MN) with a 1D transducer and a diamond Berkovich tip. The hardness values presented in this paper are averages taken from 6 and 25 indentations for the pure Au coating and the Au-MoS_2 coating, respectively. The indentation depth was ranged between 20 and 50 nm by varying the normal load between 0.04 mN and 0.3 mN. The same nanoindentation instrument and transducer was used for surface pull-off force measurements with a spherical diamond tip with a 50μm tip radius. The pull-off force measurements were performed using the displacement control feedback. The maximum displacement throughout the test was 60 nm with a hold time of one second. The pull-off force was measured from the retracting adhesion force on the unloading curves [18]. Each test consisted of 10 indentation repeated at the same position, with the last five pull-off force measurements being averaged.

An AFM (Veeco Nanoman, Santa Barbara, CA) was used in closed loop contact mode to characterize the radius, roughness, and the area function of the spherical tip used for microtribology experiments. This characterization was performed because at the smaller length scale diamond indenters typically deviate from the ideal spherical shape [19]. Therefore, it is crucial to obtain an accurate, measured area function for determination of the contact pressure.

From AFM images, a tip area function was produced using a pixel counting algorithm created in Matlab (Version 7.5.0). The actual area function of the tip was used to obtain a contact pressure at any given depth and normal load. This procedure is described in more detail elsewhere [20] and is very similar to the one described by Bushby, et al. [19].

Microtribological testing was conducted using the same nanoindentation instrument described above, but with a 2D transducer capable of scratch testing and reciprocating wear testing and a diamond tip with a 50 μm radius. Sliding tests were performed under controlled ambient temperature and a relative humidity between 3.0 and 5.0%. The relative humidity was controlled by flowing compressed air, which passed through anhydrous $CaSO_4$ (desiccant), into the instrument enclosure at a high flow rate for several minutes and then a constant low flow rate throughout the sliding experiments. The results from the sliding experiments were analyzed using a custom-built analysis code with Matlab, Version 7.5.0. Images of the wear tracks were created by AFM, and the wear area was calculated using an integral function in Origin 8.1.

The sliding experiments were conducted with 8μm track lengths at a constant velocity of 4μm/sec. The normal loads used for the experiments was varied between 0.2 and 5.0 mN, which resulted in an initial Hertzian contact pressure between 0.4 and 1.2 GPa and a contact radius between 0.4μm and 1.1μm. The contact forces chosen for this study overlap with those typically found in microswitches, which can range between a few μN to about 1.0 mN [2]. The total number of sliding cycles was 800, but due to limitation on the instrument software, only 400 cycles were performed at a time and were repeated on the same position in order to achieve a

total of 800 cycles. Each sliding test consisted of three phases, 1) a pre-scan, to image the topography at a 20 μN load, 2) an oscillating scratch, where the sample is worn under a high constant load for 800 sliding cycles, and 3) a post-scan with 20 μN load to image the topography of the resulting wear trace [21]. The experimental method is described in more detail elsewhere [22].

The coefficient of friction was calculated from the lateral force divided by the normal force. The average friction coefficient for each cycle was calculated from 75(±2) data points corresponding to the central 5μm of the track. Results from three repeats of the sliding tests were averaged.

6.4. Results

6.4.1 Coating Characterization and Properties

X-ray diffraction (XRD) plots of the sputtered Au and the co-sputtered Au-MoS_2 are shown in Figure 6.1(a) and (b), respectively. The Au-MoS_2 sample reveals only Au peaks and no Mo, S or MoS_2 peaks. This suggests that the coating consists of a nanocomposite structure with crystalline Au nanoparticles surrounded by amorphous MoS_2 (as also seen with transmission electron microscopy (TEM) and XRD analysis [6]) or crystalline Au grains with MoS_2 integrated within the matrix. The XRD analysis on the Au sample shows a similar peaks as the Au-MoS_2 sample, with the Au(111) peak having much higher intensity relative to the other Au peaks and a decrease in the peak width (c.f. Figure 6.1 (a)). The grain size was calculated using the Au (111) peak and Scherrer's equation, which resulted in 37 nm and 16 nm for the Au and Au-MoS_2 samples, respectively. Crystallite size calculations conducted using integral breadths resulted in

similar values (i.e. 31 nm and 13 nm, respectively). The change in grain size with MoS_2 content was found to be the same as that observed in similar coatings [6].

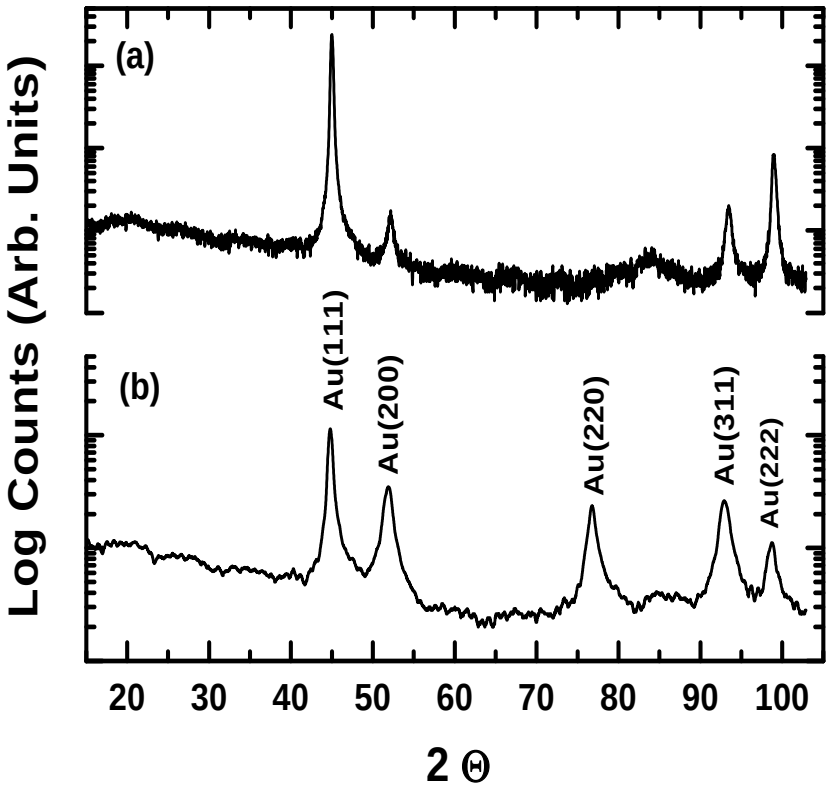

Figure 6.1. Film characterization using by x-ray diffraction for the sputtered Au sample (a) and the co-sputtered Au-MoS_2 sample (b). The crystal grain size was determined using Scherrer's method and resulted in 37nm and 16nm for the Au sample and the Au-MoS_2 sample respectively.

Other important characteristics of the coatings such as roughness, thickness, and hardness were also measured. The Au-MoS_2 coating was thicker than the pure Au coating (i.e. 515 nm and 190 nm respectively), which is simply a result of different deposition times. Despite the thickness difference, the roughness values for the coatings were very similar (i.e. 2.3 nm and 2.7 nm for

the Au-MoS_2 and the pure Au coating, respectively). The hardness was higher for the Au-MoS_2 sample (i.e. 4.1 ± 0.1 GPa) when compared to the pure Au sample (i.e. 2.9 ± 0.2 GPa).

6.4.2 Coefficient of Friction

Figure 6.2 (a) and (b) show the average coefficient of friction vs. the cycle number with a wide normal load range for the Au and Au-MoS_2 samples, respectively. For the smallest normal load (0.2 mN), the friction for the MoS_2-containing coating is higher than pure Au. At normal loads higher than 0.5 mN, the coefficient of friction was relatively similar for both samples. However, for 1.0 mN and 3.0 mN normal loads, the steady state friction for the Au-MoS_2 sample, was slightly lower when compared to the pure Au sample.

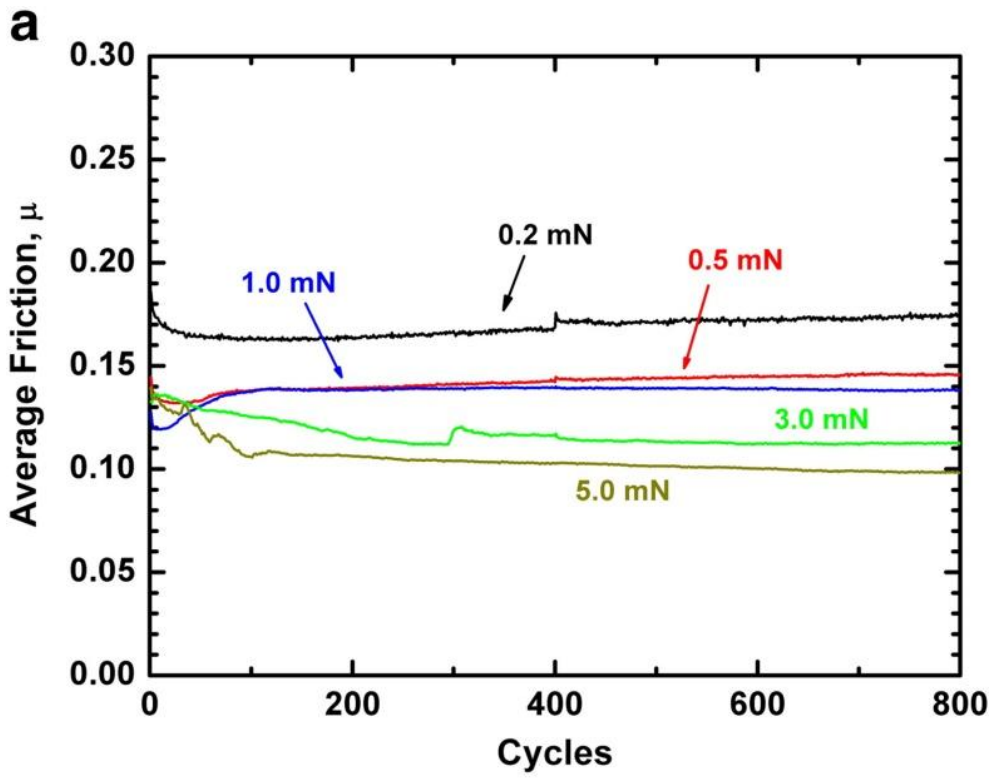

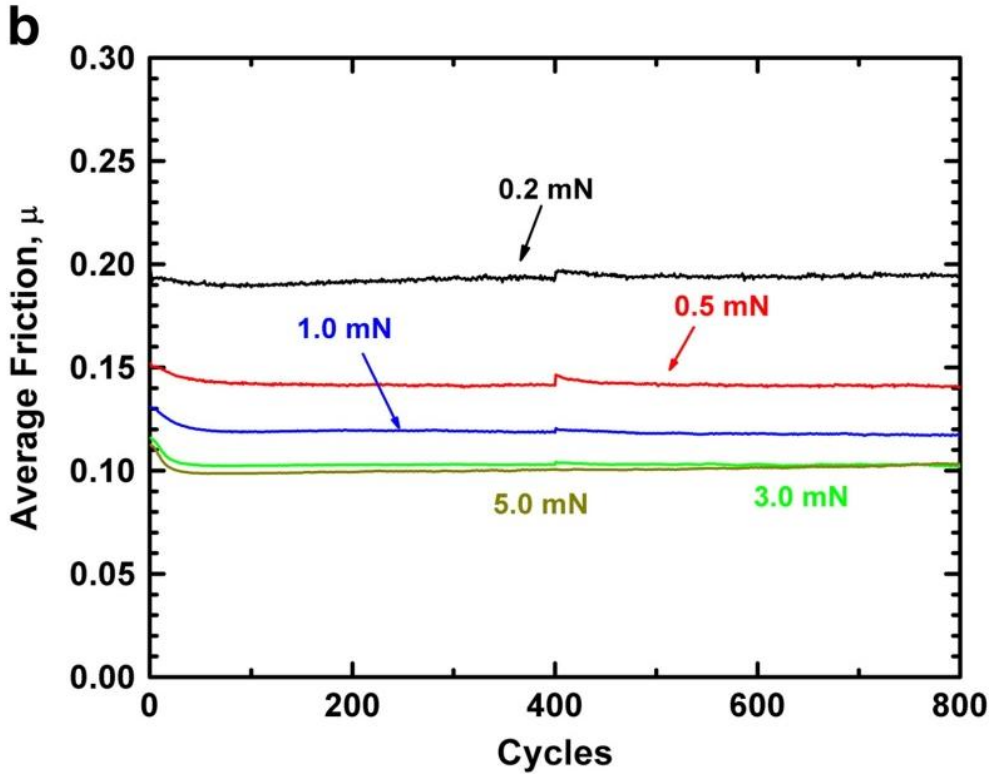

Figure 6.2. Average coefficient of friction vs. cycle with varying normal loads between 0.2mN and 5.0mN for (a) sputtered Au sample and (b) co-sputtered Au-MoS_2 sample. The coefficient of friction is averaged over the middle 5μm of the wear track from three different sliding tests. The standard deviation was between 0.02 and 0.001, but mostly in the -3 order of magnitude.

For the Au-MoS_2 sample, the coefficient of friction decreases with increasing the normal load, as expected [23]. However, this is not necessarily true for the pure Au sample (i.e. friction coefficient is similar for the 0.5 mN and 1.0 mN normal loads and for the 3.0 mN and 5.0 mN normal loads). Furthermore, during the first few cycles of the test (i.e. run in stage), the Au sample shows similar friction values for all normal loads higher than 0.2 mN (see Figure 6.2 (a)).

6.4.3 Wear Results

Figure 6.3 (a) and (b) shows AFM images of the wear tracks, which were created using a 1.0 mN normal load on the sputtered Au sample and the co-sputtered Au-MoS_2 sample, respectively. At this load, the magnitude of wear was higher for Au compared to Au-MoS_2. The morphology of the wear tracks was also noticeably different. The wear track on Au showed significant pile-up of debris along all edges of the track, but the wear track on Au-MoS_2 showed only debris at the turnaround points.

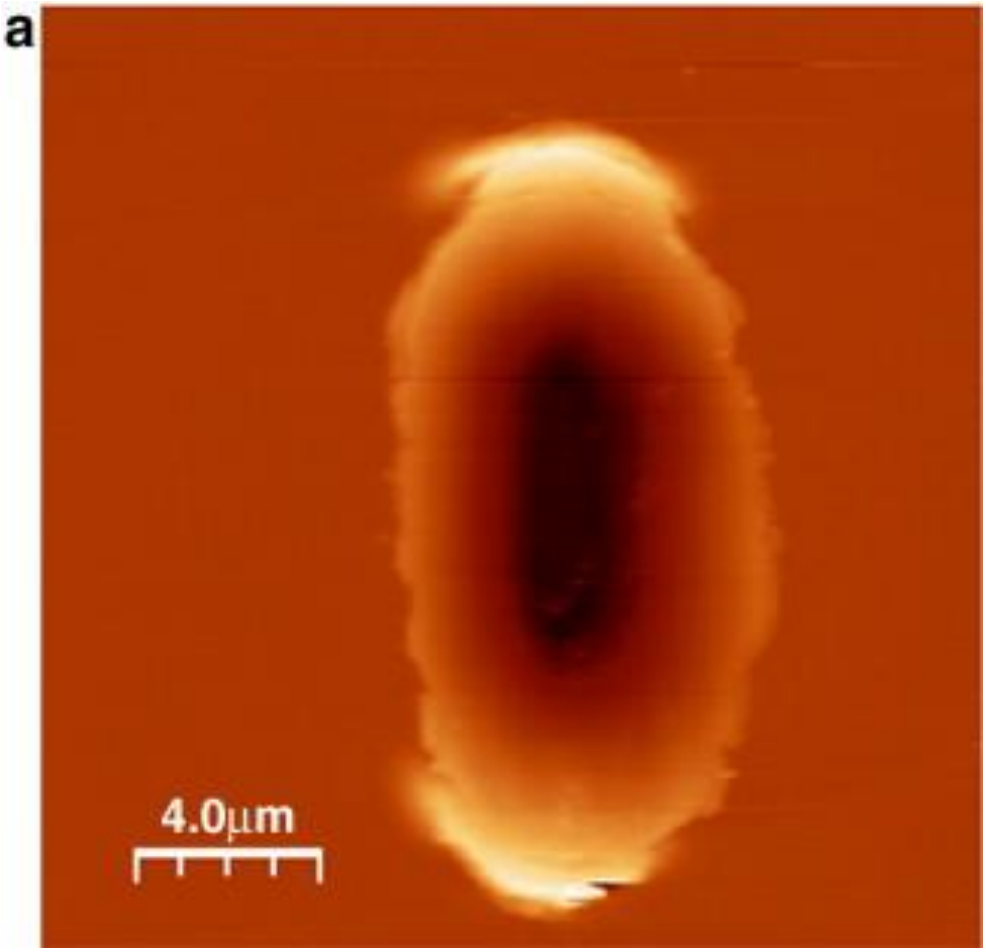

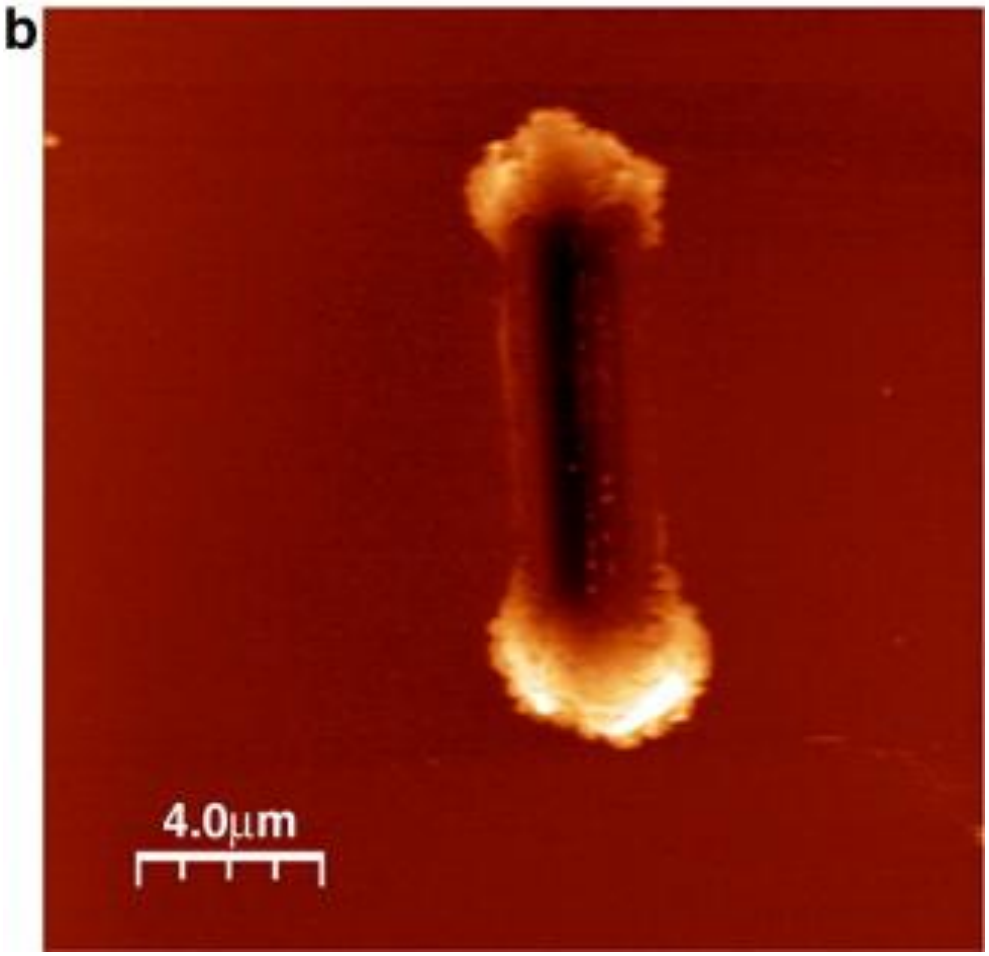

Figure. 6.3. Atomic force microscope images of a wear track, which was created using a normal load of 3.0 mN and on the (a) Au sample and (b) Au-MoS_2 sample.

Figure 6.4 shows the cross-sectional wear area vs. the normal load for the Au and the Au-MoS_2 samples. For normal loads less than 1.0 mN, very little wear is observed for both samples. However, a sharp increase in the wear area is observed for the Au sample with higher normal loads, while the wear area for the Au-MoS_2 sample remains relatively constant. The wear depth for both samples at the highest normal load was less than the actual coating thickness (i.e. 163

nm and 30 nm for the Au and the Au-MoS_2 sample, respectively), indicating that, while the magnitude of wear was different, neither coating failed by the end of the test at 800 cycles.

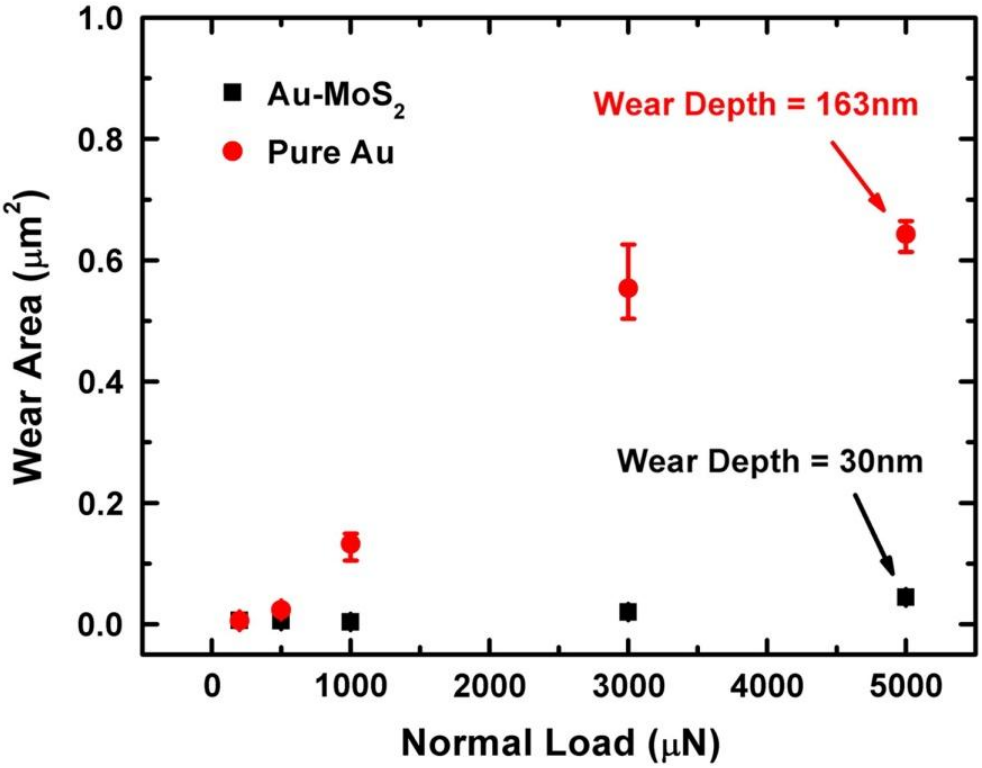

Figure 6.4. Cross-sectional wear area vs. normal load for the Au and Au-MoS_2 sample.

6.5. Discussion

6.5.1 Friction Mechanisms

Microtribological experiments on the Au and Au-MoS_2 coatings showed a slightly different behavior in the coefficient of friction. During the run in period, the Au coating showed a slight increase in the coefficient of friction with respect to the cycle number for some normal loads (i.e. 0.5mN and 1.0mN), while the Au-MoS_2 coating showed a decrease in the friction versus cycles for all normal loads higher than 0.2 mN. The initial increase in the friction coefficient for the Au

coating has previously been observed [24] for a Au-Au contact. Tian, et al. [24] believed the initial friction increase upon sliding was due to the increase in contact area due to wear that resulted in an increase in the adhesive component of friction. The decrease in friction during the run-in period for the Au-MoS_2 sample has been previously seen for MoS_2 and metal-MoS_2 coatings, where a transfer film containing MoS_2 is formed on the counterface which lowers the coefficient of friction in the first few cycles [25-26].

A simple comparison between the friction behavior of the two coatings was conducted using an Amonton's fit to steady state friction force (i.e. 800^{th} cycle) versus normal force data (see Figure 6.5 (a) and (b)). While this analysis ignores some of the nuances of the dependence of the friction on load [17,22,27], it does allow for a quick comparison to the literature. The best fit straight line gave a mean slope value of 0.110±0.005 and 0.098±0.001 for the Au and the Au-MoS_2 coating, respectively. Discussing the results for Au first, the value found here is lower when compared to the values obtained by Barriga et al. [5] for Au-Au and Cu-Au coatings ($\mu \sim 0.2$) and by Benoy and DellaCorte for Au/Cr coatings ($\mu \sim 0.4$). In both of these publications, tests were performed at higher humidity levels and a higher range of contact stresses with macroscopic length scales. Most studies of Au friction suggest that the main mechanism for generating resistance to the sliding are capillarity forces and adhesion [5,24]. In addition, Miyoshi et al. [28] suggested that gold transfers from the coating to the slider even after a single pass, which could promote even higher adhesion. Friction on Au films measured at more similar length scale to our studies, by AFM at 50 %RH, found $\mu \sim 0.18$ [10].

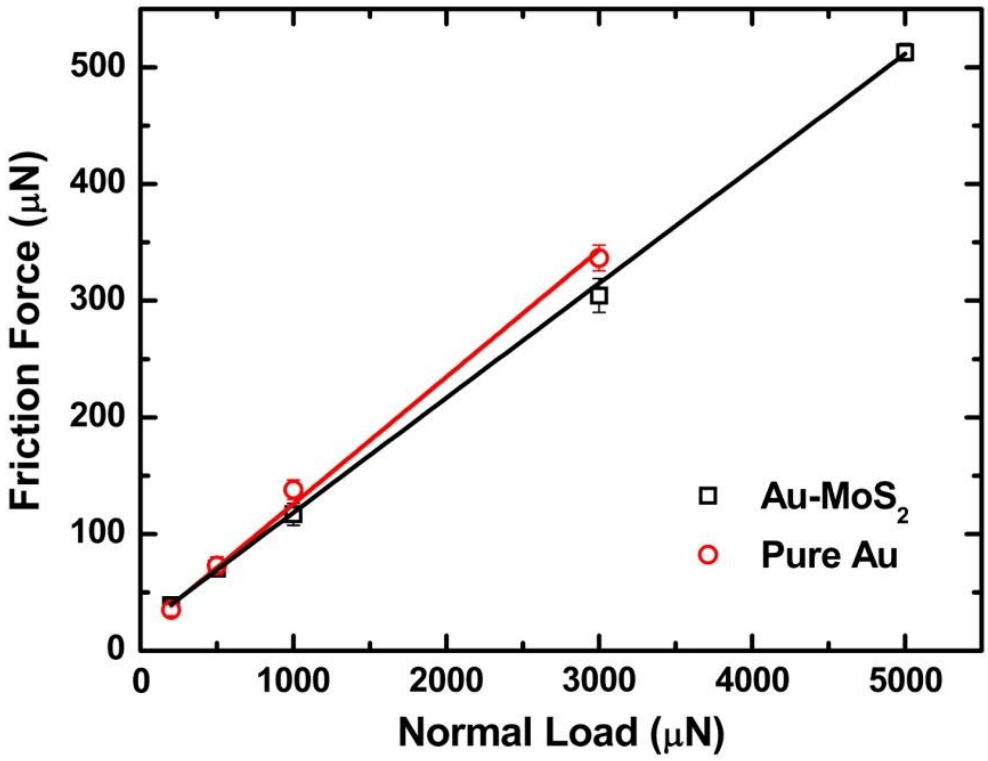

Figure 6.5. Friction force vs. normal force at steady state (800th cycle) with varying normal force between 0.2mN and 5.0mN for sputtered Au sample and co-sputtered Au-MoS_2 sample. The coefficient of friction is averaged over the middle 5μm of the wear track from three different sliding tests.

Since our sliding experiments were performed under low relative humidity, the friction force is most likely due to adhesion between the surfaces and less likely due to capillarity. The extent to which an adhesive force could play a role was explored by surface adhesion tests, which yielded a steady-state pull-off force of 15.7±0.4 μN for the pure Au and 10±1 μN for the Au-MoS_2 sample. Thus, the pull-off force for the pure Au sample was significantly higher when compared to the Au-MoS_2 sample. Using the relationship between the pull off force, F_p, and the surface energy, S:

$$S = {-2F_p}/{(3\,\pi\,R)}, \qquad \text{Eq. 6.1}$$

where R is the ideal radius of the sphere, we find the surface energy is 0.068 N/m and 0.042 N/m for the Au and Au-MoS_2 sample, respectively. The surface energy value for the pure Au sample is relatively similar to the values obtained by Barriga [5]. Furthermore, the larger pull-off force with the pure Au sample when compared to Au-MoS_2 samples was also observed for a larger scale adhesion test [6].

The differences in static adhesion by a pull-off force measurements leads to the consideration of differences in the shear strength of the interface. Previous research [23,27,29-31] has shown that the shear strength for many interfacial processes has a pressure dependence which can be approximated by:

$$S = S_o + \alpha P, \qquad \text{Eq. 6.2}$$

where S_o is the interfacial shear strength, also called the "velocity accommodation parameter," P is the contact pressure, and α represents the pressure dependence of the shear strength [27]. This equation can be re-written in terms of the coefficient of friction, such that

$$\mu = S_o/P + \alpha\,, \qquad \text{Eq. 6.3}$$

where μ is the coefficient of friction and, in this form, α is the limiting friction. Thus, from this equation we can see that the coefficient of friction is inversely proportional to the pressure. Figure 6.6 shows the plot of μ vs. *1/P* for the Au and Au-MoS_2 coatings. The pressure for this plot was calculated at the steady state condition (800^{th} cycle) using the normal force divided by

the projected area of the tip. The area was determined from the results of a pixel counting algorithm which was obtained from atomic force microscope images of the tip. The value of the tip area at the 800th cycle was calculated using the elastic depth, which was obtained from the difference in the normal displacement of the post scan (i.e. 3rd phase of the sliding experiment) and the last sliding cycle.

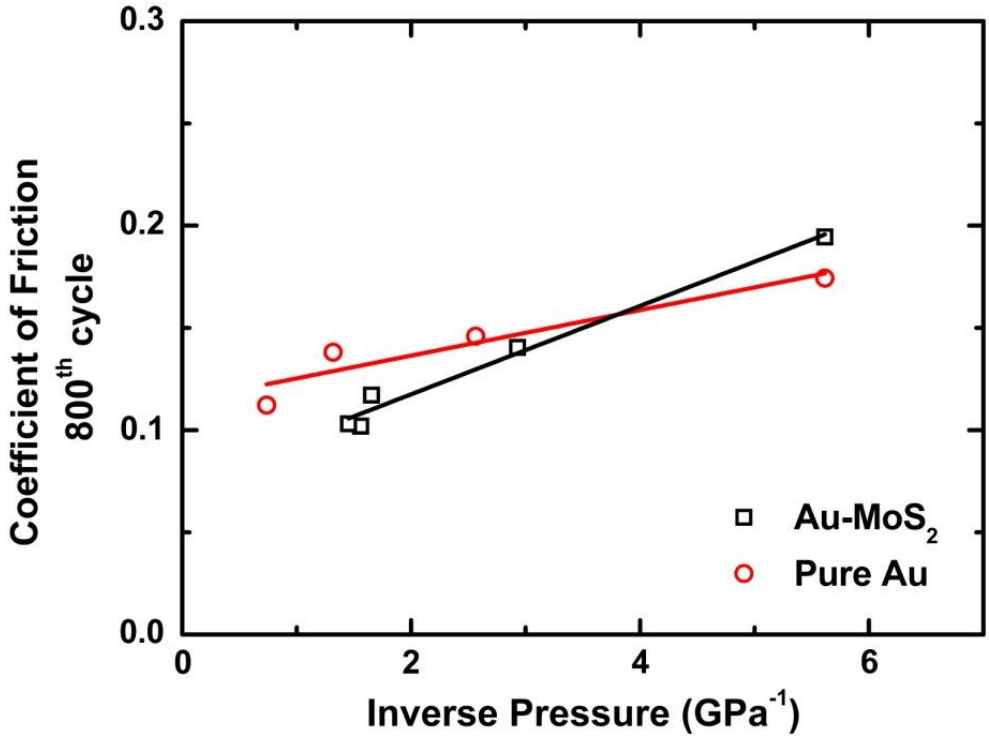

Figure 6.6. Coefficient of friction versus inverse pressure following the relationship of Eq. 2 for the sputtered Au sample and the co-sputtered Au-MoS_2 sample. The contact pressure **P** was calculated using the area function of the tip determined from closed loop AFM scans and the pixel counting algorithm.

This method of calculating the elastic depth value takes into consideration the presence of a thick transferfilm on the counterface, since the transferfilm that is present in the last cycle would also be present during the post scan. Therefore, even with the presence of a thick transferfilm, a

precise elastic depth can be obtained using this method. A straight line fit was conducted on the data for both coatings, which gave a mean slope ($\boldsymbol{S_o}$) of 11±3 MPa and 22±2 MPa for the Au and the Au-MoS_2 samples, respectively. The S_o value for the Au-MoS_2 coating, compares favorably with literature at the macroscopic scale for pure MoS_2 coatings [23] (i.e. 25±3 MPa). However, the pure Au coating revealed lower interfacial shear strength. This indicates that there may be a difference in the VAM [1,12-13] between the two coatings. The limiting friction was also different, with α=0.114±0.008 for Au and 0.074±0.005 for Au-MoS_2. Thus, the limiting friction was higher for the coating with higher adhesion. As suggested by Pendergast, et al. [10], the main wear mechanism when sliding on Au in air is by grain pull-off, which was confirmed by the increase in surface roughness on the worn area. As seen here, the addition of MoS_2 to Au decreases the grain size of the Au and decreases the pull-off force, which likely leads to less transfer of gold onto the slider. Furthermore, the VAM of the Au-MoS_2 sample is more likely the formation of an MoS_2 containing transfer film on the counterbody [6] , which should be a better solid lubricant than Au at room temperature.

6.5.2 Wear Mechanisms

The different friction mechanisms between the two coatings also correspond to the different amounts of wear seen during sliding. The wear in the Au coating increased significantly with normal loads higher than 0.5 mN, whereas the wear on the Au-MoS_2 coatings remained relatively constant (see Figure 6.4). The higher wear with the Au coating may be explained by the high adhesion between the slider and the coating. Lince et al. [6] showed that even co-sputtering a small amount of MoS_2 (i.e. 11 mol%) with Au reduces the pull-off force by a factor

of two after the first few cycles. The results presented here indicate that the addition of a small amount of MoS_2 to Au lowers the wear significantly for a microscale sliding contact with normal loads higher than 0.5mN (i.e. initial Hertzian contact stresses higher than 0.6 GPa). This result may also be explained by the lower adhesion between the slider and the coating due to the MoS_2 transfer film formation.

Kuster and Schiffmann [32] suggested that the depth during sliding can be separated into three contributions: elastic deformation, plastic deformation, and material loss. The authors used three depth values in order to calculate each wear contribution: the depth after the initial loading (D_{IL}), the depth under normal load after the last cycle of the test (D_{LC}), and the residual depth after unloading measured from the end scan (D_{RD}). Using these measurements the following equations can be derived:

$$\text{Elastic deformation} = D_{LC} - D_{RD}, \quad \text{Eq. 6.4}$$

$$\text{Material loss} = D_{LC} - D_{IL}, \quad \text{Eq. 6.5}$$

$$\text{Plastic deformation} = D_{RD} - [\text{Material loss}] = D_{RD} - (D_{LC} - D_{IL}), \quad \text{Eq. 6.6}$$

In this paper, this method was slightly modified because it was difficult to measure the wear depth from the end scan of the sliding test (due to thermal drift and material pile up at the end of the wear track). Thus, the value of D_{IL} was calculated using the elastic-plastic wear depth from an indentation test and the value of D_{RD} was calculated using the wear depth obtained with an AFM. The different depth contributions were plotted versus the normal loads for the pure Au and Au-MoS_2 coatings (see Figure 6.7 (a) and (b)). It was observed that the elastic contribution to the

sliding process, for normal loads less than 5.0 mN, is higher for the Au-MoS_2 coating when compared to the pure Au coating. Furthermore, with respect to the other two contributions (i.e. removed material and plastic deformation), the sliding behavior on the Au-MoS_2 sample is dominated by elastic deformation for normal loads higher than 1.0 mN. The highest contribution to wear of the pure Au sample, on the other hand, is the removed material, which may be due to adhesive forces.

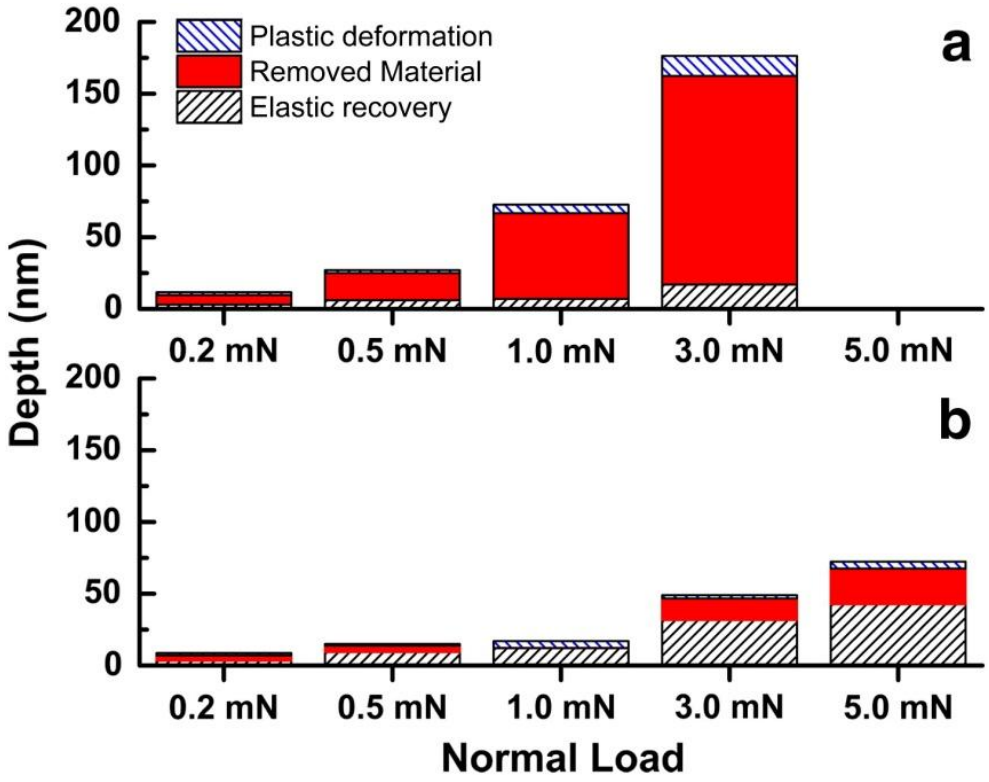

Figure 6.7. Depth for plastic deformation, removed material, and elastic deformation vs. normal force for (a) sputtered Au sample and (b) co-sputtered Au-MoS_2 sample. The different depth contributions were calculated using measurements from indentation tests, sliding tests and AFM scans. It was not possible to obtain reasonable depth contributions for the pure Au sample when using the highest normal load (i.e. 5.0 mN) because the total depth value was approaching the coating thickness.

6.6. Conclusions

The structural and microtribological properties of Au and Au-MoS_2 coatings were investigated in this paper. The addition of MoS_2 decreased the crystalline domain size, reduced adhesion and wear. The small addition of MoS_2 to the Au coating decreased the wear significantly by decreasing the amount of material loss (i.e. removed material). While the magnitude of the friction was similar for the two coatings, an analysis of the interfacial shear strength and limiting friction showed that the velocity accommodation modes were different, with Au having higher adhesion and higher limiting friction. In general, the results obtained in this paper suggest that small additions of MoS_2 to Au could be a helpful for microcomponent and microswitch applications with sliding interfaces.

Acknowledgments

The authors gratefully acknowledge financial support from Fonds québécois de la recherche sur la nature et les technologies (FQRNT), program Établisssement de nouveaux chercheurs and Lorne Trottier for the graduate Fellowship (McGill Engineering Doctoral Award). This work was also supported under The Aerospace Corporation's Mission Oriented Investigation and Experimentation program, funded by the U.S. Air Force Space and Missile Systems Center under Contract No. FA8802-09-C-0001. The diligent work by Ms. Shivani Gupta in assisting with preliminary microtribology experiments was greatly appreciated.

REFERENCES

[1] K. Holmberg, Coatings tribology : properties, mechanisms, techniques and applications in surface engineering 2ed, Elsevier Science, Amsterdam; Boston; London, 2009.

[2] S. T. Patton and J. S. Zabinski, Tribology Letters 18 (2005) 215-230

[3] D. Hyman and M. Mehregany, IEEE Transactions on components and packaging technologies 22 (1999) 357-364

[4] S. Majumder, N.E. McGruer, P.M. Zavracky, G.G. Adams, R.H. Morrison, and J. Krim, Tribology Issues and Opportunities in MEMS, Kluwer Academic Publishers, Dordrecht, 1998.

[5] J. Barriga, B. Fernández-Diaz, A. Juarros, S. I. U. Ahmed, and J. L. Arana, Tribology International 40 (2007) 1526-1530

[6] J. R. Lince, H. I. Kim, P. M. Adams, D. J. Dickrell, and M. T. Dugger, Thin Solid Films 517 (2009) 5516-5522

[7] C. W. Tan and J. Miao, Thin Solid Films 517 (2009) 4921-4925

[8] J. Kimberley, R. S. Cooney, J. Lambros, I. Chasiotis, and N. S. Barker, Sensors and Actuators A: Physical 154 (2009) 140-148

[9] S. W. Han, H. W. Lee, H. J. Lee, J. Y. Kim, J. H. Kim, C. S. Oh, and S. H. Choa, Current Applied Physics 6 (2006) e81-e85

[10] M. Pendergast, A. A. Volinsky, X. Pang, and R. Shields, in *Nanoscale Tribology-Impact for Materials and Devices* (Materials Research Society, 2008), Vol. 1085, pp. 19-24.

[11] J. R. Lince, Tribology Letters 17 (2004) 419-428

[12] I. L. Singer, S. D. Dvorak, K. J. Wahl, and T. W. Scharf, Journal of Vacuum Science & Technology A (Vacuum, Surfaces, and Films) 21 (2003) S232-S240

[13] M. Godet, Wear 100 (1984) 437-452

[14] R. R. Chromik, L. Zavalij, M.D. Johnson, and E.J. Cotts, Journal of Applied Physics 91 (2003)

[15] H.P. Klug, X-ray Diffraction Procedures for Polycrystalline and Amorphous Materials, Wiley, New York, 1974, pp.661-665.

[16] G.K. Williamson and W.H. Hall, Acta Metallurgica 1 (1953) 22-31

[17] R.R. Chromik and K.J. Wahl, in *World Tribology Congress III* (American Society of Mechanical Engineers, New York, NY, 2005), pp. 829-830.

[18] R. P. Nair and M. Zou, Surface and Coatings Technology 203 (2008) 675-679

[19] A. J. Bushby and N. M. Jennett, in *Fundamentals of Nanoindentation and Nanotribology II* (Materials Research Society, 2001), Vol. 649, pp. Q7.17.11-Q17.17.16.

[20] P. Stoyanov, D. Goldbaum, J. R. Lince, X. Zhang, and R. Chromik, Tribology Letters 40 (2010), p. 199-211

[21] K. I. Schiffmann and A. Hieke, Wear 254 (2003) 565-572

[22] P. Stoyanov, Z. Fishman, J. R. Lince, and R. R. Chromik, Surface and Coatings Technology 203 (2008) 761-765

[23] I. L. Singer, R. N. Bolster, J. Wegand, S. Fayeulle, and B. C. Stupp, Applied Physics Letters 57 (1990) 995-997

[24] H. Tian, N. Saka, and E. Rabinowicz, Wear 142 (1991) 57-85

[25] H. I. Kim and J. R. Lince, in *World Tribology Congress III* (American Society of Mechanical Engineers, New York, NY, Washington, DC, USA, 2005), pp. 819-820.

[26] S. D. Dvorak, K. J. Wahl, and I. L. Singer, Tribology Letters 28 (2007) 263-274

[27] I.L. Singer, Solid Lubrication Processes, in: I.L. Singer and H.M. Pollock, Fundamentals of Friction: Macroscopic and Microscopic Processes, Netherlands, pp. 237-261, 1992.

[28] K. Miyoshi, T. Spalvins, and D. H. Buckley, Wear 108 (1986) 169-184

[29] B. J. Briscoe and A. C. Smith, Tribology Transactions 25 (1982) 349 - 354

[30] P. W. Bridgeman, Proc. Amer. Acad. of Arts and Sciences 71 (1936)

[31] A. Erdemir, R. A. Erck, and J. Robles, Surface and Coatings Technology 49 (1991) 435-438

[32] R. L. A. Kuster and K. I. Schiffmann, Zeitschrift fuer Metallkunde/Materials Research and Advanced Techniques 95 (2004) 306-310

Chapter 7

Scaling effects between micro- and macro-tribology of a Ti-MoS_2 coating

7.1 Abstract

The tribological properties of a Ti-MoS_2 coating (9 at.% Ti) were studied at macroscopic length scales with an *in situ* tribometer and at microscopic length scales with a nanoindentation instrument with microsliding capabilities. Measurements were conducted in controlled environments at both low and high humidity (i.e. ~4%RH and ~35%RH). Reciprocating micro- and macro-sliding tests were performed with spherical diamond tip with a 50 µm radius and a sapphire tip with a radius of 3.175 mm, respectively. For both scales, the range of Hertzian contact pressures were between 0.41 GPa and 1.2 GPa. *In situ* video microscopy observations identified that the dominant velocity accommodation mode at macro-scale was interfacial sliding. However, an additional velocity accommodation mode, transfer film shearing, was also observed with higher humidity. Overall higher friction was observed with microtribology compared to macrotribology. The higher coefficient of friction was attributed to three different stages during the sliding process, which were identified with respect to different contact pressures, contact areas, tip shapes, and environmental conditions. The first two stages exhibited a solid lubrication behavior with some combination of interfacial sliding, transfer film shearing and microplowing. The transfer film thicknesses for these stages, normalized to the initial Hertzian contact radius, fell in a range of 0.001 to 0.1. For the third stage, the dominant VAM

was plowing and the normalized transfer film thickness fell below this range. Comparisons between the two scales demonstrated that for dry sliding, microscopic contacts on Ti-MoS_2 deviate slightly from macroscopic behavior, showing higher limiting friction and microplowing. For humid sliding, microscopic contacts deviate significantly from macroscopic behavior, showing plowing behavior and absence of transfer films.

Keywords: MoS_2, Ti, Microtribology, Transfer films, MEMS

7.2. Introduction

In the last decade, there have been numerous studies on the tribological and mechanical properties of alloyed molybdenum disulfide (MoS_2) and bilayered metal/MoS_2 coatings [1-18]. The most common alloying elements in these studies have been gold and titanium. When compared to pure MoS_2, coatings with these metals have shown superior lubrication properties and a significant reduction in sensitivity to humid environment [5,7,15,19]. Generally, it is believed that metal additions densify the coatings, preventing moisture penetration and oxidation [20]. There is the added benefit of increased hardness and strength [10,15,20,21].

Both pure and alloyed MoS_2 coatings exhibit similar lubrication mechanisms. It is widely accepted that the formation of thin, stable transfer films on the order of tens to hundreds of nanometers in thickness is what leads to low friction [16-18,20,22,23]. Furthermore, both the transfer film and the tribofilm, a modified layer on the wear track, have a region of basal plane oriented MoS_2 at the sliding interface [1,17,20]. Coupled with these observations of the general nature of third bodies [23,24], *in situ* tribometry has revealed direct evidence that the main velocity accommodation mode (VAM) for MoS_2 based coatings is interfacial sliding with only a small fraction of the velocity accommodated by shearing of the transfer or tribofilms [16,18,25].

Load varying experiments are often conducted on solid lubricants to identify the effect or pressure on friction and wear. The slope of a plot of friction coefficient versus inverse contact pressure provides a measure of the interfacial shear strength for the sliding process [22,26-28]. For MoS_2, especially when considering recent *in situ* observations, the interfacial shear strength,

as its name implies, is related to interfacial processes. However, some minimal influence of mechanical deformation in the transfer or tribofilms cannot be ruled out. The interfacial shear strength for MoS_2 has been measured in the literature under many circumstances for both pure, alloyed and nanocomposite coatings. The values for the shear strength range anywhere from roughly 5 to 80 MPa [1,2,18,22,27,29]. Even though there is a wide range in the literature for this value, it is comparable to the bulk mechanical shear strength (S_o = 38MPa) of fully dense MoS_2 coatings [22]. The magnitude of the interfacial shear strength often is some indication of the VAM, with lower values implying that the main VAM is interfacial sliding which typically correlates to low adhesion, low friction and easy shear. Higher interfacial shear strength values imply that there might additional VAMs such as transfer film shearing and/or plowing.

Recent studies in the literature [21,29-31] have proposed the use of MoS_2 or metal-MoS_2 coatings for micro-electromechanical systems (MEMS), such as gears and switches. The findings on the tribology of MoS_2 coatings discussed above were derived from studies using macroscopic contacts, which consist of millions of asperities, but are typically treated as a single-asperity contact for simplicity. This type of averaging does not apply for the microscopic scale, where only a few asperities may contribute to the real area of contact. Consequently, roughness and the actual contact shape play a larger role [21,31-34]. These differences between contact sizes also implicate a potential change in transfer film behavior due roughness and adhesive forces [21,31,35,36], which could furthermore impact VAMs and wear. While recent studies [21,30,31] have provided significant new insight on the microtribological performance of MoS_2 coatings, particularly with Au and Ti, direct observation of transfer films for microscale sliding contacts

was not possible due to experimental difficulties related to the small contact sizes. Thus, connections made in these studies between roughness and adhesion and third bodies were based both on the new microtribological findings and previous knowledge from literature on macroscopic contacts.

The goal of this study was to provide a direct comparison between the macro- and microtribological performances of Ti-MoS_2 coatings. A better understanding of third bodies and transfer films was aspired at both scales with varying the contact pressures and humidity levels. A 'real time' study of the transfer film behavior and VAMs at the macro-scale was conducted with an *in situ* tribometer with video microscopy capabilities. On the micro-scale, transfer films were analyzed *ex situ* on the counterface (i.e. nanoindentation tips) by means of atomic force microscopy. Differences in the friction and wear behavior at both length scales were attributed to different "stages" of lubrication as identified by VAMs. Changes between the stages were correlated to differences in contact pressure, contact area, tip roughness and humidity.

7.3. Experimental Procedure

In this work, co-sputtered Ti-MoS_2 coatings with 9 at.% Ti was studied. The titanium concentration was measured using energy dispersive spectrometry (EDS) in a field emission gun scanning electron microscope (Hitachi 4700-S FEG-SEM, Japan). The Ti-MoS_2 sample was produced by Teer Coatings, Ltd. (Worcestershire, UK) using a close field unbalanced magnetron sputtering ion plating (CFUBMSIP) system operated in DC mode [15]. Surface characterization

on these coatings was performed using a inVia Raman microscope (Renishaw, Gloucestershire, UK) with a 514.5 nm Ar+ laser in order to obtain information regarding phase identification, bonding and degree of crystallinity.

The mechanical properties of the coating were measured using a nanoindentation instrument (Hysitron, Inc. Minneapolis, MN, USA) with a 1D transducer and a diamond Berkovich tip. The values presented in this paper were obtained using an indentation depth of 170 nm and are averages of ten measurements. The same nanoindentation instrument was also used for the microtribological properties with a 2D transducer and a diamond spherical tip (50μm radius). This tip was characterized using an atomic force microscope (Veeco Nanoman 3100, Santa Barbara, CA, USA) operated with closed loop scanning in tapping mode. This characterization was performed in order to obtain an accurate area function of the tip at any given depth, a technique that is described in detail elsewhere [21].

For microtribology, the length of the wear tracks was 8 μm and the velocity was kept constant at 4 μm/sec. The normal load was varied between 0.2 and 5.0 mN, which resulted in an initial Hertzian contact pressure between 0.4 and 1.2 GPa and a initial Hertzian contact radius of 0.4 and 1.1 μm. Due to limitations by the instrument software, only 400 cycles were performed at a time, and were repeated on the same position in order to achieve a total of 800 cycles. The friction results were analyzed using a custom-built analysis code written with Matlab software. The coefficient of friction was calculated from the lateral force divided by the normal force. The

average friction coefficient for each cycle was calculated from 75 ± 2 data points corresponding to the central 5 μm of the track.

All sliding tests were performed at low (i.e. between 3 and 5%) and at high (i.e. between 30 and 40%) relative humidity levels while the temperature was kept at ambient conditions (~295 K). The low relative humidity level was controlled using compressed air, which passed through anhydrous $CaSO_4$ desiccant and into the instrument enclosure at a high flow rate for a few minutes and then a constant low flow rate throughout the sliding experiments.

Macroscopic sliding tests were performed with a pin-on-flat reciprocating *in situ* tribometer that was custom-built to allow for video microscopical investigations of the sliding interface. The generic design of the instrument was based on an experimental setup first described by DesCartes and Berthier [37], subsequently demonstrated in detail by various authors in the groups of Singer and Wahl [16,18,23,38-42] and recently reviewed in 2008 [43]. Tests were performed using a hemispherical sapphire counterface with a radius of 3.175 mm. Birefringence from the sapphire was eliminated by inserting a polarizing film into the light path. Video microscopy was conducted through the counterface to examine third body formation and transfer film dynamics. Videos were captured using a commercially available camcorder with a pixel resolution of 853 x 480 at 29.97 frames per second. The use of a 20x ultra-long working distance objective lens allowed for resolving 1.2 μm per pixel. Using the transparent hemisphere on a flat surface resulted in the occurrence of optical interface fringes (Newton's rings), which were used to calculate the thickness of the transfer film (third body material trapped between the coating

and the ball) at selected cycles. This analysis technique is described in details elsewhere [44]. *Ex situ* transfer film thickness measurements were performed using a noncontact profiler (Wyko NT 8000 Optical Profiler, Veeco Instruments).

Each sliding test at the macro-scale was performed for a total of 1200 cycles with initial track length of 8 mm at a constant sliding velocity of 3 mm/sec. The tests were run as 'stripe test', where the track length is decreased after 200 cycles to 6 mm, after 400 cycles to 4 mm, and after 800 cycles to 2 mm. The normal load was varied between 1.2 and 29.8 N, which also resulted in contact pressures between 0.4 and 1.2 GPa and contact radii between 30 and 90 μm. Lateral forces were determined at a sampling rate of 800 Hz by means of a calibrated piezoelectric force sensor, which was housed within the sample stage. Force data from turning points (approximately 12 % at each end) was omitted. An average friction coefficient, μ, was calculated using the lateral force divided by the normal load. Environmental conditions (i.e. temperature and humidity levels) for the macrotribological tests were kept within the same range as with the microtribological tests. Wear area measurements of macroscopic wear scars were performed using the same noncontact profiler that was used for transfer film thickness measurements.

Table 7.1 shows a comparison between the parameters of the macro- and microtribological setups. The range of initial Hertzian contact pressures was kept similar between the two scales. Due to the differences for the size of the tips and the capabilities for normal load, the contact pressures for the two scales was the same despite the significantly smaller contact radius at the

micro-scale. Unless otherwise noted, the term “contact pressure” will henceforth refer to the initial Hertzian contact pressure as calculated in Table 7.1.

Table 7.1. Comparison of the experimental parameters for the macro- and microtribology experiments. The contact pressure and radius are calculated from Hertzian contact mechanics [45].

	Counterface Material / Radius (μm)	**Normal Load (mN)**	**Contact Pressure (GPa)**	**Contact radius (μm)**
Macrotribology	Sapphire / 3.175×10^3	1197 - 29822	0.4-1.2	30-90
Microtribology	Diamond / 50	0.2-5.0	0.4-1.2	0.39-1.15

7.4. Results and Discussion

7.4.1 Coating Characterization and Properties

Figure 7.1 shows the coating characterization using Raman spectroscopy. No evidence of peaks that could be assigned to crystalline MoS_2 was found. However, the broad feature between roughly 200 and 500 cm^{-1} is the typical feature observed for an amorphous or poorly crystalline MoS_2 coating [17,21]. The reduced modulus and the hardness for the Ti-MoS_2 coating was measured to be 170.6 ± 1.7 GPa and 5.7 ±0.1 GPa respectively. The addition of Ti resulted in better mechanical properties compared to sputtered pure MoS_2 coatings [21] (i.e. E_r = 29 ±5 and H = 1.2 ± 0.4). The thickness and RMS roughness of the coating was 1.1 μm and 4.4 nm, respectively.

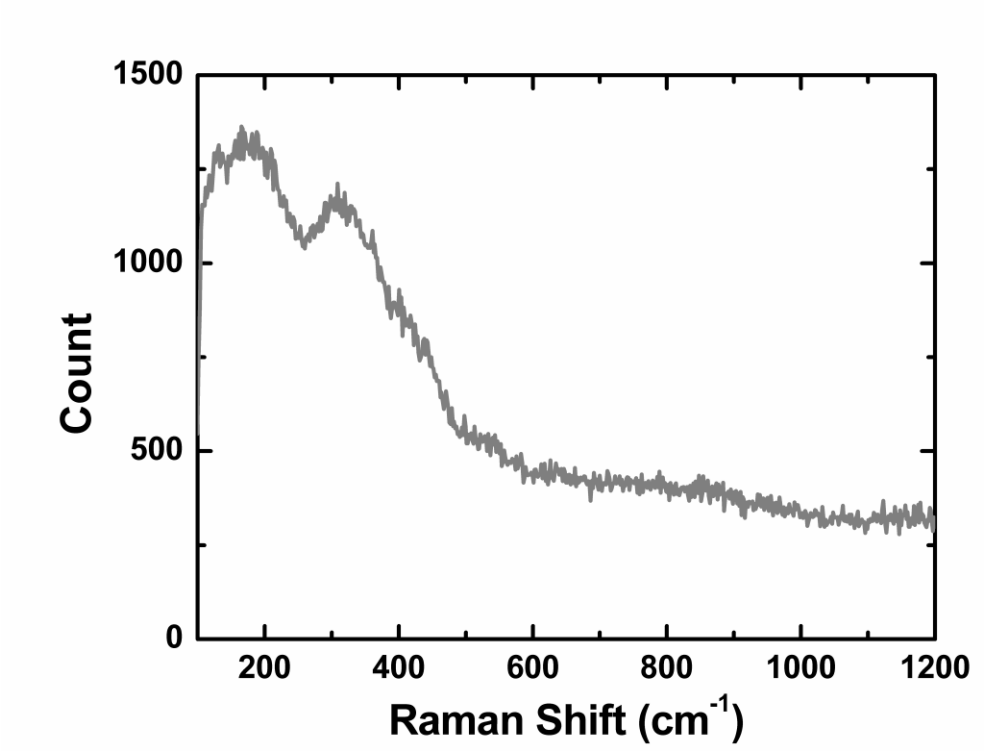

Figure 7.1. Raman spectroscopy scan for the as-prepared Ti-MoS_2 coating

The increase in hardness with the addition of titanium is consistent with literature [10,46] on similar coatings. Ding et al. [10] showed that the hardness of such coatings increases with increasing the titanium concentration and the maximum hardness is observed with 20.2at% Ti. The increase in hardness of MoS_2 with the addition of a metal was explained due to solution hardening effect [47] and/ or coating densification [48].

7.4.2 Macrotribology

7.4.2.1 Friction behavior

Figure 7.2 shows the average coefficient of friction vs. cycle for representative macrotribology tests with contact pressures between 0.5 and 1.2 GPa at (a) 4% and (b) 35% relative humidity. The steady state coefficient of friction (i.e. after 800 cycles) for both humidity levels and all contact pressures falls below 0.1, which is good agreement with literature [10] on similar coatings and environmental conditions. For most contact pressures a significant decrease in friction was observed during the run in stage (i.e. first 50 cycles). After the run in stage, the friction continuous to decrease slightly and eventually becomes constant (i.e. steady state). The steady state coefficient of friction (i.e. 800^{th} to 1200^{th} cycle) decreases with increasing the normal load for both humidity levels. However, higher steady state friction was observed overall with higher humidity (i.e. a difference of 0.025 for the 1.2 GPa contact pressure).

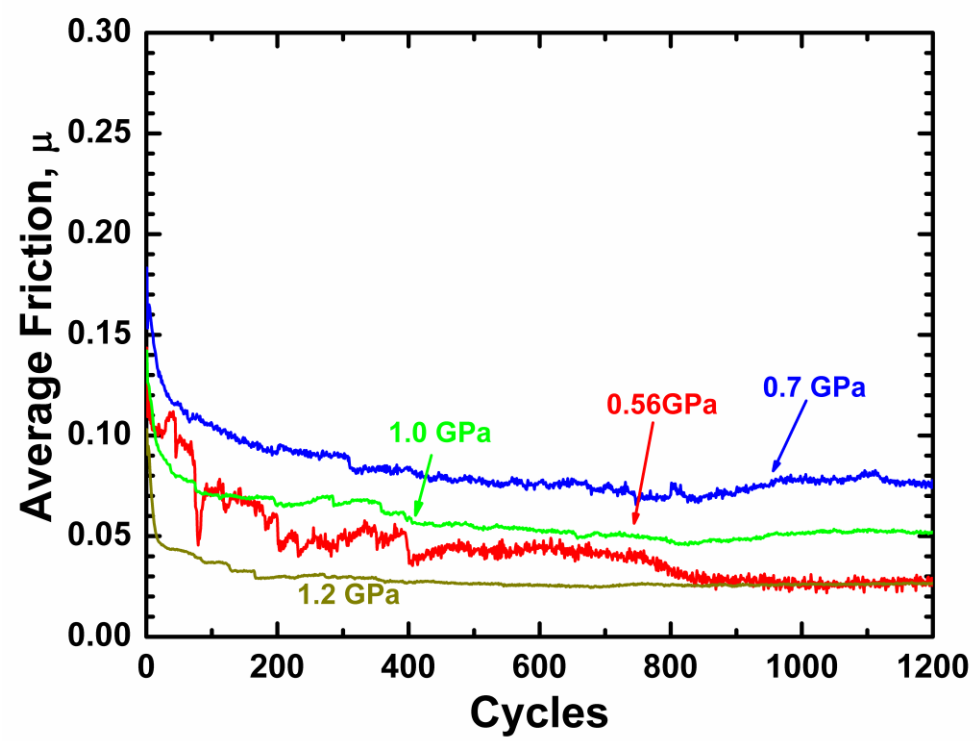

(a)

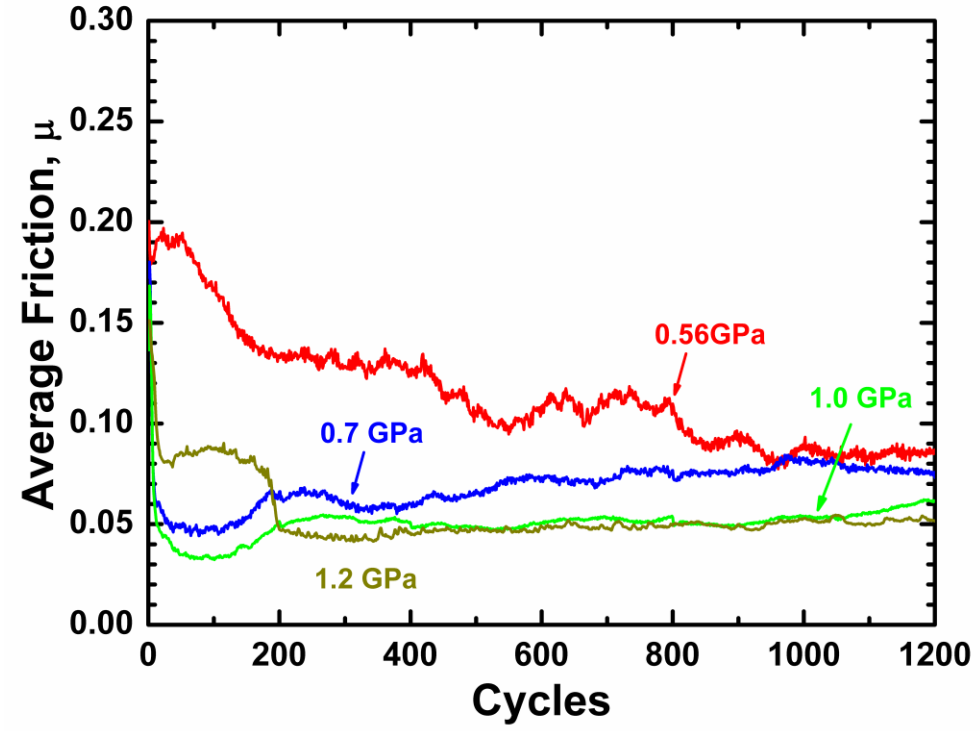

(b)

Figure 7.2. Average coefficient of friction vs. cycle for macrotribological testing with initial Hertzian contact pressures between 0.5 and 1.2 GPa at (a) 4% and (b) 35% relative humidity

7.4.2.2 Wear behavior

The cross-sectional wear area of the macrotribological tests is shown vs. the contact pressure in Figure 7.3 for the low and high humidity level. The wear area increased with increasing contact pressure for both humidity levels. However, the tests performed at higher humidity showed higher wear for all contact pressures compared to the wear for the low humidity tests. For the two highest contact pressures the difference in wear area was more than 30 μm^2, corresponding to a difference in maximum depth of 250 nm.

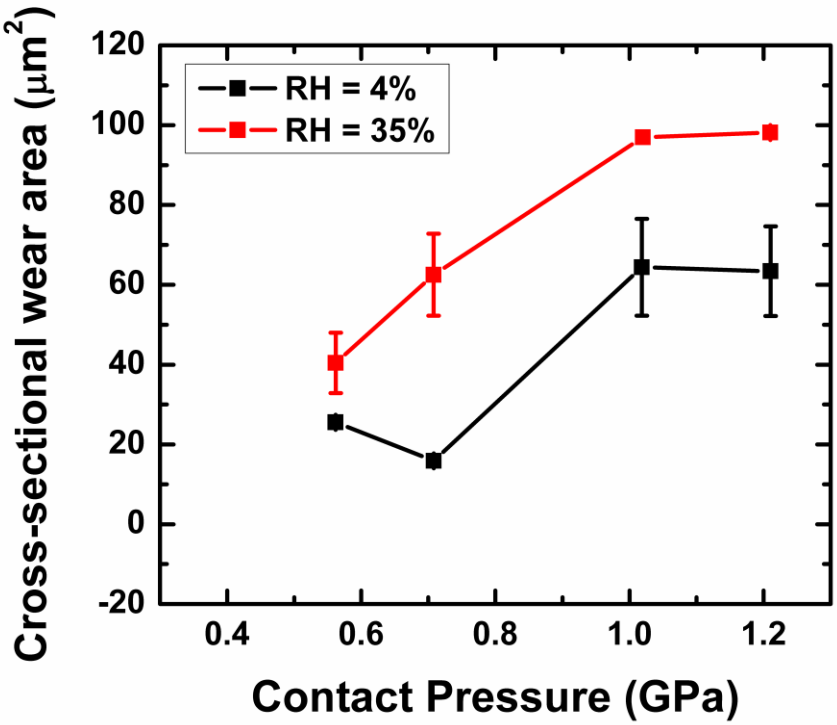

Figure 7.3. Cross-sectional wear area vs. contact pressure for macrotribological testing at low and high humidity levels.

7.4.2.3 In situ Tribometry and Wear Track Analysis

In situ test video was used to monitor the formation of transfer films and motion of third bodies. Figures 7.4 (a) and (b) show images taken at three different cycles (1st pass, 110th cycle, and 1000th cycle) for the tests performed with 0.7 GPa and 1.2 GPa contact pressure, respectively. The contact radius increased with increasing the normal load. From images like those in Figure 7.4, the contact radius was approximately 50 µm and 90 µm for the 0.7 GPa and 1.2 GPa contact pressures, respectively. These measurements agreed well with calculations from the Hertzian contact model, which were calculated to be 51.8 µm and 88.6 µm, respectively.

The tests performed at a pressure of 0.7 GPa showed very little material transfer during the first pass of the sliding test (see Figure 7.4(a)). *In situ* images from the 110th cycle showed a transfer film within the contact region and debris particles around the contact area. The growth of the transfer film during these early cycles correlated to a decrease in the coefficient of friction as seen in Figure 7.2 (a). At higher cycles (i.e. 1000th), even more material was transferred to the counterface; thick debris pads were seen on both sides of the contact area. Compared to the 110th cycle, significantly higher amount of fine debris particles were observed surrounding the contact region at cycle 1000. The increase in material transfer with the higher cycle number correlates with the decrease in friction from 0.103 to 0.077 going from cycle 110 to cycle 1000.

A similar behavior in the evolution of transferred material was observed with the higher contact pressure of 1.2 GPa (see Figure 7.4 (b)). For this contact pressure, even after the first pass, a small amount of the coating material was transferred to the counterface. By cycle 110, additional

material was transferred to the contact zone and fine debris particles were scattered around the contact area. The amount of material transfer was more when compared to the behavior with a contact pressure of 0.7 GPa. At cycle 1000, the transfer film in the contact zone appeared to be relatively smooth with some thick debris pads on both sides of the contact zone and more fine debris particles surrounding the contact, as seen with the 0.7 GPa contact pressure. For all contact pressures at low humidity, the *in situ* videos revealed only barely discernable evidence of motions of the transfer film, an indication that the main VAM was interfacial sliding. This observation for Ti-MoS_2 coatings is consistent with what has been observed for other solid lubricant coatings with a significant MoS_2 content [16,25,49].

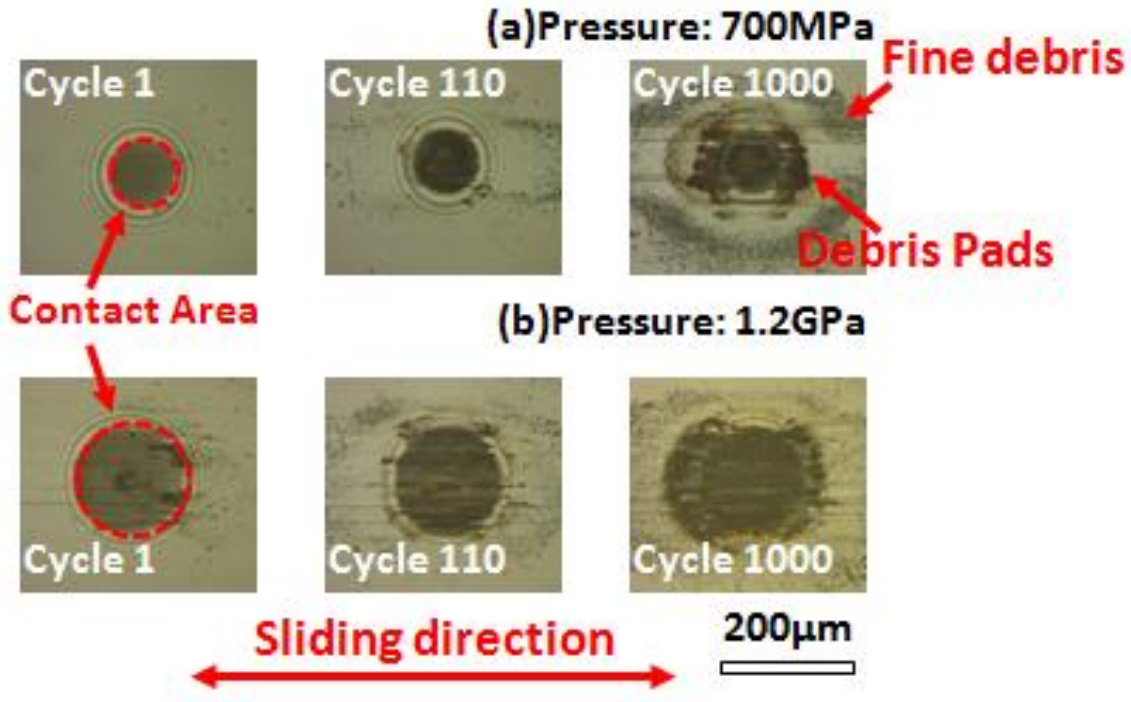

Figure 7.4. *In situ* images taken at low humidity levels for (a) 700MPa and (b) 1.2GPa contact pressures. The dark circular features are the contact regions, where additional features within this area are transfer films. Interference fringes (Newton's rings) are also observable. Features outside of the contact regions are debris attached to the sapphire slider, including small debris particles and pads of agglomerated debris seen just outside the contact region.

Figure 7.5 shows *in situ* images for the tests performed at higher humidity using (a) 0.7 GPa and (b) 1.2 GPa contact pressures. During the first pass, the behavior of the transferred material was similar to that observed for low humidity levels, where nearly no visible material transfer was observed for either contact pressure. However, as the test progressed, material was transferred to the counterface within and outside the contact region, as can be seen in the image for the 110^{th} cycle. Subsequently, even more material was transferred onto the counterface (see image for the 1000^{th} cycle). However, the transfer film in the contact zone does not appear to be uniform (i.e. see variation in contrast in contact region of Figure 7.5). Furthermore, the transfer film appeared to have an elliptical shape with the major axis perpendicular to the sliding direction, whereas the transfer film at low humidity remained circular in shape throughout the whole test. The evolution of debris transfer around the contact zone was also slightly different when compared to the behavior at low relative humidity. The debris particles on the counterface at low relative humidity were closer to the contact region, whereas the debris particles at higher humidity levels were further away from the contact zone. The difference in the debris behavior between the two humidity levels is explained by fact that the debris particles at low humidity levels adhere more strongly to the counterface in comparison to debris at higher humidity. This was confirmed with the *in situ* videos, where movement of debris particles was observed throughout the sliding test at high humidity levels. Figure 7.6 shows *in situ* images of a single cycle going in one direction. Some debris particles that are present in the beginning of the cycle get moved around or disappear from the counterface when sliding towards the end of the wear track. A similar behavior was also seen with the transfer film within the contact zone, where the bottom of the transfer film (i.e. surface of the transfer film that is in contact with the wear track) moves in the

opposite direction of the sliding, while the surface of the transfer film that is adhered to the slider remains on the same position. This is an indication that the transfer film at high humidity levels was not as stable and exhibited transfer film shearing to varying degrees throughout the test. Therefore, even though the velocity was mainly accommodated by interfacial sliding, there was also a second VAM of interfilm shearing at higher humidity. This has been observed previously in MoS_2 containing solid lubricant coatings [16,23,49].

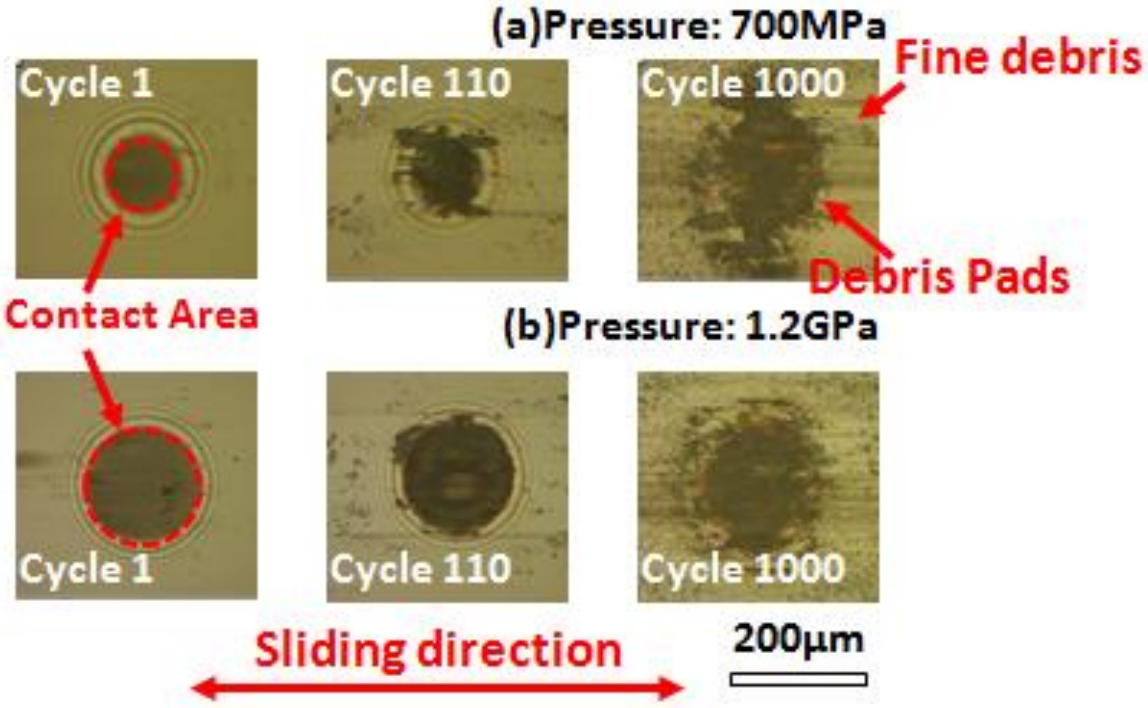

Figure 7.5. *In situ* images taken at high humidity levels for (a) 0.7 GPa and (b) 1.2 GPa initial Hertzian contact pressures.

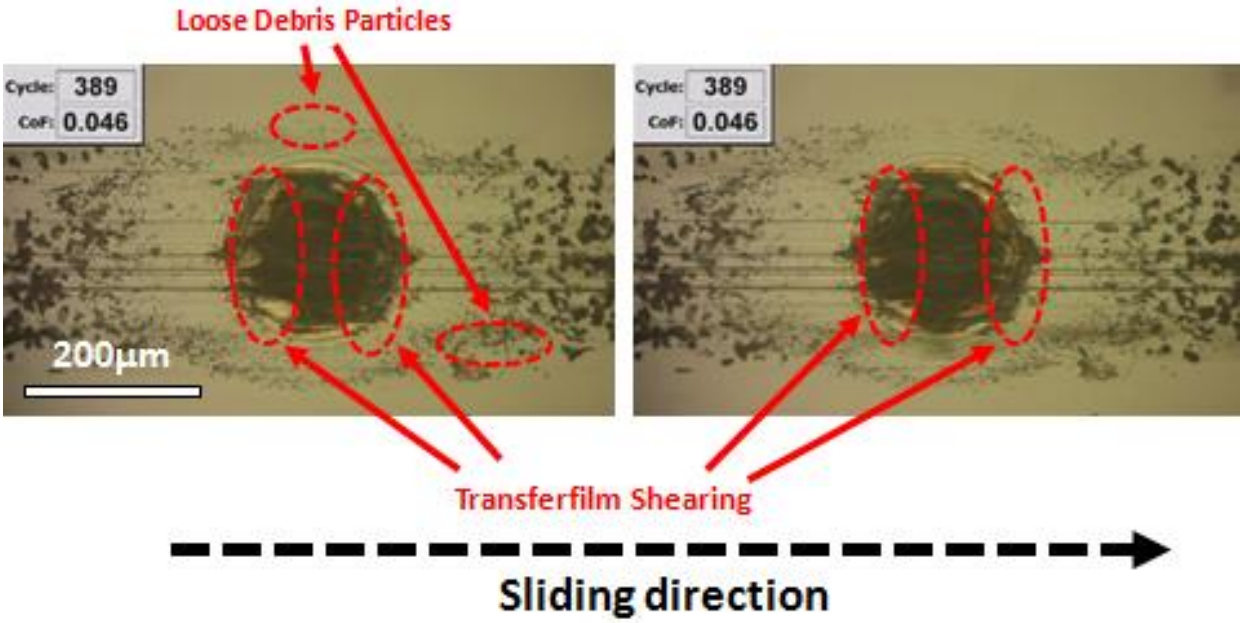

Figure 7.6. *In situ* images of a single cycle going in one direction taken at high humidity using 1.2 GPa initial Hertzian contact pressure. One image was captured in the beginning of the wear track and the other towards the end. It was observed that some debris particles that were present in the beginning of the cycle got moved around or disappeared from the counteface when sliding towards the end of the wear track. The transferfilm within the contact zone was observed to be not as stable and exhibited transfer film shearing to varying degrees throughout the sliding.

The fact that the debris particles don't adhere strongly to the counterface at high humidity levels was also confirmed with *ex situ* observation of the wear track. The middle section of the wear track was scanned using an atomic force microscope and is shown in Figure 7.7 for the tests performed using a contact pressure of 1.0 GPa at (a) 4% and (b) 35% relative humidity. In the case of the test performed at higher humidity level, debris particles were observed on the wear track. For the low humidity tests, virtually no debris particles were seen on the worn surface. This indicates that wear debris formed in humid environments tended to re-deposit on the wear

track throughout the sliding test, whereas the debris formed in dry air tended to remain on the counterface around the transfer film.

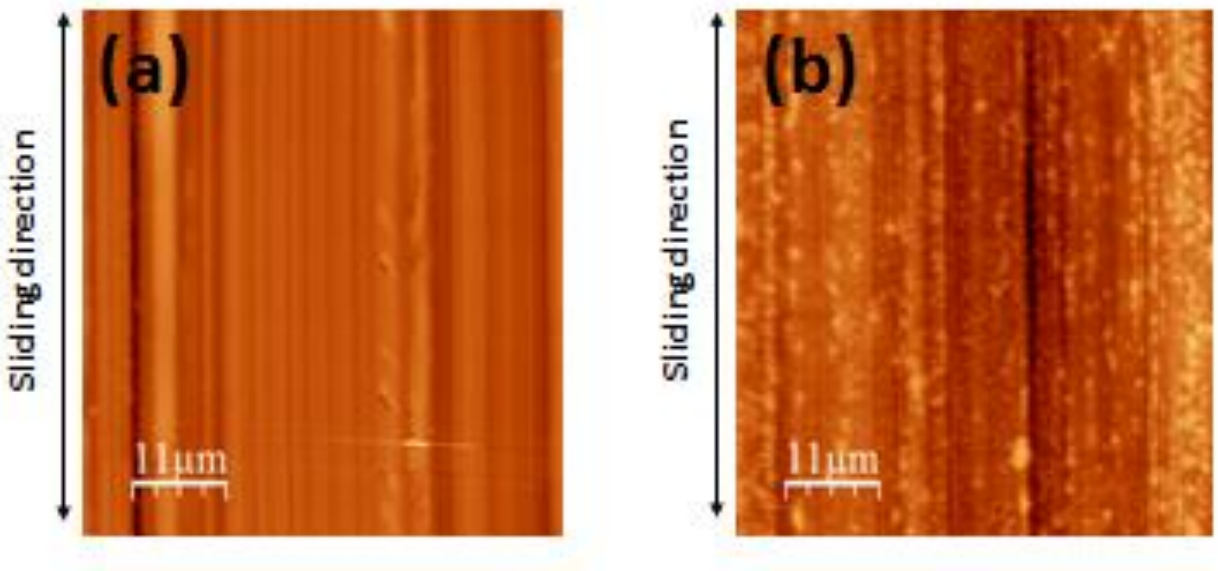

Figure 7.7. Characterization of wear tracks from macrotribology testing using an atomic force microscope for (a) low humidity and (b) high humidity using a contact pressure of 1.0GPa.

Figure 7.8 (a) shows the wear track characterization using Raman microscopy for the low and high relative humidity levels at a constant contact pressure of 1.0 GPa. For both conditions, MoS_2 peaks were observed that were not found for the unworn surface (see Figure 7.1). This indicates that a MoS_2 tribofilm was formed on the worn surface. These tribofilms typically consist of a nanoscale region of MoS_2 with greater crystallinity than the parent coating and often have their basal planes parallel to the sliding direction [1,17,20].

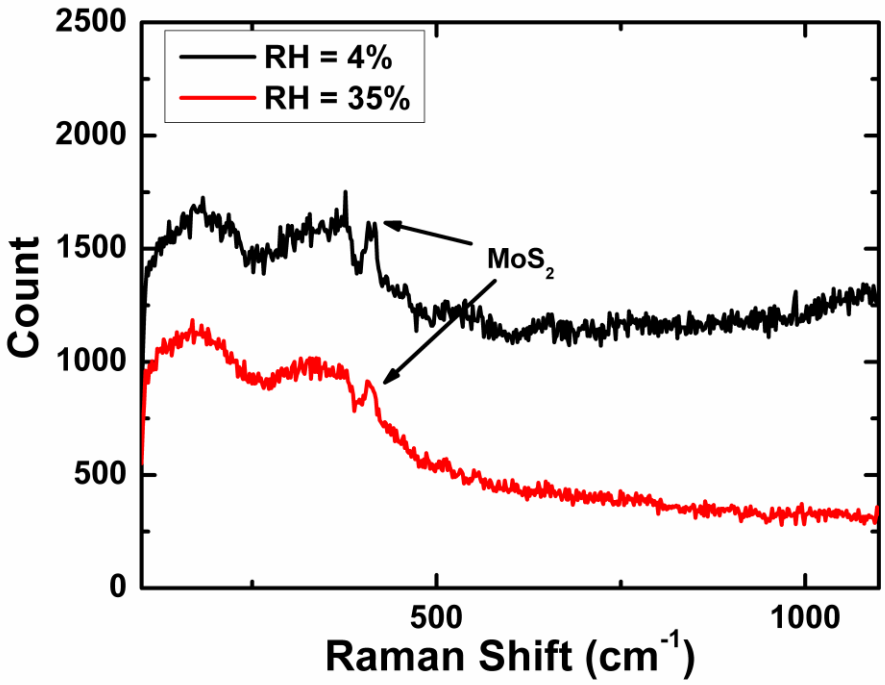

Figure 7.8. Characterization of wear tracks from macrotribology testing using Raman spectroscopy on Ti-MoS_2 carried out at a contact pressure of 1.0 GPa and both high relative humidity (bottom curve) and low relative humidity (top curve).

7.4.2.4 Transfer film Analysis and Measurements

Due to the formation of the debris pads (see Figures. 7.4 and 7.5), *in situ* measurements of the transfer film thickness were only obtainable up to somewhere between cycle 150 and 300. Despite this limitation, the Newton's ring method [44] was used to calculate average transfer film thickness for all the test conditions with results for cycle 200 presented in Table 7.2. Generally, for low humidity, the transfer films were between 10 and 60 nm and, for high humidity, the transfer films were between roughly 100 and 250 nm. The greater variability in the

transfer film thickness at high humidity may be due to transfer film shearing that would lead to more frequent changes to the transfer film thickness and morphology.

Transfer films were also examined *ex situ* with non-contact optical profilometry. Measurements were obtained for three contact pressures at both humidities and also for two tests (see Table 7.2). The thickest transfer film was observed for the highest contact pressure (i.e. 1.2 GPa) for both humidity levels. There was, however, no significant difference in the transfer film thickness between the two humidity levels for any of the three contact pressures. Also, the transfer film thickness for the end of the test was consistently between 200 and 400 nm, with one measurement of 150 nm.

Comparing the *in situ* results near cycle 200 and the *ex situ* results at cycle 1200 showed that the transfer film thickness increased with sliding for all contact pressures and humidity conditions. In fact, the thickness changed generally from between 10 and 150 nm at cycle 200 to a few hundred nanometers at cycle 1200. This trend has been observed previously in other studies of MoS_2 coatings. For a pure MoS_2 coating, Chromik, et al. [16] observed a similar increase in transfer film thickness over 1200 cycles in dry sliding tests with an initial Hertzian contact pressure of 0.9 GPa.

Chemical composition of transfer films was determined by elemental analysis using EDS. Results for both humidity levels at the contact pressure of 1.0 GPa showed that the transfer film

consisted of molybdenum, sulfur and titanium. Analysis for other contact pressures showed similar results.

Table 7.2. Transfer film thickness measurements for macrotribology testing for high and low humidity and various contact pressures. The results from two tests are presented in each column where available. Entries for the tests are entered in the same order so that comparisons can be made between *in situ* and *ex situ* measurements that are test specific.

	Transfer film Thickness (nm)			
Initial Hertzian Contact Pressure (GPa)	**Low Humidity**		**High Humidity**	
	***In situ* – cycle 200**	***Ex situ* – cycle 1200**	***In situ* – cycle 200**	***Ex situ* – cycle 1200**
0.56	35, 41	350, 200	119, 89	350, 225
1	10, 59	300, 150	260, 92	325, 275
1.2	30, n/a*	350, 350	140, n/a**	350, 400

** transfer film was very thin and unmeasurable*
***measurements not obtained due to debris pads covering the Newton's rings*

7.4.3 Microtribology

7.4.3.1 Friction behavior

Microtribology measurements of average coefficient of friction vs. cycle at (a) 4% and (b) 35% relative humidity are shown in Figure 7.9. For all tests, the friction showed a significant decrease in the first few cycles, during the run-in stage, and then increased slightly and finally became relatively constant after the 300th cycle up to the end of the test (i.e. steady state stage). The friction behavior at the micro-scale was very similar to the behavior at the macro-scale; the coefficient of friction decreased with increasing contact pressure and on average higher friction values were observed at the higher humidity level.

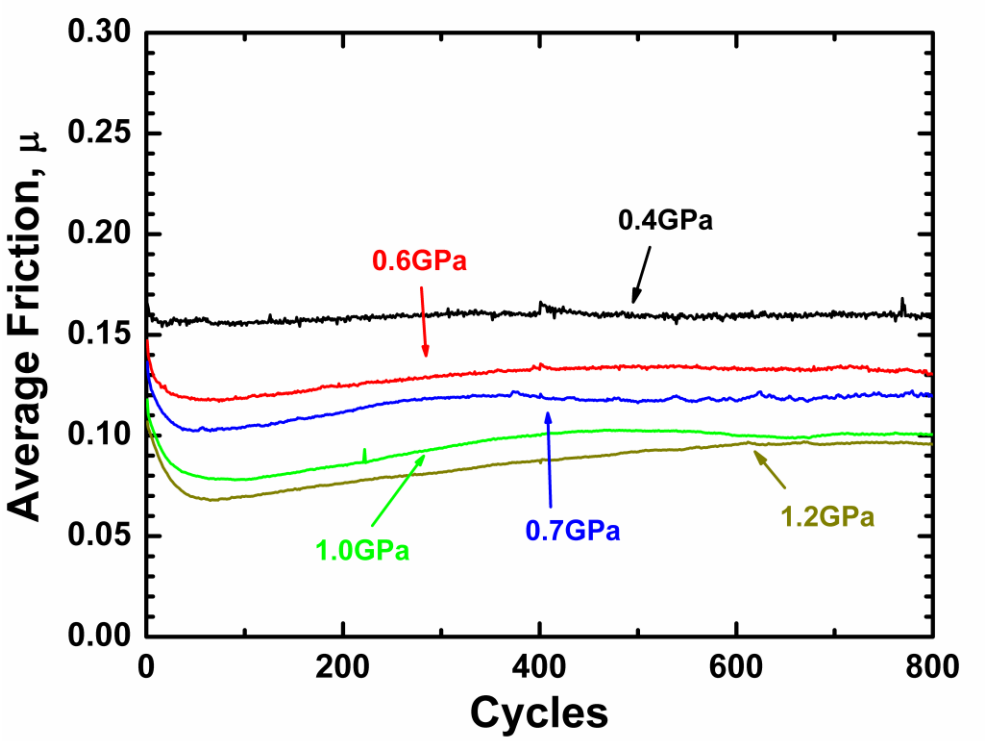

(a)

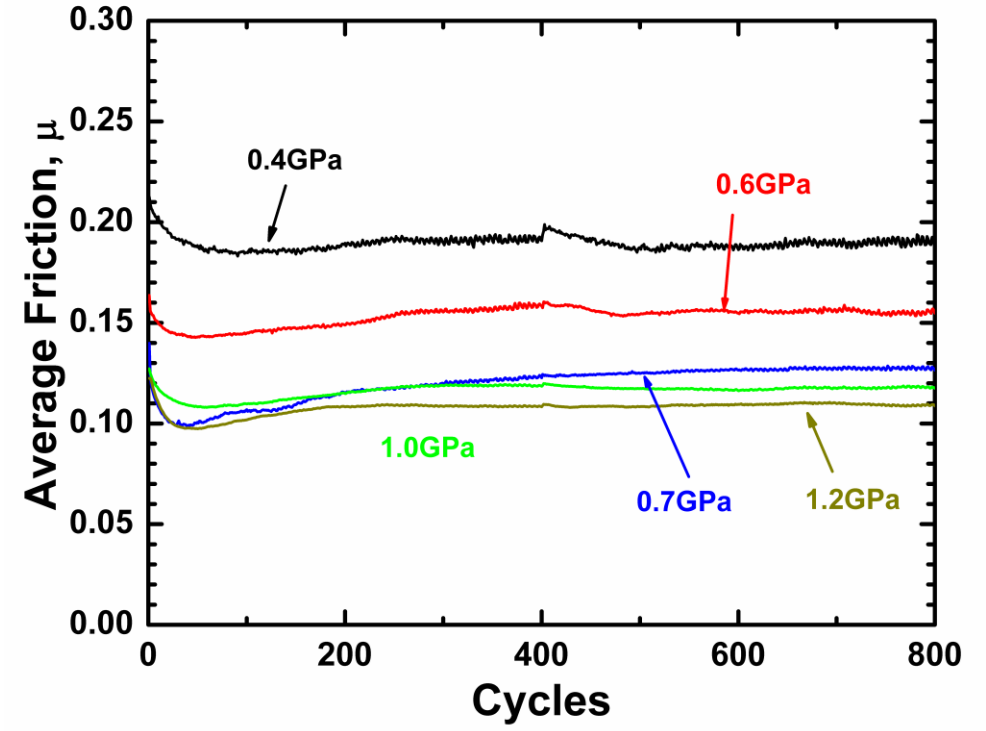

(b)

Figure 7.9. Average coefficient of friction vs. cycle for microtribological tests withinitial Hertzian contact pressures between 0.4 and 1.2 GPa at (a) 4% and (b) 35% relative humidity

7.4.3.2 Wear behavior

The cross-sectional wear area for both humidity levels increased with increasing the contact pressure (see Figure 7.10). This wear behavior was very similar to that observed for the macrotribology. However, at the micro-scale, no significant difference in wear was observed between the two humidity levels.

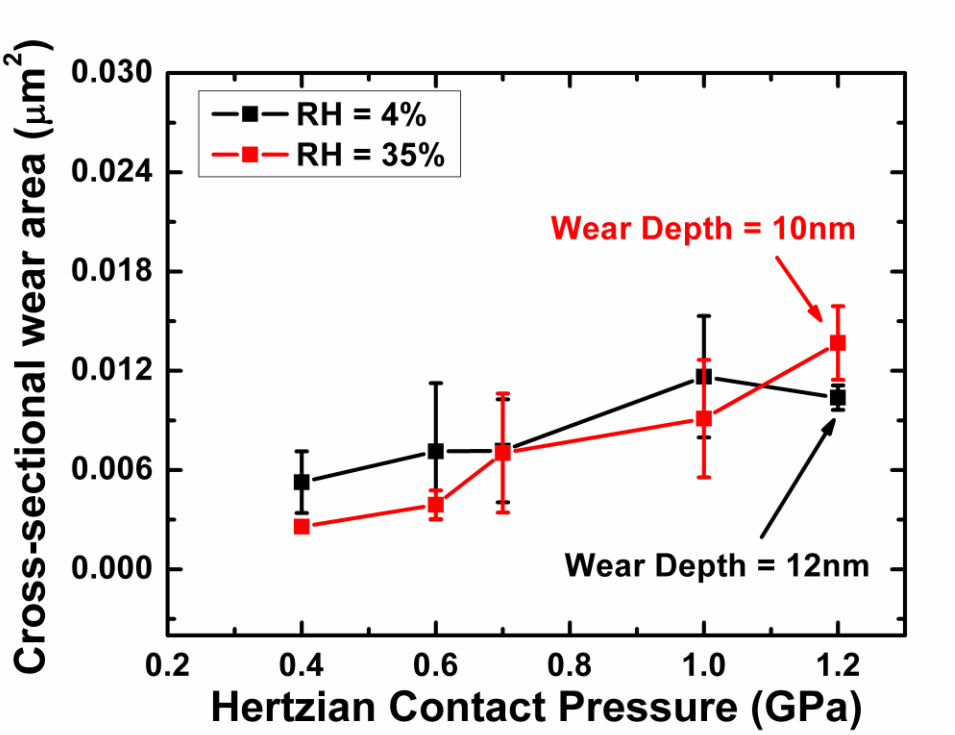

Figure 7.10. Cross-sectional wear area vs. normal load for the microtribological tests for low and high humidity levels

7.4.3.3 Ex situ analysis of transfer material and wear track

Ex situ analysis of the wear track showed similar wear track morphology to macrotribology. The worn surface at higher humidity was rougher and more debris particles were observed when compared to the wear track for the dry conditions (see Figure 7.11). This suggested that, at the

micro-scale, the debris particles tended to re-deposit on the wear track throughout the sliding test, similar to the macro-scale. Further similarities between the worn surfaces at the micro-scale and at the macro-scale were also seen with Raman spectroscopy (see Figure 7.12). Peaks consistent with crystalline MoS_2 were observed at the low humidity tests, which indicated that there was also a tribo-film formation at the micro-scale. With no sharp peak for MoS_2 for higher humidity, the tribofilm formation was less pronounced than for lower humidity.

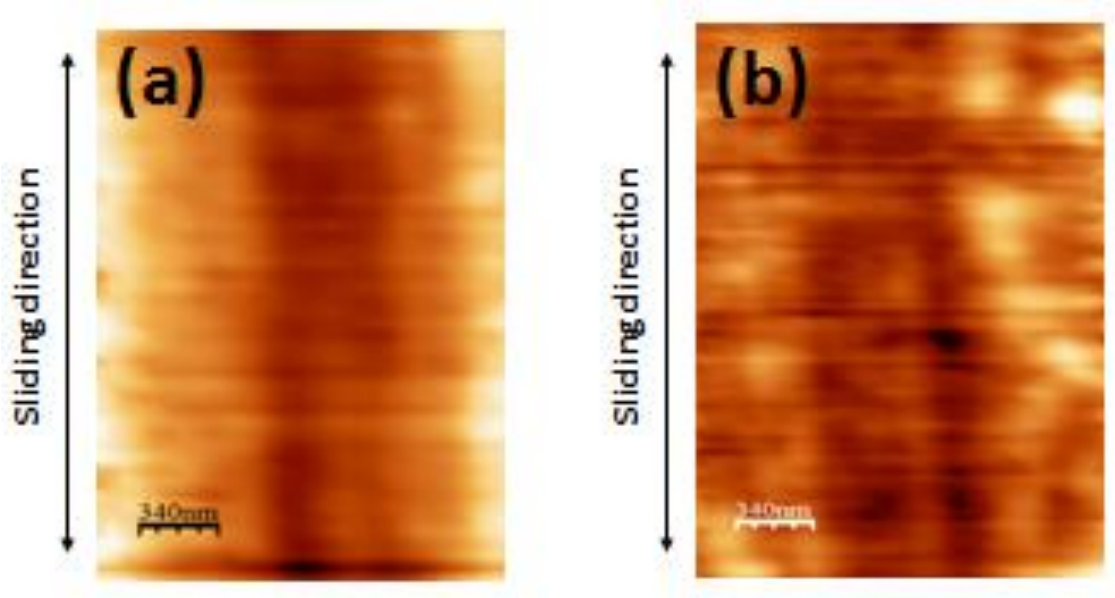

Figure 7.11. *Ex situ* wear track characterization using an atomic force microscope for (a) low relative humidity and (b) high relative humidity using a contact pressure of 1.0GPa

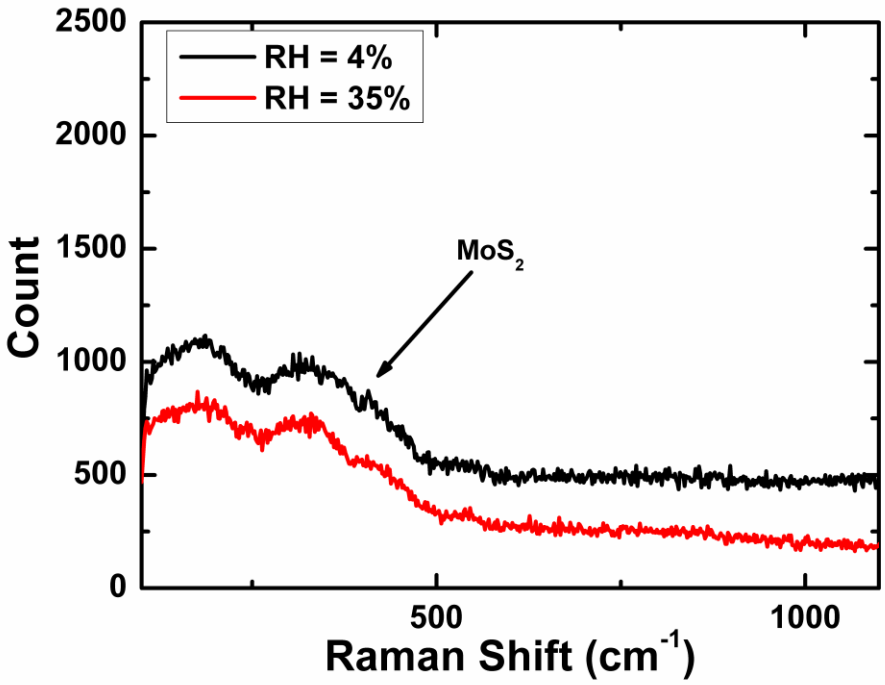

Figure 7.12. Wear track characterization using Raman microscopy for microtribology for the tests performed with a contact pressure of 1.2GPa

Ex situ analysis on the nanoindentation tip were performed at the end of the sliding tests using an AFM and are shown in Figures 7.13 (a) and (b) for low and high humidity levels, respectively. These images revealed the presence of transferred material onto the counterface. The behavior of material transfer at the micro-scale was similar to that found for the macro-scale. At low humidity, material transfer was found in the contact zone, indicated by dashed circles. Due to the flattening process of these AFM images, debris pads on either side of the contact appear to be at the same height as the transfer film itself. Fine debris particles were also seen near the contact region.

For both humidity levels, the amount of debris particles was significantly higher with the increasing contact pressures. For higher humidity, however, less debris particles were observed around the contact area for all contact pressures when compared to the tests at low humidity levels. Furthermore, the debris particles at high relative humidity are more scattered compared to the debris at low humidity. Within the contact zone (i.e. black circles in Figure 7.13), a transfer film was observed only for the low humidity tests with all contact pressures.

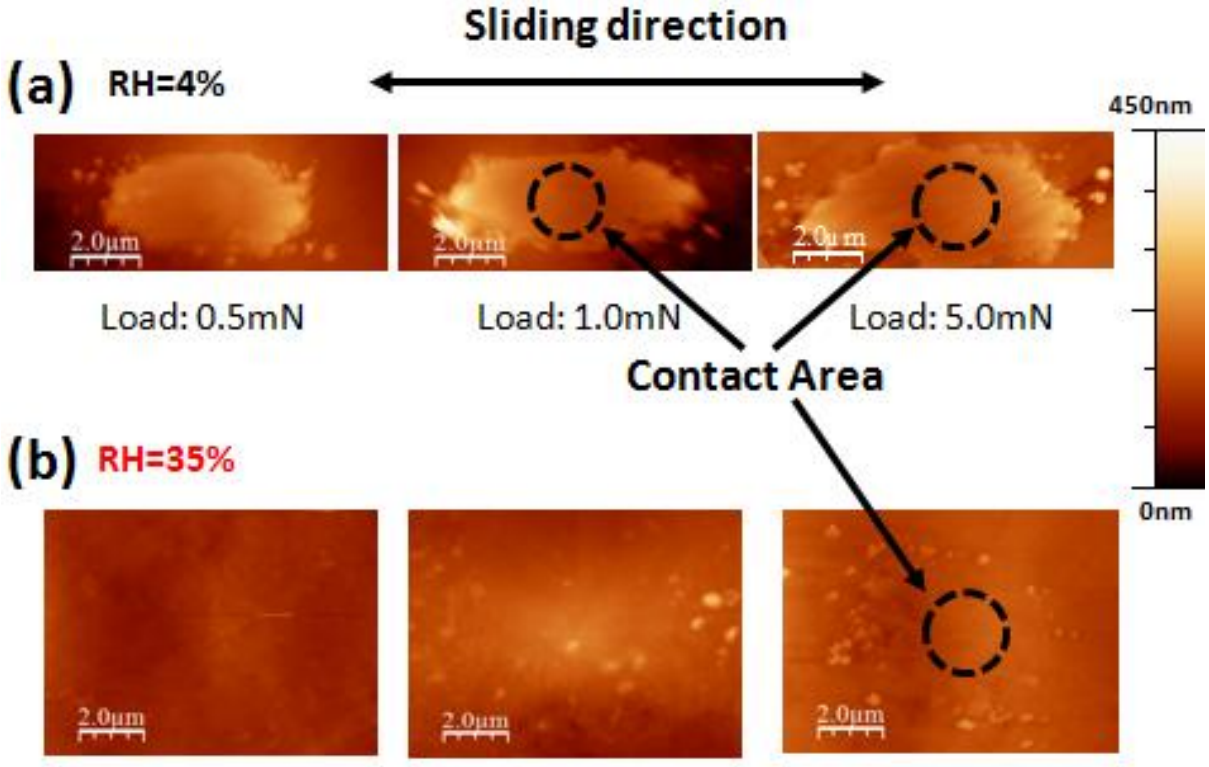

Figure 7.13. *Ex situ* analysis using atomic force microscopy for the nanoindentation tip for (a) low and (b) high humidity levels. Results are presented for three different loads.

Thickness measurements of the transfer film at the micro-scale were performed using cross sections of the atomic force microscopy images in Figure 7.13. The transfer film thickness was determined by subtracting a fitted sphere from the AFM cross section data. The transfer film

thickness for various contact pressures is shown in Table 7.3 for low and high humidity levels. It was observed for low humidity levels that the transfer film thickness for microtribology falls between 15 and 30 nm. No transfer film thicknesses were obtained for the high humidity tests because the values were either zero or were within the error of the measurement (i.e. roughness of the tip). Based on the roughness of the tip and the error analysis for our method, the thickest transfer film that could remain undetectable is roughly 5 nm.

Table 7.3. Transfer film thickness measurements for microtribological tests for low humidity and various contact pressures.

	Transfer film Thickness (nm)	
Initial Hertzian Contact Pressure (GPa)	***Ex situ* - cycle 800**	
	Low Humidity	High Humidity
0.56	30	n/a*
0.7	15	
1.2	20	

**transfer film was very thin and not measurable*

7.4.4 Comparison of Macro- to Microtribology

7.4.4.1 Role of transfer film and debris on the friction behavior

In situ tribometry and *ex situ* wear track analysis revealed information regarding the sliding process in terms of the transferred material and the tribofilm (i.e. surface of the wear track). The increase in the coefficient of friction with higher humidity levels at the macro- and at the micro-scale was associated with differences in the evolution of the transfer film formation; *in situ* observations at the macro-scale revealed a more stable and uniform transfer film at low relative humidity. Further *in situ* observation suggested that the higher friction values in humid

environments could also be due to a second VAM (i.e. transfer film shearing) and the presence of loose debris particles on the counterface. *Ex situ* analysis for the high humidity tests also revealed significantly higher amount of debris particles on the wear track, which indicates that the debris particles get re-deposited from the counterface onto the wear track, whereas in dry conditions these particles remain on the tip throughout the whole sliding procedure. This has also been previously observed in literature for Pb-Mo-S coatings [18], where the third bodies adhered securely to the counterface. More debris particles on the worn surface associated with higher friction has also previously been observed with Ti-MoS_2 coatings [50] and the friction rise was explained by the debris plowing against the softer transfer film. One possible explanation on why debris particles behave differently in dry air tests (i.e. remain on the counterface throughout the whole sliding test) when compared to the debris particles in humid environment could be due to the difference in their properties. The 'humid' debris particles are formed in humid environment possibly by a surface chemical interaction with moisture, whereas the 'dry' debris are formed with the nearly absence of moisture and therefore tend to be more stable and adherent.

7.4.4.2 Comparisons between Macro and Microtribology - Velocity Accommodation Modes

When conducting load varying experiments, a common analysis for solid lubricants is a determination of the interfacial shear strength, S_o and the limiting friction coefficient [1,49,51-53], α. To derive the form of this relationship, one first writes the friction force, F_f as the product of a shear strength, S and the contact area, A:

$$\mathbf{F_f = S \bullet A} \qquad (7.1)$$

There is then a common assumption that the shear strength is dependent on the contact pressure, P, with the form

$$\mathbf{S = S_o + \alpha P} \quad (7.2)$$

This equation has been shown to be valid for cases where lubrication takes place by thin, solid interfacial films that create a weak interface [22,26,28]. For MoS_2, this is believed to be the case when transfer films form allowing for sliding of basal planes against one another. If one measures friction coefficient, μ, with the traditional definition of friction force divided by normal force, Eq 1 and Eq 2 can be combined to provide this relationship between μ and P:

$$\mathbf{\mu = \alpha + S_o / P} \quad (7.3)$$

Thus, by conducting load varying experiments with some knowledge of the contact area and measurement of the friction coefficient, a determination of α and S_o may be made through plots of μ vs. 1/ P.

For macroscopic tribology experiments, it is common practice to use the initial Hertzian contact pressure for P in Eq. 3. If the coating or material follows Hertzian behavior, the friction force is directly proportional to the normal force to the 2/3 power. For our macroscopic experiments, the exponent, m, for the relationship $F \alpha L^m$, was found to be 0.72 and 0.73 for high and low humidity, respectively. It is not uncommon that this analysis will deviate slightly from Hertzian contact mechanics [1,54].

The steady state coefficient of friction (averaged over up to five sliding tests) was plotted vs. the inverse Hertzian contact pressure for macrotribology tests (see Figure 7.14). From the least square fits to a straight line, an interfacial shear strength of 46(±9) MPa and 44(±6) MPa were found for low and high humidity, respectively. While there was evidence for interfilm shearing at high humidity (see Figure 7.6) and differences in wear (see Figure 7.3), velocity was accommodated in both environments predominantly by interfacial sliding of transfer film versus the wear track. Thus, the general sliding behavior was not significantly affected by humidity, which has previously been observed with similar Ti-MoS_2 coatings [10,47]. However, in comparison to other material additives with MoS_2, it has been shown that the interfacial shear strength increases for higher humidity. Sharf et al. [1] showed that the interfacial shear strength of MoS_2/Sb_2O_3/Au nanocomposites almost doubled (i.e. from 20 to 38 MPa) with changing the environment from dry nitrogen to 50% relative humidity. Furthermore, Dvorak et al. [18] , studying Pb-Mo-S coatings, found the interfacial shear strength increased from 16.5 MPa to 39 MPa when changing from dry air to 50% relative humidity.

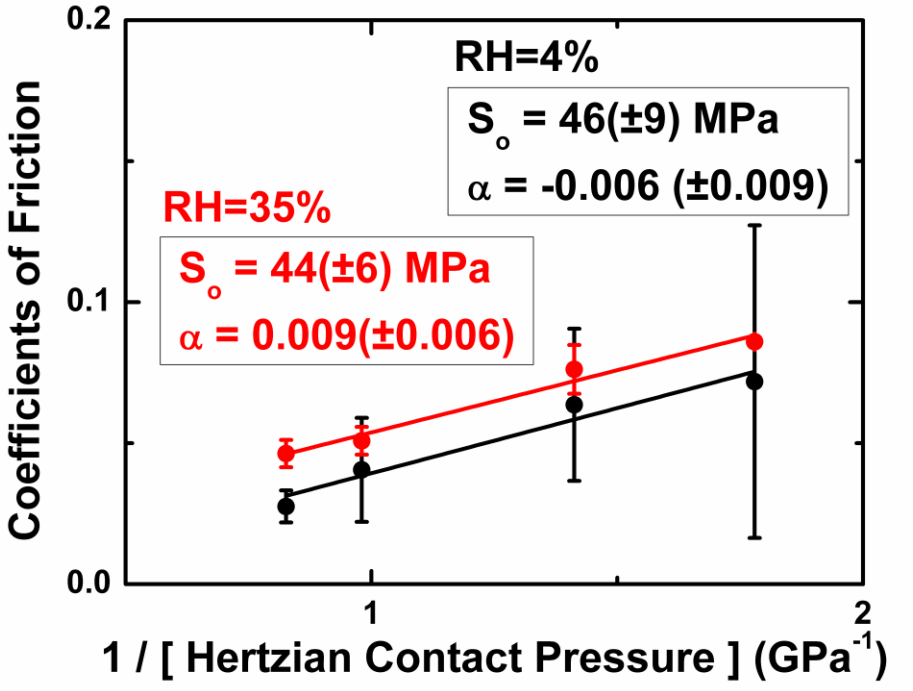

Figure 7.14. Steady state coefficient of friction vs. inverse contact pressure for macrotribology

Similar behavior, as observed with the interfacial shear strength, was also seen with the limiting coefficient of friction (α), which was -0.006 ± 0.009 and 0.009 ± 0.006 for the low and high humidity, respectively. Comparing these values to the literature mentioned above, the difference between the (α) values between high and low humidity was comparable to the study of Dvorak et al. [18] on Pb-Mo-S coating, which showed a difference of 0.019. Scharf et al. [1], studying MoS_2/Sb_2O_3/Au nanocomposites, showed a difference of 0.05 between the dry and humid tests.

It is generally true that over some range of contact pressure for dry sliding with MoS_2, a transfer film is created and near Hertzian behavior is observed with minimal wear. In these cases, a low

limiting friction coefficient is observed, in cases of vacuum extremely low [27,49] (0.001) and in cases of dry nitrogen [1,52], generally about 0.01. Our experiments were performed in dry air at 4% RH and in humid environment at 35-40% RH. Even though both testing conditions are in an environment that contains oxygen, our alpha values fall between the values for dry nitrogen and vacuum. In terms of the interfacial shear strength, the values for both humidities were also very similar to that observed for most other studies of dry sliding on MoS_2 containing coatings [1,16,49]. Thus, the VAM was similar to these other studies. In fact, our *in situ* observations demonstrate interfacial sliding, which is the same VAM observed for other studies using *in situ* tribology [16,49].

For microtribology, it is not possible to use the Hertzian contact pressure in Eq. 3. Spherical diamond tips deviate significantly from a spherical shape [33] and make it necessary to determine the real contact area. A technique developed in our group, which is described in previous work [21,31], was used here to determine the contact pressure realized during steady state sliding. Using this quantity, a plot of friction versus inverse contact pressure was constructed (see Figure 7.15).

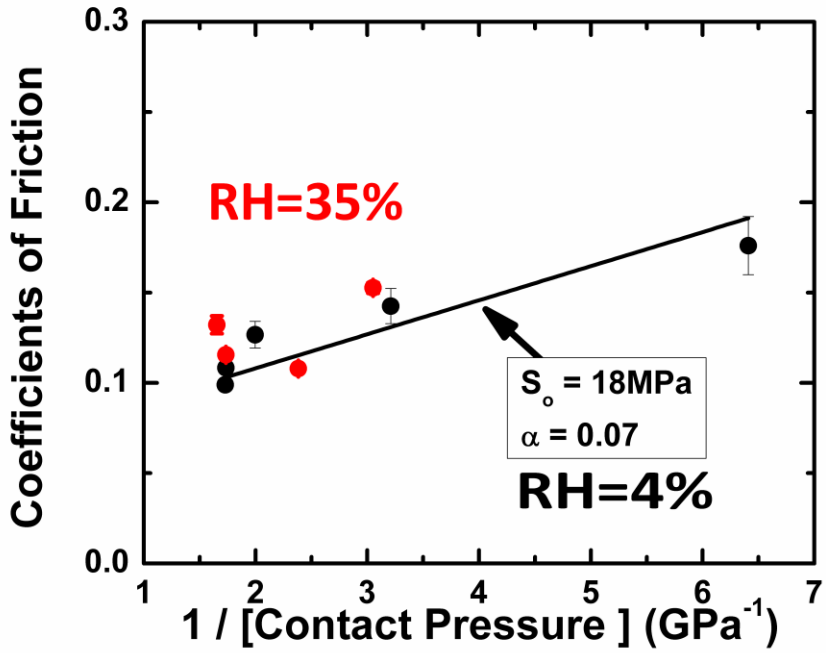

Figure 7.15. Steady state coefficient of friction vs. inverse contact pressure for microtribology at low and high relative humidity

Considering first the results at low humidity, a least square fit to a straight line revealed the mean slope (S_o = 18 MPa) and an intercept (α = 0.085). From these results, the interfacial shear strength was lower at the micro-scale compared to the macro-scale. However, the results obtained here were nearly identical to those obtained for microtribology studies on a similar Ti-MoS_2 coating with lower Ti content [21]. Also in this previous study, comparisons of the interfacial shear strength for three coatings were correlated to the level of adhesion by pull-off force measurements. Thus, the interfacial shear strength provided meaningful comparisons for different coatings tested at the same length scale. Here however, the comparisons between different scales must be conducted more carefully. The first clue that microtribology was

different from macrotribology was that the limiting friction for dry sliding was not the typical low value and was instead 0.085. This was an indication that the VAM may not be pure interfacial sliding. Even more compelling, results at higher humidity demonstrated a significant deviation from the typical behavior (see Figure 7.15) and do not follow a linear trend on a plot of friction versus inverse pressure. Thus, at higher humidity, microtribology appears to not follow the same VAM as macrotribology. Another indication that microtribology deviates from the near Hertzian behavior of macrotribology is that the exponent m for F vs. L^m was 0.83 for both high and low humidity.

To explore this different behavior at microtribology, we consider that there may be an additional VAM, such as plowing. Schiffman, et al. [55] used an empirical relationship to fit friction force versus normal force data with both elastic and plastic components:

$$\mu = \mu_e + \mu_p \tag{7.4}$$

where μ_e is the elastic/adhesive component and μ_p is the plastic/ plowing term. The two contributions of the coefficient of friction can be modeled by the following equation [30,55]:

$$\mu = \mu_e + \mu_p = c_1 L^{(-1/3)} + c_2 L^m \tag{7.5}$$

where the first term is the Herztian contribution and the second term is the plowing component. L is the normal load and *m* can be related to the yield strength and the strain hardening index. We propose that in Eq. (7.4), μ_e depends on the interfacial shear strength and μ_p could be dependent on the material properties (i.e. hardness and yield strength) and the tip shape/ roughness. The coefficient of friction was plotted vs. the normal load (not shown) and the data was fitted according to Eq. (7.5) with c_1, c_2, and m, being the constants, which can be obtained for the fit.

This fitting procedure was performed for eleven different cycles varying from the 19th to the 799th. The elastic (blue) and the plastic (red) contributions to the friction were then calculated for each normal load and plotted vs. cycle in Figures 7.16 (a) and (b) for the low and high relative humidity respectively. It was observed that for all normal loads the elastic component with the low humidity is lower compared to the high humidity tests. This was consistent with the overall lower friction values at the lower humidity levels, as seen in Figure 7.9. The plastic contribution of the coefficient of friction, on the other hand, shows a different behavior. For low humidity, the plastic component was independent of normal load, whereas at high humidity the plowing contribution increases with increasing the normal load. This was directly related to the *m* value in Eq. (7.5), which was between 0.3 and 1.0 for the high humidity tests and between 0.01 and 0.1 for the low humidity test. The values for high humidity were in a range where there is definitely a plowing component to the sliding process [55]. However, for lower humidity, the *m* values were lower and L^m becomes nearly one. Thus, the plowing component (μ_p) converts to c_2 (~0.06), which was similar to the α value obtained from Eq. (7.2). This indicates that the sliding mechanism for this condition was mainly elastic. However, due to the deviation from the Hertzian relationship (i.e. $F \alpha L^{0.83}$) and the high limiting coefficient of friction, there may also be some small scale plowing events which we will call "micro-plowing"

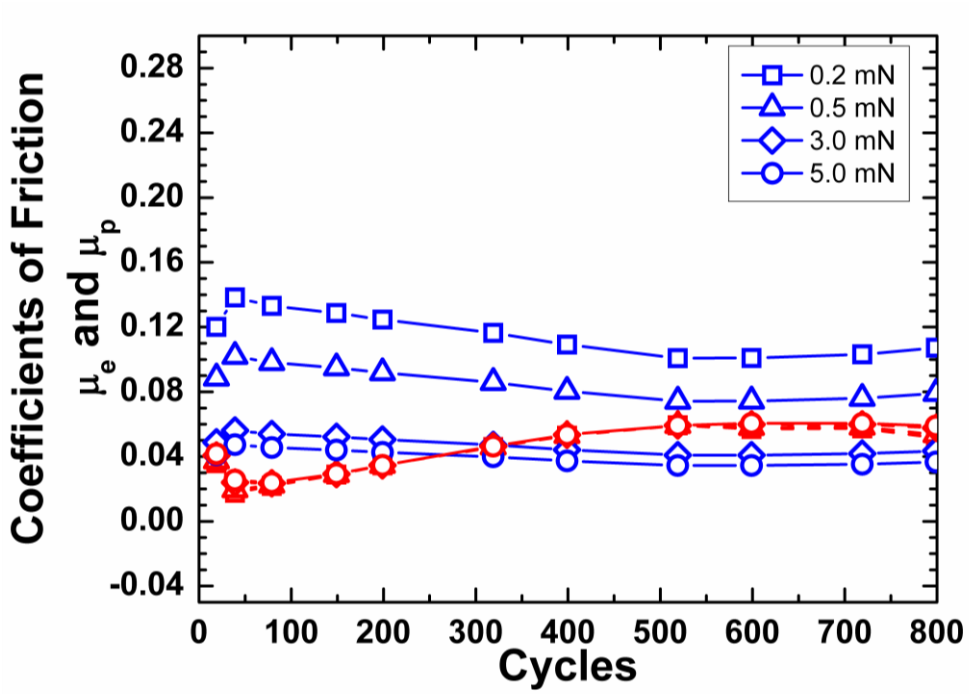

(a)

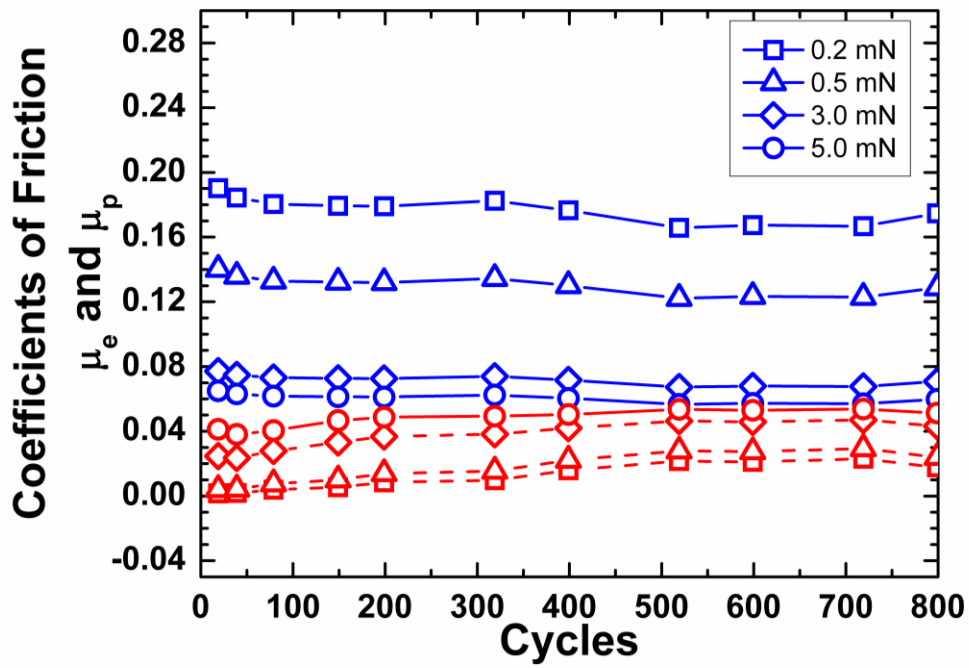

(b)

Figure 7.16. Elastic (blue) and plastic (red) contributions to the coefficient of friction vs. cycle for (a) 4% relative humidity and (b) 35% relative humidity.

Differences in VAM are often demonstrated in the appearance of third bodies. To be able to compare scales, we plot the transfer film thickness normalized to the Hertzian contact radius versus the Hertzian contact radius. For macrotribology, the range of normalized transfer film thickness has an upper limit of 0.01, meaning for a typical contact radius of 50 microns, the transfer film would be at most 500 nm. For dry sliding with microtribology, the normalized transfer film thickness was higher, being between 0.01 and 0.1. This means for a typical contact radius of 5 microns, the transfer film thickness is between 5 and 50 nm. For humid sliding with microtribology, the transfer film was undetectable. If we simply assume there is a 1 nm transfer film, the normalized value for high humidity would be 0.0002, much below the values shown in Figure 7.17. From this graph, a range of normalized transfer film thickness values (from ~ 0.001 to 0.1) were found that exhibit behavior with some level of solid lubrication (i.e. stable transfer film with VAMs of interfacial sliding, interfilm shearing and/or micro-plowing). If the value is below this range, as observed for humid microtribology, the VAM changes to plowing, which indicates that a transfer film is not thick and consistent enough to cover all asperities of the slider. If the value is above this range, one could assume that the transfer film will become unstable due to the shearing forces. Recent modeling by Pearson, et al. [56] demonstrated that a growth in transfer film thickness typically leads to reduction in overall stresses within coating, slider, and the transfer film itself. Thus, transfer film growth seems to be energetically favorable. However, a steady state thickness is typically reached, when stress reduction by further transfer film growth becomes marginal [56]. *In situ* tribological experiments on MoS_2 containing coatings [16] revealed that at this steady state transfer film thickness, equilibrium between transfer film growth and occasional debonding and extrusion of transfer film commences.

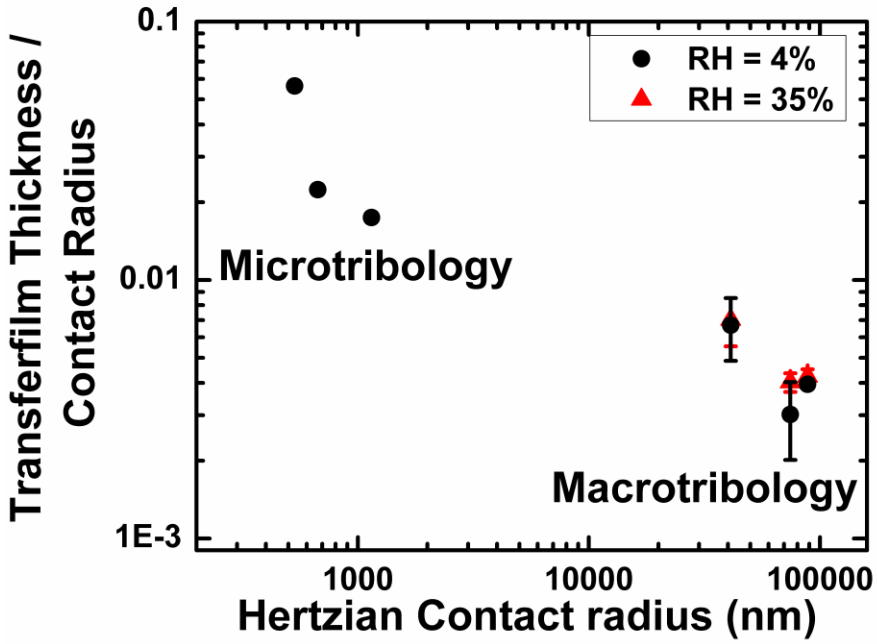

Figure 7.17. Transfer film thickness normalized by contact area vs. Hertzian contact radius for micro- and macrotribology

From the results obtained in this paper and from previous research on similar coatings [21,31], the sliding behavior of MoS_2 based coatings can be separated into three stages (i.e. solid lubrication, micro-plowing, and plowing), which are broken down by the contact pressure, contact size, tip shape, and humidity level (see Table 7.4). The first stage (solid lubrication) was typically observed with macrotribology on MoS_2 based coatings under ideal conditions (i.e. spherical tip with small roughness, and under dry air at low relative humidity). There was evidence of transfer film and tribofilm formation. Throughout this stage, the coefficient of friction decreased with increasing the normal load and followed the Hertzian contact behavior of Eq. (1). The alpha (α) component in this stage was typically small, which was consistent with

literature on similar coatings [27]. The wear mechanism was mainly due to adhesion. The second stage (i.e. micro-plowing) was observed for micro-tribology experiments with smaller contact areas compared to stage one and at low relative humidity. The friction force to normal force relationship was non-Hertzian and the (α) component was typically larger than for macrotribology. This friction behavior was seen previously with similar coatings [21]. The main wear mechanism in this stage was adhesion, but there is also some micro-plowing occurring. The low relative humidity was beneficial, but perhaps due to the reduced length scale and more discrete nature of the roughness of the tip, the sliding was not as well behaved as stage I. While transfer films and tribofilms formed the Raman signature for MoS_2 on the wear track was not as distinct as stage I. The final stage of the sliding behavior occurs when the velocity accommodation mode and wear mechanism were mainly plowing. In this case the sliding behavior followed Eq. (5) and α varied with normal load (i.e. α is proportional to L^m). During this stage, there was no stable transfer film observed, as seen in Figure 7.13 (b), and no evidence of tribofilm formation, as seen in Figure 7.12. This behavior has also previously seen at the micro-scale with Au-MoS_2 coatings [30] at high humidity and tip with a relatively rough 100 μm diamond tip.

Table 7.4. Three different stages of MoS_2 based lubricants.

	Stage I: *Solid lubrication*	**Stage II:** *Micro-Plowing*	**Stage III:** *Plowing*
Limiting Friction (α)	*~ small*	*~ big*	*~ L^m*
Friction behavior	Hertzian	non-Hertzian	non-Hertzian
General sliding behavior	solid lubricant	solid lubricant	not solid lubricant
VAM	interfacial sliding and/or interfilm shearing	interfacial sliding + micro-plowing	Interfacial sliding + plowing
Wear mechanism	adhesion	micro-plowing + adhesion	plowing
Tribofilm Formation^	Yes	Yes	No
Transfer Film Present	Yes	Yes	No

^ Evidence of increased crystallinity of MoS_2 from Raman spectroscopy.

7.5. Conclusion

The macro- and microtribological properties of co-sputtered Ti-MoS_2 coatings were investigated and compared with varying contact pressures and humidity levels. *In situ* tribometry was used to investigate third bodies for macroscale. *Ex situ* analysis with atomic force microscopy was used for microscale. Different stages for solid lubrication were identified with respect to different contact areas, tip shapes, and environmental conditions. We summarize similarities and dissimilarities between the tribological behavior between the two scales:

1) For dry sliding both scales formed transfer films, had a main VAM of interfacial sliding, and had tribofilm formation on the wear track.

2) However, for dry sliding, the friction and alpha parameter were higher for micro-scale compared to macro-scale. This change was attributed to microplowing due to tip roughness.
3) For humid sliding, both scales had an increase in friction compared to dry sliding and evidence of transfer film instability. This change with increased humidity was attributed to a modification of the adhesion between the slider and transfer film and the properties of the third bodies themselves.
4) However, for humid sliding, the instability in the transfer film let to different VAMs at the two different scales. At the macroscale, humidity led to transfer film shearing, whereas for microscale, it led to complete removal of the transfer film and the introduction of a plowing VAM. The more severe modification of the transfer film at microscale was attributed to the discrete nature of roughness of the tip leading to a multiasperity contact.
5) The transfer film thickness was normalized to the initial Hertzian contact radius for both scales. This normalized quantity showed that for values from 0.001 to 0.1, the contact exhibited behavior expected for a solid lubricant: near Hertzian contact mechanics, VAMs of interfacial sliding, interfilm shearing and only small scale plowing. For smaller values of this quantity, observed for humid conditions at microscale, plowing was observed with only possibly very thin transfer films (< 3 nm). No running conditions were observed where this normalized quantity was greater than 0.1, perhaps due to the transfer films becoming unstable due to a decrease in stiffness with respect to shearing forces.

6) Three stages of solid lubrication behavior were identified. Stage I was found at macroscale and was the same as has been shown in the literature extensively. Stage II was found for dry sliding at microscale, where evidence of plowing and adhesion effects were seen but the contact still behaved largely as a solid lubricant similar to Stage I. Finally, Stage III was observed for humid sliding at microscale, where there were no transfer films and a plowing VAM.
7) Overall, lower friction (steady state) was observed at the macro-scale (μ = 0.02 - 0.1) compared to the micro-scale (μ = 0.1 - 0.2). This difference was attributed to the higher limiting friction from an analysis of a plot of friction versus inverse contact pressure. Higher limiting friction at microscale was due to adhesion effects and the additional VAMs of microplowing (low humidity) or plowing (high humidity).
8) Increase in humidity at macroscale led to an increase in wear compared to dry sliding. However, at the microscale, the increased humidity did not lead to a significant increase in wear compared to dry sliding. This difference was attributed to VAMs. At macroscale, humid sliding led to transfer film shearing and the deposition of wear debris onto the wear track. Thus, there were multiple mechanisms available for wear, including motion and clearing of wear debris. At the microscale, while there was a plowing mechanism due to the absence of a transfer film, there was less evidence for the mechanisms seen at macroscale. Thus, the confined nature of the contact at microscale, while having a negative impact on transfer film formation, seemed to have the positive impact of confining wear debris and preventing some of the more complex wear mechanisms seen at macroscale.

Acknowledgements

The authors gratefully acknowledge financial support the Discovery Grants program of the Natural Science and Engineering Council (NSERC) of Canada, the McGill Engineering Doctoral Awardand the Canadian Foundation for Innovation, Leader's Opportunity Fund, project No. 13029. The authors acknowledge David Goldbaum, Zachary Fishman for their collaboration with the Matlab code, Guruprasad Sosale, Beinan Li for their help with the optical profiler and Francois Barthelet for collaboration with atomic force microscopy The Ti-MoS_2 coating was graciously provided by Xiaoling Zhang at Teer Coating, Ltd.

REFERENCES

1 T. W. Scharf, P. G. Kotula, and S. V. Prasad, Friction and wear mechanisms in MoS_2/Sb_2O_3/Au nanocomposite coatings, Acta Materialia 58 (2010) 4100-4109

2 J. R. Lince, Tribology of co-sputtered nanocomposite Au/MoS_2 solid lubricant films over a wide contact stress range, Tribology Letters 17 (2004) 419-428

3 T. Spalvins, Frictional and morphological properties of Au-MoS_2 films sputtered from a compact target, Thin Solid Films 118 (1984) 375-384

4 R. S. Colbert and W. G. Sawyer, Thermal dependence of the wear of molybdenum disulphide coatings, Wear 269 (2010) 719-723

5 M. C. Simmonds, A. Savan, E. Pfluger, and H. Van Swygenhoven, Mechanical and tribological performance of MoS_2 co-sputtered composites, Surface and Coatings Technology 126 (2000) 15-24

[6] B. C. Stupp, Synergistic effects of metals co-sputtered with MoS_2, Thin Solid Films 84 (1981) 257-266

[7] I. Efeoglu, Ö. Baran, F. Yetim, and S. AltIntas, Tribological characteristics of MoS_2-Nb solid lubricant film in different tribo-test conditions, Surface and Coatings Technology 203 (2008) 766-770

[8] Y. L. Su and W. H. Kao, Tribological behaviour and wear mechanism of MoS_2-Cr coatings sliding against various counterbody, Tribology International 36 (2003) 11-23

[9] W. H. Kao, Tribological properties and high speed drilling application of MoS_2-Cr coatings, Wear 258 (2005) 812-825

[10] X. Ding, X. T. Zeng, X. Y. He, and Z. Chen, Tribological properties of Cr- and Ti-doped MoS_2 composite coatings under different humidity atmosphere, Surface and Coatings Technology 205 (2010) 224-231

[11] B. C. Stupp, Performance of conventionally sputtered MoS_2 versus co-sputtered MoS_2 and Nickel, ASLE Proceedings - 3rd International Conference on Solid Lubrication (1984) 217-222

[12] R. Gilmore, M. A. Baker, P. N. Gibson, W. Gissler, M. Stoiber, P. Losbichler, and C. Mitterer, Low-friction TiN-MoS_2 coatings produced by dc magnetron co-deposition, Surface and Coatings Technology 108-109 (1998) 345-351

[13] V. C. Fox, N. Renevier, D. G. Teer, J. Hampshire, and V. Rigato, The structure of tribologically improved MoS_2-metal composite coatings and their industrial applications, Surface and Coatings Technology 116-119 (1999) 492-497

[14] V. Rigato, G. Maggioni, D. Boscarino, L. Sangaletti, L. Depero, V. C. Fox, D. Teer, and C. Santini, A study of the structural and mechanical properties of Ti-MoS_2 coatings deposited by closed field unbalanced magnetron sputter ion plating, Surface and Coatings Technology 116-119 (1999) 176-183

[15] X. Wang, Y. Xing, S. Ma, X. Zhang, K. Xu, and D. G. Teer, Microstructure and mechanical properties of MoS_2/titanium composite coatings with different titanium content, Surface and Coatings Technology 201 (2007) 5290-5293

[16] R.R. Chromik, C.C. Baker, A.A. Voevodin, and K. J. Wahl, *In situ* tribometry of solid lubricant nanocomposite coatings, Wear 262 (2007) 1239-1252

[17] K. J. Wahl, D. N. Dunn, and I. L. Singer, Wear behavior of Pb-Mo-S solid lubricating coatings, Wear 230 (1999) 175-183

[18] S. D. Dvorak, K. J. Wahl, and I. L. Singer, *In situ* analysis of third body contributions to sliding friction of a Pb-Mo-S coating in dry and humid air, Tribology Letters 28 (2007) 263-274

[19] N. M. Renevier, V. C. Fox, D. G. Teer, and J. Hampshire, Performance of low friction MoS_2/titanium composite coatings used in forming applications, Materials & Design 21 (2000) 337-343

[20] A.R. Lansdown, Molybdenum Disulphide Lubrication, Elsevier Science B.V., Amsterdam, 1999.

[21] P. Stoyanov, D. Goldbaum, J. R. Lince, X. Zhang, and R. Chromik, Microtribological Performance of Au/ MoS_2 and Ti/ MoS_2 Coatings with varying Contact Pressure, Tribology Letters 40 (2010) 199-211

[22] I.L. Singer, Solid Lubrication Processes, in: I.L. Singer and H.M. Pollock, Fundamentals of Friction: Macroscopic and Microscopic Processes, Netherlands, pp. 237-261, 1992.

[23] I. L. Singer, S. D. Dvorak, K. J. Wahl, and T. W. Scharf, Role of third bodies in friction and wear of protective coatings, Journal of Vacuum Science & Technology A 21 (2003) S232-S240

[24] M. Godet, The third-body approach: a mechanical view of wear, Wear 100 (1984) 437-452

[25] I. L. Singer, S. D. Dvorak, K. J. Wahl, and T. W. Scharf, Third body processes and friction of solid lubricants studied by *in situ* optical and Raman tribometry, in: M. Priest G. Dalmaz D. Dowson and A. A. Lubrecht, Tribology Series, Elsevier, Vol. Volume 40, pp. 327-336, 2002.

[26] B. J. Briscoe and D. C. B. Evans, The shear properties of Langmuir-Blodgett layers, Proceedings of the Royal Society of London, Series A (Mathematical and Physical Sciences) 380 (1982) 389-407

[27] I. L. Singer, R. N. Bolster, J. Wegand, S. Fayeulle, and B. C. Stupp, Hertzian stress contribution to low friction behavior of thin MoS_2 coatings, Applied Physics Letters 57 (1990) 995-997

[28] G. He and M. O. Robbins, Simulations of the kinetic friction due to adsorbed surface layers, Tribology Letters 10 (2001) 7-14

[29] T. W. Scharf, S. V. Prasad, M. T. Dugger, P. G. Kotula, R. S. Goeke, and R. K. Grubbs, Growth, structure, and tribological behavior of atomic layer-deposited tungsten

disulphide solid lubricant coatings with applications to MEMS, Acta Materialia 54 (2006) 4731-4743

30 P. Stoyanov, Z. Fishman, J. R. Lince, and R. R. Chromik, "Micro-Tribological Performance of MoS_2 Lubricants with varying Au content," Surface and Coatings Technology 203 (2008) 761-765

31 P. Stoyanov, R. R. Chromik, S. Gupta, and J. R. Lince, Micro-scale sliding contacts on Au and Au-MoS_2 coatings, Surface and Coatings Technology 205 (2010) 1449-1454

32 C. K. Bora, E. E. Flater, M. D. Street, J. M. Redmond, M. J. Starr, R. W. Carpick, and M. E. Plesha, Multiscale roughness and modeling of MEMS interfaces, Tribology Letters 19 (2005) 37-48

33 A.J. Bushby, N.M. Jennett: Determining the area function of spherical indenters for nanoindentation. In: Baker, S.P., Cook, R.F., Corcoran, S.G., Moody, N.R. (eds.) Fundamentals of Nanoindentation and Nanotribology II, vol. 649, pp. Q7.17.11–Q17.17.16. Materials Research Society, Warrendale, PA (2001)

34 B. Bhushan, Micro/nanotribology and its applications to magnetic storage devices and MEMS, Tribology International 28 (1995) 85-96

35 F.W. Delrio, M.P. De Boer, J.A. Knapp, E.D. Reedy Jr, P.J. Clews, and M.L. Dunn, The role of van der Waals forces in adhesion of micromachined surfaces, Nature Materials 4 (2005) 629-634

36 K. Komvopoulos, Surface engineering and microtribology for microelectromechanical systems, Wear 200 (1996) 305-327

[37] S. Descartes and Y. Berthier, Rheology and flows of solid third bodies: background and application to an $MoS_{1.6}$ coating, Wear 252 (2002) 546-556

[38] R. R. Chromik, A. L. Winfrey, J. Lüning, R. J. Nemanich, and K. J. Wahl, Run-in behavior of nanocrystalline diamond coatings studied by *in situ* tribometry, Wear 265 (2008) 477-489

[39] T. W. Scharf and I.L. Singer, Quantification of the thickness of carbon transfer films using Raman tribometry, Tribology Letters 14 (2003) 137-146

[40] T. W. Scharf and I. L. Singer, Role of third bodies in friction behavior of diamond-like nanocomposite coatings studied by *In Situ* tribometry, Tribology Transactions 45 (2002) 363-371

[41] T. W. Scharf and I. L. Singer, Monitoring transfer films and friction instabilities with *in situ* Raman tribometry, Tribology Letters 14 (2003) 3-8

[42] T. W. Scharf and I. L. Singer, Role of the transfer film on the friction and wear of metal carbide reinforced amorphous carbon coatings during run-in, Tribology Letters 36 (2009) 43-53

[43] K. J. Wahl and W. G. Sawyer, Observing interfacial sliding processes in solid - solid contacts, MRS Bulletin 33 (2008) 1159-1167

[44] K. J. Wahl, R. R. Chromik, and G. Y. Lee, Quantitative *in situ* measurement of transfer film thickness by a Newton's rings method, Wear 264 (2008) 731-736

[45] H. Hertz, Über die berührung fester elastischer Körper Journal für die reine und angewandte Mathematik 92 (1881) 156-171

[46] N. M. Renevier, J. Hamphire, V. C. Fox, J. Witts, T. Allen, and D. G. Teer, Advantages of using self-lubricating, hard, wear-resistant MoS2-based coatings, Surface and Coatings Technology 142-144 (2001) 67-77

[47] N. M. Renevier, V. C. Fox, D. G. Teer, and J. Hampshire, Coating characteristics and tribological properties of sputter-deposited MoS_2/metal composite coatings deposited by closed field unbalanced magnetron sputter ion plating, Surface and Coatings Technology 127 (2000) 24-37

[48] J. R. Lince, Michael R. Hilton, and A. S. Bommannavar, EXAFS of sputter-deposited MoS_2 films, Thin Solid Films 264 (1995) 120-134

[49] S. D. Dvorak, K. J. Wahl, and I. L. Singer, *In situ* analysis of third body contributions to sliding friction of a Pb-Mo-S coating in dry and humid air, Tribology Letters 28 (2007) 263-274

[50] G.Y. Lee, I. L. Singer, and K. J. Wahl, Nanoscale mechanical studies of interfacial films from sliding contacts, presented at MRS Fall Meeting, Boston, MA, 2004.

[51] B. J. Briscoe and A. C. Smith, The Interfacial Shear Strength of Molybdenum Disulfide and Graphite Films, Tribology Transactions 25 (1982) 349 - 354

[52] K. J. Wahl, L. E. Seitzman, R. N. Bolster, and I. L. Singer, Low-friction, high-endurance, ion-beam-deposited Pb-Mo-S coatings, Surface and Coatings Technology 73 (1995) 152-159

[53] J. L. Grosseau-Poussard, P. Moine, and M. Brendle, Shear strength measurements of parallel MoSx thin films, Thin Solid Films 307 (1997) 163-168

[54] U. D. Schwarz, O. Zwörner, P. Köster, and R. Wiesendanger, Quantitative analysis of the frictional properties of solid materials at low loads. I. Carbon compounds, Physical Review B 56 (1997) 6987

[55] K. I. Schiffmann and A. Hieke, Analysis of microwear experiments on thin DLC coatings: friction, wear and plastic deformation, Wear 254 (2003) 565-572

[56] J. D. Pearson, M. A. Zikry, and K. Wahl, Computational design of thin-film nanocomposite coatings for optimized stress and velocity accommodation response, Wear 267 (2009) 1137-1145

Chapter 8

8.1 Conclusions

The specific experimental conclusions have been summarized in details at the end of each chapter. In this chapter only the major global conclusions of the thesis are given.

1. The tribological properties of gold and titanium doped MoS_2 coatings were investigated at the microscopic scale. The addition of gold and titanium to molybdenum disulphide showed an increase in wear resistance and a decrease in coefficient of friction compared to pure molybdenum disulphide coatings. The improved tribological properties, at the microscopic scale, with the gold and titanium additions were attributed to an increase in the mechanical properties (i.e. hardness and reduced modulus), decrease in adhesion, and a decrease in the interfacial shear strength.

2. Direct comparison of the macro- and micro- tribological properties of co-sputtered Ti-MoS_2 coatings was performed with varying contact pressures and humidity levels. *In situ* tribometry was used at the macroscopic scale to investigate the third body behavior, whereas, at the microscale, *ex situ* analysis with an atomic force microscope was performed. Using these techniques three different stages for solid lubrication were identified based on differences in contact area, tip shapes, and environmental conditions. The first stage has been typically observed with macrotribology on MoS_2 coatings under ideal conditions. The second stage was observed for micro-tribology where the contact

size is significantly smaller compared to stage one. The main wear mechanism is still adhesion, but there is also some micro-plowing occurring. The final stage was observed for humid sliding in microtribology. In this stage, there were no transfer films and therefore the main wear mechanism was plowing.

3. Overall, lower steady state friction was observed for macrotribology compared to microtribology. The higher friction at the micro- scale was explained by the higher limiting friction value, which resulted due to adhesion effects and additional VAMs (i.e. microplowing or plowing). The microplowing or plowing at the microscopic scale was attributed to the tip roughness.

4. The influence of varying the gold content in Au-MoS_2 nanocomposite coatings on the micro-tribological properties was also investigated. Micro-sliding tests in dry environments showed that a higher Au content coating resulted in less wear and a more stable friction coefficient compared to low Au content coating. The improvement of the triobological properties with the higher gold content was attributed to a decrease in the plowing component.

5. Small amount of molybdenum disulphide was used as an additive to gold due to positive influence on the mechanical and tribological properties. It was found that the addition of 20 mol% MoS_2 to Au reduced the adhesion and limiting friction and also improved the wear resistance significantly. This coating shows potential for applications in

microcomponents and microswitches due to its wear resistance, relatively low friction and good electrical conductivity.

8.2 Contribution to original knowledge

1. The viability of Ti-MoS_2 and Au-MoS_2 nanocomposite solid lubricants at a micro- scale has been reported for the first time. The differences and similarities between micro- and macroscopic sliding behavior were identified and reported.

2. It is the first time that the transferfilm formation was investigated at the micro- scale, which was directly correlated to the tribo- film (using Raman microscopy) and different velocity accommodation modes.

3. For the first time, the micro-tribological properties of Ti-MoS_2 and Au-MoS_2 solid lubricants at the micro- scale were investigated using a variation of contact stresses and humidity levels, which were directly correlated to transferfilm formation and wear behavior.

4. It is the first time that the interfacial shear strength of solid lubricants was investigated at the micro-scale using contact pressure obtained directly from the actual contact area, which was directly correlated to shear strength values of similar coatings obtained at the macro- scale.

5. The different wear contributions (i.e. elastic, plastic, and adhesive) were reported for Ti-MoS_2 and Au-MoS_2 coatings for the first time and correlated to the mechanical properties, surface adhesion properties, and the interfacial shear strength or "velocity accommodation parameter".

6. It is the first time that direct observations of the transferfilm formation and the macro-tribological behavior of Ti-MoS_2 coatings with varying contact pressures and humidity levels using an *in situ* tribometer are reported.

8.3 Suggestions for future work

1. Transmission electron microscope (TEM) images should be performed of cross section of the wear tracks and transfer film for microtribological experiments with varying contact pressures and humidity levels. This analysis will provide inside on the behavior of the basal planes orientation, which can be compared to the sliding behavior for macroscale tribology.

2. The microtribological tests in this thesis were performed using instruments that simulate the conditions for a real device through micro- and nanotribological testing. Therefore, there is a need to investigate the viability of the Au / MoS_2 and Ti / MoS_2 coatings using real MEMS devices that are constructed as miniature tribometers. In addition, previous

literature has shown that MoS_2-based coatings can be deposited onto MEMS using successive ionic layer absorption and reaction (SILAR) technique. Future work is required to optimize the deposition of Ti or Au doped MoS_2 coatings using ALD, SILAR, or other non-line of sight processes. Consequently, the microtribological properties of such films need to be studied in a similar manner to those examined in this thesis.

3. A mixture of bilayered and cosputtered coatings should be developed in order to optimize the tribological properties. Potential coatings could be bilayered Au/ 80%Au-MoS_2 or 80%Au-MoS_2/ MoS_2. The Au-MoS_2 or pure MoS_2 layer (i.e. top layers) of such coatings will be used as a sacrificial layer, which would contribute to the formation of a stable and uniform transferfilm and therefore improve the tribological performance of the underlying layer.